A TRANSLATIONAL APPROACH TO CHARACTERIZE miRNAs INVOLVED IN EARLY CORTICAL SYNAPTIC LOSS IN SYNUCLEINOPATHIES

Dissertation der Fakultät für Biologie

der Ludwig-Maximilians-Universität München

Jeannine Sonja Norma Widmann

München, 2022

Diese Dissertation wurde unter der Leitung von Dr. Felix Strübing und Prof. Dr. Jochen Herms am Institut für Neuropathologie der Ludwig-Maximilians-Universität München angefertigt und von Prof. Dr. Hans Straka vertreten.

Erstgutachter:	Prof. Dr. Hans Straka
Zweitgutachterin:	Prof. Dr. Anja Horn-Bochtler

Tag der Abgabe:	03. August 2022
Tag der mündlichen Prüfung:	25. November 2022

Eidesstattliche Erklärung

Ich versichere hiermit an Eides statt, dass die vorgelegte Dissertation selbstständig und ohne unerlaubte Hilfsmittel angefertigt worden ist. Die vorliegende Dissertation wurde weder ganz noch teilweise bei einer anderen Prüfungskommission vorgelegt. Ich habe noch zu keinem früheren Zeitpunkt versucht, eine Dissertation einzureichen oder an einer Doktorprüfung teilzunehmen.

München, 24.01.2023

Jeannine Sonja Norma Widmann

„Von der Stirne heiß, rinnen muss der Schweiß…“

Das Lied von der Glocke,

Friedrich von Schiller, 1799

I. TABLE OF CONTENTS

II. LIST OF ABBREVIATIONS

Abbreviation	Meaning
3'UTR	three prime untranslated region
5'UTR	five prime untranslated region
AD	Alzheimer's disease
ALP	autophagy-lysosomal pathway
ALS	amyotrophic lateral sclerosis
a-OHDA	6-hydroxydopamine
APS	ammonium persulfate
Aß	amyloid beta
AST	α-Synuclein-triplication cell line
α-syn	alpha-synuclein
B2MG	ß2-microglobulin
BDNF	growth factor brain-derived neurotrophic factor
cAMP	cyclic adenosinmonophosphat
CAS	corrected α-synuclein cell line
cDNA	copy DNA
circRNA	circular RNA
CMA	chaperone-mediated autophagy
CNV	copy number variation
CO	cerebral organoid
CP	cortical plate
CREB	transcription factor cAMP response element-binding protein
CRISPR/Cas9	clustered regulatory interspaced short palindromic repeat
CRL	custom range ladder
CSF	cerebrospinal fluid
D20 … D120	Day 20 … Day 120, 20 … 120 days post CO differentiation start
DA	dopaminergic neurons
ddPCR	digital droplet PCR
DE	differentially expressed
DEG	differentially expressed gene
DLB	dementia with Lewy-bodies
DNA	deoxyribonucleic acid
DPBS	Dulbecco's phosphate buffered saline
EBs	embryoid body
ECM	extracellular matrix
EDTA	ethylendiamintetraacetat
ER	endoplasmatic reticulum
ERK1/2	extracellular signal-regulated kinase signalling pathway
FASS	fluorescent activated synaptosome sorting
FFPE	formalin-fixed, paraffin embedded
FGFR1	fibroblast growth factor receptor 1
GATA2	transcription factor GATA-binding factor 2
GCI	glial cytoplasmic inclusions
GDNF	glial cell-line derived neurotrophic factor
gRNA	guide RNA

GTP	guanosintriphosphat
GO	Gene ontology
GWAS	genome wide association studies
H-DAB	Haematoxylin and DAB (3,3'-diaminobenzidine)
hiPSC	human induced pluripotent stem cells
hMLO	human midbrain-like organoid
HRL	high resolution ladder
hsa-miRNA	*Homo sapiens* miRNA
HSP70	heat shock protein 70
IPCs	intermediate progenitor cells
iSVZ	inner subventricular zone
IZ	intermediate zone
IF	immunofluorescence immunohistochemistry
IHC	immunohistochemistry
KLF4	Kruppel-like factor 4
Lamp2A	lysosome-associated membrane protein 2
LC-MS/MS	liquid chromatography mass spectrometry/mass spectrometry
L-dopa	Levodopa
LPS	lipopolysaccharide
LUHMES cells	Lund human mesencephalic cells
mDA	mature dopaminergic neurons
MEF2	transcription factor myocyte enhancer factor 2
mGluR	metabotrophic glutamate receptor
miRISC	miRNA-induced silencing complex
miRNA	microRNA
MKL1	transcription factor megakaryoblastic leukemia 1
mmu-miRNA	*Mus musculus* miRNA
MOV10	Armitage in *D. melanogaster*
MPTP	1-methyl-4-phenyl-1,2,3,6-tetrahydropyridine
mRNA	messenger RNA
MSA	multiple systems atrophy
MZ	marginal zone
NAC	non amyloid-ß component
NCI	neuronal cytoplasmic inclusions
ncRNA	non-coding RNA
NDMC	neuronal differentiation medium with culture one supplement
NEM	neural expansion medium
NGS	next generation sequencing
NIM	neural induction medium
NSC	neural stem cells
NT	neurotransmitter
Oct4	octamer-binding transcription factor 4 (also known as *POU5F1*)
ORF	open reading frame
oRG	outer radial glia
oSVZ	outer subventricular zone
PCR	polymerase chain reaction
PD	Parkinson's disease
PDD	Parkinson's disease with dementia

PDGF	platelet-derived growth factor
PDGF mouse	Human-α-synuclein overexpressing mouse line (PDGF-h-α-syn)
PDGF.2	2-month-old PDGF mice
PDGF.3	3-month-old PDGF mice
PDL	poly-D-lysine
PFA	paraformaldehyde
piRNA	piwi RNA
pre-miRNA	precursor miRNA
pri-miRNA	primary miRNA
pSyn	phopho-α-synuclein
RBP	RNA binding protein
RhoA	Ras homolog family member A, small GTPase protein
RNA	ribonucleic acid
RNA-Seq	RNA-sequencing
Rocki	Rock Inhibitor
rpm	rounds per minute
rRNA	ribosomal RNA
RT	room temperature
RT-qPCR	real-time quantitative PCR
SH-SY5Y	human neuroblastoma cell line
siRNA	small interfering RNA
SNARE-complex	soluble N-ethylmaleimide-sensitive factor attachment receptor complex
SNCA	alpha-synuclein (α-synuclein)
snoRNA	small nucelolar RNA
snRNA	small nucelar RNA
SOX2	sex determining region Y-box 2
SRF	transcription factor serum response factor
TAE	Tris-acetate-EDTA buffer
TBE	Tris-borat-EDTA buffer
TBR2	T-box brain protein
TEMED	Tetramethylethylenediamine
TF	transcription factor
TFEB	transcription factor EB (master TF for lysosomal biogenesis)
TH	tyrosine hydroxylase
tRNA	transfer RNA
UPS	ubiquitin-proteasome system
UTR	untranslated region
v-myc	avian virus myelocytomatosis
vRG	ventricular radial glia
VZ	ventricular zone
WT	wild type
WT.2	2-month-old WT mice
WT.3	3-month-old WT mice

III. SUMMARY

Aberrant accumulation of α-synuclein protein leads to a disease called synucleinopathy, being the second largest neurodegenerative disorder worldwide. Ultimately, insoluble protein aggregates formed by α-synuclein proteins lead to the degeneration of neurons. Before the onset of any behavioural symptoms, cortical synaptic loss in PDGF mice overexpressing α-synuclein has been observed between 2 and 4.5 months of age. Remarkably, transcriptomic analysis of total cortical RNA at the onset of cortical loss could not recapitulate the differentially expressed proteins identified in synaptosomes of 3-month-old PDGF mice. Thus, post-transcriptional processes were considered to explain the observed discrepancy between gene and protein expression. Indeed, the evolutionary highly conserved miRNA 183/96/182 cluster was identified to be significantly higher expressed in PDGF mice at 2 months of age. Its specific binding to synaptically localised *eEF1A1* mRNA suggested downregulation of eEF1A1 protein and thus decreased local protein translation in activity-dependent glutamatergic synapses.

However, PDGF mice overexpress non-endogenous human *SNCA* and are therefore different from human disease, where mutations of the *SNCA* locus or copy number variations of *SNCA* are observed. Hence, murine findings during late development and early adulthood cannot be recapitulated in human post-mortem tissue, requiring model systems to translate early pathological changes observed in murine model systems to model systems of human genetic relevance. For that reason, induced pluripotent stem cells (iPSCs) harbouring a triplication of *SNCA* together with their isogenic control with a normal copy number of *SNCA* were differentiated into cortical organoids (COs). Cortical synaptic loss of glutamatergic neurons in PDGF mice could be recapitulated in AST and CAS COs during the course of time. Furthermore, steady and significantly higher expression of the miRNA 183/96/182 cluster in AST COs was detected as well. Higher expression of the miRNA 183/96/182 cluster in AST COs was correlated with a reduced density of glutamatergic neurons, possibly caused by the inability to successfully mature or maintain cytostructures of mature synapses.

In summary, the miRNA 183/96/182 cluster in glutamatergic neurons was identified to post-transcriptionally regulate *eEF1A1*, thus controlling protein synthesis locally at the synapse during neuronal development. Moreover, overexpression of α-synuclein caused a significant upregulation of the miRNA 183/96/182 cluster during neuronal development and correlated with reduced density of glutamatergic presynaptic termini. In addition, reduced synaptic density could be caused by impaired maturation and maintenance of synapses under α-synuclein overexpression conditions. Formation and maintenance of mature synaptic structures could be disrupted by decreased local protein synthesis at the spine, which would be caused by miRNA 183/96/182 cluster induced post-transcriptional silencing of *eEF1A1* mRNA translation to eEF1A1 protein.

IV. INTRODUCTION

SYNUCLEINOPATHIES

After Alzheimer's disease, synucleinopathies, also called α-synucleinopathies, are the second most common neurodegenerative disorder affecting more than 6 million individuals worldwide. It is a heterogeneous neurodegenerative disease, characterized by motor symptoms including tremor, rigidity and bradykinesia, as well as non-motor symptoms including sleep disorders, cognitive impairments and visual hallucinations. Unfortunately, although substantial effort and progress has been made in investigating the disease, no cure is available and current therapies are limited to symptomatic and supportive care (Spillantini et al. 1997; Spillantini et al. 1998; Norris et al. 2004; Moore et al. 2005; Irwin et al. 2013; Luk & Lee 2014; Ray Dorsey et al. 2018).

Collectively, synucleinopathies summarise neurodegenerative diseases with abnormal accumulation of insoluble α-synuclein protein aggregates in neuronal or glial cells. Based on clinical and neuropathological characteristics, synucleinopathies can be further subdivided into three main subtypes: Parkinson's disease with and without dementia (PDD, respectively PD), dementia with Lewy bodies (DLB) and multiple system atrophy (MSA). The subtypes show varying yet sometimes overlapping clinical phenotypes, with each subtype showing varying dynamics in disease progression and pathology prevalence (Spillantini et al. 1998; Galvin, Lee, et al. 2001; Marti et al. 2003; de Lau & Breteler 2006; McCann et al. 2013; Jellinger & Korczyn 2018).

The onset of disease is around the age of 60 years for PD and MSA. PD shows the longest average disease duration and is responsive to L-dopa treatment. Neuropathologically, PD and DLB share α-synuclein inclusions in neuronal cytoplasma (neuronal cytoplasmic inclusions, NCI) and neurites, while MSA exhibits glial cytoplasmic inclusion bodies (GCIs), most notably in oligodendrocytes (also known as Papp-Lantos-inclusions) (Spillantini et al. 1998; Jelling & Lantos 2010; McCann et al. 2013). The exact discrimination between the different subtypes is based on clinical and neuropathological hallmarks, while definition of precise distinction criteria is currently under debate (Spillantini et al. 1997; Galvin, Lee, et al. 2001; McCann et al. 2013; Koga et al. 2021).

PARKINSON'S DISEASE IS THE MOST COMMON SUBTYPE OF SYNUCLEINOPATHIES

An Essay on the Shaking Palsy is the first detailed report about PD described by James Parkinson in 1817 (Parkinson 2002). Today, PD is the most common movement disorder worldwide with a prevalence of 1% of the population over the age of 60 up to 4% of affected people at 80 years of age (de Lau & Breteler 2006). Four clinical motor symptoms define for PD: bradykinesia, rigidity, resting

tremor and postural instability (Hughes et al. 1992; Gelb et al. 1999). A neuropathological hallmark of PD is the loss of dopaminergic neurons in the substantia nigra pars compacta (SNpc) of the midbrain (Spillantini et al. 1998). Motor symptoms are therefore explained by the loss of dopaminergic neurons (DA), that normally project with their axons to the striatum as the main basal ganglia input structure (nigrostriatal pathway) (Obeso et al. 2000). Remaining neurons in the substantia nigra show axonal and cytoplasmic accumulation of protein aggregates, termed Lewy neurites or Lewy bodies (Figure 1). These protein aggregates are predominantly composed of the α-synuclein protein (Lewy 1912; Spillantini et al. 1997; Braak et al. 2003; Lill 2016).

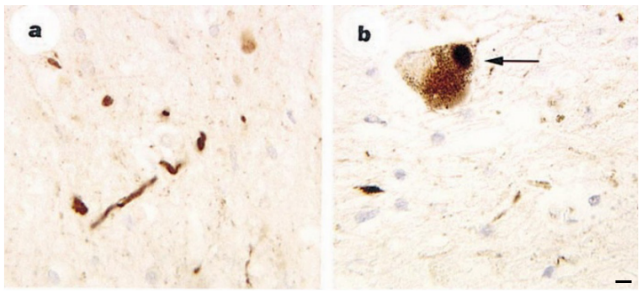

Figure 1: *Tissue from patients diagnosed with DLB immunostained for (a) α-synuclein positive Lewy neurite in substantia nigra and (b) α-synuclein-positive Lewy body in pigmented nerve cell of the substantia nigra (b). Scale bar 10 µm. (Reprinted with permission from Spillantini et al. 1997).*

Lewy pathology is not limited to specific brain areas, and disease progression throughout the brain has been categorised according to Braak staging (Braak et al. 2003). In this staging system, Lewy pathology initiates in the lower brain stem and olfactory bulb, specifically in the dorsal motor neurons of the vagus nerve in the medulla oblongata (stage 1) and extends upwards in the brain stem through the locus ceruleus in the pontine tegmentum (stage 2). With stage 3, the midbrain and specifically the substantia nigra become affected. Severe dopaminergic cell destruction in the pars compacta, pathology progression in the amygdala and thalamus together with mesocortex and allocortex involvement is observed from stage 4 onwards. Thereupon the disease is spreading into the neocortex, thus temporal, parietal and frontal lobes, which is observed along with cell death in early affected brain regions including substantia nigra, vagus nerve nuclei and locus ceruleus (stage 5). The Lewy pathology further progresses to the cerebral cortex in stage 6, where it furthermore affects motor and sensory areas (Braak & Braak 1995; Braak et al. 2003). Yet, detailed progression patterns described by the Braak staging are currently under debate, since independent post-mortem cohorts suggest refinement of the pathology progression based on different spatio-temporal disease progression observations and affected brain regions (Jellinger 2019). Moreover, only an imperfect correlation between Lewy body load and severity of cognitive impairment has been reported (Hughes et al. 1992; Parkkinen et al. 2005).

The majority of reported PD cases are idiopathic or sporadic, with unknown cause or mechanisms for disease initiation, whereas only 10 % of cases are linked to genetic mutations or gene copy number variations (compare with Figure 2). The most common genes affected by mutations are α-synuclein (*SNCA*), leucine-rich repeat kinase 2 (*LRRK2*), Parkin (*PARK2*), PTEN-induced putative kinase (*PINK1*), vacuolar protein sorting 35 complex (*VPS35*), Parkinson protein 7 (*PARK7*) and glucocerebrosidase (*GBA*). Genome-wide association studies (GWAS) further support the association between genetic variants with increased risk to develop PD (Bekris et al. 2010; Lill 2016; Chang et al. 2017).

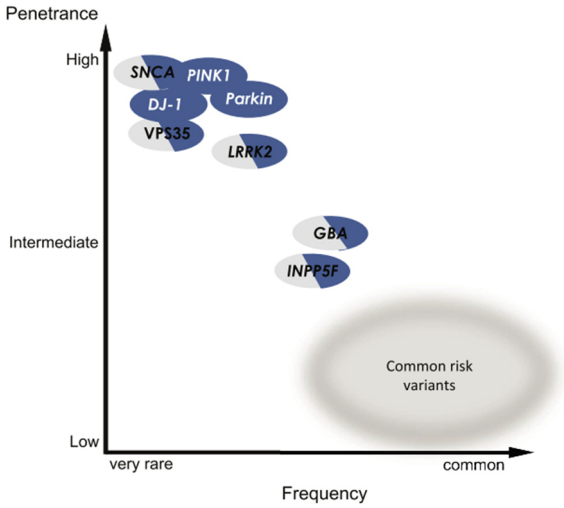

Figure 2: Schematic overview of frequency of genetic variants and respective effect size in PD-associated genes. Homozygosity is depicted as filled oval, heterozygosity is depicted as half-filled oval. (Reprinted with permission from Lill 2016).

SNCA GENE AND ALPHA-SYNUCLEIN PROTEIN

Shared neuropathological hallmarks, especially prominent in PD and DLB, are the appearance of protein inclusions in the cytoplasma and dystrophic processes of neurons as well as in glial cells. These Lewy neurites, Lewy bodies and GCIs are formed of insoluble protein aggregates of the α-synuclein protein. Although a variety of publications is available, little is known about the detailed physiological as well as disease causing mechanisms of α-synuclein (Spillantini et al. 1997; McCann et al. 2013; Koga et al. 2021; Cabrero & Morrison 2022).

Discovered for the first time in the electric organ of the pacific electric ray *Torpedo californica* (Maroteaux et al. 1988), α-synuclein is part of the synuclein protein family. These soluble proteins α-, ß-, and y-synuclein are small proteins binding to the phospholipid membrane (Clayton & George 1998), where only α-synuclein is under intensive research for its critical role in neurodegeneration and has first been mentioned in 1997 in this context (Polymeropoulos et al. 1997).

Encoded by the *SNCA* gene, alpha-synuclein (α-synuclein, 14kD, 140 amino acids) is a soluble protein. It is a neuronal, pre-synaptic nerve terminal protein that is highly conserved in vertebrates and plays

distinct roles in synaptic vesicle transport and microtubule dynamics (Spillantini et al. 1997; Moore et al. 2005; Dikiy & Eliezer 2012; Luk & Lee 2014; Snead & Eliezer 2014).

Unfortunately, the precise physiological role of α-synuclein remains elusive. However, it has been shown to be implicated in synaptic plasticity (Watson et al. 2009), neurotransmitter release (Chandra et al. 2005; Burré et al. 2010) and maintenance of the synaptic vesicle pool (Murphy et al. 2000; Dikiy & Eliezer 2012; Snead & Eliezer 2014).

The gene encoding α-synuclein, *SNCA,* is encoded on the human chromosome 4 (GRCh38 assembly), on the reverse strand with six exons (RefSeq Match NM_000345.4) and has at least 17 transcript splice variants (Ensemble.org 2021). It was the first gene identified to be causatively associated with PD (Polymeropoulos et al. 1997). By now, five missense mutations within the *SNCA* gene (A53T, A30P, E46K, H50Q, G51D) have been identified and are linked to autosomal dominant inheritance of rare familial cases of PD (Polymeropoulos et al. 1997; Singleton et al. 2003; Chartier-Harlin et al. 2004; Snead & Eliezer 2014). Less common, but also causing rare familial PD, are copy number variations (CNV) of the *SNCA* gene (Singleton et al. 2003; Chartier-Harlin et al. 2004; Ibáñez, Lohmann, et al. 2004; Bobela et al. 2014). Specifically, *SNCA* duplications clinically display typical late-onset PD, while triplications of *SNCA* lead to early-onset parkinsonism together with dementia (Chartier-Harlin et al. 2004; Farrer et al. 2004; Ibáñez, Bonnet, et al. 2004; Muenter et al. 1998).

Transcriptional regulation of *SNCA* gene expression is mediated via different ways: transcription has been shown to be activated by transcriptional activator PARP-1 (Chiba-Falek et al. 2005). Transcription factors of the GATA family and ZSCAN1 bind to elements within the promoter and the first intron to induce transcription (Scherzer et al. 2008; Clough et al. 2009; Brenner et al. 2015). This induction has also been shown to be regulated indirectly via the extracellular signal-regulated kinase/ phosphatidylinositol 3 kinase (ERK/PI3) signalling pathway (Clough & Stefanis 2007; Clough et al. 2009). Furthermore, five evolutionary conserved *cis*-regulating factors (PITX3, OCTX2, NR3C1, AR, TBP) have been identified to interact with the promoter of *SNCA* (Schüle et al. 2014). In addition, alternative splicing via posttranslational mechanisms regulates *SNCA* variant expression. Although different *SNCA* isoforms were found differently expressed in synucleinopathy subtypes, no isoform specific biological or pathological mechanism is known so far (Beyer et al. 2004; Beyer et al. 2008; Tagliafierro & Chiba-Falek 2016).

The protein α-synuclein is built of three distinct domains: The N-terminal sequence comprising of amino acid residues 1-60 folds into an α-helix structure, which allows binding to apolipoproteins thus allowing interaction with lipid membranes (Clayton & George 1998). Disease-related missense mutations in the *SNCA* gene were found predominantly located within this membrane-binding domain

(Bussell & Eliezer 2003b; Fares et al. 2014). The central domain of amino acid residues 61-95 includes the non-amyloid-ß component (NAC) region, which is unique among the synuclein family (Ueda et al. 1993; Uchihara & Giasson 2016). This hydrophobic region is prone to and critically contributing to synuclein oligomerization and protein aggregation (Ueda et al. 1993). Lastly, the proline-rich C-terminal region of residues 96-140 resolves functions in interaction with other proteins (Giasson et al. 2003; Burré et al. 2018).

Under physiological conditions, the secondary structure state of α-synuclein folds in two distinct conformational structures (compare with Figure 3): Firstly, soluble, cytosolic α-synuclein is found as a natively unfolded monomer (Weinreb et al. 1996; Kim 1997). Its second conformation is a multimeric form while binding to lipid membranes, where it forms an α-helical structure (Davidson et al. 1998; Perrin et al. 2000; Eliezer et al. 2001; Burré et al. 2018). Thereby, membrane curvature influences the final either elongated or truncated α-helix conformation of the protein, whereby vesicles of smaller diameters are preferentially bound (Davidson et al. 1998; Bussell & Eliezer 2003a; Chandra et al. 2003; Bussell et al. 2005; Burré et al. 2018).

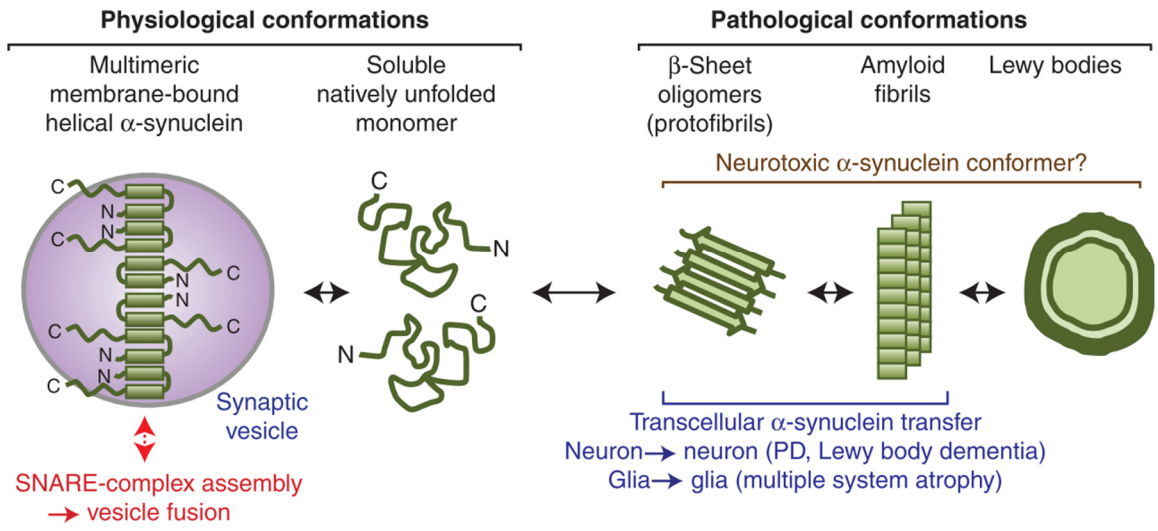

Figure 3: Illustration of α-synuclein conformations under physiological and pathological conditions. Under physiological conditions, α-synuclein appears as α-helix monomer or unfolded, while α-synuclein appears as neurotoxic oligomer under pathological conditions. (Reprinted with permission from Burré et al. 2015)

Under pathological conditions however, native α-synuclein is undergoing conformational changes and appears misfolded in a ß-sheet amyloid conformation. Further, higher-order structures being protofibrils and amyloid fibrils are subsequently formed of these multimers, which become ultimately deposited and form Lewy bodies leading to neurotoxicity including synaptic dysfunction and neuronal death (Conway et al. 1998; Narhi et al. 1999; Conway et al. 2000; Rochet et al. 2000; Ding et al. 2002; Parnetti et al. 2019).

Posttranslational modifications of α-synuclein protein further influence its binding affinities with other proteins, oligomerization and fibril formation capability and thus neurotoxicity (Burré et al. 2018): Phosphorylation of α-synuclein seems to influence the protein's structure and thus membrane binding and fibril formation capacity, with mainly serine, threonine or tyrosine residues being phosphorylated. Major de- and rephosphorylation *in vitro* occurs at the major phosphorylation sites serine 87 and serine 129 (Okochi et al. 2000; Fujiwara et al. 2002; Anderson et al. 2006), influencing aggregation patterns of α-synuclein (Waxman & Giasson 2008; Paleologou et al. 2010). In contrast, the dominant pathological modification in DLB was found to be a single phosphorylation of Serine S-129 only (Anderson et al. 2006). Tyrosine phosphorylation instead is associated with suppression of α-synuclein aggregation and toxicity at its sites Y125, Y133, Y135 (Ellis et al. 2001; Nakamura et al. 2001; Negro et al. 2001; Ahn et al. 2002). Acetylation influences its membrane affinity and aggregation resistance (Kang et al. 2012; Maltsev et al. 2012; Bartels et al. 2014; Dikiy & Eliezer 2014), while ubiquitination modifications on α-synuclein remain under investigation (Mezey et al. 1998; Gómez-Tortosa et al. 2000; Nonaka et al. 2005).

α-synuclein protein expression is enriched in different brain regions including the neocortex, hippocampus, striatum, thalamus and cerebellum (Jakes et al. 1994; Nakajo et al. 1994; Iwai et al. 1995). However, physiological expression has also been detected in other tissue, amongst others in muscle cells, CSF (cerebrospinal fluid) and blood cells (Borghi et al. 2000; El-Agnaf et al. 2003) as well as, in a pathological setting, in skin and enteric nerves and enteroendocrine cells (Donadio et al. 2017; Liddle 2018). Thereby, protein expression levels were shown to be correlated with its messenger RNA (mRNA) expression levels with overall increasing expression levels during development (Petersen et al. 1999), however detailed knowledge about molecular mechanisms underlying *SNCA* and α-synuclein expression pattern remain elusive (Burré et al. 2018).

α-synuclein first localizes to the soma of immature neurons in developing cultured neurons, and accumulates at presynaptic terminals once synapses are formed (murine (Withers et al. 1997; Hsu et al. 1998) and human (Bayer et al. 1999; Galvin, Schuck, et al. 2001)), and has been shown to be the last protein enriched within the terminals (Withers et al. 1997).

Being a neuronal, pre-synaptic terminal protein, α-synuclein is involved in synaptic plasticity through modifying vesicle trafficking at the synapse. This regulation is assumed to be indirect by altering neurotransmitter release through regulating the vesicle pools at the presynaptic termini (Burre et al. 2014; Burré et al. 2018). Being organized as multimer at the synapse, α-synuclein mediates soluble SNARE-(N-ethylmaleimide-sensitive-factor attachment receptor)-complex chaperone activity (Burre et al. 2014), regulates interaction of GTP (Guanosintriphosphat)-binding protein rab3 (RAB3GAP2) with membranes of synaptic vesicles (Chen et al. 2013) and modulates synaptic vesicle motility. It thereby

influences exo-/endocytosis by maintaining the overall size of recycling pools at individual synapses (Scott & Roy 2012; Wang et al. 2014; Burré et al. 2018). *In vitro* experiments showed α-synuclein mediated vesicle-docking inhibition without interference of the fusion process (Lai et al. 2014; Burré et al. 2018).

Furthermore, dopamine synthesis and transport are negatively influenced by α-synuclein: By keeping the enzyme tyrosine hydroxylase (TH) of the catecholamine biosynthesis pathway dephosphorylated and thus inactive, α-synuclein prevents synthesis of dopamine (Kirik et al. 2002; Perez et al. 2002; Peng et al. 2005; Wu et al. 2011). Knockout and overexpression experiments of α-synuclein to further narrow down its function on neurotransmitter release revealed controversial results from different model systems. In the context of synaptic plasticity transmission, no effect on neurotransmitter release (Chandra 2004, Watson 2009), enhanced neurotransmitter release (Steidl et al. 2003; Gureviciene et al. 2007; Gureviciene et al. 2009; Greten-Harrison et al. 2010) as well as decreased neurotransmitter release has been attributed to α-synuclein (Abeliovich et al. 2000; Cabin et al. 2002; Yavich et al. 2004; Yavich et al. 2006).

The protein's exact biological function to date remains largely elusive, as controversial reports state α-synuclein association with different compartments of the cell, suggesting additional yet different functions: Besides the location at the synapse (Withers et al. 1997; Maroteaux et al. 1988), other scientists suggest its localization with mitochondria thereby influencing mitochondrial functionality (Ellis et al. 2005; Smith et al. 2005) or leading to modifications of the ERK1/2 signalling pathway, which in turn regulates dopamine and glutamatergic signalling in neurons (Bohush et al. 2018). Nuclear localization (Schell et al. 2009) negatively influencing histone acetylation (Kontopoulos et al. 2005) or association with the endoplasmic reticulum (ER) in α-synuclein toxicity studies (Smith et al. 2005) has been proposed as well. Interactions of α-synuclein with cytoskeletal components in regard to the effect on tubulin polymerization remain controversial, because polymerization enhancement (Alim et al. 2002) as well as polymerization inhibition (Lee, Khoshaghideh, et al. 2006; Zhou et al. 2010) have been reported. Nevertheless, α-synuclein enhances phosphorylation of microtubule-associated protein tau (Jensen et al. 1999; Haggerty et al. 2011; Qureshi & Oaudel 2011), while tau and α-synuclein are presumed to seed aggregation of each other thereby possibly accelerating neuropathological cascades (Giasson et al. 2003; Burré et al. 2018).

A highly debated model is the propagation of α-synuclein throughout the brain: A prion-like spreading mechanism has been proposed after grafted neurons from fetal brain tissue were transplanted in PD-patient. Years after transplantation, they showed post-mortem Lewy bodies identical to PD-affected brain regions (Lindvall et al. 1994; Olanow et al. 2003; Kordower et al. 2008; Kurowska et al. 2011). Further *in vivo* experiments support this hypothesis: Both mutant and wild type α-synuclein injected

into murine brains resulted in propagation and aggregation of α-synuclein along synaptically connected neurons to other brain regions, including the conversion of endogenous α-synuclein into its pathologic form (Desplats et al. 2009; Luk et al. 2012). Lately, even a propagation of α-synuclein from the gut via the vagus nerve has been discussed intensively (Liddle 2018).

Two main protein degradation mechanisms are involved in α-synuclein degradation: Degradation via ubiquitin proteasome pathway (Bennett et al. 1999; McLean et al. 2001) and subsequent autophagy-lysosome system (Webb et al. 2003; Lee et al. 2003; Cuervo et al. 2004) or via chaperone-mediated autophagy (CMA) (Cuervo et al. 2004; Bandyopadhyay & Cuervo 2007). However, especially as aggregated protein, α-synuclein escapes degradation mechanisms through inhibition of proteasome activity (Lindersson et al. 2004; Emmanouilidou et al. 2010) leading to further accumulation of oligomeric proteins. Reduced levels of CMA proteins observed in PD brains (Alvarez-Erviti et al. 2010) and inhibited uptake of mutant α-synuclein to lysosomes have been reported (Cuervo & Macian 2014), suggesting impaired degradation mechanisms of α-synuclein in diseased brains.

SYNAPTIC PLASTICITY

Synaptic plasticity is describing the neurochemical activities underlying learning and memory formation and is defined as the process of synapse strengthening and weakening over time in correlation to activity (Hughes 1958). Changes in the quantity of neurotransmitters located at the synaptic membrane and differences in neurotransmitter release into the synaptic cleft are thought to modify these plastic changes (Lees & Smith 1983; Metzler-Baddeley 2007; Ferrer et al. 2007; Ferrer 2009). Coincident with the loss of neurons in PD patient brains, synaptic failure and synaptic loss are debated as synucleinopathies' underlying pathological mechanism, as cognitive impairment and dementia have been repeatedly correlated to synaptic failure (Terry et al. 1991; Villalba & Smith 2010; Picconi et al. 2012; Bellucci et al. 2016). Since the cortex is thought to be the main brain region for complex cognitive processes including thinking, learning and memory (Christoff & Gabrieli 2000), alterations in synaptic plasticity in the cortex are of special interest.

On top of that, altered regulation of dendritic spines in neurodegenerative diseases (Fiala et al. 2002; Day et al. 2006; Penzes et al. 2011; Murmu et al. 2013) is observed, together with loss of excitatory post-synapses observed in post-mortem DLB brains (Kramer & Schulz-Schaeffer 2007) and unbalanced presynaptic neurotransmitter release is reported from PD patients (Nikolaus et al. 2009). Along with the observed enrichment of α-synuclein oligomers and aggregates at the presynaptic termini (Kramer & Schulz-Schaeffer 2007), the relevance of synaptic failure as important pathophysiological mechanism is of further interest.

Synapses are essential to mediate connection and communication among neural cells. While electrical synapses propagate signals consisting of ions or small molecules via gap junctions, chemical synapses instead convert the input action potential into chemical signals. Thereby, the received electrical input leads to influx of calcium ions (Ca^{2+}) through voltage-gated channels. This influx subsequently leads to exocytosis of neurotransmitters incorporated in synaptic vesicles by fusion with the presynaptic membrane. Secreted neurotransmitters into the synaptic cleft bind to receptor molecules on the postsynaptic spines. There, ligand-gated ion channels either relay the electrical signal or respond via a second messenger, which subsequently either inhibits or excites the postsynaptic neuron (Bear & Connors 2015a) (Figure 4). Based on the variety and complexity of neurotransmitters and corresponding receptors, chemical synapses are further subdivided according to the released neurotransmitter: amino acids, amines and peptides. Furthermore, specific molecules trigger specific responses at the postsynaptic side, where for example glutamatergic synaptic transmissions are excitatory signals, while GABAergic synaptic transmissions result in inhibitory signals (Bear & Connors 2015b).

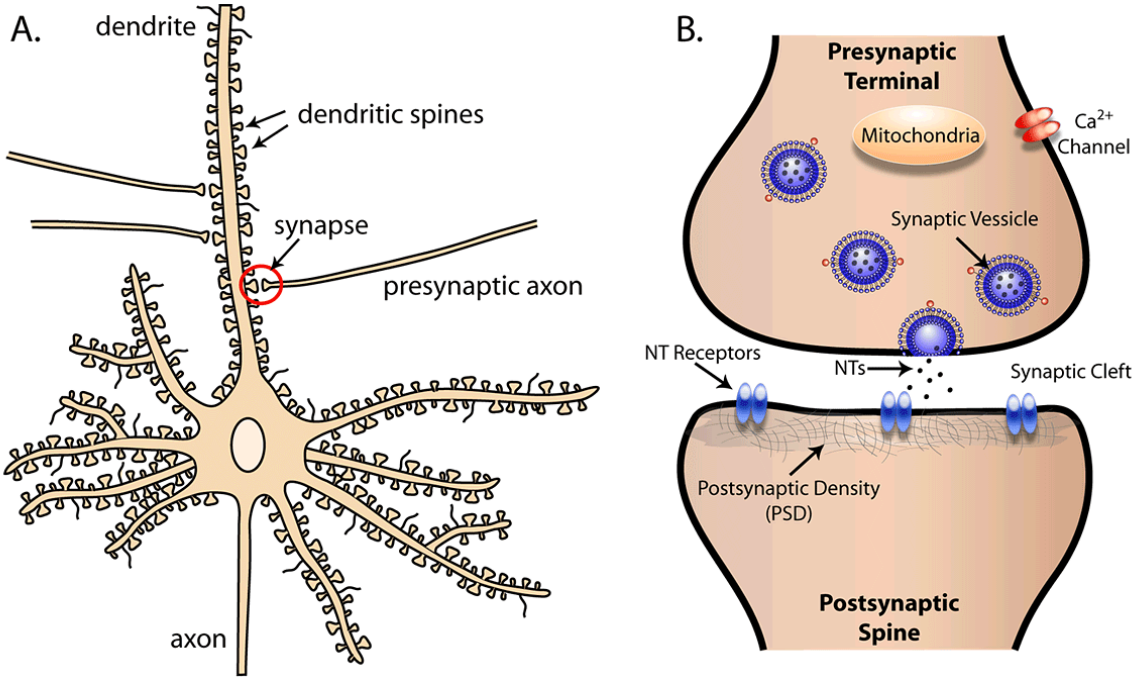

Figure 4: Dendritic spines are found along the dendrites of neuronal cells. Connection of a presynaptic axon with a spine forms a synapse (A). Synaptic vesicle within presynaptic termini can fuse with the presynaptic membrane and release neurotransmitter (NT) into the synaptic cleft. Signals are transduced upon binding of NTs to neurotransmitter receptors of the postsynaptic membrane located within the postsynaptic density (B). Abbreviations: Ca^{2+} - calcium, NT - Neurotransmitter. (Reprinted with permission from Smrt and Zhao, 2010)

Interconnectivity between neurons through small protrusions called dendritic spines have firstly been described in 1888 by Ramón y Cajal (Cajal 1888). Spines occur at different densities depending on the neuronal cell type, are highly variable and show highly dynamic changes in their morphology

dependent and independent of neuronal activity (Harris & Stevens 1988; Harris & Stevens 1989; Schikorski & Stevens 1999; Kasai et al. 2010; Rochefort & Konnerth 2012). Filopodia spines are predominantly found in developing neurons and appear as thin, hair-like protrusions lacking a defined head and are considered as transient structures with rapid turnover and with the potential to develop into dendritic spines upon synaptic input (Miller & Peters 1981; Fiala et al. 1998; Rochefort & Konnerth 2012). Thin spines have a long, thin neck and small round heads, while mushroom spines have a thin, long neck with a large head. Lastly, stubby spines have a round head and lack a neck (Jones & Powell 1969; Peters & Kaiserman-Abramof 1970; Rochefort & Konnerth 2012). Morphological changes of the spine are linked to the local biochemical signalling within the spine, whereby biochemical reactions can take place independently from the dendrite (Tashiro & Yuste 2003).

One important protein involved in the synaptic gene expression regulation machinery is the RNA binding protein FMRP (Fragile X mental retardation protein) (Van De Bor & Davis 2004), since its encoding gene *FMR1* is found mutated in neurological disease of mental retardation (Bagni & Greenough 2005; Bassell & Warren 2008). Regulated by neuronal activity, it bidirectionally shuttles as FMRP-mRNA complex between soma and dendritic spines (Antar et al. 2004; Ling et al. 2004; Antar et al. 2005; Smrt & Zhao 2010). Locally in the spine, FMRP controls activity-dependent protein synthesis: phosphorylated FMRP binds more proteins and sequesters local mRNA, including *Fmr1*, itself, thus preventing local protein translation (Ceman et al. 2003; Plante et al. 2006; Darnell & Klann 2013). Upon glutamatergic signalling activity (mGluR), FMRP becomes dephosphorylated (Narayanan et al. 2007), ubiquitinated and subsequently degraded (Hou et al. 2006; Nalavadi et al. 2012; Lannom & Ceman 2021), while the release of previously bound mRNA leads to enhanced local protein synthesis. FMRP is regulated by a physiological feedback-loop: former bound *Fmr1* mRNA becomes translated and phosphorylated, restoring the baseline levels preventing excess protein synthesis (Prieto et al. 2020). Collectively, the mGluR theory summarizes these opposing roles of mGluR signalling and FMRP protein. Accordingly, mGluR5 activation seemed to initiate protein synthesis, while FMRP suppresses it. Consequently, loss of FMRP in mental retardation disease leads to uncontrolled and excessive protein translation resulting in the observed clinical features of the disease (Bear et al. 2004).

MODEL SYSTEMS FOR SYNUCLEINOPATHIES

Within the last decades, assessment of human post-mortem tissue in combination with different model systems has helped to further shed light on synucleinopathies including PD and deepen the knowledge about its progression and underlying mechanisms.

Description and analysis of pre-mortem human pathology is limited to CSF and blood analysis for molecular markers (El-Agnaf et al. 2003), including analysis of genomic alterations (Parnetti et al. 2019), as well as different imaging techniques e.g. PET-MRI (Shang et al. 2021). Yet, these approaches only describe and accompany the progression of the disease. Ultimately, detailed analysis in human-relevant context is carried out on human post-mortem tissue. Since progression of synuclein pathology spreading is classified based on the Braak staging system, insights into early time points of disease development allow to better understand the disease. Besides post-mortem tissue analysis, several animal and cell culture system models are currently available to further investigate the onset of synucleinopathies in more depth.

IN VIVO MOUSE MODELS

Commonly, rodents are the most frequently used *in vivo* model system used for addressing research questions and genetic manipulation. Rodent animal models are further divided in toxin-based and transgenic model systems:

Pharmacological approaches aim to induce dysfunction of the motor system. The first toxin-based animal model of PD was the application of 6-hydroxydopamine (6-OHDA) constitutes (Ungerstedt 1968), leading to lesions of the nigrostriatal dopaminergic pathway accompanied by a drop in striatal dopaminergic neurons (DA) content (Jeon et al. 1995). Application of 1-methyl-4-phenyl-1,2,3,6-tetrahydropyridine (MPTP) leads to degeneration of nigral DA neurons providing the potential to mimic PD in animals (Heikkila et al. 1984), although different mice strains showed varying susceptibility to the drug (Schwarting et al. 1999). Furthermore, drugs inducing specific aspects of PD pathology in mice are in use: For example, chemical inhibition of the ubiquitin-proteasome system (UPS) leads to impaired protein degradation (McNaught et al. 2004) and inflammation in PD is recapitulated by injection of endotoxin lipopolysaccharide (LPS) inducing the innate immune response thus activating microglial cells (Bobela et al. 2014). Nevertheless, these approaches are limited to transient biochemical modifications, and mice show limited and spatially restricted α-synuclein pathology also upon repetitive application (Bobela et al. 2014).

A second approach to investigate synucleinopathies in rodent model systems is the transgenic expression of risk genes linked to PD. With α-synuclein being the first PD gene linked to autosomal dominant inheritance of rare familial forms of PD, Masliah and colleagues in 2000 generated the first α-synuclein transgenic mouse line (Masliah et al. 2000). These mice overexpress the human α-synuclein open reading frame (ORF) under the constitutively active platelet-derived growth factor (PDGF) promoter predominantly expressed in neurons. These mice are hereafter referred to as PDGF mice. They exhibit intraneuronal α-synuclein inclusions, however do not fully recapitulate human Lewy bodies across different brain regions (Masliah et al. 2000). Nevertheless, murine α-synuclein inclusions are found in comparable regions to PD patients: in the deep layers of the neocortex and in the dopaminergic neurons of the SNpc. Although these mice lack obvious neuron loss, they show motor abnormalities and loss of dopaminergic terminals, especially strong under high α-synuclein transgene expression. Accumulation of filamentous α-synuclein cytoplasmic inclusions eventually leads to complex motor deficiencies and impairments resulting in paralysis and ultimately premature death of these mice (Masliah et al. 2000). Following this approach, transgenic overexpression mouse model under different neuron-specific promoters as for example Thy-1 or tyrosine hydroxylase (TH), as well as α-synuclein mutant or truncated α-synuclein mouse lines were developed afterwards (van der Putten et al. 2000; Matsuoka et al. 2001; Tofaris et al. 2006; Garcia-Reitböck et al. 2010). The use of differently mutated α-synuclein genes under different promoters reflect and recapitulate the accumulation of filamentous, cytoplasmic α-synuclein inclusions and complex motor impairments to different extents, thus recapitulate the development of pathology with different severity, while all models show highest prevalence in aged individuals (Chesselet et al. 2012; Bobela et al. 2014).

Besides overexpression approaches, transgene injection strategies with different forms of α-synuclein to spatially restricted brain areas prevents development of physiological compensatory mechanisms during early disease development (Bobela et al. 2014). For example, stereotactic injection of recombinant adeno-associated viral (rAAV) vectors in mice delivering human α-synuclein results in loss of dopaminergic neurons (St Martin et al. 2007), while lentiviral introduction of wild type or A30P human α-synuclein leads to development of Lewy body-like pathology and neurodegeneration not only restricted to dopaminergic neurons (Lauwers et al. 2003). Nevertheless, transgene expression is restricted to its site of delivery thus resembling locally restricted pathology only. Luk et al. developed a mouse model by intracerebral injection of preformed fibrils derived from recombinant α-synuclein, where pathogenic α-synuclein was transmitted to interconnected brain regions resembling Lewy body pathology, nigral dopaminergic neuron degeneration together with motor defects (Luk et al. 2012).

Besides investigating effects of α-synuclein pathology, mouse models overexpressing other PD-linked genes were generated: Modelling idiopathic and autosomal dominant familial forms of PD is

accomplished by using *LRRK2* transgenic mice (Andres-Mateos et al. 2009; Tong et al. 2010; Li et al. 2010). Further insights in autosomal recessive forms of familial Parkinsonism are investigated using transgenic mice with alterations in expression of Parkin (Goldberg et al. 2003), *PINK1* (Kitada et al. 2007) or even knockouts of multiple genes (Kitada et al. 2009).

In summary, a variety of transgenic mice were generated, that successfully recapitulate different hallmarks of synucleinopathies by overexpression of wild type or mutant risk factors. Nevertheless, most murine model systems are comprised of transgenes derived from a different species, and resemble overexpression rather than endogenous mutations or copy number variations, thereby limiting the potential to translate findings to human context. Together with observed variances in the developed pathology, a truthful and complete recapitulation of synucleinopathies in murine models is not established yet.

IN VITRO CELL CULTURE SYSTEMS

2D CELL CULTURE

Two-dimensional cell culture *in vitro* systems allow further insights into disease onset and progression. This approach includes the cultivation of individual cell types in culture to investigate their properties combined with the ease of use for genetic manipulation. One potential origin of cells is the isolation of cells from brain tissue and subsequent cultivation in *in vitro*, so-called primary cultures (Brand & Syverton 1962). However, the potential to cultivate e.g. human dopaminergic neurons is limited due to accessibility, ethical concerns and are challenging in cultivation. Murine primary cells are easier to obtain and maintain, yet their use is limited to short culture times, missing self-renewal capacity, lack of interaction with other cell types, and the genetic background is not directly comparable to human genotypes (Falkenburger et al. 2016).

Overcoming the limitations of primary cells, one commonly used cell line is the neuroblastoma cell line SH-SY5Y, which is derived from a bone marrow biopsy of a metastatic neuroblastoma of a 4-year-old female (Biedler et al. 1978). Although not being strictly dopaminergic, its human origin, catecholaminergic neuronal properties and ease of handling makes it a widely used cell line for PD research (Xicoy et al. 2017). Another frequently used cell line is the Lund human mesencephalic (LUHMES) cell line. These neuronal cells were genetically modified for tetracycline-controlled v-*myc*-overexpression derived from female 8-week old human ventral mesencephalic tissue. Induction with tetracycline (*tet*-off) to prevent v-*myc* expression allows the neuronal differentiation into dopaminergic neurons (Lotharius & Brundin 2002; Lotharius et al. 2005).

Although there are cell lines available mimicking certain specific cell types prone to be affected by disease, different brain regions and several cell types of the human brain are susceptible to disease progression and are therefore of interest to investigate. Moreover, cell lines derived from blastomas show high genetic instability including genetic aberrations and genetic drift (Alston-Roberts et al. 2010; Gillet et al. 2013), therefore limiting in-depth and comparable transcriptional analysis.

INDUCED PLURIPOTENT STEM CELLS (IPSCS)

In 2006, the research group around Yamanaka revolutionized the toolbox of scientists: The introduction of the transcription factors OCT4, SOX2, KLF4 and c-MYC, also known as the Yamanaka-factors, into human somatic cells allowed reprogramming into induced pluripotent stem cells (iPSCs) (Takahashi & Yamanaka 2006). Besides their capacity to self-renew and thereby replenishing the stem cell pool, pluripotent cells have the potential to differentiate into any kind of germ layer tissue, i.e. ectoderm, mesoderm and endoderm, which give rise to the different cell types of the body. The fate of each cell type is determined during embryonic development, when the blastocyst forms the three different germ layers, out of which cells follow the different trajectories to form the complex cellular compositions of individual body regions (Thomson 1998). Being able to use reprogrammed cells, this discovery accelerated the possibilities to study development and disease. This powerful tool opened up a variety of applications from addressing research questions to patient-specific therapeutic approaches (Medvedev et al. 2010).

Based on cell type differentiation along clearly defined trajectories, a variety of protocols have been developed and are commonly used to guide cells to differentiate into distinct central nervous system cell types. These approaches are easy to implement, scalable and have the potential to compare different genotypes amongst each other. However, most protocols reduce the complexity and generate individual cell types rather than a complex network, e.g. specifically midbrain dopaminergic neurons or excitatory neurons only (Quadrato et al. 2017; Bianchi et al. 2018; de Rus Jacquet 2019; Rus 2019). With these differentiation protocols in hand, human derived iPSCs could be generated and differentiated into desired cell types while maintaining the genetic background and disease-associated modifications.

Conversely, for neurodegenerative research, the fetal nature of human iPSC-derived neuronal cells is contradicting the aspect to investigate degeneration-associated functions, especially since senescent cells exhibit shortened telomeres, dysfunctional mitochondria, protein aggregates, increased levels of DNA damage and altered epigenomic states. However, during reprogramming, many features seem to reverse and the cells seem to remain in a rejuvenated state upon re-differentiation. While genetic

mutations remain persistent, telomere length, mitochondria and transcriptome profiles were found to be “rested” (Lapasset et al. 2011; Ohmine et al. 2012; Mahmoudi & Brunet 2012).

To overcome reprogramming-induced rejuvenation, Miller and colleagues developed an approach to induce premature aging in iPSC-derived neurons leading to multiple age-related characteristics (Miller et al. 2013). The group used a mutated version of the nuclear envelop protein lamin A (progerin), where a mutation in the *LMNA* gene leads to aberrant accumulation of progerin protein in the nuclear membrane. This weakened its normal scaffolding function, and showed phenotypic changes including DNA damage, chromatin organization and increased mitochondrial reactive oxygen species (ROS) levels. Progerin-overexpression in iPSC-derived mature dopaminergic neurons (mDA) could also induce disease-specific phenotypes as neuromelanin accumulation and loss of tyrosine-hydroxylase expression levels and was observed in both, young donor and old donor iPSCS-derived mDA neurons (Miller et al. 2013). Somewhat surprisingly, the progerin-associated approach has not been further pursued.

Although iPSCs enable research of cell-type specific consequences based on disease-relevant genetic background, these *in vitro* approaches are highly artificial and limited by complexity, cellular diversity, cell-cell interaction and lack of tissue architecture. The most complex neuronal 2D structures achieved with differentiation protocols were the formation of neural rosettes, which are producing self-organized neuronal progenitors around ventricle-like cavities or aggregates formed by neurospheres (Reynolds et al. 1992; Zhang et al. 2001; Chambers et al. 2009; Quadrato et al. 2017). Nevertheless, complex cellular *in vitro* systems comprised of mature and differentiated cell types in a defined spatial organization were missing until recently.

3D-CELL CULTURE SYSTEMS - ORGANOIDS

With the potential of iPSCs to develop into any cell or tissue type of the body, research in the recent years generated organoids – three dimensional (3D) organ-like tissue cultures resembling multiple cell types depending on media formulation (Qian et al. 2019). Thereby, two different generation pathways have emerged: On the one hand, unguided methods which are based on the intrinsic capacity of iPSCs to form aggregates and spontaneously differentiate into complex, higher-order structures. On the other hand, differentiation can be induced by targeted supplementation of external molecules leading to lineage-specific patterning and region-specific differentiation (Qian et al. 2019).

The cultivation of cells in 3D requires an artificial extracellular matrix-like environment. These hydrogels of matrices are gelatinous protein mixtures resembling the extracellular matrix (ECM), supporting maintenance and growth of cells and play important roles in behaviour and cell fate

decision (Hughes et al. 2010; Benton et al. 2011). Commonly, these matrices contain ECM-like proteins including laminin, collagen, glycoproteins and proteoglycans, but also resemble different growth factors, e.g. bFGF, IGF-1, TGF-ß (Hughes et al. 2010). The most widely used cell culture matrix commercialized as *Matrigel* is obtained from mouse tumor cells, and therefore can be variable in composition and quality (Kozlowski et al. 2021).

The most freedom for self-organization during development is achieved following the approach published by Lancaster et al in 2013: Inducing hiPSC cells to aggregate and form ~300 µm sized embryoid bodies (EBs) with subsequent embedding in matrigel and cultivation in spinning well plates allows tissue expansion and neuronal differentiation (Lancaster et al. 2013; Lancaster & Knoblich 2014). This approach leads to the generation of cortical-like structures, including the development of a variety of cell types ranging from neural progenitors, excitatory and inhibitory neurons as well as astrocytes and oligodendrocyte cell types upon prolonged cultivation (Quadrato et al. 2017). However, major drawbacks of this approach include the heterogeneous and unpredictable cellular arrangement among different organoids, and more reproducible generation pathways are currently under investigation (Yoon et al. 2019).

External guidance of cell differentiation and temporal administration of specific molecules allows for a more accurate and precise tissue differentiation, e.g. the development of cellular structures resembling distinct brain regions such as cerebral cortex, hippocampus, cerebellum, forebrain and midbrain (Lancaster & Knoblich 2014; Muguruma et al. 2015; Pasca et al. 2015; Jo et al. 2016; Yoon et al. 2019). Although these guided approaches are less variable (Sloan et al. 2017), possible interference with iPSC self-organization and cell-cell communication cannot be excluded (Qian et al. 2019).

To investigate cell-cell interactions across different regions of the brain, separate region-specific organoid development followed by controlled fusion of multiple distinct organoids allows modelling of interacting regions and are collectively called assembloids (Birey et al. 2017; Bagley et al. 2017).

ORGANOIDS TO SOME EXTENT RECAPITULATE THE ORGANISATION OF THE HUMAN CORTEX

Being frequently affected by neurological disease and being unique compared to other animals due to its size expansion during evolution, the cortex is a brain region of great interest (Bystron et al. 2008; Rakic 2009). Therefore, cortical organoids have become the most widely used and thus best characterized model system, and studies have found similarities between the development of cortical organoids and the development of the human embryonic cortex (Camp et al. 2015; Arlotta & Pasca 2019; Qian et al. 2019; Qian et al. 2020). Although being limited by size expansion and therefore growing only to less than one tenth of the size of human embryonic cortex, cellular composition and

organization of progenitor cells of the human embryonic cortex is fairly well recapitulated in cortical organoids: SOX2 positive ventricular radial glial cells (vRG) organized in polarized structures were observed forming ventricular structure (VZ)-like structures. These are flanked by TBR2 positive intermediate progenitor cells (IPCs) forming the inner subventricular zone (iSVZ), and outer radial glia-specific marker are expressed forming an outer subventricular zone (oSVZ) within the cortical organoid (Lui et al. 2011; Kadoshima et al. 2013; Qian et al. 2016; Bershteyn et al. 2017; Li et al. 2017; Watanabe et al. 2017; Qian et al. 2019). Nevertheless, incomplete specification of cortical lamination indicated by a mix of upper and deeper layer neurons is observed (Lancaster et al. 2017; Qian et al. 2016).

Supporting the structural similarities observed with marker expression, transcriptomic profiling comparing gene expression levels showed similarities between human fetal brain tissue and cortical organoids (Camp et al. 2015; Quadrato et al. 2017; Fan et al. 2018). Although gene expression patterns and epigenetic dynamics were found to follow parallel and comparable trajectories compared to the human embryos (Luo et al. 2017; Velasco et al. 2019), comparability is limited to profiles before the third trimester due to depletion of proliferative NPCs and absent interregional cell-cell communication in organoids (Qian et al. 2019). This could also explain the lack of gyrification in developing organoids, since cortical folding is observed in late third trimester of embryonic development (Lewitus et al. 2013).

Nevertheless, emerging excitatory and inhibitory neurons within the cortical organoids have proven functionality in different electrophysiological recordings (Lancaster et al. 2013; Pasca et al. 2015). Nevertheless, less mature signals, high variability among functionality and maturation parameters and spontaneous activity have been reported. Yet, spontaneous burst-firing activities as well as robust spontaneous excitatory and inhibitory postsynaptic currents upon current injections have been shown in more mature organoids concluding neuronal function and activity (Pasca et al. 2015; Quadrato et al. 2017; Lancaster et al. 2017; Qian et al. 2019). Basic electrophysiological parameters as e.g resting membrane potential or amplitude and frequency of post-synaptic currents were detected and showed statistically significance across maturation (Pasca et al. 2015; Birey et al. 2017; Sloan et al. 2017). However, neuron-specific firing patterns were not observed (Qian et al. 2016; Qian et al. 2019). Nevertheless, synaptogenesis seemed to be abundant, and development and maturation of functional neurons during embryogenesis could be reflected within these observations (Pasca et al. 2015; Birey et al. 2017; Lancaster et al. 2017; Qian et al. 2019).

LIMITATIONS OF ORGANOIDS

Despite the great advantages and possibilities coming along with organoid model systems, 3D cell culture shows limitations. The following aspects focus on the drawbacks of using cerebral organoids

differentiated with the protocol published by Lancaster and colleagues, where iPSCs follow the intrinsic differentiation pattern along the neuroectodermal trajectory pathway (Lancaster et al. 2013; Lancaster & Knoblich 2014).

Firstly, growth of organoids is limited by size. The developing organoid lacks a vasculature system, limiting the access of nutrients and oxygen throughout the organoid, resulting in a necrotic core (Lancaster et al. 2013). This limitation is partly overcome by cultivating organoids on a shaker, which increases tissue diffusion. Yet, organoids are still limited to a size of roughly 4 mm in diameter (Lancaster et al. 2017). Continuous improvements of the protocol such as air-liquid interface culture methods (Giandomenico et al. 2019) or co-culture with endothelial-derived cells are currently under development (Shi et al. 2019).

Secondly, the neuroectodermal development trajectory allows growth of different neuronal cell types of the cerebral cortex, yet it does not give rise to immune cells in organoids, especially not to microglia, since these arise from yolk-sac derived macrophages of mesoderm-derived tissue (Alliot et al. 1999). Attempts to change media formulation or matrigel embedding time points suggested intrinsic development of microglia in cortical organoids, however with limited success (Ormel et al. 2018). Separate differentiation of cells into mature microglia followed by incorporation in a three-dimensional structure overcomes this limitation (Park et al. 2018). However, it becomes an artificial system without the intrinsic self-organization capacity.

Thirdly, high variability even among organoids of one batch challenges the reproducibility of experiments. Since unguided protocols are based on intrinsic self-regulation, it is an aspect that cannot be controlled for and can lead to natural differences upon having reached certain complexity. Embedding of EBs in artificial extracellular matrix for expansion also is a critical point in terms of variability and reproducibility (Lancaster et al. 2017; Ormel et al. 2018). Furthermore, the use of fibre microelements as floating scaffolds helped to more reproducibly shape the EBs, thereby leading to increased surface area and volume ratio with the potential for enhanced neuroectoderm development. Note that this approach is relying on extrinsic modulation and guidance as well (Lancaster et al. 2017).

Overall, organoids recapitulating distinct brain regions have been generated and allow for more extensive research to broaden knowledge about the developmental regulatory mechanisms. In summary, the lack of complex intercellular circuitries, predominantly immature cell types and incomplete tissue structure together with heterogeneous morphologies, reproducibility variance and batch differences limit the use of organoids. Nevertheless, these models provide the potential for a

deeper understanding of human genetic context aspects together with the potential for genetic manipulation.

ORGANOIDS IN NEURODEGENERATIVE RESEARCH

Collectively, organoids recapitulate the development of early brain structures (Camp et al. 2015; Fan et al. 2018; Arlotta & Pasca 2019). Still, epigenetic profiles and age of individual cells cannot be compared with an aged human being. Nonetheless, different groups currently demonstrate the usefulness of organoids in neurodegenerative research:

Human fibroblasts of patients diagnosed with a neurodegenerative disease have been cultured in the laboratory and reprogrammed into iPSCs. These iPSCs carrying mutations causing the disease have been used to cultivate organoids and were found to recapitulate certain neurodegenerative disease characteristics. Early on, organoids obtained with guided and unguided approaches demonstrated accumulation of Amyloid beta (Aß) and phosphorylated tau, hallmarks of patient with Alzheimer's disease (Raja et al. 2016; Park et al. 2018; Gonzalez et al. 2018).

In 2016, a guided protocol for hMLO (human midbrain-like organoid) generation was published by Jo and colleagues. These hMLOs recapitulate complex structural organization with characteristic cellular markers and functional dopamine-producing neurons (Jo et al. 2016). Subsequently, one of the first organoid models of PD was published in 2019, which was genetically modified to carry a mutation in *LRRK2*. The authors generated midbrain organoids with neuromelanin-expressing cells resembling dopaminergic neurons, and pathological phosphorylated α-synuclein deposits were observed. Moreover, they found enhanced dopaminergic cell death indicated by diminished dopamine transporter and TH marker expression accompanied by increased activated caspase-3 levels in LRRK2 G2019S mutant organoids (Kim et al. 2019). At the same time, organoids derived from a patient iPSC cell line carrying a mutation in the *LRRK2* gene were generated reproducing midbrain characteristics and differences in TH expression of dopaminergic cells (Smits et al. 2019). Another approach showed impaired dopaminergic neurogenesis of human midbrain organoids derived from progenitor cells lacking *PINK1* (Brown et al. 2021). A recent paper from 2021 generated midbrain organoids from an iPSCs cell line harbouring an *SNCA* triplication and compared these to an isogenic, copy number-corrected *SNCA* cell line. Elevated levels of α-synuclein expression, phosphorylated α-synuclein and aggregation along with reduction of dopaminergic neurons were observed in this study (Mohamed et al. 2021).

NON-CODING ELEMENTS OF THE GENOME

CENTRAL DOGMA OF MOLECULAR BIOLOGY

The central dogma of biology describes the flow of genetic information comprising the self-replicating capacity of the DNA (Crick 1958): information encoded on the DNA is transcribed into messenger RNA (mRNA) and subsequently translated into proteins (Figure 5).

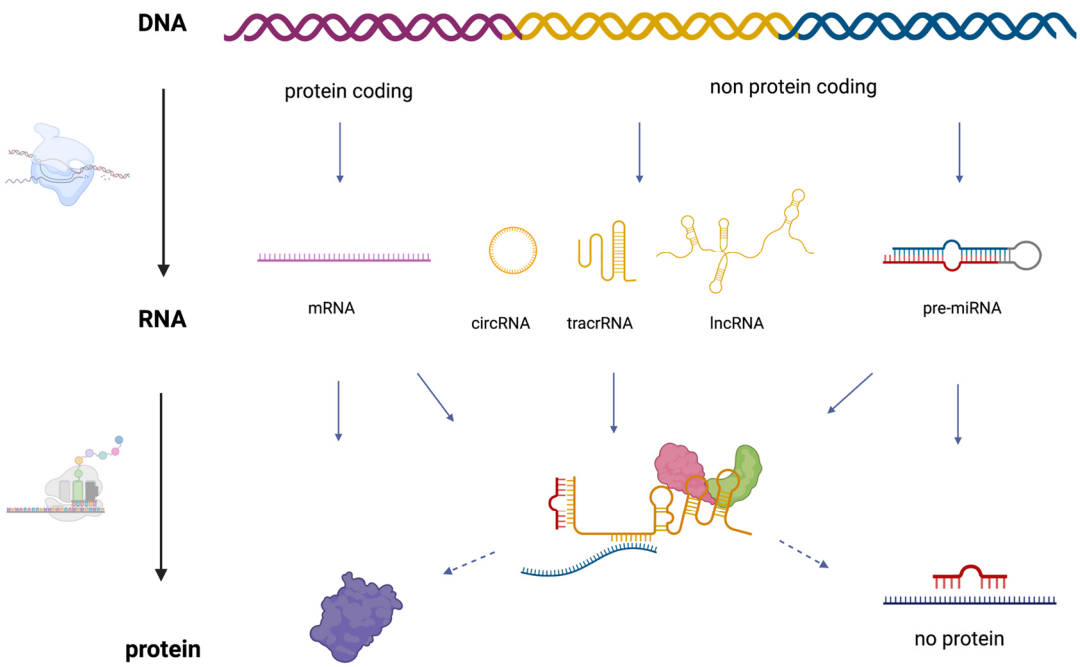

Figure 5: Central dogma of molecular biology - schematic overview of current knowledge about genetically encoded molecular regulatory mechanisms. (The figure was created with BioRender.com and adapted from Ramón y Cajal et al. 2019)

With the discovery and application of the human genome sequencing project (Lander et al. 2001; Gregory et al. 2006), it turned out that only a small percentage of DNA actually encoded for genes, while the majority of the genetic code seemed to be non-coding and was therefore considered as 'junk'. However, this view changed, as the non-coding elements were investigated in more depth. It was discovered that non-coding elements are actually not non-coding, as their name would suggest. Rather, upon transcription, non-coding elements seem to have essential roles in regulatory processes throughout the cell. Mostly, the non-coding elements show high tissue specificity, suggesting a distinct role of a specific non-coding element in a highly relevant manner (Ratti et al. 2020).

Furthermore, emerging data from NGS (next generation sequencing) and GWAS suggest that the majority of genetic elements associated with neurodegenerative diseases is actually located within the non-coding part of the genome (Figure 6), highlighting the need to investigate risk-causing variants in synucleinopathies (unpublished data).

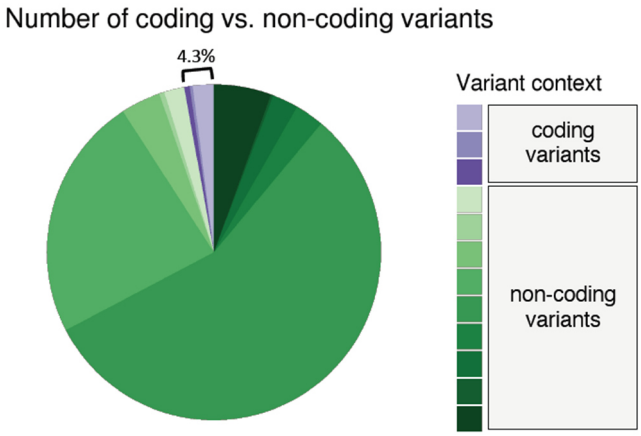

Figure 6: Number of coding vs. non-coding variants from the EMBL-EBI GWAS catalogue (04/2018). A total of 3,887 associated variants were listed when searching for keywords related to neurodegenerative diseases (including Alzheimer's disease (AD), PD, amyotrophic lateral sclerosis (ALS), dementia, amyloid and tau) with only 4.3% of elements representing coding variants. Colour shading represents different types of variant classes defined in the EMBL-EBI-GWAS catalogue (downloaded in April 2018). (Figure reprinted with permission from Dr. Felix L. Strübing).

Currently, non-coding elements are classified into two distinct categories (Figure 7): On the one hand, there are structural non-coding RNAs comprised of ribosomal RNAs (rRNA) and transfer RNAs (tRNAs) that are essential during protein biosynthesis. And on the other hand, there is the broad category of regulatory non-coding RNAs. Within the latter category, sub-classes can be divided by size into small non-coding RNAs and long non-coding RNAs. Each class has unique features, and classification and nomenclature of small and long non-coding RNAs are constantly evolving (Dahariya et al. 2019).

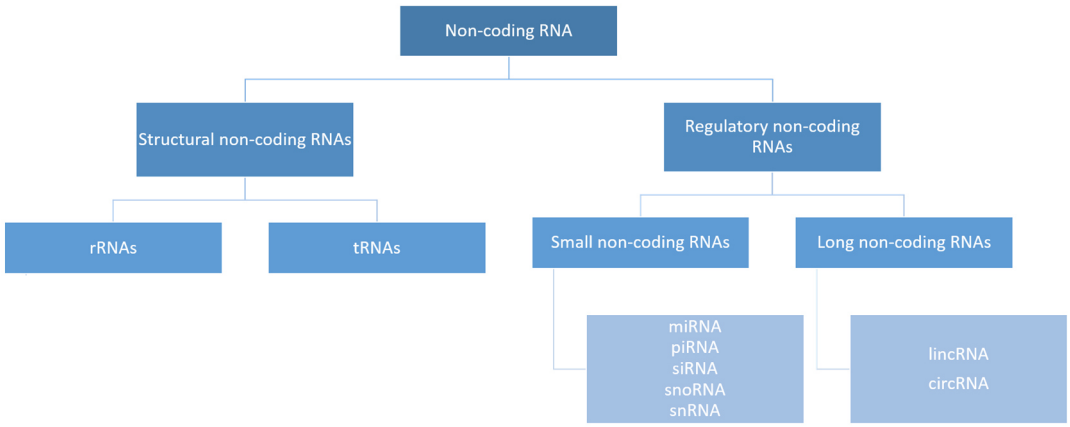

Figure 7: Schematic overview of the classification of non-coding RNAs. Abbreviations: circRNA - circular RNA, lincRNA - long intergenic non-coding RNA, piRNA - piwi RNA, rRNA - ribosomal RNA, siRNA - small interfering RNA, snoRNA - small nucleolar RNA, snRNA - small nuclear RNA, tRNA - transferRNA. (Figure adapted from Dahariya et al. 2019).

SMALL NON-CODING RNAS

A variety of small RNAs fall within the class of small non-coding elements: micro RNAs (miRNAs), PIWI-interacting RNAs (piRNAs), small interfering RNAs (siRNAs), small nuclear RNAs (snRNAs) and small nucleolar RNAs (snoRNAs) (Catalanotto et al. 2016; Dahariya et al. 2019).

MIRNAS

One of the largest classes of non-coding RNAs that has emerged as an important cell-type specific regulator within the past decades is the micro RNAs class (miRNAs). miRNAs were initially discovered in 1993 and were linked to temporal patterning processes of the model organism *Caenorhabditis elegans* (Lee et al. 1993). The first human disease associated with dysregulated miRNAs was chronic lymphocytic leukemia (Santulli et al. 2015). Now, three decades after their initial discovery, several thousand miRNAs are known and partially characterized, while tens of thousands of putative miRNAs are predicted across species (Fromm et al. 2020). Given their abundance, modulation of approx. 60 % of protein-coding genes in the human genome is contributed to by miRNAs (Friedman et al. 2009). miRNAs have emerged as fine tuners of gene expression, with their capability to influence developmental, differentiation, physiological and apoptotic processes in a spatiotemporal manner (Mukherjee et al. 2019).

MIRNA BIOGENESIS

The biogenesis of miRNAs is divided into several steps involving distinct enzymes for miRNA processing and is implemented in both the nuclear and cytoplasmic cell compartment (Figure 8) (Winter et al. 2009).

Typically, RNA polymerase II or III transcribes a long primary miRNA (pri-miRNA) transcript, which consists of a double-stranded stem of 30 base pairs, a terminal loop and two flanking unstructured single-stranded tails. Pri-miRNAs are capped and have a poly-(A) tail (Lee et al. 2003; Cai et al. 2004; Borchert et al. 2006). They are further processed into a short 65 nt stem-loop structure, termed precursor miRNAs (pre-miRNAs) (Cai et al. 2004). This is done by the microprocessor complex consisting of RNAse III enzyme Drosha and the double stranded RNA binding protein Di George critical region 8 gene (DGCR8) (Lee et al. 2003; Han et al. 2004; Han et al. 2006; Han et al. 2009). Subsequently, pre-miRNAs are translocated into the cytoplasm via Exportin5 (XOP5), which acts in complex with Ran-GTPase (Han et al. 2009). In the next step, RNAse II enzyme Dicer further shortens the immature miRNA generating a miRNA duplex (ds-miRNAs) characterized by a phosphate at the 5’ end, hydroxyl group at the 3’ end and a 2-nt overhang (Knight & Bass 2001; Bernstein et al. 2003). Subsequently, the RNA inducing silencing complex (RISC), Dicer, trans-activation response RNA binding protein (TRBP) and Argonate (AGO2) successively load the miRNA duplex onto AGO (Gregory et al. 2005; Haase et al. 2005; Lee, Hur, et al. 2006; MacRae et al. 2008). Loading the duplex in the correct orientation onto AGO2 is assured by TRBP due to its biochemical properties (Haase et al. 2005; Chendrimada et al. 2005; Lee, Hur, et al. 2006). Based on the thermodynamic properties of the ds-miRNA, the strand with the less

stable 5' end is defined as the guide strand and loaded onto AGO proteins. AGO unwinds the ds-miRNA duplex, releasing the 17-22bp long single-stranded mature miRNA and degrading the passenger strand (Gregory et al. 2005; Maniataki & Mourelatos 2005; Winter et al. 2009)

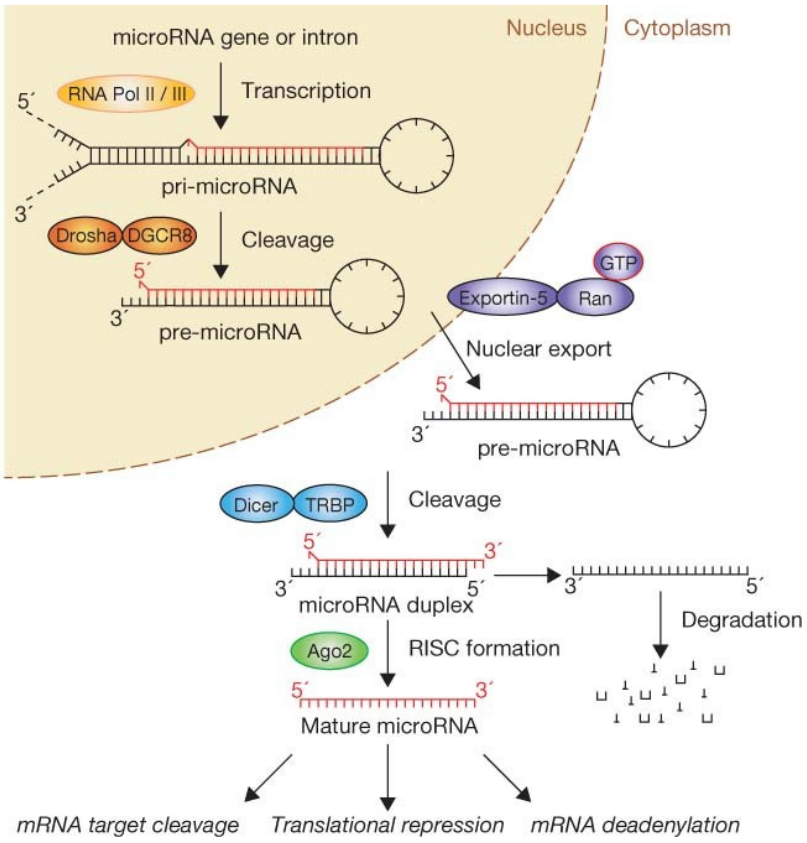

Figure 8: Linear canonical pathway of miRNA processing. miRNAs become transcribed from the DNA by RNA Pol II/III as pri-miRNA. Upon cleavage with Drosha and DGCR8, the pre-miRNA is exported from the nucleus into the cytoplasma via exportin-5. Dicer and TRBP cleavage generates the miRNA duplex, where the less thermostable strand is degraded, while the mature miRNA-strand is loaded onto AGO. Mature miRNA activity can subsequently lead to target mRNA cleavage, translational repression or mRNA deadenylation for post-transcriptional gene-regulation (Reprinted with permission from Winter et al. 2009).

Besides the described "linear" pathway of miRNA biogenesis, recent studies indicate miRNA-species with individual and distinct biogenesis pathways. For example, minor modifications of the cytoplasmic cleavage processes bypassing Drosha cleavage and alternative splicing events influence miRNA biogenesis (Okamura et al. 2007; Berezikov et al. 2007). miRNA originating from short introns rather than a miRNA gene (Hansen et al. 2016), and functional performance of even both miRNA strands (Okamura et al. 2008) have been reported as well, stressing the complexity of miRNA biogenesis.

MODE OF ACTION OF MIRNAS

Mature, single-stranded miRNAs have three main proposed mechanisms of action (Figure 8). Firstly, translational repression is achieved by miRNAs binding to their target gene of interest leading to blocking of the ribosomal translation machinery. Secondly, miRNA binding can lead to mRNA target degradation through decapping or deadenlyation and thus exposure to the mRNA degradation machineries. Thirdly, miRNA binding that generates a double-stranded RNA complex can initiate target mRNA cleavage (Winter et al. 2009).

All three modes of action are achieved through miRNA binding to its target sequence due to complementary base pairing, predominantly targeting the 3'UTR of mRNAs (Grimson et al. 2007; Didiano & Hobert 2008). While the mature miRNA has a length of up to 22bp, only the short seed sequence of miRNAs is responsible for the binding specificity and regulatory mechanisms (Chendrimada et al. 2005). Plant miRNAs require almost perfect base pairing for gene repression through cleavage (Jones-Rhoades et al. 2006), but animal miRNAs require the 6-8 nucleotide long seed sequence located at the 5' end of the miRNA for common regulation (Ellwanger et al. 2011).

On the other hand, miRNAs can also regulate the RNA transcriptome via miRNA induced post-transcriptional degradation of RNA molecules spatially restricted to distinct cell compartments. Nuclear shuttling has been proposed as a mechanism for explaining the dynamic movement of miRNAs from and to the nucleus as part of mRNA regulation, binding to pre-miRNAs prior to nuclear export or redistribution for sub-cellular storage and activity upon cellular stress (Catalanotto et al. 2016). Essential roles in regulation of alternative splicing have also been proposed, as AGO proteins have been found to interact with several splicing factors and miRNA binding sites were identified in intronic sequences (Boudreau et al. 2014).

The role of miRNA regulation is a highly complex and dynamic research field: While some experiments show that miRNAs can have multiple unique targets, meaning that one specific miRNA could potentially regulate hundreds of mRNAs, other experiments indicate target-specificity of one specific miRNA only (compare with Catalanotto et al. 2016 for more details). Thus, regulation of target transcripts by several miRNAs as combinational regulation is a key feature of mammalian miRNA's mode of action (Catalanotto et al. 2016).

ROLE OF MIRNAS AT THE SYNAPSE

Local, activity dependent regulation of gene expression at the synapse is also involving miRNA activity at different steps during dendrite development and synaptic plasticity (Figure 9) (Smrt & Zhao 2010).

For example, miR-137 expression is critical during dendritic morphogenesis and maturation (Smrt & Zhao 2010), miR-132 expression regulates dendritic development through regulation of a Rho family GTPase-activating protein (Wayman et al. 2008; Imprey et al. 2010), and miR-134 regulates dendritic spine maturation via governing protein translation of APT1 (Siegel et al. 2009). miRNAs are also active locally at the pre-synapse, as e.g. miR-124 regulates synaptic plasticity in presynaptic terminals via transcription factor CREB targeting (Rajasethupathy et al. 2009; Smrt & Zhao 2010).

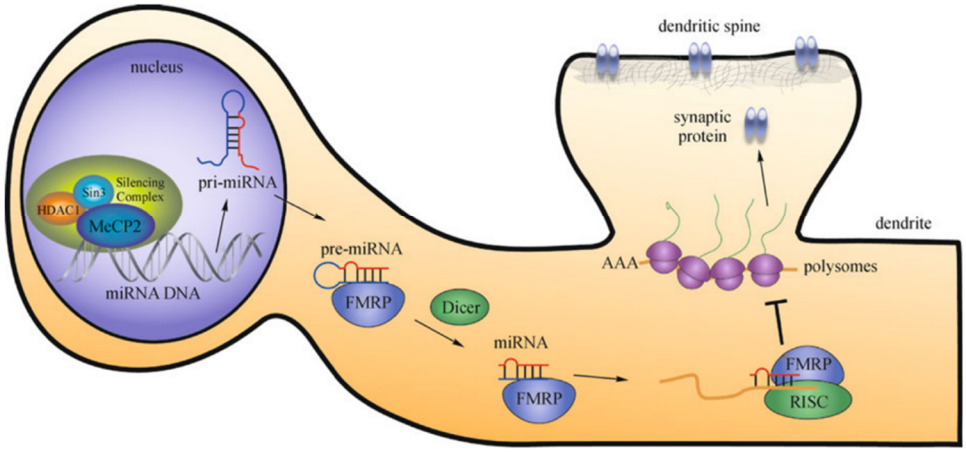

Figure 9: Overview of biogenesis of miRNAs at the synapse. miRNAs become transcribed in the nucleus from the DNA. Exported as pri-miRNA and subsequently processed as pre-miRNA, FMRP binds immature miRNA and shuttles it to distant dendrites. Locally, mature miRNA can interact with its target mRNA to negatively regulate gene expression. (Reprinted with permission from Smrt and Zhao 2010).

Furthermore, different miRNAs regulated by neuronal activity at multiple levels have been identified (Schratt 2009b). Firstly, miRNA transcription can be regulated by activity (Figure 10 a and Figure 10 d). Thereby, high signalling activity leads to activation of transcription factors, which in turn activate transcription of miRNA genes. Along the same line, signalling activity can lead to miRISC complex remodelling thus enabling target mRNA transcription. Secondly, activity can lead to miRNA shuttling along the dendrite, where miRNAs find their target genes for binding (Figure 10 b). Under basal conditions, miRNAs can be "stored" in association with an RNA binding protein as immature, double-stranded pre-miRNAs. Subsequently, signalling activity leads to dissociation of RBP allowing miRNA processing into mature miRNA (Figure 10 c) (Schratt 2009b; Smrt & Zhao 2010).

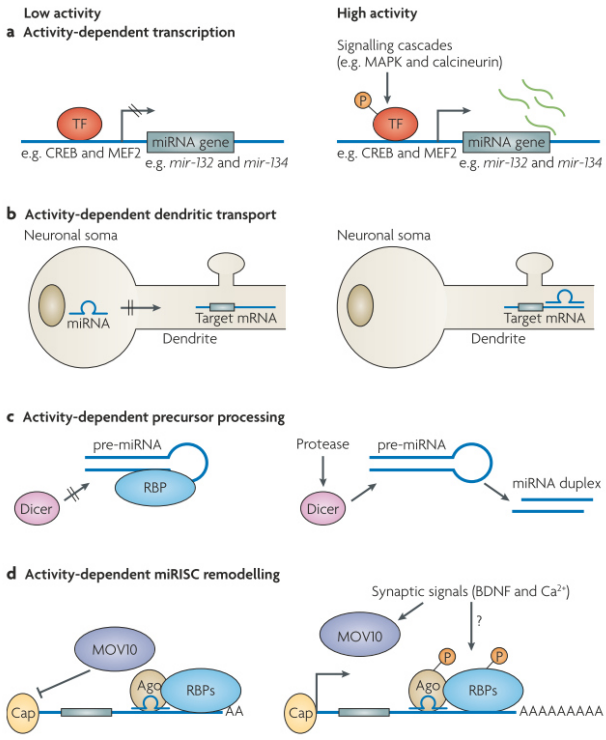

Figure 10: Schematic mode of action of miRNAs regulated by neuronal activity. Activity-dependent mechanisms include transcription of miRNA gene (a), shuttling of mature miRNA from the soma to the dendrite (b), processing of pre-mature miRNA to mature miRNA (c) and miRISC remodelling (d). Abbreviations: BNDF - growth factor brain-derived neurotrophic factor, Ca^{2+} - Calcium, CREB - transcription factor cAMP response element-binding protein, MEF2 - transcription factor myocyte enhancer factor 2, miRISC - miRNA-induced silencing complex, MOV10 - Armitage in Drosophila melanogaster, RBP - RNA binding protein, TF - transcription factor. (Reprinted with permission from Schratt 2009).

ROLE OF MIRNAS IN THE CONTEXT OF A-SYNUCLEIN EXPRESSION AND SYNUCLEINOPATHIES

In 2016, Recasens et al. summarized the role of miRNAs on targeting α-synuclein expression (compare with Figure 11 and Recasens et al. 2016). Two miRNAs that were recognized early on in regulating α-synuclein expression are miR-7 and miR-153 (Doxakis 2010). Both miRNAs appear to have a synergistic effect on *SNCA* mRNA, where their direct binding to the 3'-UTR leads to repression of α-synuclein (Doxakis 2010). The 3'UTR of *SNCA* contains binding sites for miR-34b and miR-34c, and miRNA activity has been shown to repress the expression of α-synuclein *in vitro,* while repression of both miRNAs resulted in increased α-synuclein expression (Kabaria et al. 2015). miR-214 and miR-1643 also have confirmed binding sites in the 3'UTR of *SNCA* (Lim & Song 2014; Wang et al. 2015).

Furthermore, indirect miRNA regulation of α-synuclein has been identified on different levels (Figure 11): Firstly, miRNAs have been identified in influencing signalling pathways regulating α-synuclein expression. Cellular RhoA expression leads to the activation of a transcription factor cascade, eventually influencing α-synuclein expression, where miR-133 regulates initial RhoA expression (Niu et al. 2016; Recasens et al. 2016). Binding of miR-433 to the PD-associated gene *FGF20* regulates expression of α-synuclein through its main target FGF-receptor 1 (Van Der Walt et al. 2004; Haghnejad

et al. 2015; Recasens et al. 2016). Proteolytic pathways leading to α-synuclein degradation are also modulated by miRNAs: miR-128 indirectly initiates α-synuclein degradation via the autophagy-lysosomal pathway (ALP) through activation of transcription factor *EB* promoting transcription of ALP-related genes (Decressac et al. 2013; Recasens et al. 2016). The chaperone-mediated autophagy (CMA) pathway leading to lysosomal degradation was shown to be modulated by nine different miRNAs targeting different proteins of the pathway (Recasens et al. 2016).

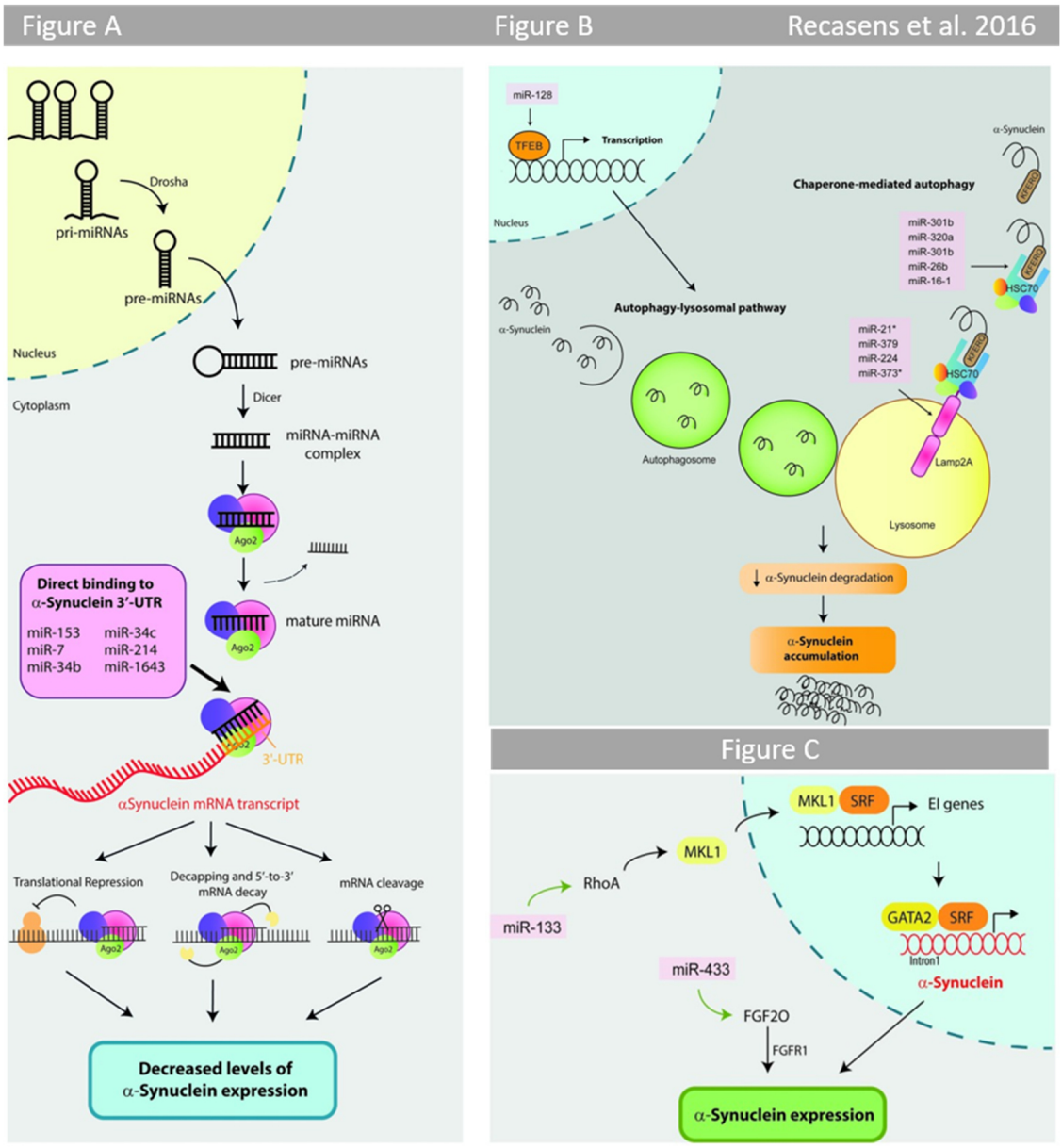

Figure 11: Role of microRNAs in the regulation of α-synuclein expression. miRNA can directly bind and thereby regulate α-synuclein expression (A), or modulate α-synuclein expression by alternating the proteolytic degradation pathway (B). miR-133 and miR-433 directly regulate α-synuclein expression via RhoA and FGF20. Abbreviations: 3'UTR - three-prime untranslated region; FGF20 – fibroblast growth factor 20, HSC70 - heat shock protein 70, Lamp2A - lysosome-associated membrane protein 2, RhoA - Ras homolog gene family member A, GATA2, MKL1, SRF and TFEB are transcription factors. (Reprinted with permission from Recasens et al. 2016).

The aggregation capacity of α-synuclein protein is also modulated by miRNAs: miR-16-1 reduces expression of chaperone HSP70 via binding of its 3'UTR sequence, which results in reduced levels of HSP70 thus increasing aggregation of α-synuclein protein (Zhang & Cheng 2014). Along the same lines, miR-494 has been associated with regulation of the chaperone DJ-1 protein levels, which are generally lower in PD patients compared to control, thus assumed to contribute to increased α-synuclein aggregation (Xionga et al. 2014).

Further key-players in synucleinopathies and specifically PD appear to be prone to miRNA regulation: miR-132 directly alters expression of transcription factor *Nurr1* (Yang et al. 2012), and reduced levels of miR-205 in PD patients are associated with increased levels of the miRNA target *LRRK2* (Xie & Chen 2016). Interestingly, *LRRK2* itself has been found to negatively control levels of let-7 and miR-184, which in turn have inhibitory effects on transcription factor *E2F1*. Increased levels of those transcription factors, however, are associated with increased neurodegeneration of specifically dopaminergic neurons (Gehrke et al. 2010). Changes in miRNA expression have also been recapitulated in overexpression model systems including mouse models (Recasens et al. 2016).

Taken together, so far, numerous miRNAs have been discovered targeting important genes involved in synucleinopathies, thus providing potential biomarkers as well as novel treatment opportunities, and clearly help to further elucidate the underlying biological regulatory network of synucleinopathies.

BACKGROUND OF THIS THESIS - CORTICAL SYNAPTIC LOSS IN PRE-SYMPTOMATIC PDGF MICE MODELLING SYNUCLEINOPATHIES

Ultimately, α-synuclein accumulation is accompanied by a loss of neurons in synucleinopathies (Spillantini et al. 1997; McCann et al. 2013; Koga et al. 2021). Thus, synapses being essential cellular structures involved in cell signalling and communication during neuronal network activity are of special interest in understanding early physiological changes in the context of α-synuclein expression. α-synuclein related dendritic spine impairments in murine mouse models have been assessed in different brain regions so far: The striatum receiving input from dopaminergic neurons (McNeill et al. 1988; Zaja-Milatovic et al. 2005; Day et al. 2006; Finkelstein et al. 2016), the *substantia nigra,* where dopaminergic loss occurs (Patt et al. 1991), the hippocampus (Winner et al. 2012) or the olfactory bulb being a suggested starting point of Lewy pathology (Neuner et al. 2014).

Recent studies provide evidence for cortical impairments including abnormally phosphorylated α-synuclein accumulation at cortical synapses observed especially in synucleinopathy-subtypes PD and DLB (Ferrer 2009). Thus, Blumenstock et al. 2016 aimed to understand the structural alterations of dendritic spines in the cortex of α-synuclein overexpression in differently aged transgenic mice. Spine dynamics across time were monitored in the PDGF mouse model overexpressing human wild type α-synuclein (PDGF-h-α-syn). Three age groups of PDGF mice were chosen for spine dynamic analysis, where 3-month-old mice were considered as “pre-symptomatic” and 6 to 12 month old mice were considered as “diseased”, having developed a PD-like phenotype (Masliah et al. 2000; Blumenstock et al. 2017). Interestingly, a progressive decrease in spine density could be observed in young adult mice between 3 and 4.5 months of age, while no difference in spine density was observed in 2-month-old mice (Blumenstock et al. 2017). Thus, this study provides *in vivo* evidence for cortical spine loss in pre-symptomatic 3-month-old animals overexpressing α-synuclein before the onset of any behavioural symptoms (Figure 12).

Since cortical neurons are comprised of glutamatergic synapses, a follow-up study has sought to understand the proteomic changes underlying glutamatergic synapses in 3-months-old PDGF mice at the presumed onset of cortical synaptic loss in this model system (Blumenstock et al. 2019). Synaptosomes of 3-month-old PDGF and wild type mice have been purified using fluorescent-activated synaptosome sorting (FASS) for vesicular glutamate transporter 1 (VGLUT1) positive excitatory glutamatergic pre-synaptic termini. Subsequently, quantification of differentially expressed proteins has been performed using nanoliquid chromatography tandem mass spectrometry (LC-MS/MS) (Blumenstock et al. 2019). Interestingly, 42 proteins were found to be significantly differentially regulated with the majority of proteins being upregulated in PDGF mice overexpressing α-synuclein (Figure 13). Overexpressed proteins were found to be involved in synaptic vesicle cycle, cytoskeleton,

ER-Golgi trafficking and metabolism (Blumenstock et al. 2019). While overall protein synthesis seemed to be increased in PDGF mice, only two proteins were found to be significantly downregulated and the steepest reduction was found for the elongation factor alpha (eEF1A1). eEF1A is one of the most abundant protein synthesis factors required for amino acid chain elongation during translation of proteins (Mateyak & Kinzy 2010). Interestingly, reduction of eEF1A1 protein immunoreactivity along with reduced PSD95 levels representing reduced synaptic density could be recapitulated in the *cingulate gyrus* of patients with DLB (Blumenstock et al. 2019).

Figure 1A – Blumenstock et al. 2017

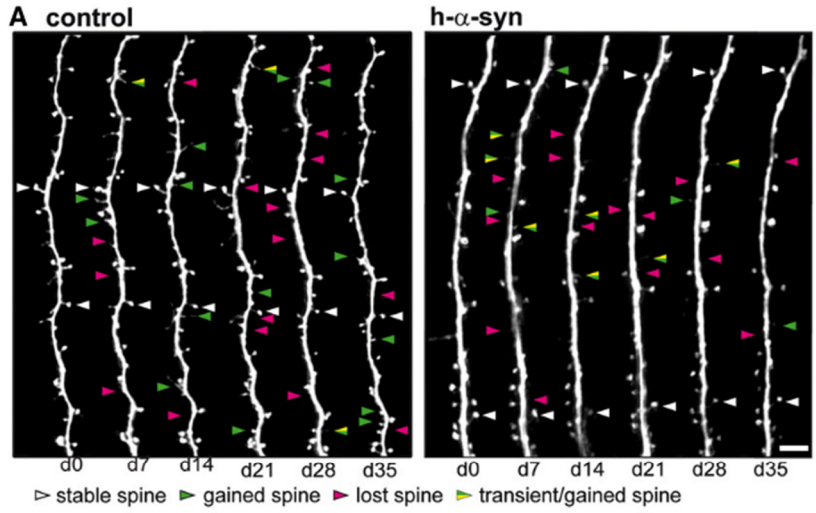

Figure 2D and 2E – Blumenstock et al. 2017

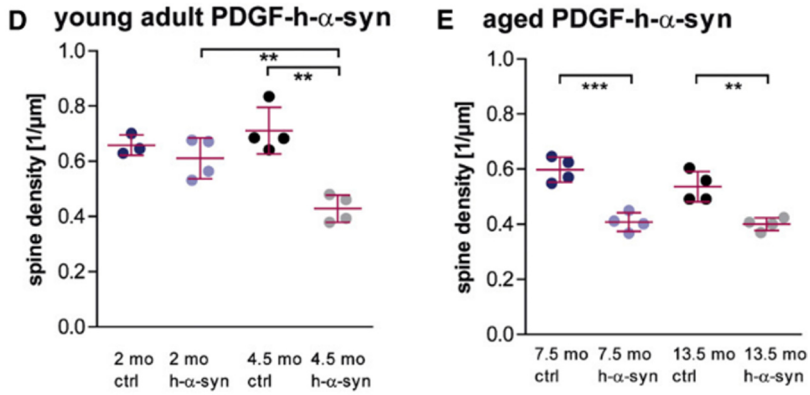

Figure 12: Excerpt from figure 1 and figure 2 from Blumenstock et al. 2017 showing representative altered spine dynamics in PDGF mice and wild type mice (Figure A) and quantification of synaptic spine density in 2-month, 4.5-month, 7.5-month and 13.5-month-old PDGF and wild type mice (Figure 2 D and 2 E). Abbreviations: ctrl - control, h-a-syn: human - a-synculein overexpressing mice, mo - months. (Reprinted with permission from Blumenstock et al. 2017).

Taken together, the results from Blumenstock et al. 2017 and 2019 demonstrate that 4.5-month-old PDGF mice show cortical synapse loss before the onset of any behavioural or neurodegenerative abnormalities. This loss has been observed to be accompanied by enhanced protein synthesis activity

in pre-synaptic termini of excitatory glutamatergic synapses, while a transcription elongation factor was found to be downregulated.

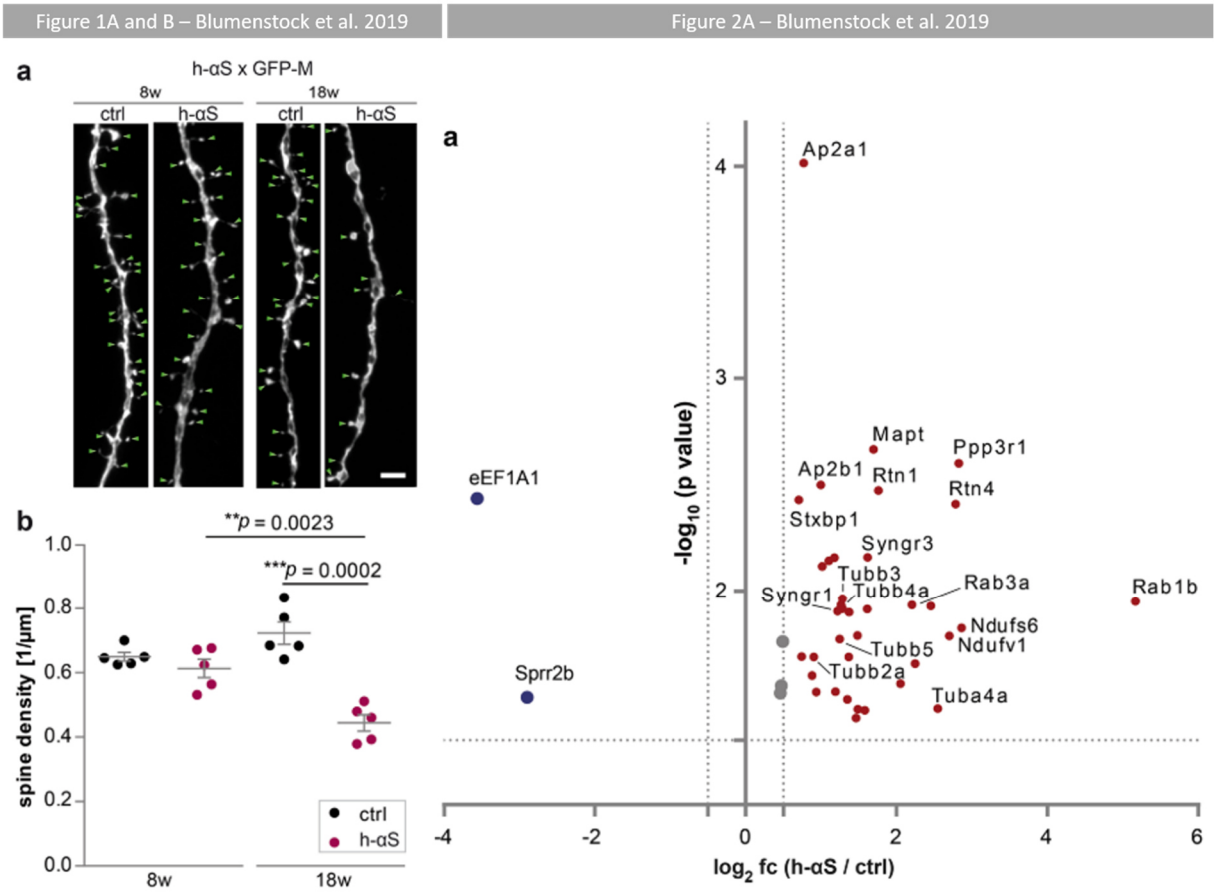

Figure 13: Excerpt from figure 1 and figure 2 from Blumenstock et al. 2019 showing representative images of altered spine density and differentially expressed proteins in synaptosomes of 3-month-old PDGF vs. wild type mice. Figure 1 A-a shows comparable spine density between PDGF and wild type mice at 8 weeks of age (2 months) and significantly reduced spine density in 18-week-old (Figure 1 A-b). Figure 2 A shows significant differentially expressed proteins in FASS-sorted excitatory, glutamatergic synapses of 3-month-old PDGF mice vs. wild type mice. Abbreviations: 8w - 8 weeks, 18w - 18 weeks. (Reprinted with permission from Blumenstock et al. 2019).

V. AIM OF THE THESIS

Synucleinopathies are the second most common neurodegenerative disease worldwide with current therapies limited to slowing down disease progression and no effective cure treatments available. Despite extensive research in this field over the last decades, fundamental understanding of basic molecular mechanisms for early disease-causing mechanisms especially at the synaptic level remain elusive.

The aim of this thesis was to investigate changes in molecular regulatory non-coding elements leading to early synaptic cortical loss in model systems of synucleinopathies. To elucidate post-transcriptional regulatory mechanisms accompanying the observed synaptic loss, transcriptomic analyses with focus on the role of non-coding regulatory elements at the onset of cortical synaptic loss were carried out in a mouse model of Parkinson's disease. Despite the great progress in molecular disease understanding, mouse models remain highly artificial systems that only partially recapitulate the human disease progression. To functionally investigate regulatory mechanisms underlying cortical synaptic loss with a human genetic background, a recently developed protocol modelling the cortical brain region derived from human iPSCs was used to generate cortical organoids. As such, a human derived iPSC cell line carrying a triplication of *SNCA* together with its isogenic control with a normal copy number of *SNCA* were differentiated into cortical organoids. These were characterised for their potential use as translational model system from mouse to human with regard to transferability of findings from non-coding elements.

VI. METHODS

ANIMALS

PDGF-h-a-syn mice bred on a C57Bl/6 background were received from QPS Austria Neuropharmacology (Grambach, Austria). Mice used throughout this thesis were kept under pathogen-free conditions in the animal facility of the Center for Neuropathology und Prion Research at the Ludwig-Maximilians-University (LMU) Munich and at the animal facility of the German Center for Neurodegenerative Disease (DZNE) Munich. Experiments conducted in this thesis were performed in accordance with the German animal protection law and approved by the Bavarian government (Az. 55.2-1-54-2532-163-13). All mice used throughout this thesis are listed in Table 1.

Table 1: List of all mice used for small RNA and long RNA sequencing

Age	Sex	Geno type	ID	Library prep	RNA isolation
2 months	F	WT	737	miRNA-Seq, long RNA-Seq	Small, long, total RNA
2 months	F	WT	716	miRNA-Seq, long RNA-Seq	small, long, total RNA
2 months	M	WT	733	miRNA-Seq, long RNA-Seq	small, long, total RNA
2 months	M	WT	719	miRNA-Seq, long RNA-Seq	small, long, total RNA
2 months	F	PDGF	713	miRNA-Seq, long RNA-Seq	small, long, total RNA
2 months	F	PDGF	715	miRNA-Seq, long RNA-Seq	small, long, total RNA
2 months	M	PDGF	721	miRNA-Seq, long RNA-Seq	small, long, total RNA
2 months	M	PDGF	718	miRNA-Seq, long RNA-Seq	small, long, total RNA
3 months	F	WT	658	miRNA-Seq, long RNA-Seq	small, long RNA
3 months	F	WT	657	miRNA-Seq, long RNA-Seq	small, long RNA
3 months	M	WT	661	miRNA-Seq, long RNA-Seq	small, long RNA
3 months	M	WT	663	miRNA-Seq, long RNA-Seq	small, long RNA
3 months	F	PDGF	656	miRNA-Seq, long RNA-Seq	small, long RNA
3 months	F	PDGF	654	miRNA-Seq, long RNA-Seq	small, long RNA
3 months	M	PDGF	662	miRNA-Seq, long RNA-Seq	small, long RNA
3 months	M	PDGF	659	miRNA-Seq, long RNA-Seq	small, long RNA
4 months	F	WT	648	miRNA-Seq	small, long RNA
4 months	F	WT	652	miRNA-Seq	small, long RNA
4 months	F	WT	653	miRNA-Seq	small, long RNA
4 months	M	WT	649	miRNA-Seq	small, long RNA
4 months	F	PDGF	647	miRNA-Seq	small, long RNA
4 months	F	PDGF	651	miRNA-Seq	small, long RNA
4 months	F	PDGF	671	miRNA-Seq	small, long RNA
4 months	M	PDGF	674	miRNA-Seq	small, long RNA
4 months	M	PDGF	675	miRNA-Seq	small, long RNA

POST-MORTEM TISSUE SAMPLES

Work with human post-mortem tissue samples in this project was granted by the local ethics committee (# 18-851). Samples were obtained from the Neurobiobank Munich (NBM), where they were collected on the basis of an informed consent according to all relevant guidelines and regulations including the guidelines of the ethics commission of the LMU, Germany (# 345-13). Case selection for this study was based on neuropathological examination and diagnosis for (early) stages of synucleinopathies. A case summary is listed in Table 2.

Table 2: List of human post-mortem tissue samples used throughout this study.

Sample code	LBD Braak	PMI (h)	Age	Sex
s1	4	96	63	M
s2	6	42	79	F
s3	1	46	65	F
s4	3	28	87	F
s5	1	79	80	F
s6	4	68	76	M
s7	1	8	90	F

CELL CULTURE

CELL LINES

In order to investigate the effect of *SNCA* gene over dosage on early cortical synaptic loss in human context, two iPSC cell lines were kindly provided by Prof. Dr. Thilo Kunath from the University of Edinburgh, Scotland. The one iPSC cell line used in this thesis was obtained from fibroblast from an Iowan family with early-onset PD harbouring an *SNCA* triplication (Singleton et al. 2003; Devine et al. 2011) and is herein referred to as AST (α-synuclein triplication iPSC cell line). The second line used is an isogenic, CRISPR-Cas9 corrected iPSC cell line with a normal copy number of *SNCA* gene, that has been generated from the AST cell line (Chen et al. 2019) and is herein referred to as CAS (corrected α-synuclein triplication cell line).

IPSC CELL CULTURE

Both the AST and CAS iPSC cell lines and subsequent differentiated cells were maintained in an incubator at 37 °C with 5 % CO_2 throughout the experiments. All media volumes provided below are given for one well of a 6-well plate if not stated otherwise. Cell culture vessels for iPSC culture were pre-coated with matrigel prior to cell plating. Therefore, matrigel (Corning, #356230) was thawed on

ice and diluted 1:100 in DMEM/F12 (Thermo Fischer, #12634010). Subsequently, the matrigel-DMEM/F12-solution was applied to the culture vessel covering the surface. The plate was incubated for at least 1 h or overnight at 37 °C. Before plating of cells, the coated wells were washed with DPBS (Thermo Fischer, #14190144) and respective culture medium was added.

THAWING AND CRYOPRESERVATION OF CELLS

Prior to thawing cells, the cell culture vessels were pre-coated with matrigel. Before thawing cells, the coated plate was washed three times with DPBS. mTesR+ medium (STEMCELL Technologies, #05825) with 2 µl of 10 mM Rock-Inhibitor (Rocki, Merck, #SCM075) for a final concentration of 10 µM was added per well and incubated at 37 °C. Frozen iPSCs were thawed in a 37 °C water bath for about one minute until the ice block detached from the tube. The cells were decanted into a falcon tube with 10 ml pre-warmed DMEM/F12 (Thermo Fischer, #12491015) and the empty cryovial was washed with 1 ml DMEM/F12. The falcon was carefully tilted to mix the cells and subsequently pelleted at 300 x g for 5 minutes at RT. The supernatant was removed and the pellet was carefully resuspended in 0.5 ml mTesR+ medium per well. The cell suspension was applied onto the plate, carefully moved with quick side-movements to evenly distribute the cells and placed in the incubator. After 24 hours, the medium was changed to remove cellular debris and Rocki. Until expansion of the cells, the medium was changed every second day until the cells reached confluency for passaging.

Cells for cryopreservation were harvested at the same time they would normally have been ready for routinely passaging at 70-80 % confluency. Each cryovial would contain cells harvested from a 70-80 % confluent 6-well plate, respectively about 1 million cells. For cryopreservation, cells were harvested using the enzyme-free passaging protocol as described below. Harvested cells were centrifuged at 300 x g for 5 minutes at RT. Without disturbing the cell pellet, the supernatant was carefully removed and gently resuspended in pre-cooled (2-8 °C) Bambanker (NIPPON Genetics, #BB02) using a serological pipette to minimize breaking of cell aggregates. 1 ml of cell suspension containing on average 1 million cells was transferred to a cryovial. Cryopreserved cell aggregates were transferred at -80 °C inside a freezing container with a cooling rate of apprx. 1 °C/min.

PASSAGING CELLS

Cells were passaged on prepared multi-well plates pre-coated with matrigel diluted 1:100 in DMEM/F12 for a minimum of 1 hour or overnight.

For routinely cell passaging, iPSCs being 70-80 % confluent were passaged as colonies using ReLeSR (Stemcell Technologies, #05872). Therefore, the consumed medium was aspirated, replaced with 1 ml ReleSR reagent and incubated for 1 minute at room temperature. ReleSR was removed and the plate was placed in the incubator for 5 minutes. Cell colonies were detached by firmly clapping at the side of the well plate and collected in 2 ml DMEM/F12 medium, centrifuged for 5 minutes at 300 x g and resuspended in the desired mTesR+ volume and evenly distributed with quick side-wards movements. Cells were routinely passaged in ratios between 1:3 and 1:6.

When starting experiments with a pre-defined number of cells, iPSC cells were harvested using gentle cell dissociation reagent (GCDR) (Stemcell Technologies, #07174) to obtain single cells. Therefore, the consumed medium was aspirated and replaced with 1 ml GCDR and incubated for 5-8 minutes at room temperature. After incubation, 1 ml of DMEM/F12 was added to the well and the cells were scratched from the bottom. The cells were collected and counted using a Neubauer counting chamber system, centrifuged for 5 minutes at 300 x g and eventually plated at the desired density.

Being re-plated as single cells, Rocki at 10 µM final concentration was added to the medium of the cells for 24 hours to improve cell attachment, recovery and prevent dissociation-induced apoptosis (Claassen et al. 2009).

DIFFERENTIATION PROTOCOLS

Pluripotent stem cells have the capacity for self-renewal in order to maintain the stem-cell pool, and specific changes in media formulation allows induction and subsequent differentiation of iPSCs into desired specific cell types along defined linages (Medvedev 2010). Differentiation protocols used throughout this thesis are provided below.

CEREBRAL ORGANOID GENERATION

In order to investigate cortical development with respect to intrinsic organization and therefore intrinsic regulation of gene expression, the unguided cortical organoid (CO) development approach by Lancaster and colleagues was followed throughout this thesis (Lancaster & Knoblich 2014). The commercially available media and protocol provided by STEMCELL Technologies was used following the manufacturer's instructions. Respectively, the STEMCELL Cerebral Organoid Kit and STEMCELL Cerebral Organoid Maturation Kit for subsequent maturation of the organoids were used (#08570 and #08571). Despite the limitations mentioned above to generate organoids with this protocol, and recent publications improving e.g. reproducibility with modifications of matrigel application of media

formulation changes, this commercially available protocol was used throughout this study to ensure overall media composition reproducibility, consistency and comparability to other studies and reports using the same organoid differentiation protocol. Compare workflow of CO generation with Figure 14. Regular media change has occasionally been performed by Federico Fierli.

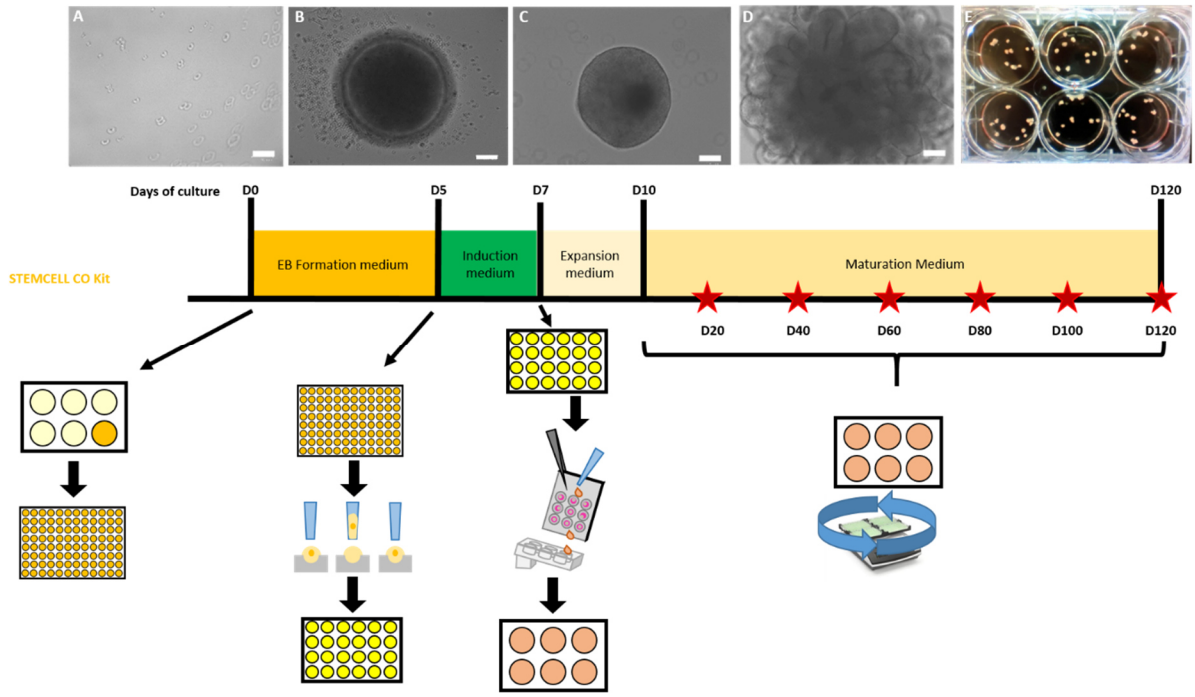

Figure 14: Schematic overview of cerebral organoid generation from iPSCs using the STEMCELL CO Kit. At day 0, one well of a confluent 6-well plate with iPSCs was harvested as single cells and plated in EB formation medium to form EBs (A). At day 5, EBs were transferred in induction medium in a 24-well plate (B). At day 7, EBs were embedded in matrigel and transferred for culture in expansion medium in a 6-well plate (C). At day 10, the medium was changed for maturation medium and cells were plated on a shaker in the incubator (D) and incubated during maturation (E, day 41). Red stars indicate harvesting time points. Harvesting time points: AST: D20 - Day 20; D40 - Day 41; D60 - Day 61; D80 - Day 82; D100 - Day 102; D120 - Day 120. CAS: D20 - Day 20; D40 - Day 41; D60 - Day 60; D80 - Day 81; D100 - Day 101; D120 - Day 119.

In brief: On day 0, CO generation was started with embryoid (EB) formation. Therefore, one 70-80 % confluent well of a 6-well plate of iPSC cell was washed with PBS and harvested with GCDR. Cells were resuspended in EB seeding medium and 100 µl of cell suspension were plated into each well of a 96-well round-bottom ultra-low attachment plate (Corning, #7007) with a concentration of 90.000 cells/well. On day 2 and day 4, 100 µl EB formation medium each was added per well. On day 5, small formed EBs were transferred with a wide-bore pipette tip onto an ultra-low attachment 24-well plate (Corning, #3473) with fresh 0.5 ml induction medium. At day 7 of the protocol, the EBs were collected with a wide-bore pipette tip and placed on an embedding sheet (Stemcell Technologies, #08579). Excess medium was removed and a 15 µl matrigel droplet was added to the EB, which was subsequently positioned in the center of the drop. After 30 minutes incubation at 37 °C degree for matrigel polymerization, the matrigel-embedded EBs were washed off the embedding sheet with expansion medium into an ultra-low attachment 6-well plate (Corning, #3471) and incubated for 3 days. At day 10, the consumed medium was replaced with fresh maturation medium and the well plate

was transferred to an orbital shaker with 75 rmp throw inside the incubator. Routinely media change was performed when consumed, which was roughly every 2-3 days. Organoids ready for harvest were taken from the plate using a 1000 µl pipette tip with a cut opening.

FIXATION AND CRYOGENIC TISSUE PROCESSING FOR IMMUNOFLUORESCENCE ANALYSIS OF COS

Using a cut 1000 µl pipette tip, COs ready for harvesting were transferred to a 50 ml falcon tube and washed three times with DPBS. Cryogenic tissue processing was performed according to the technical bulletin *Cryogenic Tissue Processing and Section Immuno-fluorescence of Cerebral Organoids* (STEMCELL Technologies, TB27171). In brief, after 16 hours fixation in 4 % PFA (Merck, #158127) at 4 °C, the COs were washed three times with 0.1 % PBS-T. Subsequent protection against freezing artefacts was achieved by embedding in 30 % sucrose solution at 4 °C until the organoids were no longer floating. The sucrose solution was replaced by pre-warmed gelatine solution and incubated at 37 °C for 60 minutes. Thereafter, the COs were transferred to embedding sheets, snap frozen in a dry ice-100 % ethanol slurry and transferred to -80 °C for long-term storage. Harvesting of COs and cryogenic tissue processing was occasionally performed by Federico Fierli.

INDUCTION OF NEURAL STEM CELLS (NSC) FROM IPSCS

NEURONAL INDUCTION AND DIFFERENTIATION OF IPSCS INTO NPCS AND NEURONS

NPC (neural progenitor cell) differentiation was induced following the protocol *Induction of Neural Stem Cells from Human Pluripotent Stem Cells Using PSC Neural Induction Medium* (Thermo Fischer, #A1647801, Pub.No. MAN0008031, rev. A.0). Neuronal differentiation of NPCs was performed following the protocol *Culture One Supplement 100X* from Gibo (Thermo Fischer, #A33202-01, Pub. No. MAN0016204, rev. 3.0) according to the manufacturer's instructions with minor modifications as outlined below (compare with Figure 15).

CULTURE PREPARATION AND NEURAL INDUCTION

In brief, undifferentiated iPSCs were maintained in mTesR+ medium until they reached 70-80 % confluency. One well of a 6-well plate was harvested using ReleSR as for routinely sub-culturing. A proportion of harvested cells was collected in a separate falcon tube and dissociated into single cells for accurate counting. As colonies, a total of 2.5 x 10^5 – 3 x 10^5 iPSC cells per well of a 6-well plate pre-coated with matrigel were plated in mTesR+. A final concentration of 10 µM Rocki was supplemented to the medium. Having reached the starting density of about 15-25 % confluency ~24 hours after

plating, the culture medium was replaced with 2.5 ml PSC Neural Induction Medium (NIM). After 48 hours of neural induction, the spent medium was replaced with 2.5 ml NIM. On day 4 of neural induction, the cells were reaching near confluency and the consumed medium was replaced with 5 ml fresh NIM. On day 6 of neural induction, the medium was replaced with 5 ml fresh NIM.

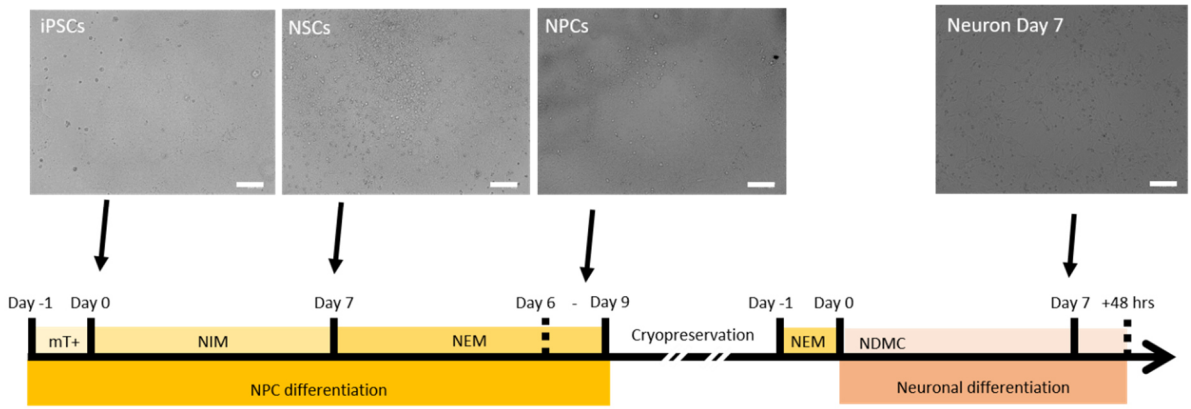

Figure 15: Schematic overview of the differentiation protocol of NPCs and neurons derived from iPSCs using the NPC and Culture One Protocol (Thermo Fischer). After 24 hours cultivation of iPSCs in culture medium, the medium was changed to NIM. At day 7, NSCs were passaged into NEM to expand the precursor cells. The NPCs were harvested and cryopreserved at confluency. For neuronal differentiation, the cryopreserved NPCs were thawed in NEM for 24 hours and neuronal differentiation was induced using NDMC. Abbreviations: mT+ - mTesR+, NDMC - neuronal differentiation medium with culture one supplement; NEM - neural expansion medium; NIM - neural induction medium; NSCs - neural stem cells; NPCs - neural precursor cells. Scale bar 100 µm.

HARVEST AND EXPANSION OF P0 NSCS

On day 7 of neural induction, neural stem cells (NSCs) (P0) were ready for harvest and expansion on prepared matrigel-coated well-plates. Spend NIM was removed from the NSC-plate and washed with 2 ml of DPBS without calcium and magnesium to prevent cell detachment. Afterwards, 1 ml of pre-warmed Accutase (Stemcell Technologies, #07920) was added to each well and incubated for 5-8 minutes at 37 °C until cell detachment from the surface of the culture vessel was observed. Cells were fully detached from the surface with a cell scraper and cell clumps were transferred to a falcon tube. Residual cells in the wells were collected with 1 ml DPBS each. The cell clumps were broken up by pipetting up and down three times and the cell suspension was passed through a 100 µm strainer and centrifuged at 300 x g for 4 minutes. The supernatant was aspirated and the pellet was re-suspended in DPBS with 3 ml per one well of a 6-well plate. Afterwards, the cells were centrifuged again at 300 x g for 4 minutes. The supernatant was removed and the cells were resuspended in complete Neural Expansion Medium (NEM) with Rocki at a final concentration of 5 µM. The cell suspension was plated at a density of 0.5 x 10^5 - 1 x 10^5 cells/cm^2 on matrigel-pre-coated well plates and evenly distributed with quick side-movements. After 24 hours, the spent medium was replaced with fresh NEM without Rocki and medium change was performed every day. Between 4-6 days after plating, NSCs reached

confluency and were ready for either expansion or cryopreservation. Subsequent expansion of cells was carried out as described above with accutase passaging and double DPBS wash by centrifugation. If the cells were passaged between P0-P4, Rocki at a final concentration of 5 µM was added to the medium to improve cell attachment, cell survival and to prevent glial expansion.

CRYOPRESERVATION OF NPCS

NSCs were passaged to NPCs P1 before cryopreservation. For cryopreservation, NPCs should have reached confluency. The spend medium was replaced with pre-warmed accutase and incubated for 5-8 minutes at 37 °C. The detached cells were collected in a falcon tube and residual cells of the well were collected with DPBS. Cell clumps were broken up by pipetting up and down three times. After centrifugation at 300 x g for 4 minutes, the supernatant was aspirated and the cells were resuspended in DPBS. After a second round of centrifugation, the cells were re-suspended in Neural Progenitor Freezing Medium (Stemcell Technologies, #05838). 1 ml of cell suspension was collected in a cryotube and frozen in a freezing container with a cooling rate of approx. 1 °C/min.

NEURONAL DIFFERENTIATION OF NPCS INTO NEURONS

COATING CULTURE VESSELS FOR DIFFERENTIATION OF NPCS INTO NEURONS

Before plating NPCs for neuronal differentiation, the respective culture vessel was coated with Poly-D-Lysine (PDL, 50 µg/mL) for two hours at room temperature. After three rounds of rinsing with distilled water, the coated plate was air-dried under the lamina flow hood. Subsequently, laminin diluted 1:100 in distilled water was added to the pre-coated plate and incubated for a minimum of two hours at 37 °C. Laminin was aspirated from the well directly before cell plating.

RECOVERY AND DIFFERENTIATION OF NSCS

Cryopreserved NPCs were thawed in a 37 °C water bath until the ice block detached from the wall. Cells were transferred dropwise in a falcon tube with 10 ml DPBS without calcium and magnesium and 1 ml of DPBS was added to the cryovial to collect residual cells. The thawed NPCs were dissociated and centrifuged at 300 x g for 5 minutes. The cell pellet was resuspended in pre-warmed NEM and plated at a density of 5 x 10^4 cells/cm^2 on PDL and laminin coated plates with Rocki (5 µM final concentration). The plate was moved with quick side-wards movements to evenly distribute the cells and incubated at

37 °C. After 24 hours, the medium was changed to NDMC medium (Neuronal Differentiation Medium with Culture One Supplement) to induce neuronal differentiation. The spent medium was replaced every second or third day. Therefore, half the spent medium was aspirated and the same volume of fresh NDMC was added per well.

TRANSFECTION OF CELLS

iPSCs differentiated into NPCs and subsequently into neurons were transfected with small molecules. Therefore, commercially synthesised miRNAS (Merck) were diluted with RNAse free water to a final concentration of 1 µM. Subsequently, the small molecules at 100 nM concentration were applied directly to cells into the culture medium and incubated for 48 hours. No transfection-helping agent was used, and no media change was performed within the incubation time.

MOLECULAR BIOLOGY METHODS

cDNA SYNTHESIS

cDNA synthesis of mature miRNAs was performed using the TaqMan™ Advanced miRNA cDNA Synthesis Kit (Thermo Fischer, #A28007) with 0.1 ng small RNA input according to the manufacturer's instructions.

cDNA synthesis of small and long RNA was performed using the SuperScript IV VILO MasterMix (Thermo Fischer, #11756050) with up to 2 µg RNA input according to the manufacturer's instructions. cDNA synthesis including genomic DNA removal of isolated RNA from the *in vitro* pull down experiment was performed using SuperScript IV VILO MasterMix with ezDNase (Thermo Fischer, #11766050) according to the manufacturer's instructions.

DROPLET DIGITAL POLYMERASE CHAIN REACTION - DDPCR

The ddPCR technology was used to determine copies per µl of target gene of interest. Analysis of TaqMan based probes was performed using ddPCR Supermix for Probes (No dUTP) (BioRad, #1863023), direct quantification of target copy number was performed using QX200™ ddPCR™ EvaGreen® Supermix (BioRad, #1864033) workflow. Neither genomic, nor cDNA was enzymatically digested prior to PCR-amplification. Primers were designed using the primer3 webtool (Koressaar & Remm 2007; Untergasser et al. 2012; Koressaar et al. 2018) using the settings described in *BioRad ddPCR application Bulletin_6407*, page 14.

Master mixes were prepared using the volumes indicated below. Upon master mix ingredient combination, thoroughly vortexed sample DNA was added as last step with a volume of 5 µl to the 0.2 ml PCR tube. Reverse transcribed RNA into cDNA was diluted to obtain the desired input concentration (0.02 ng/µl of cDNA converted from long RNA and 5 µl input of 1:100 diluted miRAMP reaction in nuclease free water). Subsequently, 20 µl of master mix-sample DNA mix was added to the sample wells of the DG8™ cartridges (BioRad, #1864008). Following the eight sample mixes, 70 µl of the respective droplet generation oil was applied to each respective oil well and the cartridge was sealed with DG8™ Gaskets (BioRad, #1863009) and) placed in the QX200TM droplet generator (BioRad, #1864002) for droplet generation.

Specific droplet generation oil was used for each supermix used in the master mix, respectively droplet generation oil for EvaGreen (BioRad, #1864005) or droplet generation oil for Probes (BioRad, #1863005). Subsequently, generated droplets were slowly transferred to 96-well PCR plates using a pipetting volume of ~42.6 µl. Having transferred all samples to the PCR well plate, the plate was

covered with a PCR plate heat seal foil (BioRad, #1814040) and sealed at 180 °C. The sealed plate was transferred to a PCR cycler (Eppendorf Mastercycler X50s) and the PCR reaction was performed using the settings indicated in Table 3. Having completed the PCR run, the plate was transferred to the QX200 Droplet Reader (BioRad, #1864003) and run analysis was performed.

Table 3: Overview of ddPCR master mix reaction setup and respective PCR settings (ramp rate 2°C/sec).

Eva Green reaction mix setup

Component	Volume (22 µl)	Final concentration
QX200™ddPCR™EvaGreen® Supermix (2X)	11 µl	1x
Forward primer (1 µM)	2 µl	Up to 250 nM
Reverse primer (1 µM)	2 µl	Up to 250 nM
DNA input	5 µl	Variable
Water	2 µl	

EvaGreen PCR settings

Cycling step	Temperature	Time	Cycles
Enzyme activation	95 °C	5 min	1
Denaturation	95 °C	30 sec	40
Annealing & extension	60 °C	1 min	
Signal stabilization	4 °C	5 min	1
	90 °C	5 min	1
Hold	4 °C	∞	1

Probe-based reaction Mix setup

Component	Volume (22 µl)	Final concentration
ddPCR Supermix for Probes (No dUTP) (2X)	11 µl	1x
miRAssay (FAM)	1 µl	Up to 250 nM
DNA input	5 µl	variable
Water	5 µl	

Probe-based PCR settings

Cycling step	Temperature	Time	Cycles
Enzyme activation	95 °C	10 min	1
Denaturation	94 °C	30 sec	40
Annealing & extension	60 °C	1 min	
Enzyme deactivation	98 °C	10 min	1
Hold	4 °C	∞	1

ddPCR-BASED LIBRARY QUANTIFICATION

In order to obtain accurate concentration values of each Illumina library for optimized pooling with equimolar balanced libraries, each individual library was quantified using the ddPCR™ Library Quantification Kit for Illumina TruSeq (BioRad, #186-3040) following the manufacturer's instructions. The concentration of the libraries was accessed with a final dilution of 10^{-7} to 10^{-8} in DNAase and RNAse free water. Only nM concentrations that were not differing more than 10 % between the two accessed library dilutions were used for downstream applications. The determined copies/µl were multiplied by

the dilution factor and by 5 to account for the DNA dilution in the master mix. The nM concentration was obtained using the following formula:

Equation 1:

$$\frac{calculated\,\frac{copies}{\mu l} * 10^6\,\frac{\mu l}{L}}{6.023 * 10^{23}\,\frac{copies}{mol}} = concentration\ in\ nM$$

RT-qPCR-BASED LIBRARY QUANTIFICATION

Illumina library quantification using RT-qPCR was performed using the *NGS Library Quantification Kit (for small RNA-seq)* (Norgen, #61600) following the manufacturer's instructions. The library concentration was calculated by determining the concentration of 10^{-3} and 10^{-4} fold diluted libraries relative to the standard curve.

GENOMIC DNA ISOLATION

Genomic DNA was isolated using the QIAamp DNA Mini Kit (Qiagen, #51304). In brief, cell pellets were resuspended in 200 µl PBS, 20 µl protease K and 200 µl buffer AL was added to the sample, pulse-vortexed and incubated at 56 °C for 10 minutes. The following purification steps were carried out on the QIAcube following the automated protocol *QIAamp DNA mini, blood and body fluids, manual lysis*, with 100 µl elution volume.

GELS FOR SIZE-SEPARATION OF NUCLEIC ACIDS

DNA was separated by size using different percentages of agarose (Serva, #11406.03). The gels were stained with 1-5 µl SYBR™ Gold Nucleic Acid Stain (Invitrogen, #S11494) or SYBR™ Safe DNA gel stain (Invitrogen, #S33102) in 50 ml TAE buffer. DNA fragments with less than 500 bp of length were separated on 2 % gels, DNA fragments longer than 500 bp were separated on 1 % gels. Usually, 6 µl of DNA ladder was loaded per lane. A 1:10 diluted ladder was loaded on SYBR™ Gold stained gels.

Adapter-ligated miRNA for Illumina sequencing was separated by size on an 8 % poly-acrylamide gel as described below.

NUCLEIC ACID CONCENTRATION QUANTIFICATION

Concentration quantification of isolated RNA was performed using Qubit™ RNA assay kits (Thermo Fischer, #Q32852) for long RNAs and the Qubit™ microRNA assay kit (Thermo Fischer, #Q32880) for small RNAs including miRNAs. DNA concentrations were determined using Quibit™ dsDNA HS and BR assay kits (Thermo Fischer, #Q32851 and #Q32850). For each kit, reagent and buffer were combined in a ratio 1:200 to obtain the final working solution. Typically, 2 µl of sample were mixed with 198 µl of working solution for sample concentration measurement using the Qubit fluorometer (Thermo Fischer, #Q33238).

POLYMERASE CHAIN REACTION (PCR) AMPLIFICATION

PCR amplification of cDNA was performed using the Q5® High-Fidelity 2x Master Mix (NEB, #M0492S) according to the manufacturer's instructions. The primer melting temperature (Tm) was calculated using the Tm calculator from NEB (https://tmcalculator.neb.com/#!/main), and the amplification time was adjusted to the expected amplicon length (30 sec/kb).

RNA ISOLATION

RNA isolation was performed using different approaches depending on the starting material and required output.

Total RNA from frozen mouse cortical tissue was isolated using the RNeasy kit (Qiagen, #74104). For RNA isolation of cerebral organoids and human cortical tissue, RNA was isolated using the protocol to separate small and long RNA following the miRNeasy Kit (Qiagen, # 217004). Long RNA was isolated in part A using RNeasy MiniSpin columns, followed by part B using RNeasy MinElute spin columns for enrichment of RNA fractions smaller than 200 nucleotides.

In brief, up to 50 mg of cryofrozen cortical tissue or cerebral organoids or up to 2 million pelleted cells were manually dissociated and homogenated in 700 µl QIAZOLE lysis reagent (Qiagen, #79306) using a plastic pistil and incubated at room temperature for 5 minutes. For RNA separation from proteins and DNA, 140 µl chloroform was added to the tube and vortexed for 15 minutes followed by 3 minutes incubation at room temperature. After phase separation by 15 minutes centrifugation at 12.000 x g at 4 °C, the upper aqueous phase of approx. 350 µl was transferred to a fresh 2 ml tube and placed in the QIAcube. The following steps including RNA binding to the purification column, ethanol washing steps and final RNA elution in RNase free water were performed using the automated QIAcube protocol

following the automated protocols for either total RNA isolation or RNA isolation separated into long RNA (part A) and small RNA (part B) of the respective kits.

ILLUMINA LIBRARY PREPARATION AND SEQUENCING

MIRNA LIBRARY PREPARATION, POOLING AND SEQUENCING

RNA isolation and library-preparation of 2-month, 3-month and 4-month old PDGF mice for miRNA sequencing has been performed by Jiao Geng (Geng 2019). Small RNA isolation from frozen cortical mouse and subsequent library preparation was performed following the TrueSeq® Small RNA Library Prep Reference Guide (#15004197 v02, July 2016). 50 ng of small RNA was used as input for library preparation following the manufacturer's instructions (Geng 2019).

Previously adapter-ligated and PCR-amplified library preparations of 2-month, 3-month and 4-month-old mice (Geng 2019) have been re-used for this thesis for miRNA sequencing. In order to obtain correctly balanced samples on the flow cell, 25 µl of each adapter-ligated library with 5 µl loading dye was loaded individually on a 8 % poly-acrylamide gels for isolation of correctly ligated and amplified miRNA libraries only (compare with Figure 16). Each poly-acrylamide gel ran in 1 x TBE buffer at 80 V for ~2 hours until the pink loading dye font left the gel, and was post-stained with 5 µl SYBR™ Gold Nucleic Acid Gel Stain Adapter in 50 ml TBE for 10 minutes. Addition of 130 nt long adapters to miRNAs with an average length of 22 nt required isolation of 145-160 bp long fragments. Thus, separation of adapter dimers from correctly ligated adapters to the miRNA was required. Bands of adapter-ligated miRNAs were isolated between 145 and 160 bp range using the gel cutter of the seqmatic gel extraction kit (Seqmatic, #TC-025).

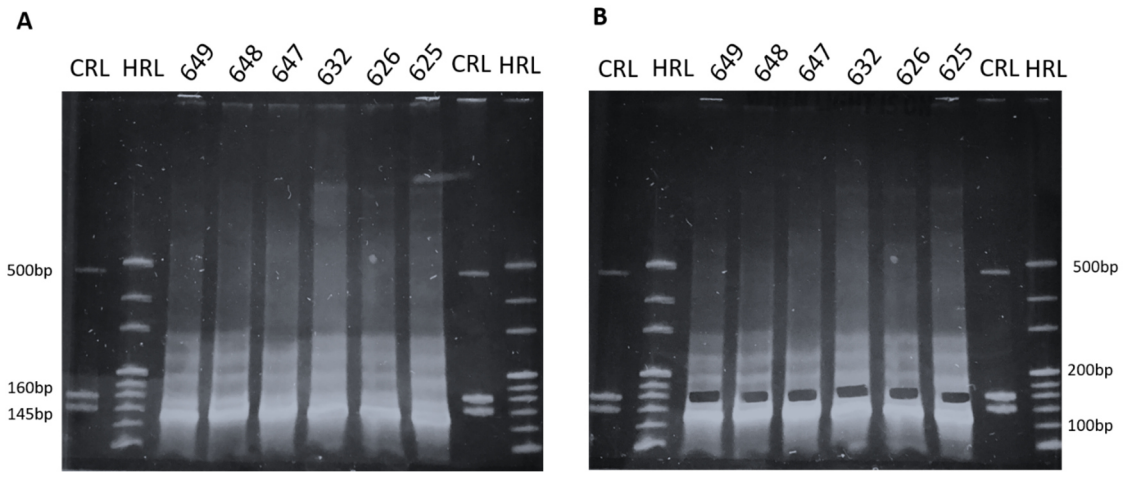

Figure 16: Representative 8 % poly-acrylamide gel before (A) and after (B) isolation of correctly sized miRNA sequencing library. Ladders CRL and HRL allow correct size determination. Numbers 649,648,647,632,626 and 625 represent libraries of respective animals as listed in Table 1. Abbreviations: bp - pase bairs; CRL - custom RNA ladder; HRL - high resolution ladder.

The isolated acrylamide pieces were placed in a 0.5 ml gel breaker tube placed within an 2 ml collection tube and centrifuged for 14.000 x g for 2 minutes. Collected gel debris was dissolved in 200 µl ultra-pure water and incubated rotating over night at room temperature. The partially dissolved gel debris was centrifuged at 600 x g for 10 seconds through a 5 µm filter into a 2 ml collection tube. The flow-through was used for library concentration determination with subsequent conversion of units into nM:

Equation 2:

$$\frac{measured\ concentration\ \frac{ng}{\mu l} * 10^6}{600\ \frac{g}{mol}\ x\ average\ library\ size\ (300bp)} = library\ concentration\ in\ nM$$

All libraries were pooled to obtain a library pool with a final concentration of 4 nM of each library. To prepare the library pool for sequencing, the library pool was denatured following the standard normalization method using 0.2 M NaOH and subsequently diluted as described in the *NextSeq 500 and NextSeq 550 Sequencing Systems - Denature and Dilute Libraries Guide* (Document #115048776 v16, July 2020). The denatured and diluted library pool with a concentration of 1.8 pM was loaded on the NextSeq 550 on a High Output Flow cell cartridge (1 x 75 cycles) (Illumina, #20024906) and sequencing was performed on a NextSeq550 platform (Illumina, SY-415-1002).

miRNA TARGET PULL DOWN LIBRARY PREPARATION, POOLING AND SEQUENCING

Library preparation of miRNA target RNA isolated from the *in vitro* miRNA target pull down was performed following the *SMART-Seq® Stranded Kit User Manual* (Takara, #634444, Version 041922). 7 µl of RNA was used as input following the ultra-low input protocol (no Post-PCR1 pooling, 10 PCR1 cycles, 13 PCR2 cycles, 2 final clean-ups and 12 µl final elution volume). Each library was quantified using the ddPCR library quantification protocol.

For the library pool, 1 nM of each library was combined and subsequently denatured using 0.1 N NaOH. Following the standard normalization method (protocol A), the library pool was diluted to 0.8 pM as described in *MiniSeq Systems Denature and Dilute Libraries Guide* (Document #1000000002697 v09, April 2021). The library pool was sequenced using the Mini Seq Mid-Output flow cell (2x 175 cycles) (Ilumina, #FC-420-1004) and sequencing was performed on the Illumina® MiniSeq™ system (Illumina).

LONG RNA LIBRARY PREPARATION, POOLING AND SEQUENCING

Starting quality of long RNA isolated from PDGF mice was determined using a Bioanalyzer (Agilent) and quantified using the Quibit HS dsDNA assay. The library preparation was performed with 1 µg initial RNA input following the protocol *TruSeq Stranded Total RNA* (Document #1000000040499 v00, October 2017). Library quality and concentration was quantified using the Agilent 2100 Bioanalyzer using the Agilent High Sensitivity DNA Kit (Agilent, #5067-4626) followed ddPCR library quantification.

For the library pool, 4 nM of each long RNA library was combined. Subsequently, the library pool was denatured using the standard normalization method (protocol A) using 0.2 N NaOH and subsequently diluted with HT1 hybridization buffer to 1.8 pM as described in *the NextSeq500 and NextSeq500 Sequencing Systems – Denature and Dilute Libraries Guide* (Document #150487776 v16, July 2020). The library pool was loaded on the NextSeq500 using the High Output Flow cell cartridge (300 cycles) (Illumina, #20024908) and sequencing was performed on the NextSeq550 platform (Illumina, SY-415-1002).

SEQUENCING DATA ANALYSIS

Illumina sequencing data analysis was done in collaboration on a pipeline provided and written by Dr. Felix L. Strübing as follows:

Short RNA sequencing and miRNA pulldown sequencing were performed using High- and Mid-Output flow cells (1x75 and 2x150 cycles, respectively) on an Illumina MiniSeq. Long RNA sequencing was performed on an Illumina NextSeq 550 with a High-Output 300 cycle flow cell.

Demultiplexed RNA-seq *fastq* files were aligned with STAR 2.7.0 to the GRCm39 reference genome using Gencode v29M annotation files in the case of long RNA-seq data (pull down included). Small RNA-seq data was aligned using bowtie2 with the “very-sensitive-local” option to the mm10 reference genome with miRbase v22 annotation files.

Reads were quantified at the exon or mature miRNA feature level with Rsubread 2.10.0 without counting multi-mappers. Differential expression was carried out with edgeR 3.38.1. For quantifying the transgene expression within the RNA-seq data, the PDGF-asyn transgene sequence was added to the annotation files. Generalized linear models corrected for sex were fit, and Likelihood-Ratio tests were carried out. All results were adjusted for multiple comparisons using the False Discovery Rate (FDR), and a significance threshold of FDR < 0.1 and an absolute log2-fold change of > 0.5 was defined. Plots were created with ggplot2 version 3.3.6. All computations were carried out in R version 4.2.0. Figure 18, Figure 20 and Figure 38 were prepared by Dr. Felix Strübing.

IN VITRO MIRNA TARGET PULLDOWN ASSAY

Identification of *in vitro* miRNA target RNAs was based on the biotinylated micro-RNA pulldown assay described by Phatak and Donahue (Phatak & Donahue 2017) and was performed with modifications as described below. The experimental procedure is schematically depicted in Figure 17.

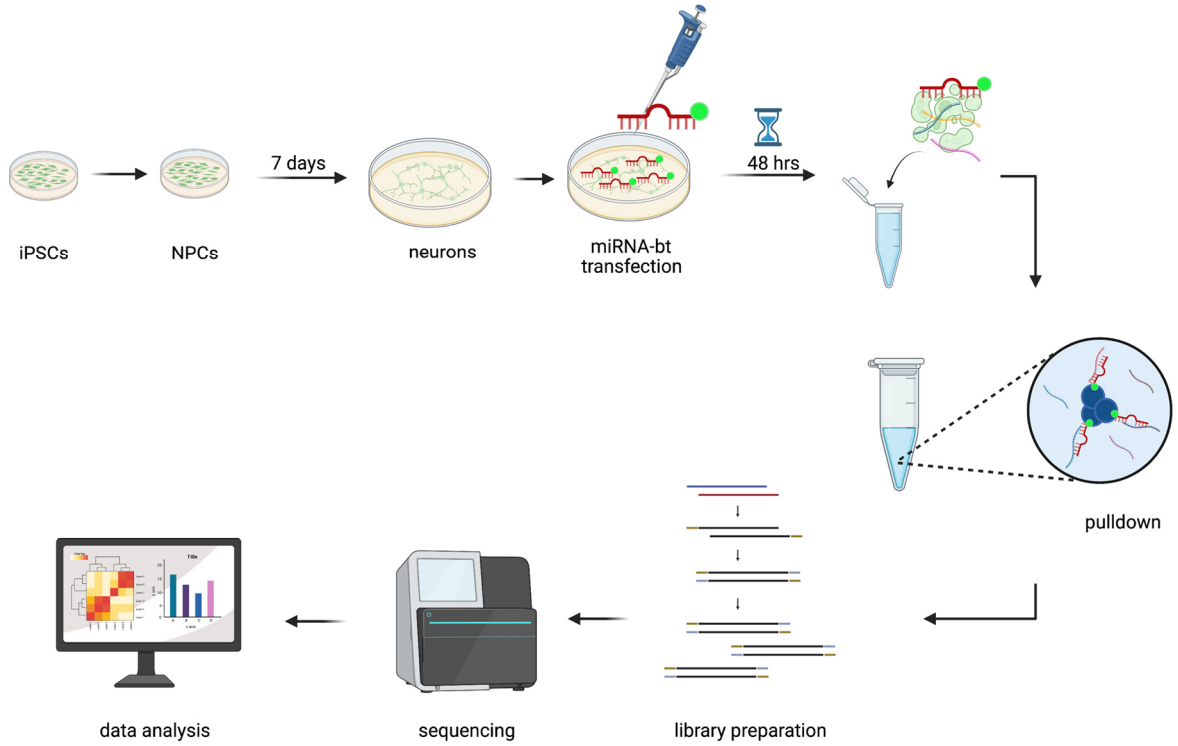

Figure 17: Schematic workflow of the in vitro pulldown of miRNA targets. AST and CAS iPSCs were differentiated into NPCs and subsequently neurons. After 7 days in NDMC medium, 100 nM biotinylated miRNA (miRNA-bt) specific for each miRNA of the cluster was added to the neurons. After 48 hourfs of incubation, the cells were harvested and lysed. The cell lysates were incubated with streptavidin beads to purify miRNA-bt with specifically bound RNA. Following RNA isolation, a library was prepared and sequenced on a MiniSeq platform followed by data analysis. The biotinylated miRNA pulldown assay was adapted and modified from Phatak and Donahue 2017. Abbreviation: bt - biotin. NDMC - neuronal differentiation medium with culture one supplement. The figure was created with Biorender.com

AST and CAS iPSCs were differentiated into NPCs and subsequently into neurons as described above under *Material and Methods - cell culture – differentiation protocols*. For the miRNA pulldown experiment, $5*10^4$ cells/cm^2 were plated on a PLO and laminin coated 6-well culture plate and incubated for 24 hours in NEM supplemented with 5 µM Rocki before changing to NDMC. After seven days in differentiation medium, 100 nM of commercially synthesised miRNA labelled with a biotin tag at the 3'end (Merck) were transfected per well and incubated for 48 hours at 37 °C in 5 % CO_2.

Subsequently, cell lysates were prepared as follows: Each well was washed with ice-cold PBS, harvested with StemPro Accutase (Thermo Fisher, #A1110501), pooled and centrifuged at 2000 x g for

5 minutes at 4 °C to collect the cell pellet. The cell pellets were mixed by pipetting with 550 µl lysis buffer supplemented with protease inhibitor (Thermo Fisher Scientific, #78430) and RNAse inhibitor (Thermo Fisher Scientific, #EO0381), and incubated on ice for 10 minutes. The lysates were centrifuged at 4 °C and 18.000 x g for 10 minutes and the supernatant was collected in a new tube.

Four hours in advance, streptavidin beads were prepared as follows: Per sample, 50 µl beads (Dyna beads M-280 streptavidin, Thermo Fisher Scientific, #11205D) were prepared for coating. The beads were washed three times with 500 µl solution A, and washed twice with 500 µl solution B. Afterwards, the beads were washed three times with 1 ml lysis buffer and incubated with 550 µl lysis buffer and 10 µl yeast tRNA (Thermo Fisher Scientific, #AM7119) on a rotator at 4 °C for 2 hours. Washing the beads was performed as follows: The microcentrifuge tube containing the beads was incubated with the respective solution for 2 minutes, and then placed on a magnetic stand for another 2 minutes. Excess solution was removed without touching or taking out the magnetic beads.

Pulldown of RNA bound to biotinylated miRNAs was performed as follows: After incubation of the beads with coating solution, the tube was placed on a magnetic stand and washed once with 1 ml lysis buffer. 500 µl cell lysates were added to the beads and incubated rotating at 4 °C overnight. The remaining 50 µl cell lysate was saved as “Input” at -80 °C. After overnight incubation, the cell lysate-bead mix tube was placed on a magnetic stand and the beads were washed 4 times with 1 ml lysis buffer each.

Subsequent total RNA isolation was performed as follows: Per input and pulldown bead sample, 750 µl Qiazol and 250 µl water were mixed and placed at -20 °C for 2 hours. After thawing the mixture at room temperature, 200 µl chloroform was added to each sample, vortexed for 45 seconds and incubated at room temperature for 3 minutes. After centrifugation at 4 °C 18.000 x g for 15 minutes in a pre-chilled centrifuge, the upper aqueous phase (~750 µl) was transferred to a new tube and RNA isolation was performed using the RNeasy Micro Kit (Qiagen, #74004), following the procedure in the RNeasy Micro Handbook, Appendix C: *RNA Cleanup after Lysis and Homogenization with QIAzol® Lysis Reagent* (Version March 2021). Briefly, 750 µl of 70 % ethanol was added and mixed by vortexing. Each sample was transferred to an RNeasy MinElute spin column, centrifuged for 1 minute at > 8.000 x g and the supernatant was discarded. Subsequently, each column was washed with 500 µl RPE buffer and centrifuged (> 8.000 x g, 1 minute), followed by 500 µl of 80 % ethanol and centrifuged (> 8.000 x g, 2 minutes). The spin column was transferred to a new collection tube and dried with open lid in the centrifuge at full speed for 5 minutes. RNA was eluted in 14 µl EB buffer.

Subsequent library preparation was performed following the *SMART-Seq® Stranded Kit User Manual* (Takara, #634444, Version 041922) following the ultra-low input workflow with 10 PCR1 cylces,

13 PCR2 cycles and two rounds of final AMPure bead (Beckman, #A63881) clean-ups, eluted in 12 µl Tris-buffer. Library quality and concentration was quantified using the Agilent 2100 Bioanalyzer and the Agilent High Sensitivity DNA Kit (Agilent, #5067-4626) followed by ddPCR library quantification. The final library pool was sequenced on an Illumina® MiniSeq™ system.

IMMUNOFLUORESCENCE (IF) AND IMMUNOHISTOCHEMISTRY (IHC)

IF STAINING OF 2D CELL CULTURE CELLS

Cells were grown on PDL and laminin coated glass coverslips as described above. For the fixation procedure, the cells were washed with DPBS and incubated with 4 % PFA for 15 minutes. Next, the coverslips were washed three times with PBS and kept at 4 °C for short-term storage. The coverslips were pre-blocked for 2 hours at room temperature in 5 % goat serum (#FG9023, Merck) with 0.5 % PBS-T (Triton X-100). The primary antibody solution was incubated over night with 5 % goat serum in 0.1 % PBS-T (Triton X-100) at 4 °C. After 3 x 5 minutes PBS wash, the secondary antibody was incubated for 2 hours at room temperature with 5 % goat serum in 0.1 % PBS-T (Triton X-100). Afterwards, the slides were washed 3 x 10 minutes with PBS and were mounted using Roti Mount Fluor Care (Carl Roth, #HP19.1) mounting medium. The used antibodies are listed in Table 7.

IF STAINING OF CRYOPRESERVED COS

PFA-fixed and in gelatin-sucrose solution embedded and snap-frozen COs were thawed for 30 minutes at -20 °C. Subsequently, each CO was trimmed and cut on a Cryostat (Cryostar NX70). Subsequently, 10 µm and 20 µm thick sections were cut on Superfrost Plus slides (VWR, # 48311-703) with the block set to -22 °C and the knife set to -17 °C. The slides were kept at -20 °C for long-term storage.

Cryopreserved COs were prepared for immunofluorescence staining as follows: Comparable depths of organoids were used for staining with one antibody mix. Therefore, cryosections were post-fixed for 10 minutes in 4 % formalin and washed three times with PBS. Slides were shortly kept in 37 °C warm water to dissolve the gelatin embedding solution. Next, the sections were pre-blocked for 2 hours in 5 % goat serum (#FG9023, Merck) with 0.3 % PBS-T (Triton X-100) at room temperature. Subsequently, the primary antibody mix was applied over night at 4 °C. After 3 x 5 minutes PBS wash, the secondary antibody was incubated for 2 hours at room temperature with 5 % goat serum in 0.1 % PBS-T (Triton X-100). Afterwards, the slides were washed 3 x 10 minutes in PBS and were mounted using Roti Mount Fluor Care (Carl Roth, #HP19.1) mounting medium. The used antibodies are listed in Table 7.

IHC STAINING OF PARAFFIN-EMBEDDED COS

Organoids were washed three times for 10 minutes with PBS and transferred for fixation to 4 % formalin. Thereafter, tissue processing including paraffin embedding, vibratome cutting and antibody IHC staining was performed by Michael Schmidt in accordance with the guidelines and protocols at the histology lab of the Center for Neuropathology (ZNP) at the LMU. In brief, formalin-fixed tissue was embedded in paraffin and cut on a vibratome in 10 µm thick sections. Following xylol and ethanol de-paraffination, the slides were stained on an automated IHC tissue stainer using antibodies listed in Table 7.

IMAGING AND IMAGE ANALYSIS

IF images were acquired using the confocal microscope Stellaris 5 (Leica). Analysis of IF synaptic marker expression in iPSC-derived neurons was performed as follows: six images were acquired per coverslip, with three coverslip replicates for each condition. For IF synaptic marker analysis in organoids, images were acquired as follows: Per organoid, eight images evenly distributed alongside the organoid within 200 µm from the edge, and three images within the core of the organoid were acquired. Total tissue slices of IHC-stained organoids were imaged by Hartmut Leithäuser using the slide scanner Axioscan 7 (Zeiss).

All images were analysed using Fiji software. For synaptic density analysis of 2D cell culture, the fluorescent synaptic signal distribution was quantified and the synaptic counts over total MAP2-positive area was quantified using the Fiji-tool plug-in *Analyze Particles*. Synaptic density analysis in organoids was measured and quantified as area in percent using the Fiji-tool plug-in *Analyze Particles*. To quantify marker expression in FFPE-embedded COs, each organoid with the respective staining was quantified for its area of H-DAB positive staining versus the H-DAB negative staining of the organoid using *the* Fiji-tool plug-in *Colour Deconvolution2*.

All computations were carried out using R studio version 4.2.0 with the following libraries: *ggplot2, dplyr, tidiverse, ggstatsplot and ggpubr*.

VII. MATERIALS

BUFFERS, MEDIA AND SOLUTIONS

Table 4: Summary of buffer, media and solutions used throughout this thesis

TAE buffer (50 x stock) – pH 7.6		
Tris base	242 g	Merck, #741883
Galacial acetic acid	57.1 ml	Merck, #137130
0.5 M EDTA	100 ml	Merck, #E5134
ddH_20	1 l	

TAE buffer (1 x, 50 ml)	
TAE buffer (50x)	10 ml
ddH_20	490 ml

TBE buffer (10 x stock) – pH 7.6		
Tris base	108 g	Merck, #741883
Boric acid	55 g	Merck, #B0394
EDTA	7.5 g	Merck, #E5134
ddH_20	1 l	

TBE buffer (1 x, 500 ml)	
TBE buffer (10x)	50 ml
ddH_20	450 ml

PBS-TX100 (0.3 %)		
PBS	50 ml	Thermo Fischer, #10010023
Triton X-100	150 µl	Merck, #T8787

PBS-Tween (0,1 %)		
PBS	1 l	Thermo Fischer, #10010023
Tween® 20	1 ml	Merck, #P9416

Lysis buffer (pulldown assay) (1 x, 500 ml)		
20 mM Tris-HCL (pH 7.5)	1.759 g	Merck, #108315
100 mM KCl	3.727 g	Merck, #529552
5 mM $MgCl_2$	0.508 g	Merck, #208337
0.3 % IGEPAL	1.5 ml	Merck, #I8896

Solution A (pulldown assay) (1 x, 50 ml)		
0.1 M NaOH	0.2 g	Merck, #S5881
0.05 M NaCl	0.161 g	Merck, #S9888

Solution B (pulldown assay) (10 x, 50 ml)		
1 M NaCl	2.922 g	Merck, #S9888

GELS FOR NUCLEIC ACID PURIFICATION

Table 5: Summary of gels used for nucleic acid purification

8 % poly-acrylamide gel (6 ml for 2 gels)		
30 % acrylamide	3.2 ml	Merck, #A3699
5 x TBE	2.4 ml	
10 % APS	200 µl	Merck, A3678
TEMED	10 µl	Roth, #H225

2 % agarose gel		
agarose	0.5 g	Serva, #11406
1 x TAE	50 ml	

CELL CULTURE

The following table provides media composition and cell culture kits used in this thesis (Table 6).

Table 6: Summary of media and kits used for cerebral organoid and NPC and neuron differentiation protocols.

Cerebral Organoid Kit (STEMCELL, #08570 and #08571)					
EB seeding medium			**EB formation medium**		
Basal Medium 1	40 ml	#08572	Basal Medium 1	40 ml	#08572
Supplement A	10 ml	#08574	Supplement A	10 ml	#08574
10 mM Rocki	15 µl	Merck, #Y0503			
Induction medium			**Expansion medium**		
Basal Medium 1	49.5 ml	#08572	Basal Medium 2	24.25 ml	#08573
Supplement B	0.5 ml	#08575	Supplement C	0.25 ml	#08576
			Supplement D	0.5 ml	#08577
Maturation medium					
Basal Medium 2	44 ml	#08573			
Supplement E	1 ml	#08578			

Additional material (Thermo Fischer)					
Rock Inhibitor (10 nM)			**Matrigel-coating (1:100)**		
Y27632	2 mg	Merck, #Y0503	Matrigel	10 µl	Corning, #356230
Distilled water	0.625 ml	#15230162	Advanced DMEM/F12	1 ml	#12634010
Sucrose solution (30 %)			**Gelatin solution**		
sucrose	30 g	Merck, #S0389	sucrose	10 g	Merck, #S0389
DPBS	100 ml	#141900144	gelatin	7.5 g	Merck, #G9391
			PBS	100 ml	#70011044

NPC generation media (Thermo Fischer, #MAN0008031)					
PSC Neural Induction Medium			**Neural Expansion Medium**		
Neurobasal® Medium	49 ml	#A1647801	Neurobasal® Medium	49 ml	#A1647801
Neural Induction Supplement	1 ml	#A1647801	Advanced DMEM/F12	49 ml	#12634
			Neural Induction Supplement	2 ml	#A1647801

Table 6 continues on the next page

Neuronal differentiation medium (Thermo Fischer, #MAN0016204, Rev. 3.0)			
NDMC (Neuronal Differentiation Medium Culture One Supplement)	**Final conc.**	**100 ml**	**Catalogue number (#) of Thermo Fischer**
Neurobasal® Medium	50 %	50 ml	#10888-022
DMEM-F/12 with GlutaMax	50 %	50 ml	#10565018
N-2 supplement (100 x)	1 x	1 ml	#17502001
B27 supplement w/o Vitamin A	1 x	2 ml	#12587001
Culture One Supplement (100 x)	1 x	1 ml	#A33202-01
Ascobic acid	200 µM	100 µl	Merck, #A8960
BDNF	20 ng/ml	200 µl	Peprotech, #450-02
GDNF	10 ng/ml	100 µl	Peprotech, 450-10
Laminin	2 µg/ml	60 µl	Corning, #354232
dcAMP	1 µM	5 µl	Merck, #D0627
Penicillin-Streptomycin	1 x	1ml	#15070-63

Poly-D-Lysine coating (50 µg/ml)			**Laminin-coating (1:100)**		
Poly-D-lysine	1 ml	#A3890401	Laminin mouse protein, natural	1 ml	#23017015
DPBS, calcium, magnesium	1 ml	#14080048	distilled water	99 ml	#15230162

ANTIBODIES

The following table provides antibodies used for immunohistochemistry on FFPE-embedded tissue and immunofluorescent staining (Table 7).

Table 7: Summary of all antigens used for immunohistological and immunofluorescent analysis.

Antigen	Species	Dilution IF	Dilution FFPE	Company
DAPI	-	1:1000		Thermo Fischer, #D1306
GFAP	Rabbit		1:500*	Dako, #Z0334
Ki67 (clone MIB-1)	Mouse		1:500*	Zeta Corporation, #Z2305
MAP2	Mouse	1:40.000	1:40.000*	Merck, #M4403
Nestin	Mouse		1:100*	BD Bioscience, #554002
NeuN (clone A60)	Mouse		1:300*	Millipore, #MAB377
PSD95	Rabbit	1:200		Thermo Fischer, #51-6900
Synaptophysin (MRG-40)	Rabbit		1:100*	Cell Marque, #336R-98
VGLUT1	Guinea pig	1:200		SYSY, #135304
α-synuclein	Mouse		1:2000*	BD Bioscience, #610787
p-α-synuclein	Rabbit		1:200*	Abcam, #ab59264

* dilutions used and validated at ZNP histology diagnostics (LMU)

Secondary Antibodies
Alexa Fluor 488, Alexa Fluor 546, Alexa Fluor 594 and Alexa Fluor 647. Secondary antibodies were originating from different species, and were used depending on the primary antibody species. All Alexa Fluor secondary antibodies were supplied by Thermo Fischer.

OLIGONUCLEOTIDES

The following table summarises oligonucleotides used for sequencing analysis (Table 8). All oligonucleotides were commercially synthesised by Merck if not stated otherwise.

Table 8: Summary of oligonucleotides used throughout this thesis

Primer name	Sequence 5' -> 3'	Originating from:
miRAssay hsa-miR-96-5p	uuuggcacuagcacauuuuugcu	A25576/478215_mir (Thermo Fischer)
miRAssay hsa-miR-183-5p	uauggcacugguagaauucacu	A25576/477937_mir (Thermo Fischer)
miRAssay hsa-miR-182-5p	uuuggcaaugguagaacucacacu	A25576/477935_mir (Thermo Fischer)
miRAssay hsa-miR-191-5p	caacggaaucccaaaagcagcug	A25576/477952_mir (Thermo Fischer)
miRAssay hsa-miR-423-5p	ugaggggcagagagcgagacuuu	A25576/478090_mir (Thermo Fischer)
hsa-miR96-5p-biotin	uuuggcacuagcacauuuuugcu	Designed on hsa-miRNA-96-5p
hsa-miR182-5p-biotin	uuuggcaaugguagaacucacacu	Designed on hsa-miRNA-182-5p
hsa-miR183-5p-biotin	uauggcacugguagaauucacu	Designed on hsa-miRNA-183-5p
hsa-miRscramble-biotin	ucaccggguguaaaucagcuug	Adapted from a Qiagen scramble
Anti-miRNA96	[+A][+G][+T][+G][+C][+C][+A][+A]	Designed on hsa-miR96-5p
Anti-miRNA182	[+A][+T][+T][+G][+C][+C][+A][+A]	Designed on hsa-miR182-5p
Anti-miRNA183	[+A][+G][+T][+G][+C][+C][+A][+T]	Designed on hsa-miR183-5p
Anti-miRNAscramble	[+A][+C][+C][+C][+G][+G][+G][+T]	Adapted from Qiagen scramble
JWS20_SNCA_E1_gDNA_f	AAAGGCCAAGGAGGGAGTT	Devine et al. 2011, Suppl. S1
JWS21_SNCA_E1_gDNA_r	ATCCTAACCCATCACTCATGAAC	Devine et al. 2011, Suppl. S1
JWS22_SNCA_E4_gDNA_f	CCTGTGGATCCTGACAATGA	Devine et al. 2011, Suppl. S1
JWS23_SNCA_E4_gDNA_r	TGCAAGTTGTCCACGTAATGA	Devine et al. 2011, Suppl. S1
JWS26_B2MG_gDNA_fwd	CTCACGTCATCCAGCAGAGA	Devine et al. 2011, Suppl. S1
JWS27_B2MG_gDNA_rev	AGTGGGGTGAATTCAGTGT	Devine et al. 2011, Suppl. S1
JWS40_SNCA_cDNA_fwd	AGCAGGGAGCATTGCAGCA	Designed on NM_000345.4
JWS41_SNCA_cDNA_rev	TCATTGTCAGGATCCACAGGCA	Designed on NM_000345.4
JWS44_VGLUT1_ddPCR_f	CATGAACCCCCTCACGAAGT	Designed on NM_020309.4 (*SLC11A7*)
JWS45_VGLUT1_ddPCR_r	TGAGCAGCAGGTAGAACGTC	Designed on NM_020309.4 (*SLC11A7*)
JWS46_PSD95_ddPCR_f	GAGTTGCAGGTGAACGGGA	Designed on NM_001321075.3 (*DLG4*)
JWS47_PSD95_ddPCR_r	ATGCTGTCGTTGACCCTGAG	Designed on NM_001321075.3 (*DLG4*)
JWS54_eEF1A1_ddPCR_f	TCGCCGTTCTGGTAAAAAGC	Designed on NM_001402.6
JWS55_eEF1A1_ddPCR_r	GAACAGCAAAGCGACCCAAA	Designed on NM_001402.6

VIII. RESULTS

NON-CODING RNAS INVOLVED IN CORTICAL SYNAPTIC LOSS IN MOUSE MODEL SYSTEM

TRANSCRIPTOMIC CHANGES IN 3-MONTH-OLD A-SYNUCLEIN OVEREXPRESSING MICE

Synucleinopathies are categorised by the abnormal accumulation of α-synuclein and neuronal loss in post-mortem tissue (Spillantini et al. 1997; McCann et al. 2013). Recent studies shed light on early pathological impairments of the cortex in synucleinopathy subtype PD (Neuner et al. 2014). In the murine PDGF mouse models for PD, Blumenstock et al. in 2017 identified an onset of cortical synaptic loss at 3 months of age, which is before the onset of behavioural impairments. Subsequently in 2019, Blumenstock et al. investigated the proteome of synaptosomes in 3-month-old PDGF versus wild type mice. In VGLUT1-positive synaptosomes, 42 proteins were identified to be significantly differentially expressed. Only two proteins were significantly downregulated, namely the Eukaryotic Translation Elongation Factor 1 Alpha 1 (eEF1A1) and Small Proline Rich Protein 2B (Sprr2b) (Blumenstock et al. 2019). Based on these findings, their transcriptomes were investigated, with a special focus on whether transcriptomic changes could recapitulate the observed proteomic dysbalance. Therefore, RNA-Seq was performed in cortical tissue of 2 and 3-month-old PDGF and wild type (WT) mice.

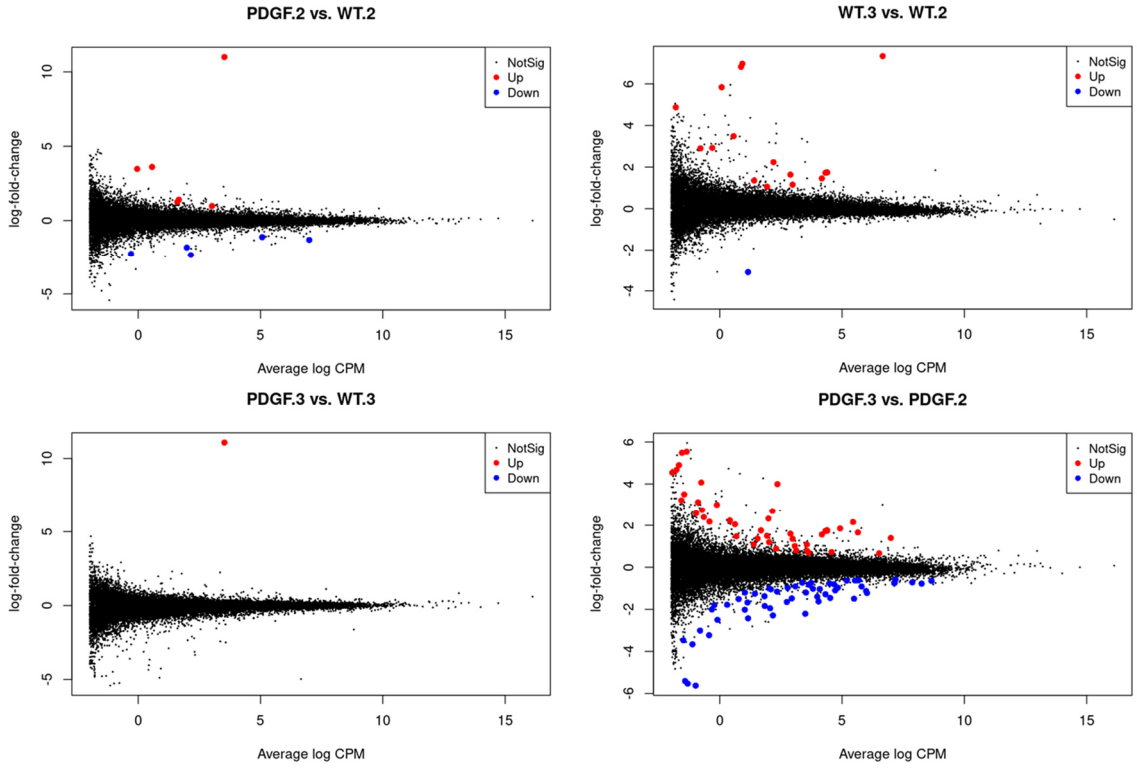

Figure 18: Mean-average plots of RNA-Seq expression analysis of 2-month and 3-month-old PDGF and WT mice. Expression changes are depicted at the y-axis in log2-scale and average log CPM on the x-axis. Non-significantly regulated genes are depicted as black points, significantly up-regulated genes as red points and significantly downregulated genes as blue points. Sample size: 2-month WT = 4n; 2-month PDGF = 4n; 3-month WT = 4n; 3-months PDGF = 4n; balanced for two males and two females each. Abbreviations: CPM - counts per million. PDGF.2 - PDGF mice at 2 months of age, PDGF.3 - PDGF mice at 3 months of age, WT.2 - WT mice at 2 months of age, WT.3 - WT mice at 2 months of age.

Figure 18 shows mean-average plots of the transcriptomic changes observed in 2-month and 3-month-old PDGF mice compared to wild type mice. Comparing gene expression of 2-month-old PDGF (PDGF.2) versus 2-month-old WT mice (WT.2), only five genes were significantly downregulated and five genes were significantly upregulated. The highest differentially expressed gene was the *SNCA* transgene in PDGF mice. In 3-month-old PDGF (PDGF.3) versus 3-month-old WT mice (WT.3), only the transgene *SNCA* was differentially expressed. Comparing gene expression changes between wild type mice at 2 months (WT.2) and 3 months of age (WT.3), 15 genes were identified to be significantly upregulated, while only one gene was identified to be significantly downregulated. Comparing gene expression changes in PDGF mice between 2-month (PDGF.2) and 3-months-old mice (PDGF.3), 41 genes were significantly upregulated and 54 were identified to be significantly downregulated.

To investigate similarities and differences of transcriptomic and proteomic changes in PDGF mice, the RNA-Seq dataset was compared to the proteomic changes of fluorescence-activated synaptosome sorting (FASS) from Blumenstock and colleagues in 2019. However, only the transgene *SNCA* was identified to be differentially expressed in PDGF.3 versus WT.3. In contrast, numerous differentially expressed genes were identified between genotypes during the development of the mice between 2 and 3 months, suggesting overall high transcriptional activity. More than 90 genes were differentially expressed in PDGF.3 vs. PDGF.2, suggesting altered transcriptional dynamics in these mice.

Since no differentially expressed (DE) genes were found in PDGF.3 versus WT.3, transcriptomic changes from PDGF.3 to PDGF.2 were compared to the FASS proteome of PDGF.3 and WT.3. Therefore, the non-DE genes were compared to the non-DE proteins, which showed an overlap of 92 % (Figure 19). Thus, the total RNA transcriptome from whole cortex could also detect the proteins expressed specifically in synaptosomes. However, comparing the overlap of DE genes with the DE FASS proteins indicated an overlap of only one gene (2.3 %), being *Actn1.* This gene encodes the protein alpha-actinin1, an F-actin cross-linking protein anchoring actin to intracellular structures (Uniprot 2022). However, the fold change showed inverse directionalities: The log2-fold change in the transcriptomic dataset was -0.55 (PDGF.3 vs. PDGF.2), while the fold change in the FASS proteomic dataset was 2.79 (PDGF.3 vs. WT.3). However, no significant difference in gene expression of the FASS candidate eEF1A1, nor its structurally highly similar isoform eEF1A2 could be observed. Interestingly, overall low comparability of shared results between RNA-Seq and LC-MS/MS datasets has been observed in PD patient brains (Riley et al. 2014).

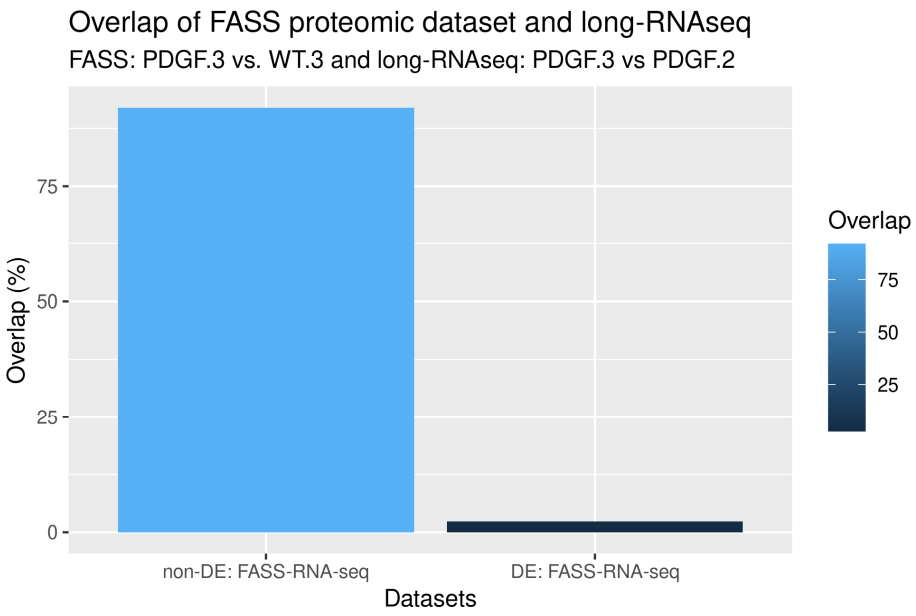

Figure 19: Overlap of genes identified with RNA-Seq and with proteins identified in a published FASS proteomic dataset (Blumenstock et al. 2019) in PDGF and WT mice. An overlap of 92 % percent was detected for non-differentially expressed genes and non-differentially expressed proteins. Only 2 % overlap was observed for significantly differentially expressed genes and significantly differentially expressed proteins. Abbreviations: DE - differentially expressed, FASS - fluorescent-activated synaptosome sorting. PDGF.2 - PDGF mice at 2 months of age, PDGF.3 - PDGF mice at 3 months of age, WT.3 – wild type at 3 months of age.

Overall, more DEGs were found to be downregulated in the PDGF.3 vs. PDGF.2 comparison, while the proteins identified in the PDGF.3 versus WT.3 synaptosomes were found to be primarily upregulated. This was in line with the observed poor comparability of transcriptomic and proteomic dataset. Together with the observation that high transcriptional dynamics were observed in the PDGF.3 vs PDGF.2 and between PDGF.3 and WT.3, it was hypothesised that post-transcriptional modifications could explain the observed discrepancy. Therefore, a role of non-coding genes was considered for further examinations. Because miRNAs are known as post-transcriptionally acting fine-tuners of gene expression (Schratt 2009a), efforts were focused on miRNAs for their involvement in cortical synaptic loss in PDGF mice.

DIFFERENTIAL EXPRESSION OF THE MIRNA 183/96/182 CLUSTER IN THE PDGF A-SYNUCLEIN MOUSE MODEL AT 2 MONTHS OF AGE

Potentially dysregulated post-transcriptional modifications could explain the discrepancy observed between the transcriptomic and proteomic changes in PDGF mice at 3 months of age. Therefore, cortical miRNA expression changes were analysed in 2-month, 3-month and 4-month-old mice, representing time points before, at and after the onset of cortical synapse loss.

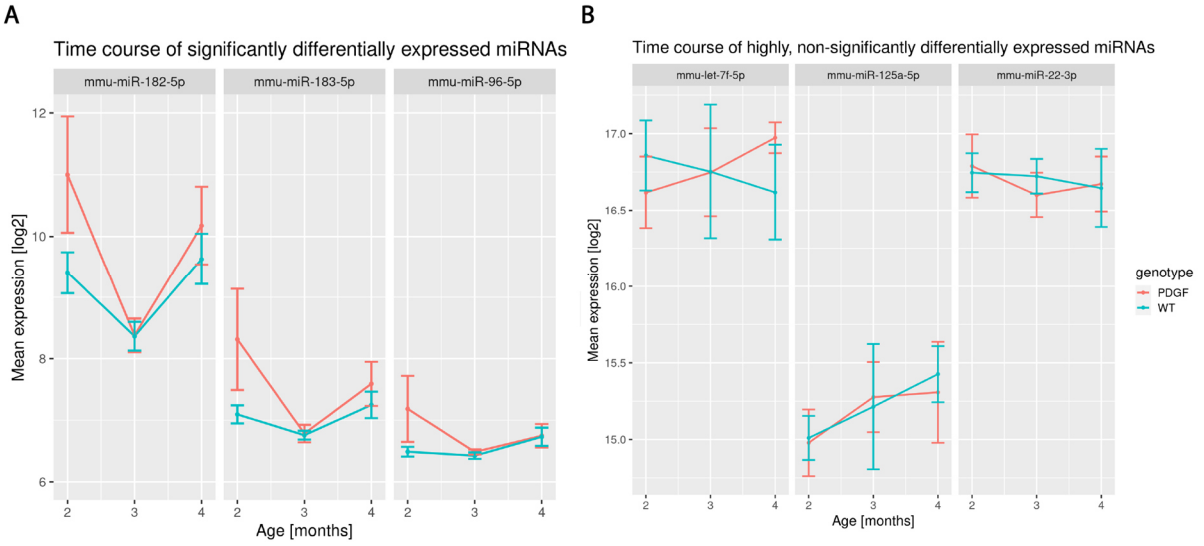

Figure 20: Mean expression levels on log2 scale of significantly differentially expressed miRNAs in 2-month, 3-month and 4-month-old PDGF and WT mice (A). Mean expression levels of highly, non-significantly differentially expressed miRNAs in 2-month, 3-month and 4-month-old PDGF and WT mice (B). Error bars represent standard error of the mean.

The miRNA-Seq analysis revealed a total of 443 expressed miRNAs. Out of these genes, three out of four miRNAs were identified to be significantly differentially expressed at 2 months of age, namely mmu-miR-182-5p, mmu-miR-183-5p and mmu-miR-96-5p (Figure 20 A). These miRNAs show a significantly higher expression in 2-month-old PDGF mice compared to WT mice. Upon high miRNA expression levels in 2-month-old mice, a drop in expression levels in both, PDGF and WT mice was observed from 2-month to 3-month-old mice. This drop was observed for all three differentially expressed miRNAs. At 3 months of age, no significant difference in expression could be observed anymore. Further on, the expression levels of miRNAs increased again from 3 to 4-month-old mice, however remained non-significantly different between PDGF and WT mice. Nevertheless, a drop of miRNA expression between two and three-month-old mice was not observed in other highly, but non-differentially expressed miRNAs (Figure 20 B), suggesting this phenomenon to be biological rather than a technical artefact.

Intriguingly, the three differentially expressed miRNAs were found to be in close proximity to each other on the murine chromosome 6qA3, known as miRNA 183/96/182 cluster (Xu et al. 2007; Dambal

et al. 2015; Zhou et al. 2021). Furthermore, this miRNA 183/96/182 cluster was reported to be evolutionary highly conserved across species as indicated by almost identical seed sequences (Lim et al. 2003; Pierce et al. 2008; Dambal et al. 2015). Interestingly, a knockout of mmu-miR-183 leads to retinal degeneration characterized by less prominent ribbon synapses of photoreceptors (Lumayag et al. 2013) and hsa-miR-96 was found dysregulated in cortical post-mortem tissue of patients diagnosed for synucleinopathy subtype MSA (Ubhi et al. 2014).

In summary, the miRNA 183/96/182 cluster was identified to be significantly higher expressed in 2-month-old PDGF versus wild type mice. At the presumed onset of cortical synaptic loss in 3-month-old PDGF mice, a drop in expression of all three miRNAs was observed in both genotypes. This drop resulted in similar expression levels between both genotypes, which persisted in 3 and 4-month-old mice.

Subsequently, the expression of the evolutionary conserved miRNA 183/96/182 cluster was assessed in human cortical post-mortem tissue to explore the translatability of this finding.

DIFFERENTIAL MIRNA 183/96/182 CLUSTER EXPRESSION CANNOT BE RECAPITULATED IN HUMAN CORTICAL POST-MORTEM TISSUE

The usage of murine model systems in the context of fundamental research has achieved great success in understanding essential disease-associated pathological and molecular mechanisms as well as causal relationships in synucleinopathies. However, murine model systems are highly artificial models. The PDGF mice constitutively overexpress the human *SNCA* gene, while the endogenous *Snca* gene is physiologically regulated (Masliah et al. 2000). In contrast, human patients diagnosed for synucleinopathies with alterations of *SNCA* predominantly show genetic mutations in the *SNCA* loci or copy number variations as duplications of triplications of the *SNCA* gene (Eriksen et al. 2005). Therfore, the relevance of murine findings is limitted in its potential to be translated to human-relevant context (compare with Figure 21).

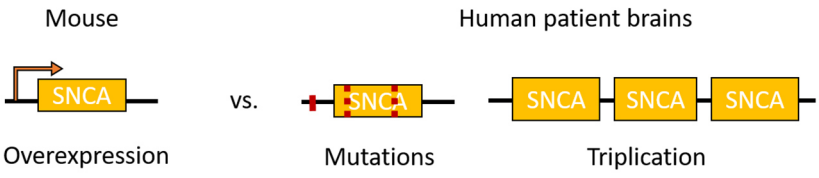

Figure 21: Schematic illustration of SNCA gene in murine mouse model versus human patient brains. PDGF mouse models systems overexpress human SNCA under a constitutive active promoter. Instead, genomic alterations of the SNCA loci in human patients are linked to mutations in the genomic loci of SNCA or copy number variations as duplications of triplications of SNCA.

In order to investigate the miRNA 183/96/182 cluster expression changes in human, RNA was isolated from human cortical cryofrozen tissue of synucleinopathy cases (Braak 1-6), reverse transcribed into cDNA and analysed for specific miRNA expression (Figure 22). Surprisingly, almost no expression of any of the miRNAs of the miRNA 183/96/182 cluster was identified in any of the seven different tissues tested. However, expression of endogenous "housekeeping" hsa-miR-191 and hsa-miR-423 was detected in each tissue. In summary, miRNA 183/96/182 cluster expression could not be detected in human cortical tissue of synucleinopathy patients.

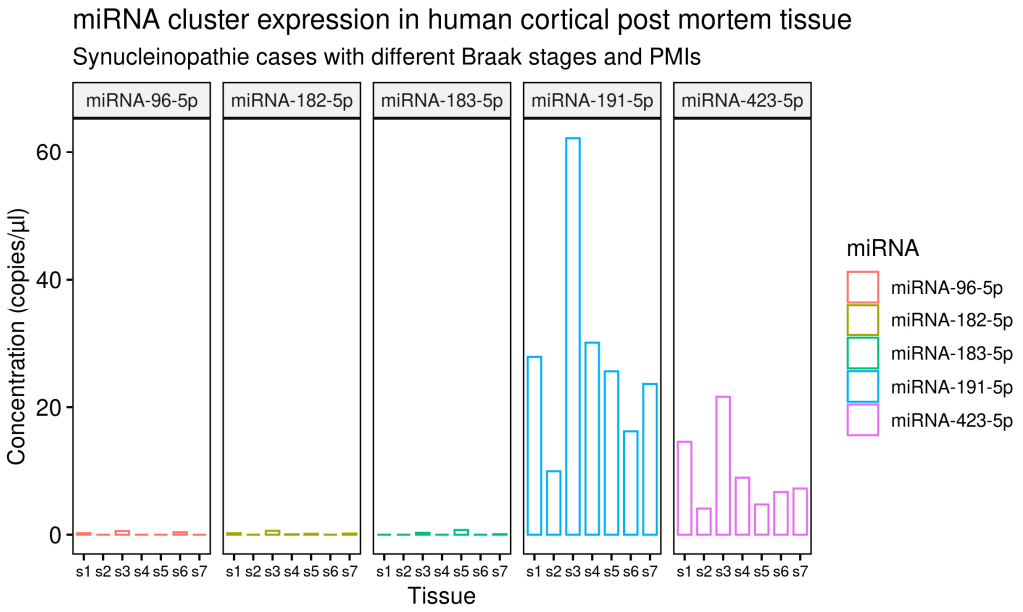

Figure 22: miRNA 183/96/182 cluster expression in human cortical post-mortem tissue of synucleinopathy cases. No expression was observed for any miRNA of the miRNA 183/96/182 cluster in seven different human cortical post-mortem tissues. Expression of control endogenous miRNA was observed in each tissue tested. A list with LBD Braak stages and PMIs for each sample is provided in material and methods. cDNA input: 5 µl of a 1:100 dilution of miRAMP reaction product (with initially 0.1 ng RNA input). Abbreviation: LBD braak - Lewy body disease Braak stages, s1 through s7 - human cortical synucleinopathy tissue cases 1 through 7, PMIs - post-mortem intervals.

Significantly different expression of the miRNA 183/96/182 cluster was observed only in young PDGF mice and before the onset of behavioural symptoms. Therefore, new model systems to investigate early molecular changes in a human-relevant context were required for investigating the role of the miRNA 183/96/182 cluster.

IPSC-DERIVED AST AND CAS CEREBRAL ORGANOIDS AS A MODEL SYSTEM FOR SYNUCLEINOPATHIES

To investigate murine findings in a human relevant context, existing conventional cellular models predominantly rely on overexpression of the transgene of interest (Eriksen et al. 2005) and do not recapitulate the genomic architecture in a disease-relevant context. The emergence of reprogramming technology allowed the generation of human-derived iPSCs carrying the genetic background of disease patients (Takahashi & Yamanaka 2006). This provides a powerful tool for investigation and translation of murine findings to human genetic alterations.

To investigate the effect of *SNCA* gene dosage in a human context, Devine and colleagues (Devine et al. 2011) generated two iPSC cell lines from fibroblast cultures derived from a *SNCA* triplication patient and an unaffected relative. The female donor carrying the *SNCA* triplication was first mentioned in 1998, where the Iowan kindred was described with a family history of early-onset Parkinsonism and dementia (Muenter et al. 1998; Gwinn et al. 2011). The generated *SNCA*-triplication iPSCs (herein referred to as AST - α-synuclein triplication) were successfully differentiated into midbrain dopaminergic neurons, recapitulating doubled α-synuclein protein expression levels compared to the generated control iPSC cell line with a normal copy number of *SNCA* gene (Devine et al. 2011).

In a follow-up publication from 2019, the authors used the CRISPR/Cas9 technology to generate iPSC cell lines corrected for a normal copy number of genomic *SNCA*, as well as genomic deletion of *SNCA* (Chen et al. 2019). Using this technology, the AST cell line from 2011 was used to "erase" additional *SNCA* alleles, leading to a genomically identical iPSC cell line with normal copy numbers of *SNCA*. This isogenic-corrected AST cell line is herein referred to as CAS (corrected α-synuclein triplication). Both cell lines, AST carrying a triplication of *SNCA*, as well as isogenic CAS with the corrected copy number of *SNCA*, were used as model systems in this thesis.

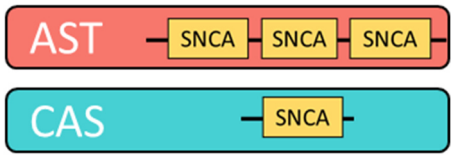

Figure 23: Schematic overview of SNCA copy number difference. Abbreviations: AST - α-synuclein triplication; CAS - corrected α-synuclein triplication.

QUANTITATIVE GENOMIC GENOTYPING OF AST AND CAS CELL LINES

AST and CAS cell lines were genotyped to verify the copy number difference of the *SNCA* gene on the genomic DNA. Therefore, quantitative genomic PCR assessing the copy number of *SNCA* exon 1 and SNCA exon 4 was carried out as described before (Devine et al. 2011). The CRISPR/Cas9-induced correction used a gRNA targeting the region of the *SNCA* exon 1, which lead to a deletion of the genomic region of the first exon only, leaving the *SNCA* exons downstream unaffected. Deletion of the first coding exon resulted in successful inhibition of *SNCA* gene expression (Devine et al. 2011; Chen et al. 2019). Therefore, *SNCA* exon 4 was expected to show four copies of genomic exons, with the triplication of *SNCA* located on one allele (Devine et al. 2011) in both cell lines. With the gRNA-induced cut in *SNCA* exon 1, only two copies from both alleles were expected in the corrected cell line. The copy number of *SNCA* was normalized to ß2-microglobulin (B2MG) representing a normal set of genes with one gene on each allele. Relative to B2MG, quantitative genomic PCR indicated four copies of *SNCA* exon 1 and four copies of *SNCA* exon 4 for the AST cell line. In contrast for the CAS cell line, two copies of *SCNA* exon 1 and four copies of *SNCA* exon 4 confirm the genomic deletion of two of the four genes (Figure 24).

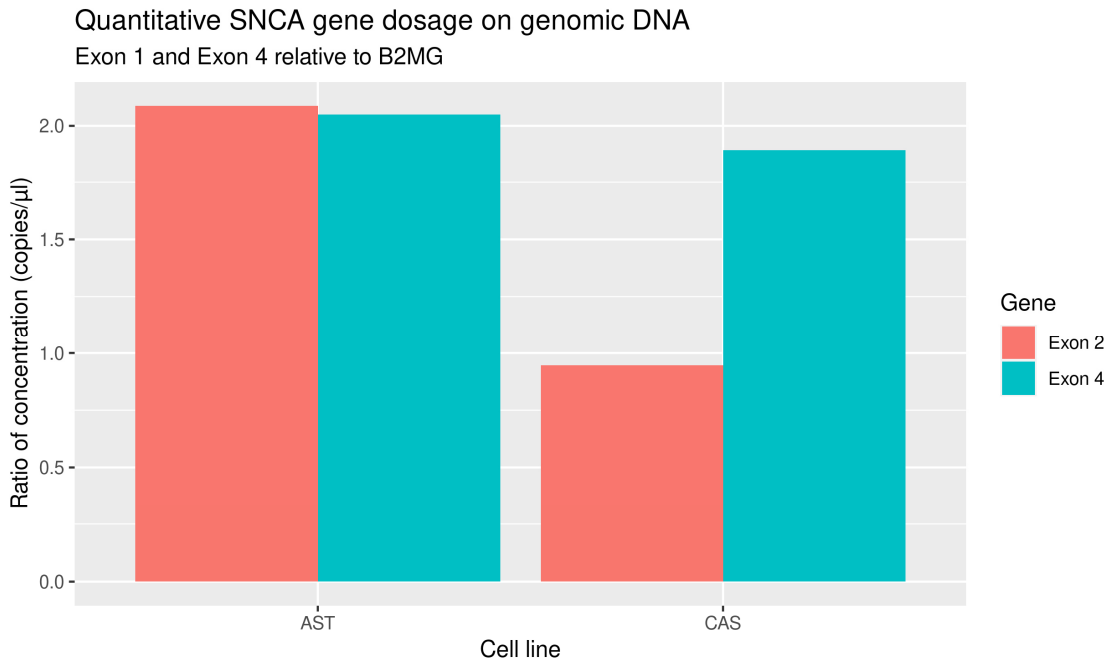

Figure 24: Quantitative genomic PCR for *SNCA* exons 1 and exon 4 relative to gene dosage of B2MG in AST and CAS cell line. Relative expression of SNCA exon 1 and SNCA exon 4 is depicted relative to B2MG (ß2-microglobulin) expression.

AST and CAS iPSCs are genetically identical and only differ in their *SNCA* copy number (Figure 24 and Devine et al. 2011, Chen et al. 2019). Although providing a human genetic background, conventional human cell culture systems lack cellular diversity, cell-to-cell contacts and the complex spatial

organization present in the brain environment. To address differences induced by *SNCA* overexpression with human genetic background in a more complex system, cortical organoids (COs) were generated from AST and CAS iPSC cell lines. The COs were generated as described in material and methods and were harvested for characterization at six time points, every 20 days from day 20 onwards.

DIFFERENCES IN *SNCA* GENE AND A-SYNUCLEIN PROTEIN EXPRESSION IN AST AND CAS COS

In the original publication from 2011, AST iPSCs differentiated into dopaminergic neurons showed a significant increase in both, *SNCA* (gene) and α-synuclein (protein) expression compared to an unaffected relative (Devine et al. 2011). Consequently, it was investigated if a significant difference in expression of *SNCA* and α-synuclein was also observed during AST and CAS cortical organoid differentiation (Figure 25). Three organoids per harvesting time point and genotype were formalin-fixed, paraffin-embedded, and stained for the expression of α-synuclein at different time points. Of note, the interpretation of this analysis is limited by low sample sizes especially at day 60 and day 80.

Generally, expression of α-synuclein in AST and CAS organoids showed a steady increase in expression until day 80 (Figure 25 A). However, this tendency showed no significant difference, and AST COs showed significantly more α-synuclein expression compared to CAS COs only at day 40. Furthermore, α-synuclein expression seemed to decline at day 120 for both AST and CAS COs.

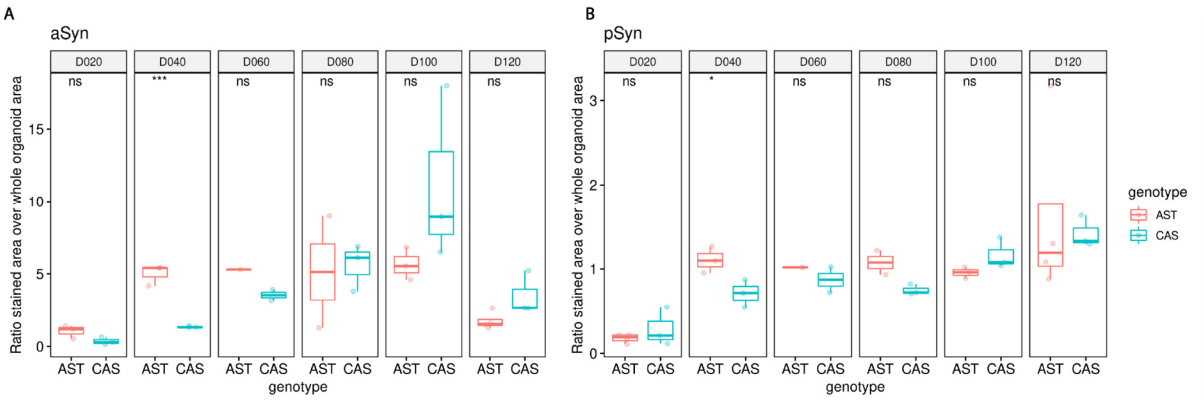

*Figure 25: Analysis of α-synuclein expression (A) and phospho-α-synuclein expression (B) relative to the whole organoid slice in AST and CAS cortical organoids at six different time points. n= 3 organoids per time point and cell line (day 60: AST: n=1, CAS: n=2, day 80: AST: n=2, day 120: AST: n=4); statistical analysis: two-sided anova; error bars: SE; p-value: p≤0.05 = *, p<0.01 = **, p<0.001 = ***. Abbreviations: aSyn - α -synuclein, pSyn - phospho-α-synuclein.*

PD pathology is accompanied by post-translational modifications of α-synuclein, and phosphorylation of α-synuclein has been reported to enhance its toxicity and potential to self-aggregate (Fujiwara et al.

2002; Anderson et al. 2006; Burré et al. 2018). Therefore, the expression of phosphorylated α-synuclein was assessed during the course of AST and CAS CO differentiation. Detected expression levels were relatively comparable during the time course with a shallow increase until day 120. However, overall expression levels were very low and a significant difference between AST and CAS COs was observed only at day 40 in AST COs (Figure 25 B).

Following the characterization of α-synuclein, the expression of *SNCA* (RNA) was investigated in the AST and CAS COs (Figure 26). At day 20, similar expression levels of *SNCA* were observed in both COs. At day 40, significantly more *SNCA* expression was detected in AST COs. Surprisingly, expression of *SNCA* RNA showed a reduction in AST COs from day 60 onwards, while its expression in CAS organoids remained significantly higher from day 60 through day 80 and day 100, and a tendency but not significant higher expression was observed at day 120.

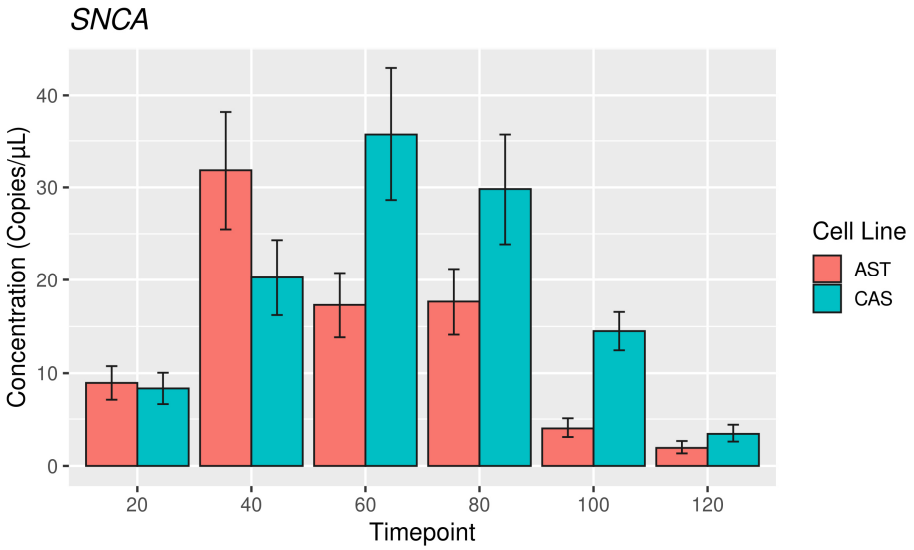

Figure 26: Expression of SNCA RNA in AST and CAS cortical organoids during the time course day 20 until day 120. n= 5 organoids per time point and cell line, statistical analysis: two-sided ANOVA, error bars: Poisson 95 % confidence interval based on direct quantification through ddPCR.

In summary, AST COs show significantly more RNA and protein expression of α-synuclein at day 40. However, while the levels of α-synuclein protein remain comparable until day 120, RNA expression of *SNCA* was significantly decreased at day 60, day 80, and day 100 in AST COs.

PHENOTYPIC SIZE DIFFERENCE OF AST AND CAS IPSCS DIFFERENTIATED INTO CEREBRAL ORGANOIDS

The unexpected significantly reduced expression of *SNCA* during the late time points suggested to investigate how *SNCA* copy number variation could potentially influence development or neuronal maturation. Interestingly, already during the cultivation of AST and CAS COs, a phenotypic size difference was observed between the two genotypes (Figure 27 and Figure 28). For each harvesting time point, the area of the organoid in relation to the well size was quantified for each cell line (Figure 27). After 20 days in culture, AST organoids were significantly bigger in size compared to CAS organoids and little size variability was observed within each organoid group. After 40 days of culture, the AST and CAS organoids were comparable in size. During the course of time, both COs continued to grow, however AST CO growth rate remained reduced compared to CAS CO growth. Starting from day 60 onwards until day 120, CAS COs remained significantly bigger in size compared to AST COs. Both, CAS and especially AST COs showed a high variability of the organoid size for the late time points, yet the size difference remained significant between AST and CAS for day 60, day 80, day 100 and day 120 (Figure 27).

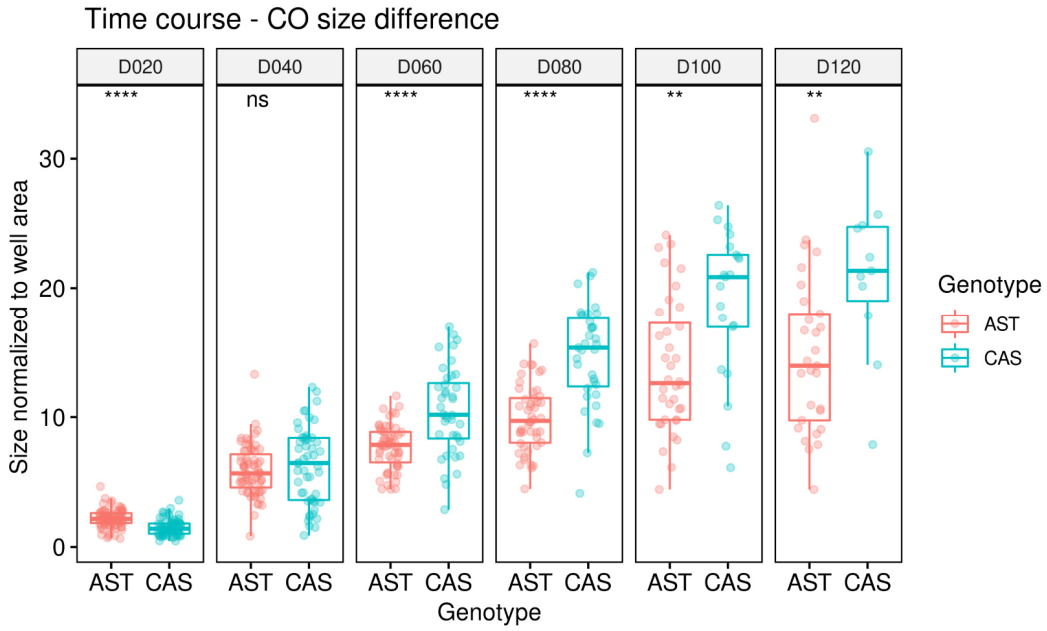

Figure 27: Size difference of AST and CAS COs at the six different harvesting time points. Y-axis depicts size of organoid relative to the well area of the six-well plate it was cultured in (no unit). Statistical test used: Two-sided ANOVA. p-values: D20: p= 1e^{-9}; D40: p= 0.42; D60: p= 4.9e^{-7}; D80: p= 1.1e-9; D100: p= 0.0013; D120: p= 0.0089.

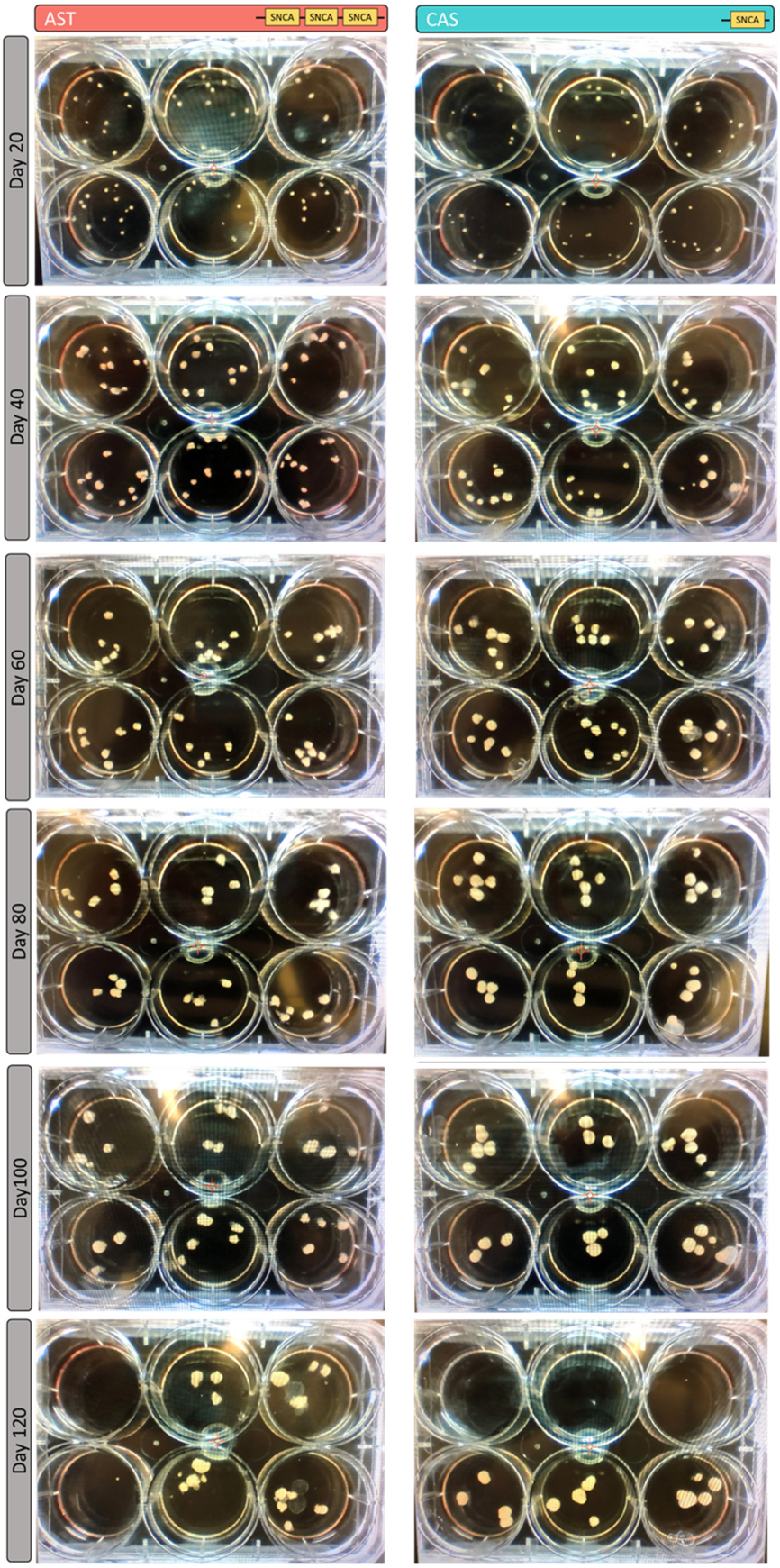

Figure 28: Representative images of AST and CAS COs visualizing phenotypic size difference of COs cultured in 6-well cell culture vessel at all six different harvesting time points. Diameter of one 6-well: 3,496 cm. Fused organoids of both genotypes appeared throughout the cultivation time.

AST AND CAS COS SHOW NO DIFFERENCE IN NEURONAL MATURATION OR DIFFERENTIATION BASED ON IHC ANALYSIS

For basic characterization of maturation differences between the AST and CAS COs, three organoids per harvesting time point were PFA-fixed and paraffin embedded for further analysis and are herein referred to as FFPE-COs (formalin-fixed, paraffin embedded cortical organoids). All FFPE-COs were stained for neuronal maturation and cell type specific markers, namely α-synuclein, GFAP, Ki67, MAP2, Nestin, NeuN and synaptophysin (Figure 29, Figure 30, Figure 31).

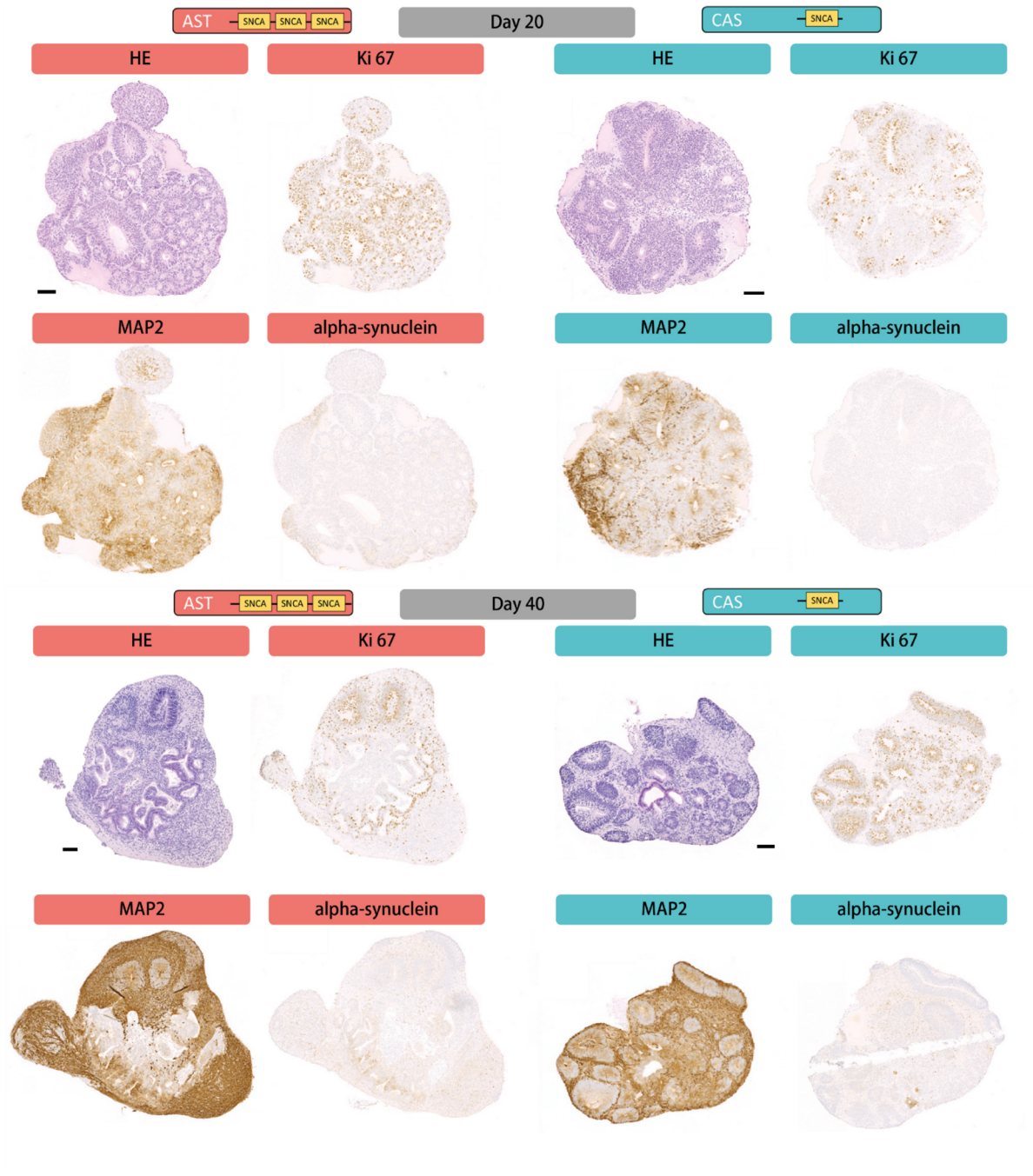

Figure 29: Representative images of AST and CAS COs at day 20 and day 40 stained for selected markers. HE - overview; Ki6 proliferation marker; MAP2 - neuronal marker; alpha - α-synuclein. Scale bar: 100 µm.

At day 20, the HE overview stain of AST and CAS COs exhibited ventricular-like structures across the whole organoid (Figure 29). Staining with the proliferation marker Ki67 indicated proliferative cells in the cores of these ventricular zones. Neuronal maturation already after 20 days in culture was observed by a positive signal for MAP2 marker, sparing out the ventricular zones with proliferative cells. Sparse labelling of α-synuclein confirmed early protein expression in both COs. At day 40, the HE overview staining still resembled the ventricular like structures for both genotypes, as well as ongoing proliferation. More intense MAP2-staining emphasised ongoing neuronal maturation, together with more intensive expression of α-synuclein for AST and CAS COs (Figure 29).

At day 60, ventricular structures were still observed for both genotypes (Figure 30). The representative AST CO at day 60 showed a lateral structure, reminiscent of the choroid plexus. Both genotypes stained positive for post-mitotic marker NeuN, especially in the periphery of the organoids. MAP2 and α-synuclein were both more intensively stained sparing out the ventricular structures. After 80 days in culture, only less prominent ventricular zones with the HE stain were observed in both genotypes. Neuronal nature of organoids was further indicated by positive stain for NeuN and MAP2. In addition, an intensive α-synuclein expression was observed in both COs. The representative AST CO at day 80 shows a fused organoid. However, first traces of absence of MAP2-positive signal in the core of the organoid was observed in both organoid genotypes at day 80, and is clearly visible in the CAS CO (Figure 30).

After 100 days in culture, the HE overview staining did not resemble ventricular structures anymore and represented a rather uniform and homogenous cell composition (Figure 31). Expression of the neuronal marker MAP2 and α-synuclein remained more restricted to the periphery of the organoid, leaving a bigger core of unstained tissue in both genotypes. However, positive signal for the synaptic marker synaptophysin was still observed in both genotypes. At 120 days in culture, the HE overview stain indicated a very homogeneous cell composition. Positive marker expression of MAP2, α-synuclein and synaptophysin was predominantly restricted to the outer periphery of the organoid (Figure 31).

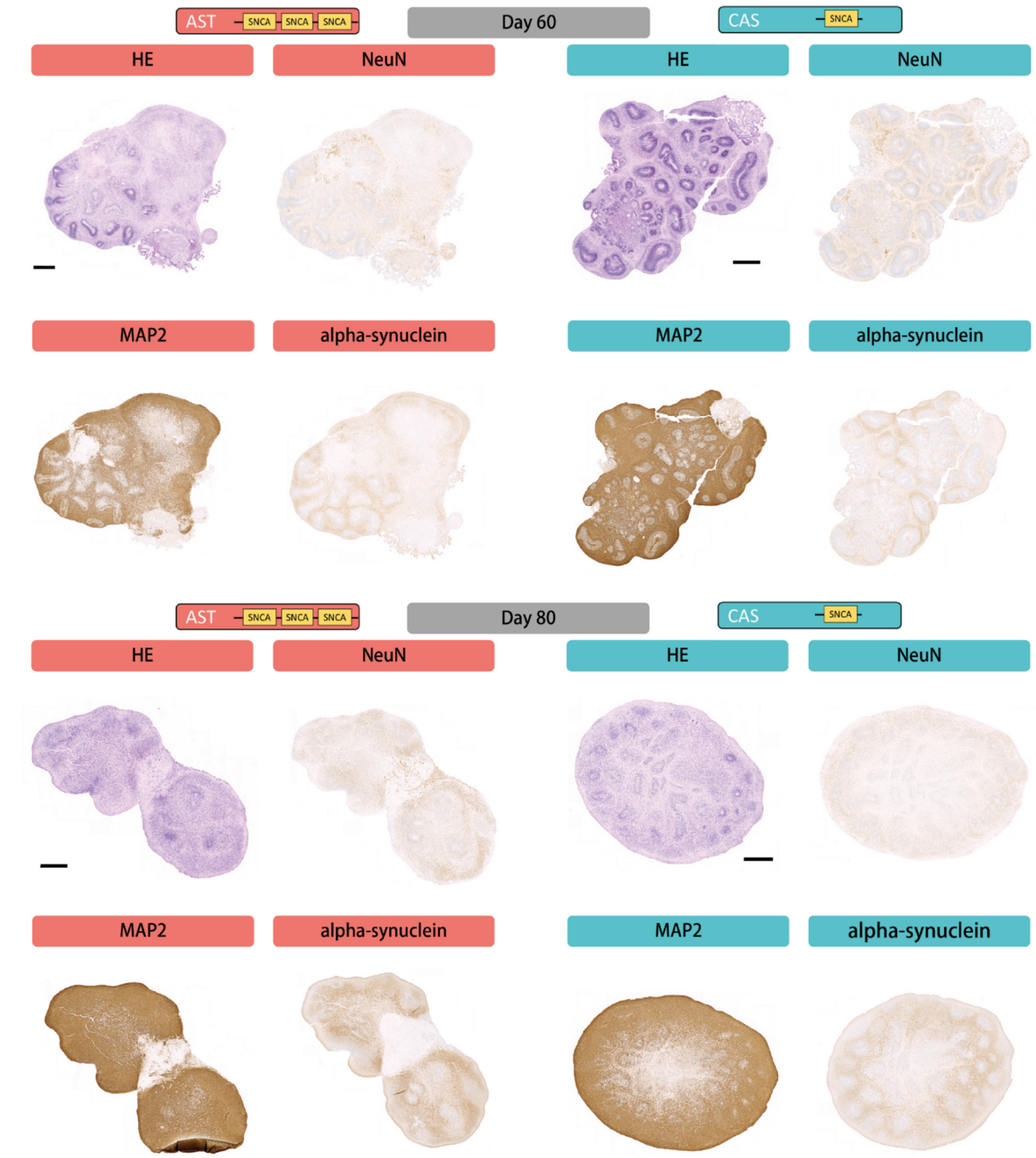

Figure 30: Representative images of AST and CAS COs at day 60 and day 80 stained for selected markers. HE - overview; MAP2 - neuronal marker; NeuN - post-mitotic neuronal marker; alpha - α-synuclein. Scale bar: 500 µm.

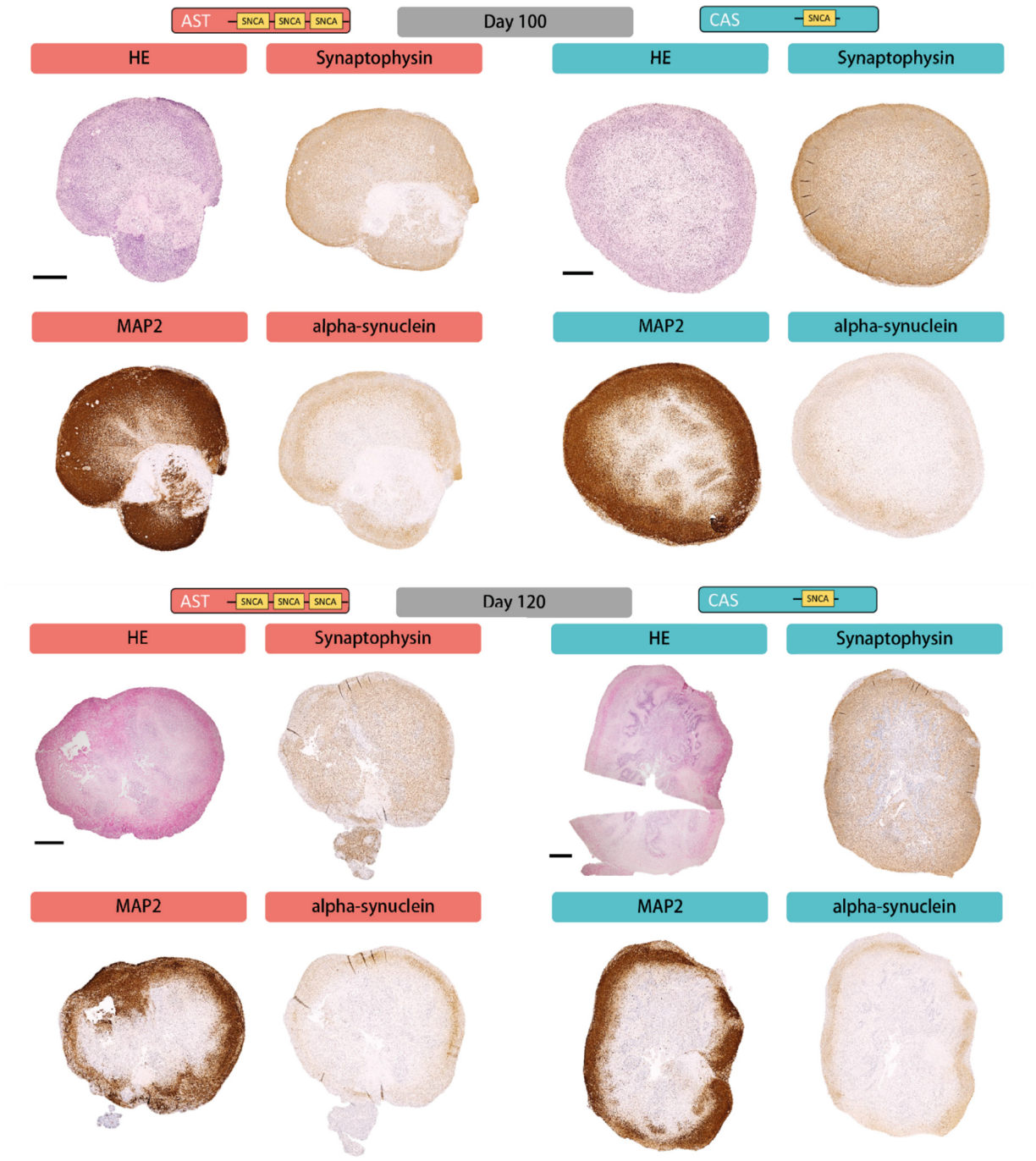

Figure 31: Representative images of AST and CAS COs at day 100 and day 120 stained for selected markers. HE - overview; MAP2 - neuronal marker; synaptophysin - synaptic marker; alpha - α-synuclein. Scale bar: 500 µm.

To quantify and investigate potential differences in marker expression in FFPE-COs, each organoid with the respective staining was quantified for its area of H-DAB positive staining versus the negative staining area of the organoid (Figure 32).

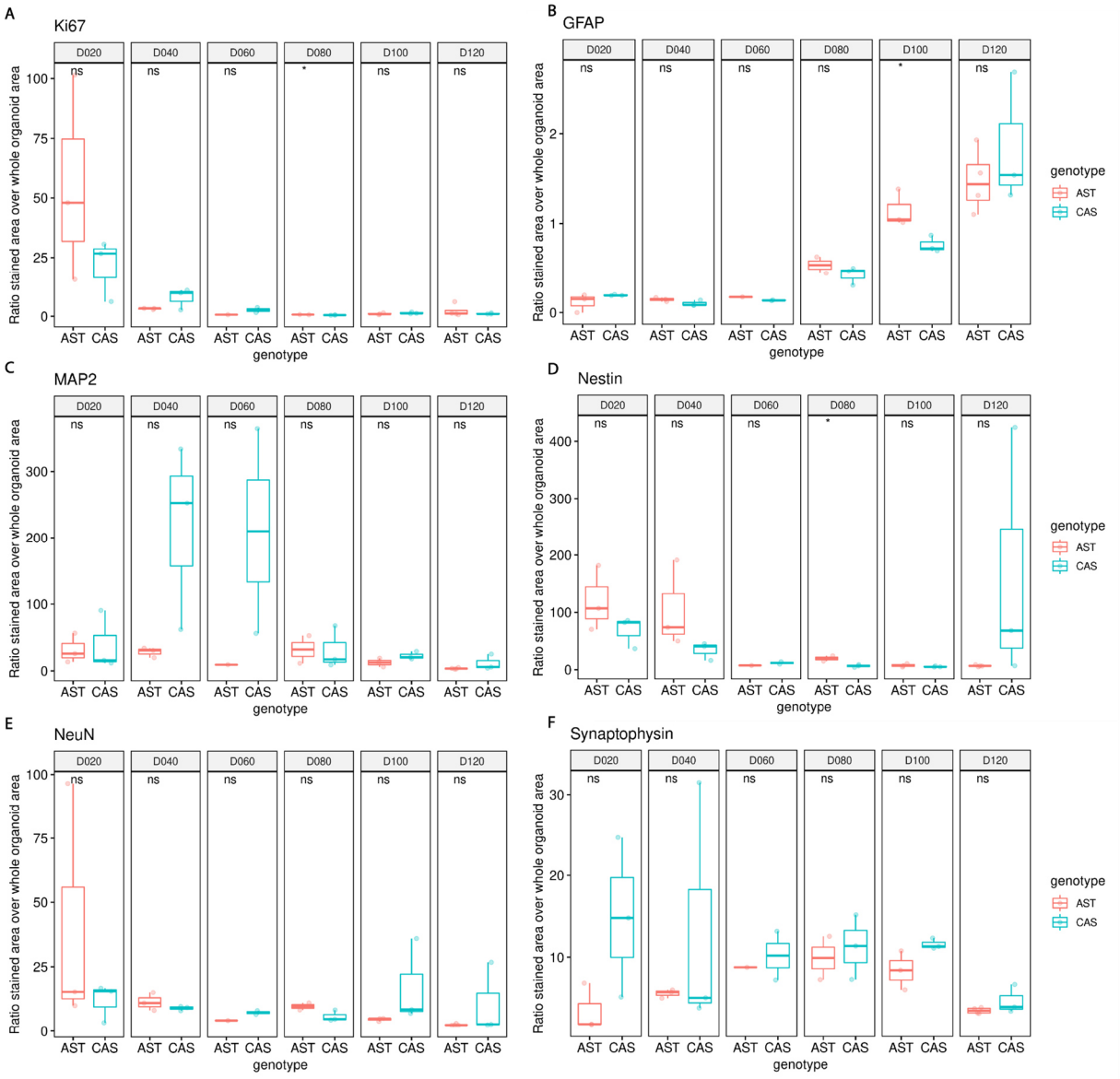

*Figure 32: Analysis of marker expression relative to the whole organoid slice in AST and CAS cortical organoids at six different time points. Proliferation marker Ki67 (A), glial protein marker GFAP (B), neuroepithelial marker (MAP2), immature neurons marker (Nestin), post-mitotic neurons marker (NeuN) and synaptic marker (synaptophysin). n= 3 organoids per time point and cell line (day 60: AST: n=1, CAS: n=2, day 80, AST: n=2, day 120: AST: n=4. Thus, data from time point D60 and D80 have to be considered with caution); statistical analysis: two-sided ANOVA; error bars: SE; p-value: p≤0.05 = *, p<0.01 = **, p<0.001 = ***.*

The proliferation marker Ki67 showed high relative expression in AST and CAS COs during the first days in culture, but decreased with differentiation progression. No significant difference was found between the two groups during the course of time (Figure 32 A).

The GFAP marker showed an increase in expression in both AST and CAS COs only starting from day 80 onwards. Significantly more GFAP expression was observed in AST COs compared to CAS COs at day 100. Nevertheless, overall low marker expression was observed for GFAP (Figure 32 B).

Characterizing the neuronal maturation of the COs, the neuronal marker MAP2 was expressed already at day 20. It increased with its relative expression until day 40 with high variance in CAS organoids, and declined until day 120 for AST and CAS COs. No significant differences were observed between AST and CAS COs during the course of time (Figure 32 C).

The marker for maturing neurons, Nestin, showed a relatively consistent expression throughout differentiation, with a peak of expression during the early time points. A significant difference was observed only between AST and CAS COs at day 80, with higher Nestin expression in AST COs (Figure 32 D).

The post-mitotic neuronal marker NeuN showed comparable expression throughout differentiation, whereby its relative expression slightly declined until day 120. NeuN expression did not differ significantly during the course of time between AST and CAS COs, however showed high variance in AST at day 20, and in CAS at day 100 and day 120 (Figure 32 E).

Expression of the synaptic marker synaptophysin was steadily increasing during the course of time until it peaked at day 100, and declined until day 120. No significant difference in marker expression of synaptophysin was observed between AST and CAS COs. High variance was detected at day 20 and day 40 in CAS organoids and showed a tendency to a higher but no significantly different expression during these time points (Figure 32 F).

In summary, AST and CAS COs appeared to successfully undergo neuronal maturation based on this IHC quantification. However, no clear significant difference in maturation of differentiation caused by α-synuclein overexpression could be observed. Nevertheless, this analysis method has limited significance due to the high variability within organoids. After around 80 days in culture, the organoids started to form a necrotic core, indicated by lack of positive marker stain.

SYNAPTIC LOSS IN PDGF MICE CAN BE RECAPITULATED IN AST AND CAS COS

In the PDGF mouse model for Parkinson's Disease, overexpression of *SNCA* lead to cortical, glutamatergic synaptic loss at 3 months of age (Blumenstock et al. 2017; Blumenstock et al. 2019). It was therefore investigated if a change in synaptic density could be recapitulated in AST and CAS cortical organoids. In FFPE-COs, a tendency but not significantly higher expression of synaptophysin was observed in CAS COs during the course of time (Figure 32).

It was therefore investigated if the *SNCA* copy number difference in AST and CAS COs had an influence on specifically glutamatergic synaptic density after varying times in culture. Therefore, four COs per time point per cell line were harvested, PFA-fixed and cryopreserved for immunofluorescent staining analysis. Organoids were stained for the nuclei marker DAPI, the neuronal marker MAP2, the glutamatergic pre-synaptic marker VGLUT1 and the post-synaptic marker PSD95. Images were analysed for their density of marker expression in the periphery and core of the organoid (Figure 33). A representative overview of the synaptic staining in AST and CAS COs is provided below (Figure 34).

A steady increase in protein expression during the course of time in AST and CAS COs was observed for the pre-synaptic glutamatergic marker VGLUT1. Interestingly, expression of VGLUT1 was significantly higher in CAS COs during all time points assessed. VGLUT1 expression in AST COs increased only slightly from day 20 to day 100, and seemed to be reduced at day 120. Instead, VLGUT1 expression in CAS COs seemed to steadily increase during the course of time. However, the variance of CAS organoids was showing overall more inconsistency, especially for the late time points (Figure 33 A).

The gene *SLC17A7* encodes for the protein VGLUT1, and is hereafter referred to as *VGLUT1*. The expression pattern of VGLUT1 protein correlated with the expression of *VGLUT1* RNA (Figure 33 C). Already at day 20, significantly more *VGLUT1* was observed in CAS COs. At day 40, RNA expression levels were comparable. However, from day 40 onwards, *VGLUT1* expression levels of AST COs were significantly lower than expression levels in CAS and remained overall rather low. In CAS COs, a peak of *VGLUT1* expression was observed at day 60, which declined during the course of time. At day 120, no significant difference between AST and CAS *VGLUT1* expression could be observed.

A similar increase in expression of the post-synaptic marker PSD95 was observed for AST and CAS COs (Figure 33 B). A significantly higher density of PSD95 marker expression was observed in CAS organoids at day 20 and day 40, and no significant difference was observed at day 60 and day 120. In contrast, at day 80 and day 100, significantly more PSD95 expression was observed in AST organoids. For both genotypes, a reduction in expression was observed at day 120 compared to day 100. Collectively, a relatively large variance of data points was observed for the PSD95 marker for all time points, especially for AST COs (Figure 33 B).

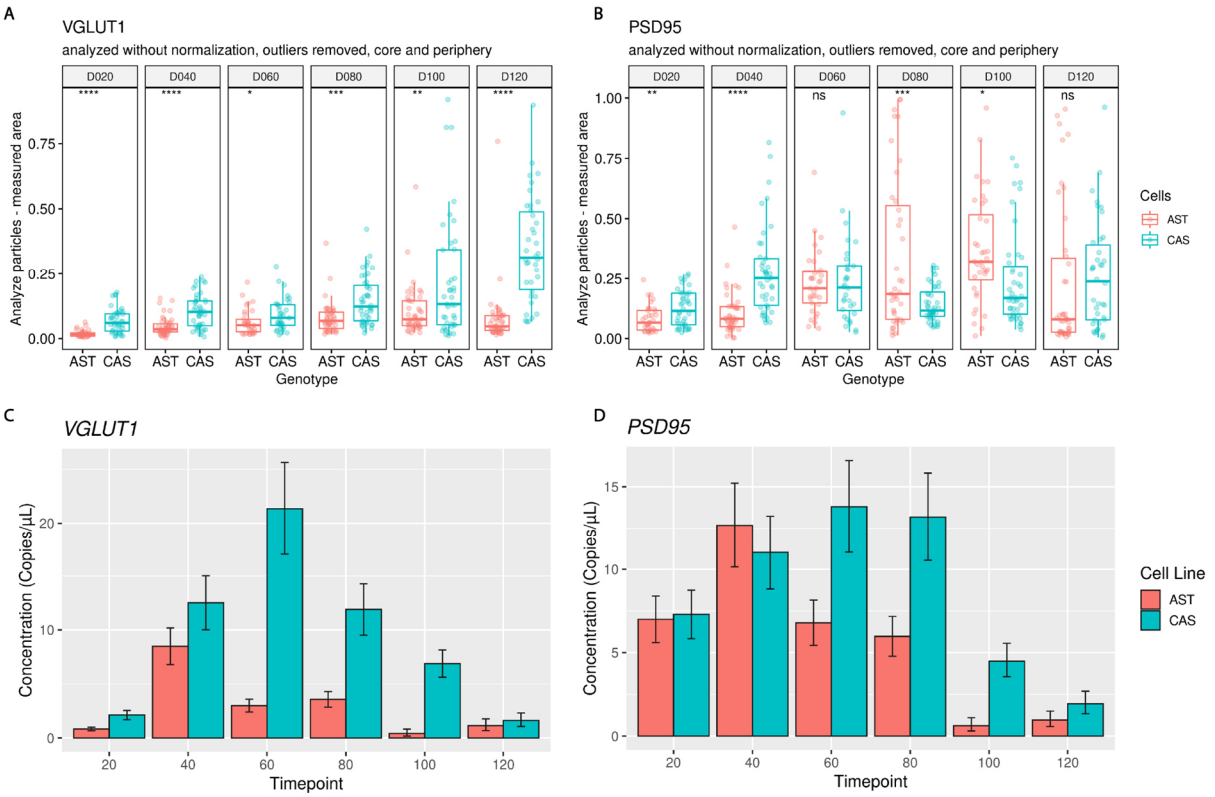

Figure 33: Quantification of synaptic marker expression in AST and CAS COs during the course of time. Pre-synaptic glutamatergic marker VGLUT1 (A,C) and post-synaptic marker PSD95 (B, D) were analysed for their IF protein expression (A, B) and RNA expression (C, D). For the IF-based protein quantification, values are depicted as analysed particles across the acquired image (within 200 µm of the edge and within the periphery). Statistical analysis of IF-analysis: two-sided ANOVA. n= 8 periphery images and 3 core images per CO, with 4 COs per cell line per time point (Exceptions: AST day 20 and day 60: n= 3 COs, CAS day 20: n= 3 COs). RNA expression analysis: n= 5 organoids per time point and cell line, error bars: Poisson 95 % confidence interval based on direct quantification through ddPCR. p-values: (A) D20: p= 1.6e^{-7}; D40: p= 1.4e^{-6}, D60: p= 0.032; D80: p= 0.00012; D100: p= 0.0042; D120: p= 3.2e^{-11}. (B) D20: p= 0.0092; D40: p= 1.9e^{-7}, D60: p= 0.85; D80: p= 0.00019; D100: p= 0.01; D120: p=0.57.

The gene *DLG4* encodes for the protein PSD95, and is hereafter referred to as *PSD95*. The expression pattern of *PSD95* differed in the RNA expression analysis (Figure 33 D). No significant difference in expression was observed at day 20 and day 40. From day 40 onwards, AST *PSD95* RNA showed reduced expression and remained significantly lower expressed compared to CAS COs. Only at day 120, expression levels of *PSD95* were comparable in AST and CAS COs. The peak of expression of *PSD95* was observed at day 60 in AST COs and at day 80 in CAS COs.

Nevertheless, AST and CAS COs appeared to have formed functional excitatory synapses as indicated by synaptic marker expression in close proximity to each other (Figure 35).

In summary, RNA and protein expression of the pre-synaptic, glutamatergic marker VGLUT1 appeared significantly reduced in AST COs during the course of time. The post-synaptic marker PSD95 seemed to be significantly lower expressed in AST COs during the early time points, while a reduction in RNA

expression was observed at later time points. Yet, differences in expression of RNA and protein levels were observed at day 80 and day 100 in AST and CAS COs.

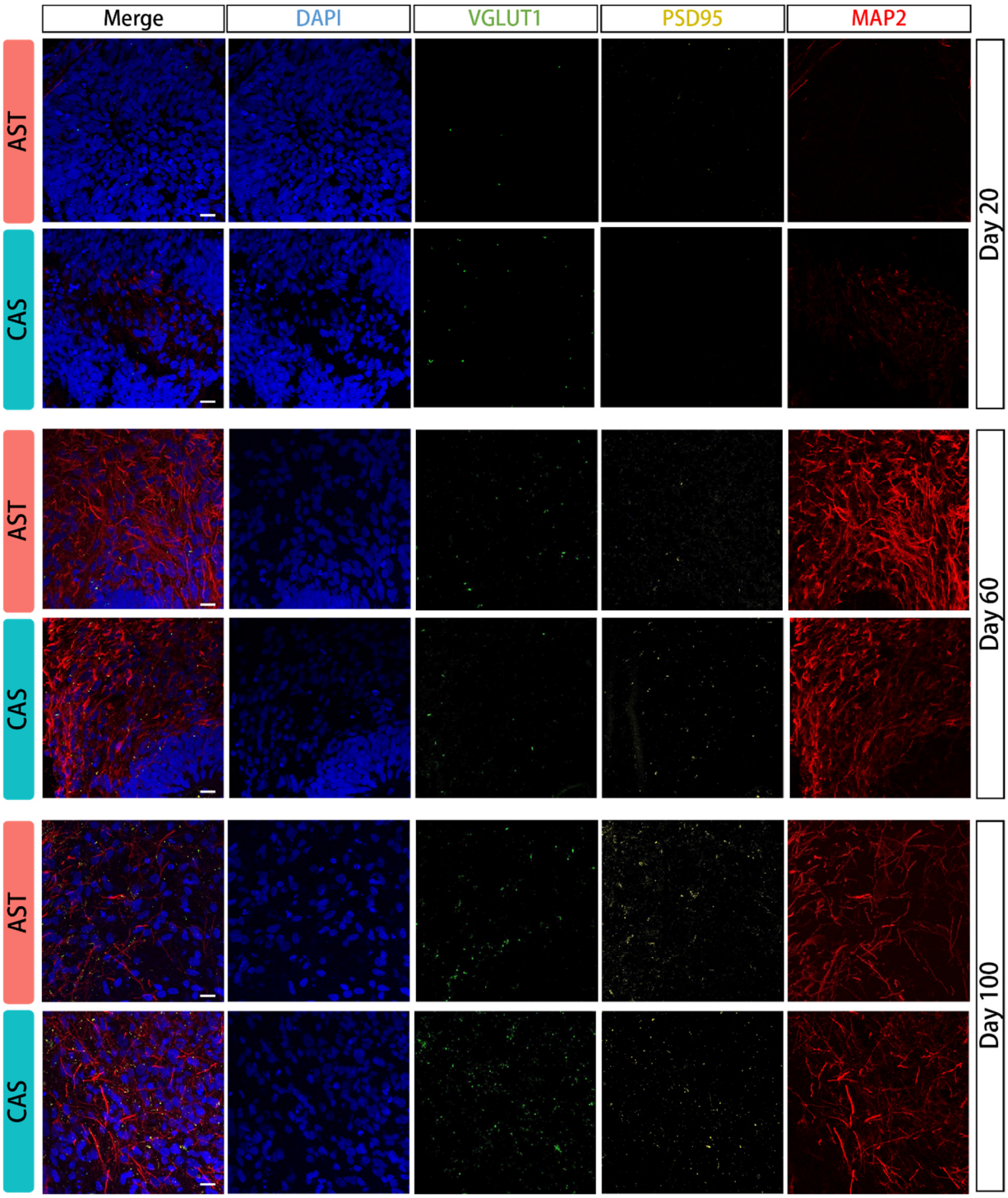

Figure 34: Representative overview of AST and CAS COs stained for synaptic marker expression. Synaptic marker expression is indicated by the pre-synaptic marker VGLUT1, the post-synaptic marker PSD95 and the neuronal marker MAP2. Images were acquired within 200 µm from the edge of the organoid. Scale bar: 20 µm.

Collectively, the cortical synaptic loss of VGLUT1-positive cells observed in the PDGF mouse model could be recapitulated in the AST and CAS model system. The significantly higher density of glutamatergic synapses in CAS COs appeared persistent throughout the course of time.

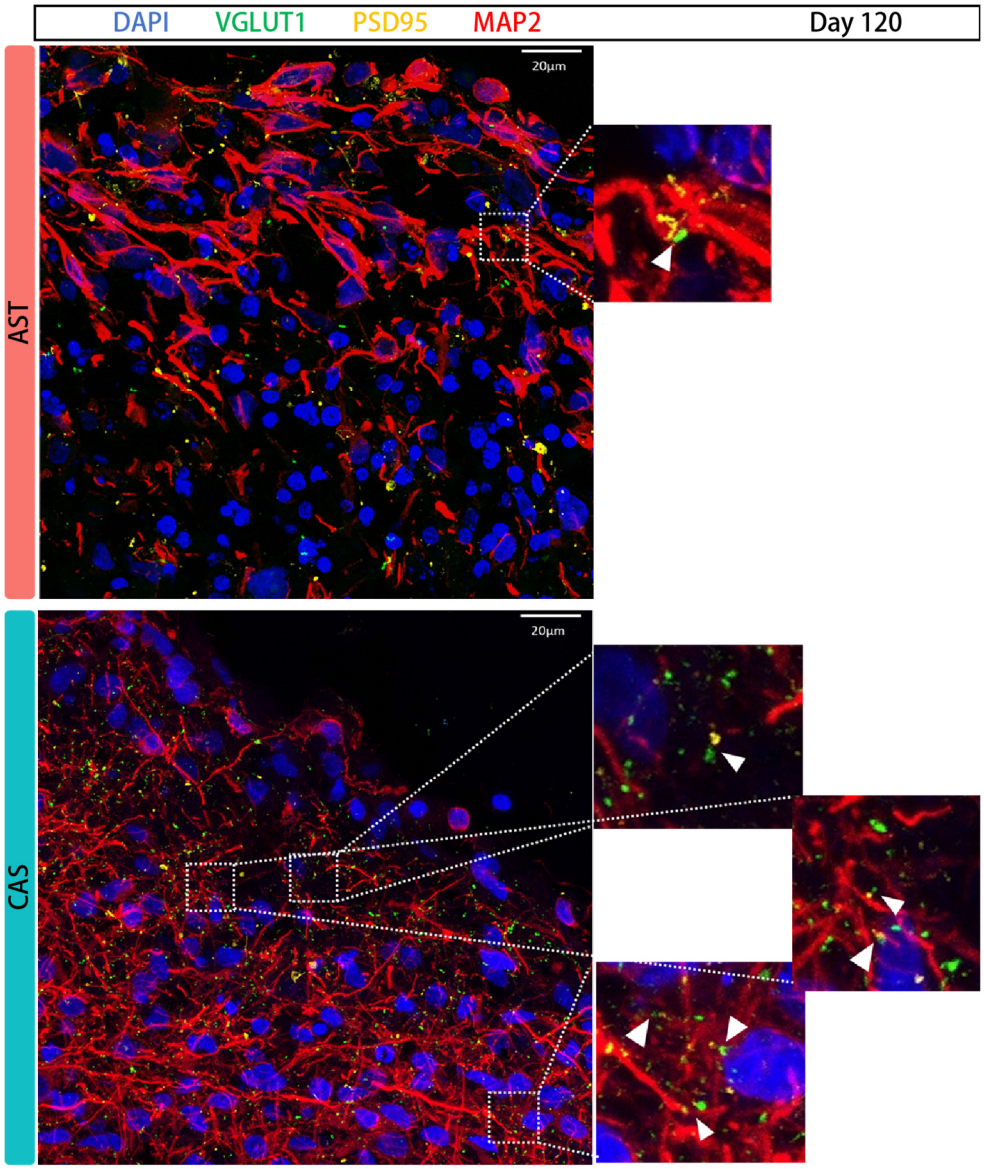

Figure 35: Representative synaptic marker expression in AST and CAS COs after 120 days in culture. Synaptic marker expression is indicated by the pre-synaptic marker VGLUT1, the post-synaptic marker PSD95 and the neuronal marker MAP2 and nuclear stain DAPI. Arrow heads point at pre and post-synaptic marker in close proximity to each other. Scale bar 20 µm.

MIRNA 183/96/182 CLUSTER DYNAMICS AND DIRECTIONALITY RECAPITULATED IN AST AND CAS COS

Characterization of AST and CAS organoids has shown complex maturation of cells into neuronal cell types along with the expression of synaptic markers. Therefore, it was investigated whether the miRNA 183/96/182 cluster expression observed in the murine PDGF models could be recapitulated in the AST and CAS CO model system with a human genetic background.

Thus, the expression of the miRNA 183/96/182 cluster was assessed in both AST and CAS organoids for six different time points using ddPCR (Figure 36). Indeed, all three hsa-miRNAs of the cluster showed a similar expression pattern across time: At day 20 and day 40, the miRNAs showed a significantly higher expression in the AST organoids compared to the CAS organoids. Between day 40 and day 60, the miRNA expression dropped in both genotypes and was significantly lower in AST COs compared to CAS COs. However, for AST organoids, the expression dropped below the expression levels at day 20, and showed a significant increase again at day 100 only. Instead, for the CAS organoids, the expression levels did not drop as much as in the AST organoids, and miRNA expression at day 60 was significantly higher in CAS compared to AST organoids and declined gradually until day 120.

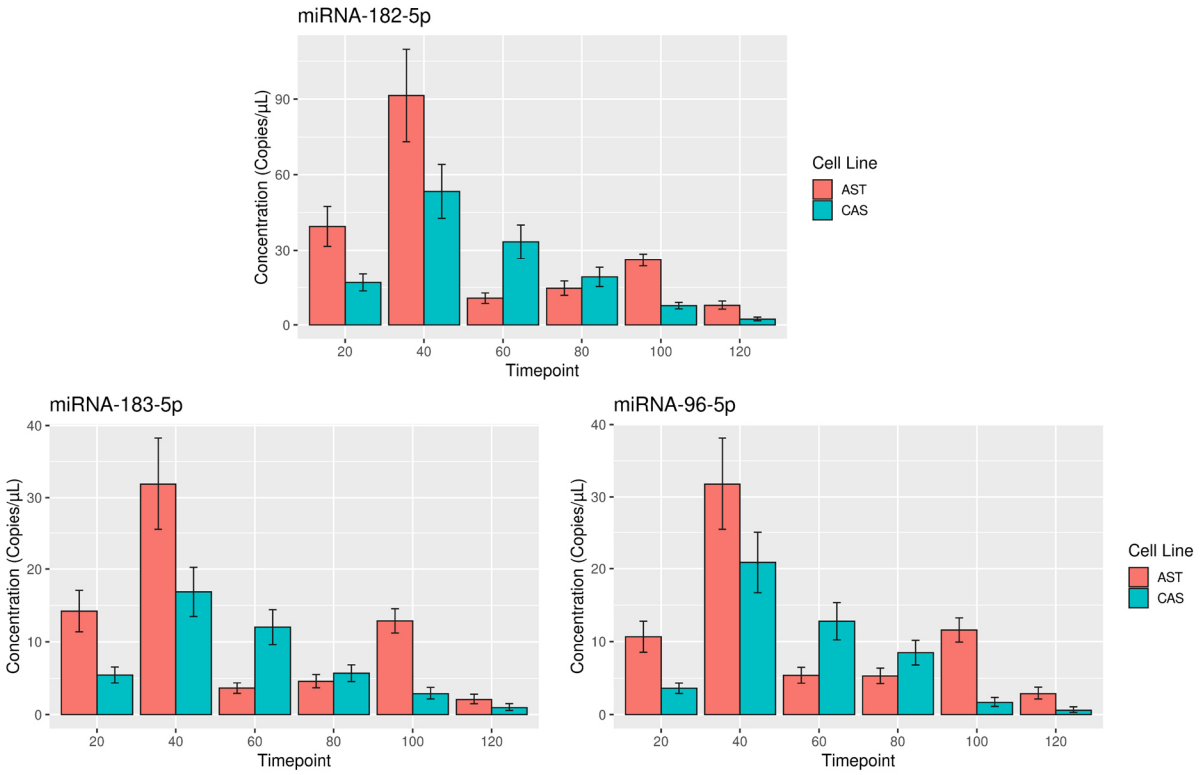

Figure 36: miRNA 183/96/182 cluster expression in AST and CAS cortical organoids at six different time points. n= 5 organoids per time point and cell line, error bars: Poisson 95 % confidence interval based on direct quantification through ddPCR.

Comparing this data set to the miRNA-Seq expression analysis in 2-month and 3-month-old PDGF mice demonstrated, that the significantly higher expression of the miRNA cluster in the *SNCA*

overexpression mouse model was recapitulated on the human side in the AST and CAS cortical organoids. Moreover, hsa-miR-182 was the highest expressed miRNA of the cluster, which was consistent with mmu-miR182 showing the highest expression in PDGF mice.

MIRNA 183/96/182 CLUSTER TARGETS EUKARYOTIC TRANSLATION ELONGATION FACTOR *EEF1A1* MRNA IN AST AND CAS IPSC DERIVED NEURONS

The significantly higher expression of the miRNA 183/96/182 cluster was observed in PDGF mice at 2 months of age. A drop in expression of the miRNA cluster was observed at 3 months, which is the presumed onset of cortical synaptic loss in PDGF mice (Blumenstock et al. 2017). Proteomic analysis of synaptosomes in 3-month-old PDGF mice revealed differential expression of proteins in PDGF mice compared to WT mice (Blumenstock et al. 2019). Since miRNAs can function as post-transcriptional regulators of gene expression (Schratt 2009a), reduced translation of their target genes into proteins would be expected. Hence, it was bioinformatically tested if the miRNA 183/96/182 cluster would bind mRNA of any of the synaptosome proteins seen as decreased in 3-month-old PDGF mice, namely *eEF1A1* and *Sprr2b*. In addition, the isoform *eEF1A2* was tested for potential miRNA binding sites, since the proteomic assay used by Blumentstock et al. might have been unable to differentiate between these two highly related isoforms. Using targetscan.org (Agarwal et al. 2015; McGeary et al. 2019), only one poorly conserved binding site was found for miRNA-182-5p on *eEF1A1* (human genome), and one poorly conserved binding site for miR-183-5p on *SPRR2B* (Table 9). No further binding sites were identified.

Table 9: Overview of bioinformatically predicted binding sites in the 3'UTR of genes for the miRNA 183/96/182 cluster miRNAs (human and mice) (targetscan.org, Release 8.0, September 2021).

Gene	miR183 sites		miR96 sites		miR182 sites	
	Human	Mouse	Human	Mouse	Human	Mouse
eEF1A1	0	0	0	0	1	0
eEF1A2	0	0	0	0	0	0
SPRR2b	1	0	0	0	0	0

Consequently, the bioinformatically predicted miRNA 183/96/182 cluster binding site was investigated using an *in vitro* pulldown based on Phatak & Donahue 2017.

Therefore, AST and CAS iPSCs were first differentiated into NPCs and subsequently into a mixed neuronal culture resembling the phenotype of synapses. Neurons after one week in culture medium were first characterized for their potential as model system for the *in vitro* pulldown (Figure 37).

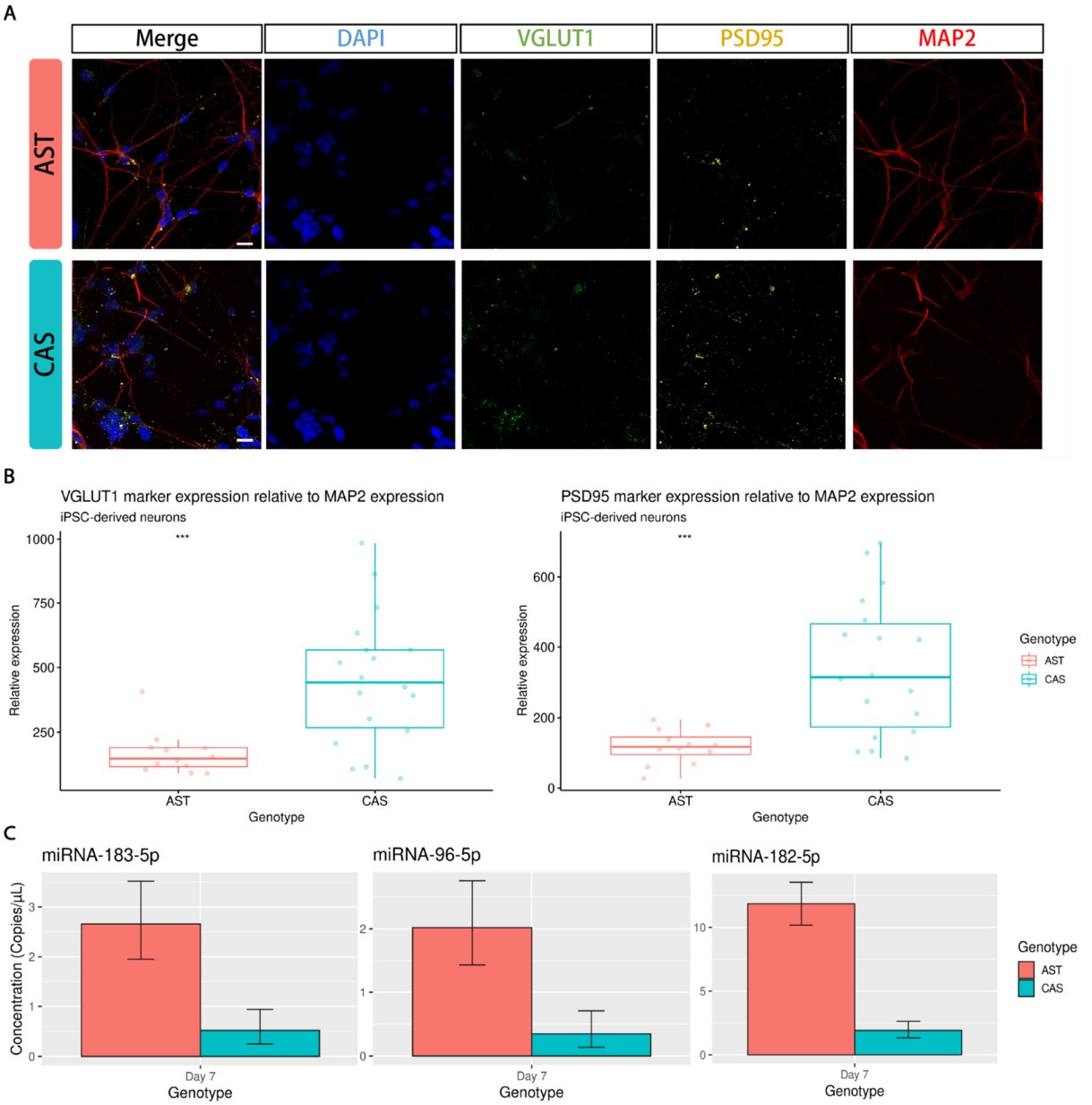

Figure 37: Characterization of AST and CAS iPSC derived neurons as in vitro model system for a miRNA in vitro pulldown. (A) Representative immunofluorescent staining of excitatory synapses and neuronal marker MAP2 (A). Quantification of VGLUT1 and PSD95 marker expression (B) and miRNA 183/96/182 cluster expression (C) in AST and CAS iPSC derived neurons cultivated for 7 days in neuronal culture medium. Statistical analysis: (B) two-sided ANOVA. n= 3 coverslips with 6 images per genotype. p-values: (VGLUT1) p= 0.00093, (PSD95) p= 0.00054. (C) n= RNA of 4 wells per cell line, error bars: Poisson 95 % confidence interval based on direct quantification through ddPCR.

Successful differentiation of iPSCs into neurons was confirmed with synaptic VGLUT1 and PSD95 marker expression after one week in neuronal culture medium (Figure 37 A). Moreover, also the iPSC-derived AST and CAS neurons showed a significant difference in synaptic marker expression after one week in neuronal medium (Figure 37 B). Additionally, miRNA expression analysis confirmed miRNA 183/96/182 cluster expression in AST and CAS iPSC derived neurons. Moreover, the analysis showed a significantly higher expression of each miRNA of the miRNA 183/96/182 cluster in the cell line harbouring the triplication of *SNCA* (Figure 37 C). Thus, 7 days of cultivation of AST and CAS iPSC

derived neurons in neuronal culture medium resembled excitatory synaptic loss and differential expression of the miRNA 183/96/182 cluster in AST-derived iPSCs and was therefore chosen as model system for the *in vitro* pulldown.

The NPC derived neuronal cells after 7 days in neuronal cultivation medium were transfected each with 100 nM of each biotinylated miRNA of the cluster separately, and with a biotinylated scrambled miRNA as control. After 48 hours, the neurons were harvested and lysed. Streptavidin-coated magnetic beads were then used to purify the RNA specifically bound to the miRNA of interest for further library preparation and Illumina sequencing. Altogether, after background correction, 10277 individual genes (AST iPSC derived neurons) and 11199 individual genes (CAS iPSC derived neurons) were identified to bind to the miRNA 183/96/182 cluster in the *in vitro* pulldown experiment. Background correction was performed as follows: All gene counts of the individual miRNA samples (hereafter referred to as miRNA mix) were summarized, and all gene counts identified in the miRNA scramble sample were subtracted from the total counts of the mixed miRNAs. Gene ontology (GO) enrichment analysis was performed of all genes bound by the miRNA mix after background correction (Figure 38). This GO enrichment analysis provided an overview of the classification and grouping based on association with cellular components and molecular functions of the mRNAs bound to the miRNA 183/96/182 cluster identified by the pulldown in CAS iPSC derived neurons. Strong enrichment in the GO for cellular compartments was identified for intracellular membrane-bound organelles and considerable enrichment was observed for postsynaptic density, asymmetric synapse and dendrite (Figure 38 A). The GO enrichment for the molecular function revealed enrichment for RNA binding, GTPase binding, regulatory element binding, microtubule and tubulin binding (Figure 38 B).

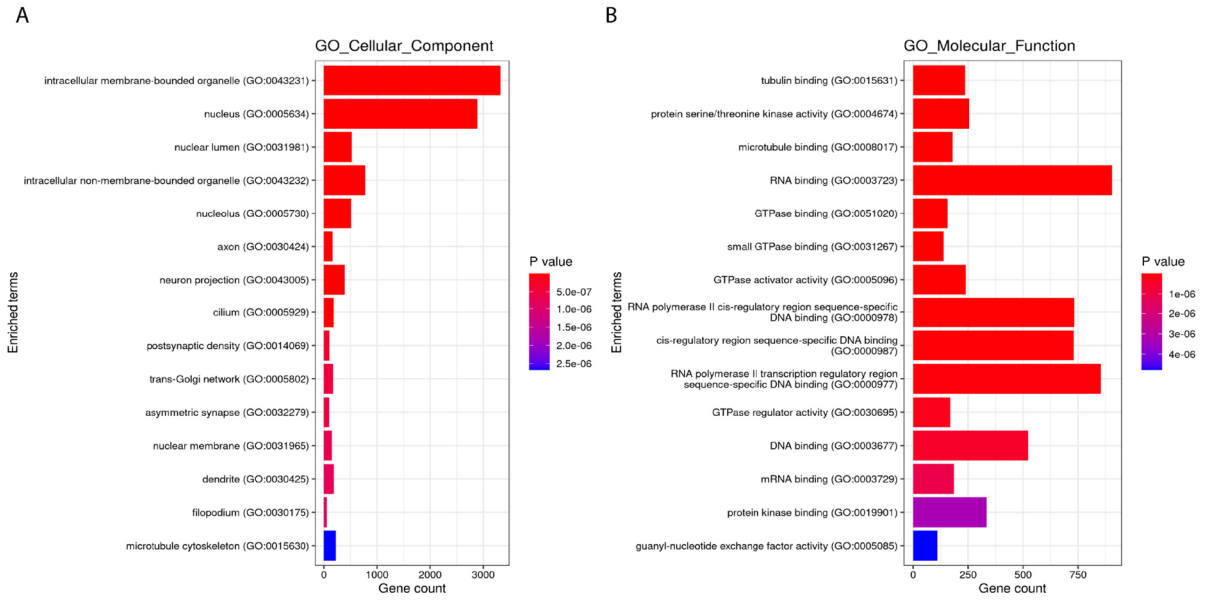

Figure 38: GO enrichment analysis of mRNAs bound to the miRNA 183/96/182 cluster identified by the pulldown in CAS iPSC derived neurons. GO term for cellular component (A) and molecular function (B). Annotations were performed with the GO database release 2021.

Among the more than 10000 identified genes, *eEF1A1* was identified to be bound by each miRNA of the miRNA 183/96/182 cluster in both genotypes after background correction. In contrast, neither binding of *eEF1A2* nor *SPRR2b* was identified with the pulldown. Specific binding of *eEF1A1* was furthermore confirmed with a PCR. Therefore, RNA isolated from the pulldown sample (that was used for the library preparation) and total RNA input from the pulldown cell lysates was converted into cDNA. A PCR with primers specifically targeting eEF1A1 confirmed specific binding of *eEF1A1* to the miRNA 183/96/182 cluster on an agarose gel (Figure 39), as amplicons were found in both the AST and CAS miRNA mix samples. An amplicon was also found in AST RNA scramble, however no amplicon was detected in the CAS RNA scramble. Evidence for *eEF1A1* in the input RNA was found in all four samples tested. Of note: No conclusion can be drawn from the amplicon intensity, as the RNA input and thus cDNA input is not comparable across samples.

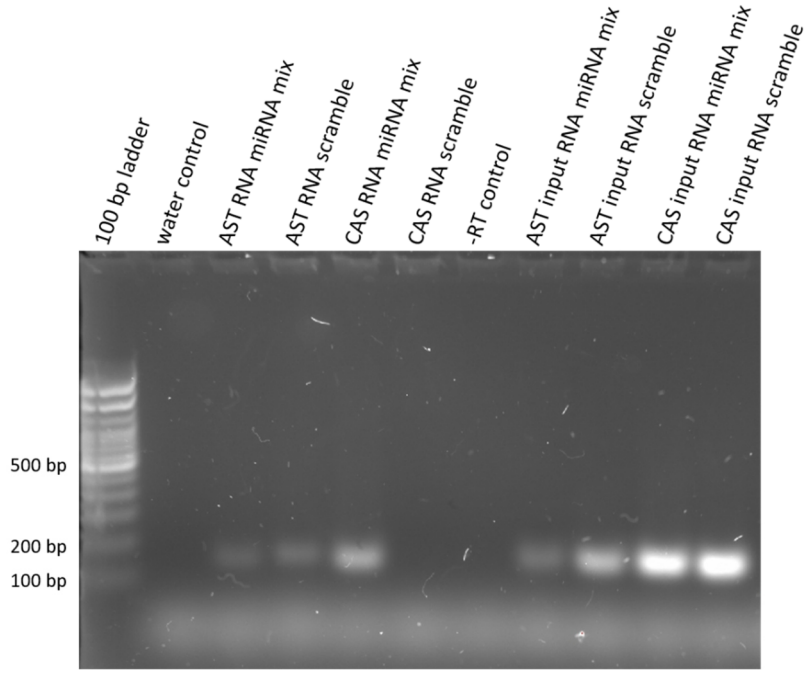

Figure 39: A 2 % agarose gel confirming eEF1A1 expression in AST and CAS pulldown samples. Amplicons were detected in the AST and CAS pulldown miRNA mix (mix of 183/96/182 RNA samples) and in the AST pulldown RNA scramble. No amplicon was detected in the CAS pulldown RNA scramble. Amplicons were detected in the input RNA of all samples. No amplicon was detected in the negative controls (water and no reverse transcriptase (-RT)). Expected length of the eEF1A1 amplicon: 140 bp. Amplicon intensity is not conclusive, since different cDNA input was used because RNA concentration of the pulldown was too low to quantify with a Qubit or Bioanalyzer. Abbreviations: bp - base pairs, miRNA mix - pulldown RNA also used for library preparation, input RNA - total RNA input of cell lysates before pulldown, RT - reverse transcriptase.

Collectively, this pulldown experiment confirmed *in vitro* binding of *eEF1A1* mRNA by the miRNA 183/96/182 cluster in AST and CAS iPSC derived neurons, and was further validated with a PCR detecting *eEF1A1* in the AST and CAS RNA mix samples but not in the CAS scramble sample.

IX. DISCUSSION

DIFFERENTIALLY EXPRESSED MIRNA 183/96/182 CLUSTER IN PDGF MICE BEFORE THE ONSET OF CORTICAL SYNAPTIC LOSS

Synucleinopathies collectively summarise neurodegenerative diseases characterized by the accumulation of α-synuclein protein aggregates (Spillantini et al. 1998; McCann et al. 2013; Luk & Lee 2014; Snead & Eliezer 2014; Burré et al. 2018). Unfortunately, the underlying molecular mechanisms are only poorly understood, and successful disease-modifying therapies have not been established yet (Ray Dorsey et al. 2018). Early on, mutations in the gene *SNCA* encoding for α-synuclein were of special interest in understanding synucleinopathies (Polymeropoulos et al. 1997). Mutations in the *SNCA* locus have a low prevalence in PD patients, yet they show a high penetrance for development of a fully-fledged phenotypic disease (Lill 2016). Within the past few years, early pathological changes caused by aberrant *SNCA* expression affecting the human cortex have attracted growing interest (Neuner et al. 2014; Blumenstock et al. 2017).

One approach to understand the causal role of *SNCA* in complex systems is the use of murine model systems. Out of these, one model system is a mouse line overexpressing human *SNCA* under the constitutive active PDGFß promoter (Masliah et al. 2000), hereafter referred to as PDGF mouse. Characterizing cortical alterations in synucleinopathies, PDGF mice at 3 months of age showed reduced cortical synaptic density before the onset of any behavioural deficits (Blumenstock et al. 2017). Consequently, it was investigated if *SNCA* overexpression leads to dysbalanced protein expression in synaptosomes of 3-month-old mice. Indeed, the proteome of PDGF mice synaptosomes showed dysregulated protein expression, with overall upregulation of 40 proteins and significantly reduced expression of the Eukaryotic Translation Elongation Factor 1 Alpha 1 (eEF1A1) and the Small Proline-rich Protein 2B (Sprr2b) compared to wild type mice (Blumenstock et al. 2019).

Based on these observations, RNA expression analysis of cortical tissue in 2 and 3-month-old PDGF mice aimed to elucidate transcription changes. It was of special interest whether the previously observed proteomic changes could be recapitulated. Surprisingly, only a few significantly differentially expressed genes were identified between PDGF and wild type mice: Only 11 genes were differentially expressed between 2-month-old mice, and only the transgene *SNCA* was identified as significantly differentially expressed when comparing 3-month-old mice. In contrast, considerably more differentially expressed genes were observed between 2 and 3-month-old mice of the same genotype: In wild type mice, 16 genes were significantly differentially expressed, while even more than 90 genes were significantly differentially expressed in PDGF mice. This generally suggests elevated dynamic transcription and important changes during the mouse brain development from 2 to 3 months. Indeed,

with 2 months of age, mice are still considered being pre-mature. Between 3 and 6 months of age, mice are considered mature adults (Flurkey et al. 2007). This latter, post-development phase is generally considered the reference group for mouse experiments, when no phenotypes related to senescence have been observed (Flurkey et al. 2007). Interestingly, overall more significantly differentially expressed genes thus enhanced transcriptional dynamic was observed specifically in PDGF mice during this step of development.

Comparing the genes that were expressed at detectable levels in whole brain lysates with the synaptic proteome of PDGF.3 and WT.3 mice, an overlap of over 90 % indicated that the transcriptomic analysis was sensitive enough to identify genes encoding for proteins of the synaptosomes. However, it cannot be excluded that using whole brain lysates might have masked subtle differences in gene expression specifically at the synapse. The only significantly differentially regulated protein of the synaptosome that was detected with differential transcriptomic expression analysis was *Actn1,* encoding for the actin filaments (F-actin) cross-linking protein alpha-actinin 1 protein. Interestingly, an isoform of *ACTN1* was identified to be exclusively expressed in the brain (Kremerskothen et al. 2002). It seems to be required for tethering of PSD-95 protein to postsynaptic membrane sites (Matt 2018), thus being a bundling protein anchoring alpha-actinin 1 to intracellular structures (Uniprot 2022). Importantly, development and maintenance of young synapses relies on F-actin assembly (Zhang & Benson 2001). In contrast, at the end stages of synaptogenesis, the maintenance of synaptic ultrastructure becomes independent of F-actin and relies on other scaffolding proteins as for example Bassoon (pre-synaptic) or PSD95 (post-synaptic) proteins (Garner et al. 2000; Zhang & Benson 2001). Thus, transcriptional downregulation of *Actn1* from 2 to 3-month-old PDGF mice could reflect a reduced requirement of F-actin-dependent synaptic strengthening. In contrast, enhanced alpha-actinin 1 levels in synaptosomes of 3-month-old PDGF mice could suggest ongoing synaptic development and maturation of young synapses, delays and impairments in F-actin-dependent proper synapse formation or an inability to strengthen and maintain mature synapses.

A divergence of proteomic and transcriptomic changes in PDGF mice at 3 months of age was observed. Consequently, it was further investigated whether the most prominent fine-tuners of gene expression, microRNAs, could contribute to this phenomenon upon overexpression of *SNCA*. Therefore, miRNA sequencing was performed on PDGF and wild type mice before the onset of synaptic loss during development (2 months), in mature mice at the onset of synaptic loss (3 months) and with an observed phenotype of synaptic loss (4 months).

The miRNA expression analysis revealed three miRNAs being significantly differentially expressed in 2-month-old PDGF versus WT mice, namely mmu-miRNA182-5p, mmu-miRNA183-5p and mmu-miRNA96-5p. Following initially high expression levels, all three miRNAs showed a drop in

expression from 2 months of age to 3 months of age, and remained lower and non-significantly differentially expressed at 3 and 4 months of age. A slight increase in miRNA expression was observed from 3 months to 4 months in both genotypes. This drop observed for the three miRNAs did not seem to be a technical artefact, as highly expressed but non-significantly differentially expressed miRNAs did not recapitulate this drop between 2 and 3 months of age. Indeed, miRNAs are reported to play important but distinct roles during development as well as during homeostatic maintenance of cells (He & Hannon 2004). Thus, miRNA expression levels show spatiotemporal dynamics that appear to be developmentally regulated.

Moreover, it turned out that all three identified miRNAs, miRNA-183-5p, miRNA-96-5p and miRNA182-5p, belong to a known miRNA cluster (miRNA 183/96/182 cluster), since they are located in close proximity to each other on the murine and likewise on the human genome (Lim et al. 2003; Xu et al. 2007; Dambal et al. 2015; Zhou et al. 2021). Furthermore, the seed sequence of each miRNA is almost identical across the cluster, where the sequences differ with only one base to each other. This sequence is highly conserved across species, and can be evolutionary traced back to protostomes and deuterostomes, thus about 600 million years ago (Lim et al. 2003; Pierce et al. 2008; Dambal et al. 2015; Zhou et al. 2021). Transcribed as a polycistronic gene, this miRNA cluster is encoded with varying intergenic spacing, but high sequence similarity and similar chromosomal order between species (Griffiths-Jones 2004; Griffiths-Jones et al. 2008; Kozomara & Griffiths-Jones 2011; Kozomara & Griffiths-Jones 2014; Dambal et al. 2015). In humans, the miRNA 183/96/182 cluster sequences are almost identical to the murine sequences, with only a few base pairs mismatch of the mature miRNA sequence, but identical seed sequences (Xu et al. 2007; Kozomara & Griffiths-Jones 2011; Dambal et al. 2015; Zhou et al. 2021).

The miRNA 183/96/182 cluster has already been studied in a synaptic context in the retina: Lumayag and colleagues identified less prominent ribbon synapses of photoreceptors and enhanced retinal degeneration in mice lacking mmu-miR-183 (Lumayag et al. 2013). Krol and colleagues identified the expression of the miRNA 183/96/182 cluster in the retina being regulated by light sensitivity with a rapid turn-over between pre-miRNA and mature miRNA (Krol et al. 2015). In 2020, Peskova and colleagues investigated the miRNA 183/96/182 cluster expression changes during retina development using human iPSCs differentiated into retinal organoids. Similar to the observed drop in expression in the PDGF mice, the retinal miRNA 183/96/182 cluster expression also shows dynamic expression changes during development of the retinal organoid. With comparably high expression in undifferentiated iPSCs, the expression of each miRNA of the cluster, and especially for hsa-miR-182, steadily decreased until day 56, and started to increase again until maturation of the organoid at 84

days in culture. Inhibition of the cluster led to enhanced neuronal retinal expansion (Peskova et al. 2020).

Expression of the miRNA 183/96/182 cluster has also been identified in the context of human synucleinopathies: Ubhi and colleagues have investigated dysregulated miRNAs in MSA and identified disease-related alterations of hsa-miR-96 expression. Hsa-miR-96 was identified to be upregulated in MSA patient tissue, whilst protein levels of its target genes *SLC1A1* and *SLC6A6* (members of the solute carrier protein family) were downregulated (Ubhi et al. 2014). More recently, levels of hsa-miR-96 in blood serum samples have been identified as a potential biomarker to tell apart MSA from PD. While levels of hsa-miR-96 were found to be elevated in MSA patients, hsa-miR-96 was absent in PD patients' blood samples (Vallelunga et al. 2021).

Collectively, these findings underline a potentially important role of the miRNA 183/96/182 cluster in the context of synaptic regulation during development, but also in the context of synucleinopathies.

LACK OF MIRNA 183/96/182 CLUSTER EXPRESSION IN HUMAN CORTICAL SYNUCLEINOPATHY TISSUE

A significant difference in expression of the miRNA 183/96/182 cluster in cortical tissue of PDGF mice was observed before the onset of cortical synaptic loss. Since the miRNA cluster was reported to be highly evolutionary conserved, its expression was further investigated in human samples. Therefore, expression of the three individual miRNAs was investigated in human cortical post-mortem tissue. However, no expression of either of the miRNAs of the miRNA 183/96/182 cluster was detected in seven different patients diagnosed with synucleinopathies. The assessed cases differed in their post-mortem intervals (PMI), which ranged from 8 to 96 hours. Although samples with a high PMI typically suggest impaired and fragmented RNA (Koppelkamm et al. 2011), the integrity of RNA seemed to be sufficiently well to detect miRNA expression, confirmed by the detection of two different control miRNAs. Interestingly, Ubhi and colleagues identified hsa-miR-96 significantly upregulated in the frontal cortex of MSA patients compared to healthy patients. However, no significant difference in expression of hsa-miR-96 in DLB, PD and CBD was detected in their study (Ubhi et al. 2014). Having analysed tissue from the same region, it suggests that hsa-miR-96 seems to play a relevant role in the cortex in synucleinopathy-subtype MSA. However, since no expression was detected in the seven examined human post-mortem cases that had different forms of synucleinopathies, hsa-miR-96 aberrant expression might be restricted to MSA-patient derived tissue. Indeed, the MSA-subtype is characterized by glial-specific inclusions and was not represented in this study.

Nevertheless, synucleinopathy pathology is not restricted to *SNCA* copy number variation but is also observed sporadically or upon genetic mutations of the *SNCA* locus (Lill 2016). Unfortunately, genetic alterations of the *SNCA* locus were unknown for the human tissue samples used in this study. Since miRNA 183/96/182 cluster expression was observed early during development and before the onset of a disease phenotype in mice, miRNA levels could have been altered in the selected human samples long before death, rendering the measurement of early changes in expression levels impossible.

Moreover, the PDGF mouse model was generated by constitutive overexpression of the human *SNCA* transgene and therefore represents a highly artificial system. Although formation of intraneuronal α-synuclein inclusions is observed, the loss of neurons is not fully recapitulated in PDGF mouse models (Masliah et al. 2000). Furthermore, the overexpression of a non-endogenous gene is not well recapitulating the genetic background observed in human synucleinopathy patients, where predominantly mutations of the *SNCA* locus, as well as copy number variations are observed (Polymeropoulos et al. 1997; Singleton et al. 2003; Farrer et al. 2004; Snead & Eliezer 2014).

AST AND CAS CORTICAL ORGANOIDS AS MODEL SYSTEM WITH HUMAN GENETIC BACKGROUND

Since mouse model systems do not fully recapitulate the genetic background observed in human patients suffering from synucleinopathies, iPSCs derived from patients harbouring genetic mutations of the *SNCA* locus would allow to investigate and translate murine findings to a human-relevant context. Therefore, the dynamics of the miRNA cluster in a more complex environment with human genetic background were investigated. Cortical organoids (COs) were chosen as a suitable model system, as they resemble cortical brain structures with complex three-dimensional networks of neuronal cells including cell-cell contacts and communication (Lancaster et al. 2013; Lancaster & Knoblich 2014). Consequently, COs of AST and CAS iPSCs were generated and investigated for differences caused by *SNCA* overdosage during 120 days in culture with a special interest in to what extent AST and CAS COs would present a suitable model system for synucleinopathies.

AST COS SHOW A REDUCTION IN *SNCA* RNA EXPRESSION AFTER 60 DAYS IN CULTURE

Having grown the AST and CAS COs, it was first tested whether the triplication of the *SNCA* locus would also lead to increased α-synuclein expression *in vitro*. This has been shown before, where the AST iPSCs used in this thesis to generate COs were successfully differentiated into dopaminergic neurons by Devine and colleagues. These AST iPSC-derived dopaminergic neurons had elevated α-synuclein and *SNCA* levels compared to a healthy controls (Devine et al. 2011).

Quantification of IHC-stained slices of AST and CAS COs throughout the course of time showed a steady increase of α-synuclein expression until day 100, followed by a slight reduction at day 120. Decreased levels could be explained by the emergence of a necrotic core leading to a reduction of staining-positive areas. Overall, α-synuclein expression showed a tendency for higher expression in AST COs, but was only significantly higher at 40 days. A more quantitative analysis of protein composition, e.g. through western blot or LC-MS/MS analysis, are required to support this notion. Interestingly, the phosphorylated and thus pathological form of a-synuclein showed overall low staining levels, yet significantly more phospho-α-synuclein at day 40 in AST. This suggests that the COs are capable of forming oligomeric α-synuclein aggregates *in vitro,* which could eventually lead to toxic aggregates. Surprisingly, levels of *SNCA* RNA expression changed through the course of time: While significantly more *SNCA* was identified in AST COs at day 20 and day 40, its expression was reduced after day 40. In contrast, CAS COs showed increasing *SNCA* expression until day 60, before expression levels decreased again. Strikingly, *SNCA* expression in AST COs was significantly higher at day 40, but significantly lower compared to CAS at day 60, day 80 and day 100. While *SNCA* was observed to be differentially expressed in AST and CAS COs by ddPCR, α-synuclein expression was observed to be comparable at these time points based on IHC-quantification. This could suggest that the cells could have sensed the overproduction of α-synuclein mRNA, downregulating its translation, or in turn also reducing transcription to prevent over-representation of the mRNA.

Cortical organoids do typically not contain mature dopaminergic but rather glutamatergic neurons and the different susceptibility of both neuron types to *SNCA* overproduction must be considered. Interestingly, contradicting reports about *SNCA* expression in synucleinopathy patients have been reported (Chiba-Falek et al. 2005): While a loss of 15-20 % of *SNCA* mRNA expression was observed in the *substantia nigra* (containing mostly dopaminergic neurons) from PD patients, no alterations were found in the frontal cortex of these patients (Neystat et al. 1999). In contrast, another publication reported 50 % loss of *SNCA* mRNA expression in neurons of the *substantia nigra* and frontal cortex (Kingsbury et al. 2004). On the other hand, elevated *SNCA* mRNA expression levels have been detected in *substantia nigra* mature dopaminergic neurons from PD patients (Gründemann et al. 2008). Transgenic mice overexpressing human α-synuclein fused to a membrane-targeting signal sequence showed specific expression in the cortex at glutamatergic synapses. However, no signal was detected in dopaminergic neurons of the *substantia nigra* (Frahm et al. 2018). Thus, different susceptibility of neuronal subtypes to α-synuclein is present (Brazdis et al. 2021), which could explain the observed reduction of *SNCA* expression in AST COs. However, it cannot be excluded that AST COs show increased apoptosis from day 40 onwards. This could explain the observed overall reduced RNA transcript

expression levels, making the expression changes in the context of downregulation caused by intrinsically sensed α-synuclein less likely.

SNCA OVEREXPRESSION INDUCES GROWTH STAGNATION IN COS, HOWEVER NO ROBUST DIFFERENCE IN MATURATION COULD BE OBSERVED

Subsequently, it was tested whether *SNCA* copy number variation would influence growth, maturation or differentiation of AST and CAS COs. Indeed, during the first 20 days of cultivation, AST COs were significantly bigger in size compared to CAS COs. However, at 40 days, the COs were comparable in size. Subsequently, the COs continued to grow during the course of time, however AST COs seemed to grow slower and remained significantly smaller than CAS COs. This observed size difference could be due to differences in cell number or soma size. Interestingly, midbrain organoids generated of the AST and CAS cell line were also smaller when carrying the genomic *SNCA* triplication (Mohamed et al. 2021). In addition, primary culture of E18 cortical neurons overexpressing α-synuclein have shown reduced soma size suggesting α-synuclein induced cortical atrophy in PD mouse models (Fang et al. 2017). This suggests impairments caused by α-synuclein overexpression already early during development. Therefore, a comparison of soma sizes and cell number of AST and CAS COs is required to further elucidate the observed phenotypic size difference.

Furthermore, it was investigated whether the size difference could be explained by differences in maturation or differentiation of AST and CAS COs using IHC and subsequent quantification. Of note: These data have to be interpreted with caution, as low sample size and lack of additional proteomic analysis of the whole organoid limits the explanatory power of IHC quantification.

During day 20 and day 40, AST and CAS COs showed many ventricular-like structures in the growing organoids. This on-going proliferation was confirmed by expression of the proliferation-marker Ki67 only early during the course of time. A tendency to prematurely reduced proliferation capacity in AST COs could be seen at day 40, however, a significant difference was observed at day 80 only.

In contrast, little GFAP expression was appreciated from day 80 onwards in both COs, and AST COs showed significantly higher levels of GFAP at day 100. This observation correlates with the appearance of necrotic cores within the organoids from day 80 onwards. These necrotic cores increase during the growth of organoids and appear due to limited nutrient and oxygen distribution caused by a lack of a vasculature system (Lancaster et al. 2017). Moreover, gliosis can precede apoptosis (Sofroniew 2014), thus could be correlated to the premature GFAP expression in AST COs. Indeed, more dead cells were observed in AST CO culture vessels at later time points indicated by a blurred culture medium.

Although AST COs were smaller in size during the late time points, enhanced gliosis and thus enhanced apoptosis was observed in COs with *SNCA* over-dosage. Organoids at day 120 presented a very large necrotic core with very large marker-negative areas. Thus, data collected at day 100 and day 120 have to be analysed with caution and could explain the reduced overall marker expression at later stages.

Differences in maturation of COs were assessed by analysis of neuronal marker expression. Very high expression of the microtubule-associated protein MAP2 confirmed neuroepithelial identity of CO cells throughout the course of time. Predominantly maturing cells were observed early during maturation at day 20 and day 40. This was characterized by expression of Nestin staining for intermediate filament proteins in nerve cells. Overall, a small number of post-mitotic NeuN positive cells was observed throughout the course of time. In parallel, an increase in the synaptic marker synaptophysin was seen, suggesting successful maturation of nerve cells and formation of synapses within both CO genotypes. An increase of synaptophysin staining could be observed from day 20 onwards until day 80, followed by a drop in expression, which could be explained by the described necrotic core at late stages.

Collectively, successful neuronal maturation of both AST and CAS COs could be confirmed. Nevertheless, no significant difference in neuronal maturation was observed between AST and CAS COs. However, differences in marker expression could be masked by the high variability in marker expression and low sample size especially at day 60 and day 80. Given the high variability of the individual organoids, potential differences could be lost by analysis of different sectional planes. Consequently, western blot or proteomic analysis (e.g. LC-MS/MS) of the total organoid are required to comprehensively quantify differences in protein expression in AST and CAS COs during the course of time.

GLUTAMATERGIC SYNAPTIC LOSS IN AST COS

Loss of cortical glutamatergic synapses was observed in PDGF mice before the onset of behavioural symptoms (Blumenstock et al. 2017). Since no difference in synaptophysin expression was detected in AST and CAS COs, a more detailed synaptic quantification was performed using immunofluorescent and RNA expression analysis. Indeed, during the course of time, significantly lower expression of the pre-synaptic glutamatergic marker VGLUT1 was detected in AST COs. This was confirmed by RNA expression analysis, where significantly less *VGLUT1* expression was observed at all time points assessed but day 40. Interestingly, *VGLUT1* RNA expression peaked in AST COs already at day 40, and later at day 60 in CAS COs.

Similar results were observed for the post-synaptic marker PSD95. Significantly more PSD95 was detected in CAS COs at day 20 and day 40 and no significant difference was observed at day 60 and

day 120. Surprisingly, significantly more PSD95 was detected in AST COs at day 80 and day 100. However, *PSD95* RNA expression did not reflect this observed pattern: At day 20 and day 40, no significant difference was observed. Yet, from day 60 onwards, significantly more *PSD95* RNA was detected in CAS COs. As for *VGLUT1*, *PSD95* expression in AST peaked at day 40, while the peak in CAS COs was observed at day 60. Especially at day 80 and day 100, significantly more *PSD95* RNA expression was observed in CAS COs, while significantly more protein expression was observed in AST COs. However, a large variance in PSD95 marker density was observed throughout the quantification especially for AST COs and might be caused by high variability of organoids. In addition, apoptotic and proteolytic synapses could lead to larger fluorescent signals. Generally, elimination of synapses requires disassembly of the actin filament network (Meng et al. 2015). Successively, clearance of proteins and cellular debris is performed by microglial phagocytosis (Fu et al. 2014). However, microglia are mesoderm derived tissue, and not produced during the neuroectodermal differentiation of the cerebral organoid protocol used in this thesis (Alliot et al. 1999; Lancaster et al. 2013; Park et al. 2018; Ormel et al. 2018). Accordingly, proteolytic post-synapses could release PSD95 protein into the extracellular matrix, no longer resembling well-organized complexes, leading to the relatively large fluorescent signals.

Collectively, a reduction of glutamatergic synapses in cortical organoids could be detected upon overdosage of *SNCA*. These findings recapitulate the observed cortical synapse loss in PDGF mouse lines. Furthermore, while RNA expression levels appeared comparable until day 40, the onset of synaptic RNA transcript reduction in AST and CAS COs was observed later than for the proteins. There, already at day 20, fewer pre-synaptic glutamatergic termini were observed in AST COs. Potential post-translational modifications, unsuccessful protein incorporation, and even unsuccessful formation or maintenance of mature synapses could lead to the observed phenotype.

Of note: A turnover towards reduced RNA expression during the course of time could be observed in AST and CAS organoids. Reduced RNA transcription rates could be explained by overall reduced need of mRNA template for newly generated proteins as well as an overall reduced cellular homeostasis after prolonged time in culture, linked to nutrient and oxygen shortage. Most likely, overall RNA transcription could be diminished by the relatively large size of the necrotic core. While only few healthy neuronal marker-positive cells were observed at the periphery of organoids at later time points, the necrotic core was increased in size from day 80 onwards and correlated with decreased RNA transcript expression. The highest expression of RNA transcripts was observed at day 60 in CAS COs. However, the turnover towards reduced RNA expression of assessed RNA transcripts in AST was already observed at day 40. Thus, this seemed to be caused by overdosage of *SNCA*, since AST and CAS are genetically identical apart from the *SNCA* loci. Collectively, the AST and CAS CO differentiation

model confirms early-on reduced RNA transcriptional activity in AST accompanied by premature apoptosis and degeneration of cells caused by α-synuclein overexpression.

MIRNA 183/96/182 CLUSTER DYNAMICS RECAPITULATED IN AST AND CAS COS

Since cortical synaptic loss could be recapitulated in AST and CAS COs, it was further investigated whether the observed translational changes and specifically the expression dynamics of the miRNA 183/96/182 cluster could be recapitulated as well. Indeed, expression of all three miRNAs of the cluster was seen in AST and CAS COs with a similar dynamic as detected in PDGF mice. In addition, hsa-miR-182 showed the highest expression among the cluster miRNAs also in AST and CAS COs. Furthermore, a more precise difference in expression dynamics could be appreciated: at day 20 and day 40, significantly more miRNA expression was seen in AST COs. The peak of expression in both CO genotypes was at day 40, followed by a drop in expression from day 60 onwards. While expression levels in CAS COs remained low, a significant increase in AST COs at day 100 was detected.

Furthermore, significantly higher expression of the miRNA 183/96/182 cluster in AST COs has been appreciated from the first assessed time point onwards. Thus, overexpression of the miRNA 183/96/182 cluster also in AST COs is correlated with a reduced density of glutamatergic neurons as it was detected in PDGF mice. This reduced difference in synaptic density could possibly be caused by an inability to successfully mature into synapses or reduced ability to maintain mature synapses. In parallel, reduced levels of post-synaptic termini were seen during the early time points, suggesting also delayed formation and/or reduced ability to maintain mature post-synapses in AST COs within the first 40 days in culture.

In summary, AST and CAS COs seem to recapitulate and translate findings observed in PDGF mice making them a suitable model system to investigate synaptic loss upon α-synuclein overexpression in a human genetic background.

MIRNA 183/96/182 CLUSTER PREDOMINANTLY BINDS CYTOSKELETAL PROTEINS – AND *EEF1A1* MRNA

miRNA expression dynamics were comparable between PDGF mice and AST COs. Thus, it was further investigated how the miRNA 183/96/182 cluster could possibly induce post-transcriptional changes eventually leading to the observed cortical synaptic loss. Therefore, an *in vitro* RNA pulldown in AST and CAS iPSCs derived neurons was performed to identify mRNAs bound to each individual miRNA of the cluster and more than 10000 genes being bound by the miRNA 183/96/182 cluster were identified with this approach. GO enrichment analysis for the cellular component in CAS iPSC derived neurons

revealed association with intracellular membrane bound organelles, as e.g. the nucleus or vesicles. In addition, association with postsynaptic density, asymmetric synapses and dendrites further supported the role of the miRNA 183/96/182 cluster in the synaptic context. GO enrichment analysis for the molecular function in CAS iPSC derived neurons showed enrichment for RNA binding, RNA regulatory region sequence binding. This was expected, as the identified mRNAs were recognized upon binding of a post-transcriptional regulator. Interestingly, enrichment for genes associated with tubulin binding, microtubule binding and GTPase binding suggested involvements in structural and regulatory modulation.

Among all genes identified with this pulldown, the *eEF1A1* mRNA was found to be bound by each individual miRNA in AST and CAS iPSC derived neurons. Although binding of *eEF1A1* mRNA was bioinformatically predicted for hsa-miR-182 only, the *in vitro* pulldown confirmed specific binding for each miRNA of the miRNA 183/96/182 cluster in iPSC derived neurons. Interestingly, recent reports suggest, that not only perfect base pairing of the seed sequence to its target genes would be required for regulatory function (Chipman & Pasquinelli 2019). Moreover, no binding to the isoform *eEF1A2* nor to *SPRR2b* was identified with this *in vitro* pulldown. An agarose gel furthermore showed successful amplification of *eEF1A1* in the input RNA, confirming its basal expression in the input lysates. Positive amplification was furthermore detected in the RNA isolated from the AST miRNA mix and CAS miRNA mix, confirming its specific binding by the miRNAs of the cluster. No amplicon was detected in the CAS RNA scramble, however an amplicon was detected in the AST RNA scramble control. Therefore, background correction was performed on the sequenced library to correct the results for unspecific binding to the scramble miRNA. In addition, it has to be kept in mind that this experimental approach for analysing the miRNA binding to the 3'UTR is no final conclusive evidence. It requires further conformation with e.g. a 3'UTR dual Luciferase gene reporter assay.

In summary, the *in vitro* pulldown to identify targets of the miRNA 183/96/182 cluster in AST and CAS iPSC derived neurons confirmed specific binding of each miRNA to *eEF1A1* mRNA, which is downregulated as protein in VGLUT1 positive synaptosomes in 3-month-old PDGF mice.

MIRNA 183/96/182 CLUSTER REGULATES LOCAL PROTEIN SYNTHESIS IN THE SPINE. IT IS DYSBALANCED IN SYNAPSES OVEREXPRESSING A-SYNUCLEIN AND LEADS TO IMPAIRED MATURATION AND MAINTENANCE OF YOUNG SYNAPSES

eEF1A was reported to be an important modulator of structural plasticity in dendritic spines (Mendoza 2021). Thus, binding of the miRNA 183/96/182 cluster specifically to *eEF1A1* mRNA suggests a relevant physiological role in regulating local protein synthesis at the synapse.

In glutamatergic, excitatory synapses, local protein translation has been shown to be activity-dependent (Bramham & Wells 2007; Martin & Ephrussi 2009; Muddashetty et al. 2011). Under physiological conditions, local protein synthesis is suppressed in an inactivated synapse (Muddashetty et al. 2011). This translational regulation of dendritically localized mRNA is mediated by the Fragile X Mental Retardation Protein (FMRP) (Ashley et al. 1993; Li et al. 2001). In a phosphorylated state, FMRP blocks protein translation by ribosome stalling through segregation of mRNA and proteins of the translation machinery (Rao & Steward 1991; Torre & Steward 1992; Li et al. 2001; Ceman et al. 2003; Darnell et al. 2011; Chen et al. 2015). Moreover, translational repression was reported to be regulated by FMRP binding directly to the ribosome (Laggerbauer et al. 2001; Chen et al. 2015). Interestingly, *FMR1* mRNA, which encodes for FMRP, was reported in dendrites and its translation seemes to be regulated by group 1 metabotropic glutamate receptor (mGluR) signalling (Bassell & Warren 2008).

mGluR signalling activates the synapse, whereby FMRP becomes ubiquitinated and subsequently degraded through the ubiquitin proteasome pathway (Hou et al. 2006; Andres-Mateos et al. 2009; Lannom & Ceman 2021). De-phosphorylated and ubiquitinated FMRP thereby releases previously bound proteins and mRNAs, enabling their translation (Hou et al. 2006; Narayanan et al. 2007; Nalavadi et al. 2012; Lannom & Ceman 2021). Consequently, local protein synthesis of previously bound mRNA, including *Fmr1* itself, is enabled (Angenstein et al. 1998; Ceman et al. 2003; Antar et al. 2004; Plante et al. 2006; Darnell & Klann 2013). Newly synthesised FMRP proteins could become phosphorylated, thus sequestering mRNA and proteins again. Consequently, this physiological feedback loop would enable the reconstitution of suppressed protein translation in the inactive synapse upon activating stimuli (Muddashetty et al. 2011). Interestingly, loss of FMRP leads to increased basal translation (Ifrim et al. 2015), and to elevated local protein synthesis in synapses (Qin et al. 2005; Dölen et al. 2007; Qin et al. 2013). In addition, de-phosphorylated FMRP also releases previously bound miRNA machinery complexes as e.g. the protein Dicer, enabling miRNA binding to target-mRNAs (Plante et al. 2006; Cheever & Ceman 2009).

The *in vitro* pulldown confirmed that the miRNA 183/96/182 cluster can bind to *eEF1A1* mRNA, thus leading to its reduced translation. Consequently, less eEF1A1 protein is synthesized, which was

observed in synaptosomes of 3-month-old PCGF mice. Accordingly, the miRNA cluster indirectly regulates the ribosomal translation machinery by targeted degradation of *eEF1A1* mRNA. Under physiological conditions, this would resemble a second control feedback loop that fine-tunes protein translation during synaptic activity.

However, this physiological control-mechanism of the miRNA 183/96/182 cluster seems to cause unexpected consequences in synapses with genomic *SNCA* copy number variations. For easier understanding, a synapse overexpressing α-synuclein is herein referred to as α-synuclein synapse.

In α-synuclein synapses, elevated mGluR signalling has been reported in PDGF mice (Price et al. 2010). This leads to elevated synaptic activity, including enhanced protein synthesis and reduced levels of phosphorylated FMRP protein, as it becomes ubiquitinated and degraded more frequently. Indeed, reduced levels of FMRP protein have been described in mice overexpressing α-synuclein at three months of age (Tan et al. 2020). Less FMRP protein implies more unbound and therefore available mRNAs and miRNAs at the spine. This significantly elevated abundance of miRNAs has been identified in this thesis specifically for the miRNA 183/96/182 cluster expression under α-synuclein overexpression conditions in PDGF mice at 2 months of age. Elevated expression levels of miRNA 183/96/182 furthermore suggests enhanced binding of *eEF1A1* mRNA. Consequently, enhanced post-transcriptional binding to *eEF1A1* mRNA would lead to reduced levels of eEF1A1 protein expression. These significantly reduced expression levels of eEF1A1 protein in VGLUT1-positive synaptosomes of 3-month-old PDGF mice have been reported by Blumenstock and colleagues in 2019. Consequently, reduction of the eEF1A1 protein levels would lead to reduced overall protein translation locally in the synapse. Furthermore, reduction of protein synthesis has been correlated with synaptic weakening (Sutton & Schuman 2005; Pfeiffer & Huber 2006; Portera-Cailliau 2012), which results in a phenotypic loss of synapses. This phenotypic synaptic loss has been observed in PDGF mice at 4.5 months of age (Blumenstock et al. 2017).

Nevertheless, mRNA expression levels of *eEF1A1* were not seen as differentially expressed in transcriptomic expression analysis at 2 and 3-month-old PDGF mice. However, this analysis was performed on total RNA of whole cortical tissue. Moreover, eEF1A is one of the most abundant proteins of protein synthesis (Mateyak & Kinzy 2010). Accordingly, subtle synaptic *eEF1A1* mRNA expression changes would possibly be masked in total RNA expression analysis.

In summary, elevated levels of miRNA 183/96/182 cluster in α-synuclein overexpression mice are thought to decrease local protein synthesis at the synapse through direct binding to *eEF1A1* mRNA, of which the protein is an essential part of the translation machinery. Consequently, reduced overall

protein translation would lead to synapse weakening, ultimately observed as synaptic loss. Compare with Figure 40 for a graphical summary of the hypothesis.

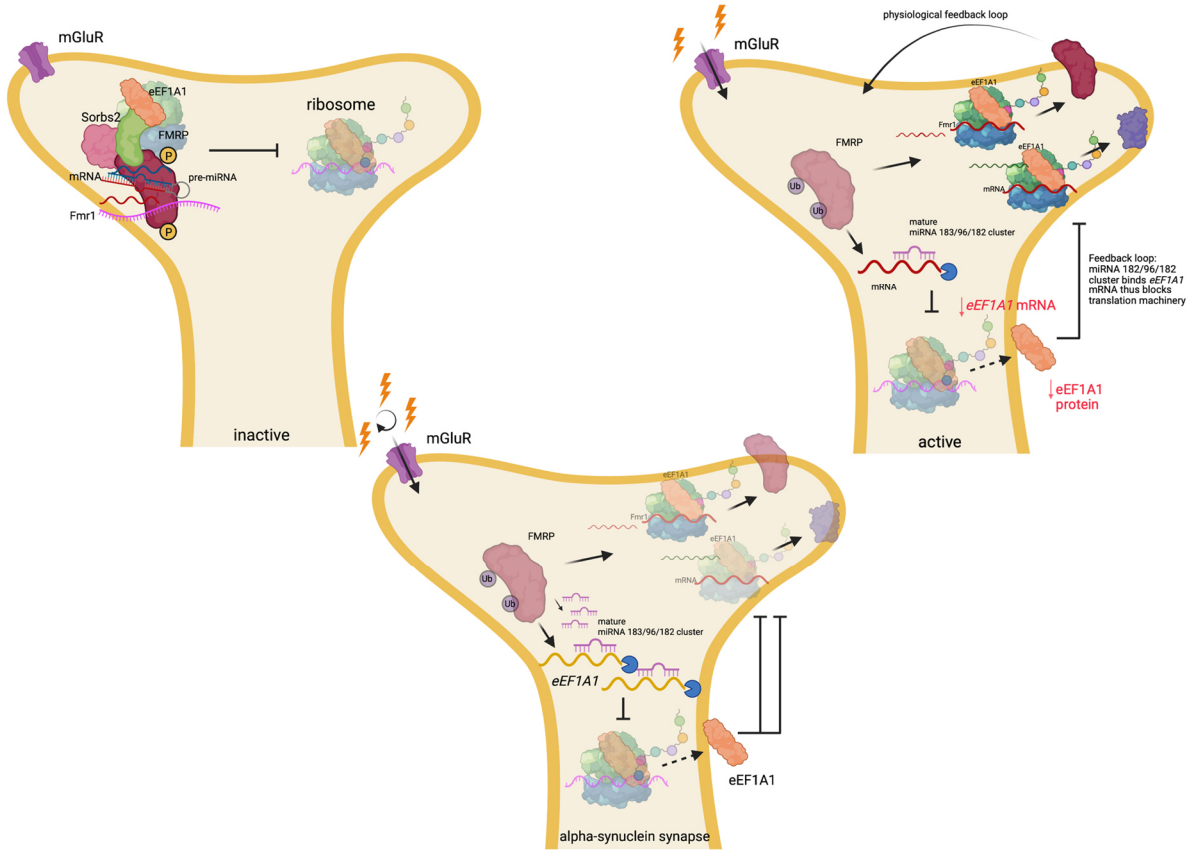

Figure 40: Graphical summary of the hypothesis that the miRNA 183/96/182 cluster regulates local protein synthesis in the spine. In an inactive synapse, local protein translation is suppressed by sequestered proteins and mRNAs. Upon mGluR-induced local protein synthesis, FMRP becomes dephosphorylated and ubiquitinated, thus releasing previously bound mRNAs and proteins. A physiological feedback loop by local translation of FMRP allows to restore supressed protein synthesis. This thesis proposes a second regulatory mechanism, where the miRNA 183/96/182 cluster binds eEF1A1 mRNA thus blocking eEF1A1 protein translation and consequently reducing the local synaptic protein synthesis. In synapses overexpressing α-synuclein, enhanced mGluR-signalling leads to reduced levels of FMRP protein. Thus, less mRNA, proteins and miRNA are bound. Thus, the observed higher expression of the miRNA 183/96/182 cluster could lead to more binding to eEF1A1 mRNA thus reducing eEF1A1 protein levels and consequently reducing local protein synthesis. In addition, reduced overall protein synthesis is correlated with synaptic weakening. Dysbalanced miRNA 183/96/182 cluster expression in synapses overexpressing α-synuclein might lead to impaired maturation and/or maintenance of young synapses, phenotypically observed as synaptic loss. The figure was created with BioRender.com.

Conversely, it can be furthermore hypothesised that the observed synaptic loss could instead be attributed to difficulties in successful maturation and/or impaired maintenance of α-synuclein synapses. Indeed, GO enrichment analysis for molecular functions of the genes identified by the *in vitro* pulldown of the miRNA 183/96/182 cluster in CAS iPSC derived neurons showed an association with microtubule and tubulin binding. Moreover, 28 out of 40 differentially upregulated proteins of the synaptosome in PDGF mice at 3 months of age were assigned to cytoskeletal proteins (eleven proteins), proteins related to metabolism (seven proteins), chaperones (three proteins) or catalytic enzymes (seven proteins) (Blumenstock et al. 2019). The cytoskeletal proteins were composed of

genes encoding for tubulin proteins, which are subject to tightly regulated spatial and temporal expression patterns in the developing brain, where the precise expression patterns are required for proper cortical development (Romaniello et al. 2018).

In addition, eEF1A was reported to regulate actin dynamics (Mendoza et al. 2021) and was reported to bind to the postsynaptic density via actin (Cho et al. 2004; Fernández et al. 2009; Cho et al. 2012). Likewise, regulation of cytoskeletal dynamics of F-actin and microtubules has been assigned to eEF1A (Yang et al. 1990; Liu et al. 1996; Gross & Gross Kinzy 2005; Bunai et al. 2006; Iketani et al. 2013). No difference in synaptic density in 2-month-old mice but differentially upregulated proteins in synaptosomes at 3 months of age suggest that successful formation and maturation of synapses or maintenance of synapses could be impaired in 3-month-old PDGF mice. Hence, a developmentally weakened or young mature but impaired α-synuclein synapse could enhance expression of cytoskeletal proteins to strengthen the synapse. However, *SNCA* overexpression induced miRNA 183/96/182 cluster overexpression at 2 months of age during late development would prevent local protein translation by negatively regulating *eEF1A1* mRNA translation. Indeed, control of translation and actin dynamics in dendritic spines has been reported to be controlled by isoform eEF1A2 in mature neurons (Mendoza et al. 2021). Thus, reduced local protein synthesis would further prevent the required enhanced translation of necessary cytoskeletal proteins, impairing the final maturation and maintenance of young mature synapses. Likewise, impaired maturation and maintenance of synaptic spines, and accordingly visibly reduced density of spines, could lead to the observed phenotype of synaptic loss. Of note, no significant difference in synaptic density was observed in 2-month-old PDGF mice. Nevertheless, complete and absolute maturation as well as defects in maintenance of synaptic cytoarchitecture were observed to be impaired in 3-month-old mature PDGF mice, which was preceding and possibly caused by overexpression of the miRNA 183/96/182 cluster in 2-month-old PDGF mice.

Importantly, eEF1A has two isoforms in vertebrates: *eEF1A1* is predominantly expressed during neurodevelopment and becomes replaced by predominantly *eEF1A2* expression in neurons (Mendoza et al. 2021; Wefers et al. 2022). The nucleotide identity of the two isoforms of *eEF1A* is 75%, however the 5'- and 3'-untranslated regions (UTRs) differ from each other: *eEF1A2* resembles a longer 3' UTR, suggesting more post-transcriptional regulation potential (Browne & Proud 2002; Wefers et al. 2022). Nevertheless, the proteins of the two *eEF1A* isoforms encode 92 % identical proteins in mammals (Soares et al. 2009). It should be kept in mind that LC-MS/MS might not be sensitive enough to discriminate between highly identical isoforms. Accordingly, no distinct conclusion can be drawn regarding specific eEF1A1 or eEF2A2 protein expression in PDGF mice without western blot analysis. Furthermore, a recent publication investigated the expression and subcellular distribution of both

eEF1A mRNA isoforms (Wefers et al. 2022). Investigating the subcellular localization in cultured primary hippocampal neurons, *eEF1A1* mRNA localization was recognized in dendrites and synapses during dendritogenesis and synaptogenesis. In contrast, *eEF1A2* mRNA was found to be predominantly expressed in the soma of neurons. Moreover, co-expression of both isoforms was identified in mature hippocampal neurons, where *eEF1A1* remained the predominantly expressed variant in dendrites (Wefers et al. 2022). Nevertheless, significant reduction of eEF1A1 staining intensity was observed in mature human cortical brain tissue from synucleinopathy patients without visible α-synuclein pathology (Blumenstock et al. 2019), and reduction of synaptic plasticity has been correlated to reduced expression of eEF1A in several neurodegenerative disorders (Moreno et al. 2012; Garcia-Esparcia et al. 2015; Delaidelli et al. 2019; Blumenstock et al. 2019).

In this study, the miRNA 183/96/182 cluster was found to bind *eEF1A1 in vitro*. However, only one perfect 7-mer matche of hsa-miR-182 seed sequence on the 3' UTR of human was bioinformatically predicted. Nevertheless, reports suggest that even among miRNAs of the same cluster, imperfect base-pairing over perfect base-pairing of the seed sequence, pairing depending on additional base pairing or even temperature sensitivity would influence subcellular-specific binding (Carmel et al. 2012; Bartel 2018; Chipman & Pasquinelli 2019). Therefore, the drop in miRNA 183/96/182 cluster expression could be explained by changes in *eEF1A* isoform expression, where the post-transcriptional regulation of the miRNA 183/96/182 cluster would not be required any longer for isoform *eEF1A2* regulation. This switch in isoform expression seemed to be correlated with neurodevelopment of the neuron (Wefers et al. 2022). Thus, it could be hypothesised that the drop in miRNA 183/96/182 cluster expression from 2 to 3-month-old mice could even be required for the shift between *eEF1A1* and *eEF1A2* mRNA expression during late development and maturation of neuronal cells. Consequently, slight disturbances of the tightly regulated miRNA expression patterns might lead to unintended severe disturbances in the development and maintenance of synapses. However, clinical symptoms upon *SNCA* overdosage are observed long after the onset of pathological changes. Accordingly, the brain in its complexity might be able to compensate developmental deficits, which would enable proper function throughout the years even with underlying genetic risk factors.

MIRNA 183/96/182 CLUSTER DYNAMICS

Interestingly, AST and CAS COs seemed to resolve the miRNA expression dynamics more precisely, since a significant increase of miRNA 183/96/182 cluster expression was observed at day 100 exclusively in AST COs. However, analysis of a later time point in 18 month old, thus senescent PDGF

mice, could detect comparable expression levels of the miRNA cluster as for 4-month-old mice, without a significant difference between PDGF and wild type mice (data not shown).

Notably, miRNAs are reported to resemble distinct roles depending on their subcellular localization and temporal expression (He and Hannon 2004). The drop in miRNA expression was observed in PDGF mice from 2 to 3 months, thus during the shift from development to post-developmental mature mice (Flurkey et al. 2007). Therefore, the miRNA 183/96/182 cluster expression could be required in two distinct regulatory functions for normal cellular homeostasis: During development, the miRNA 183/96/182 cluster seemed to be required for control of local protein synthesis in the synapse. Its reduced expression correlates with the switch from development to maturation, emphasising a relevant regulatory role. In contrast, in mature and aged neurons, the miRNA 183/96/182 cluster could take on a different role other than regulating local protein synthesis, especially since isoform *eEF1A2* rather than *eEF1A1* is predominantly expressed in mature synapses, which was not bound to the miRNA 183/96/182 cluster in the pulldown experiments. Nevertheless, a variety of cytoskeletal mRNAs were identified to directly bind to each miRNA of the cluster, suggesting that the miRNA 183/96/182 cluster in post-developmental and mature neurons could regulate actin dynamics required during synaptic plasticity. Still, a different subcellular localization of the miRNA cluster associated with a different regulatory role in mature cells cannot be excluded, but would require further investigation.

Several questions remain to be elucidated: How does SNCA overexpression lead to increased abundance of miRNA 183/96/182 expression? Is the dynamic expression of the miRNA 183/96/182 cluster attributed to the switch in maturation state of synapses, which might be correlated or even possibly caused by differences in *eEF1A1* and *eEF1A2* expression? Does the expression of the miRNA 183/96/182 cluster in mature neurons conduct similar molecular functions or does it post-transcriptionally regulate different (cytoskeletal) proteins? What is the role and potential contribution of the other genes identified with the *in vitro* pulldown?

X. CONCLUSION

In summary, this thesis proposes a regulatory mechanism related to local protein translation during the development of glutamatergic synapses. Controlled regulation of protein synthesis would be mediated by post-transcriptional binding of the miRNA 183/96/182 cluster to *eEF1A1* mRNA, which encodes an essential component of the protein translation machinery. This mechanism is thought to occur during specific developmental stages in glutamatergic synapses, and might be diminished or replaced in mature synapses.

During development and maturation of young synapses, elevated expression of the miRNA 183/96/182 cluster caused by α-synuclein overexpression leads to enhanced repression of local translation through reduced levels of eEF1A1 protein expression in glutamatergic synapses. Consequently, overall protein synthesis is reduced and leads to weakening of synapses. Elevated expression of cytoskeletal proteins in young mature synapses along with elevated α-synuclein expression suggest impairments in the final formation or maintenance of mature synapses. A deficiency in successful stabilization of the synaptic cytoskeleton in combination with abnormally reduced local protein translation ultimately leads to a reduction in synaptic density.

In addition, this thesis proposes an *in vitro* model system to translate murine findings to a human-relevant context, and to investigate effects of α-synuclein overexpression with a human genetic background. AST and CAS derived COs are capable of recapitulating phenotypic abnormalities of the murine α-synuclein overexpressing PDGF models. Differences in growth, *SNCA* and α-synuclein expression, as well as glutamatergic synaptic loss in correlation with miRNA 183/96/182 cluster dynamics were observed in AST and CAS COs cultivated for several months.

Collectively, these findings underline the need for developmental model systems and translational research to better understand neurodegenerative diseases.

XI. ACKNOWLEDGEMENTS

Dr. Felix Strübing - thank you so much. For always having an open door for me, for your feedback, your advice and your support for all our exciting, disappointing and surprising results, for promoting and challenging me throughout this thesis!

Prof. Dr. Jochen Herms - thank you for providing me this research environment with all these techniques, methods, tool and equipment that I could use throughout this thesis, and for your feedback and support guiding me into the right directions!

Prof. Dr. Hans Straka - thank you for supervising this thesis as first referee and asking the right questions during my progress reports. Thank you for your time and your incomparable support throughout my journey at university! Thank you for everything!

Furthermore, I would like to kindly thank *Prof. Dr. Anja Horn-Bochtler* for taking over the second correction of my thesis. Furthermore, I would like to thank my thesis examination committee consisting of *Prof. Dr. Nicolas Gompel, Prof. Dr. Silke Robatzek, Prof. Dr. Herwig Stibor* and *Prof. Dr. Wolfgang Enard* for their time and associated effort. Likewise, I would like to thank *Prof. Dr. Tilo Kunath* for our collaboration and providing us the AST and CAS iPSCs for our experiments.

Dr. Alexander Beck - thank you so much for all your valued help and advice regarding cell culture, showing me how to do iPSC culture. I learned a lot from you, and you saved my cell culture schedule more than once with your stock and backup of materials...!

Federico - It was a pleasure to have you and accompanying you during your master thesis in our lab! And of course, a very big thank you for doing routinely media changes for me when my wrist was violated. *Ben* - thank you for our lunch breaks, if it was outside freezing during the winter following the current in-house guidelines. And for your patience listening to my monologues trying to find the best cell culture schedules.

During my time in the lab, many people have shared the office with me and were cheering up my daily lab life: *Jiao* and *Fang* for your good mood, *Christina, Kaltra, Pia* and *Marbod* for our discussions about cell culture and in the end *Teo* and *Carsten*. Thank you for all the chats and nice moments, as well as the intense discussions not only about lab problems! I would also like to express my gratitude to the "lab at the DZNE": *Kathi* for our nice time and always answering my questions and helping me to find things at the DZNE lab, *Caro* for the nice chats and your patching test-run, *Jose* for always providing me a fresh aliquot of antibodies, *Katrin* for helping me with the administrative jungle, *Paul* and *Lars* for your scientific advice and feedback, and *Mochen* for your support and advice regarding any questions concerning our microscope.

Vanessa thank for our time in the lab, the shared happy and sad moments (showers and 80 % ethanol...). Furthermore, thank you *Susi*, *Mourad* and *Sonja* for answering my questions related to any administrative matter and for the open door, *Melanie*!

The beautiful pictures would not haven half as beautiful without the help of the histology lab. In this sense thank you *Esther*, *Christiane*, *Susanne, Nemira* and especially *Michael* for your work and help integrating the cutting and staining of FFPE-embedded organoids into the workflow, and *Hartmut Leithäuser* for digitalizing sections on the microscope slide scanner for me. Any DNA analysis would not have been so successful without the help of *Michael* and *Virginie*, and especially *Janina* - thank you for always having a fresh 1M NaOH or Tris-HCl aliquot for me!

Viktoria, thank you for your help with the communication with the Neurobiobank Munich. Not forgetting to mention that I'm very grateful for your last-minute media changes! *Peer*, you helped me with all the IT questions I had, even if it was as simple as just installing a plug in for a software but you didn't lose your patience. Thank you! *Otto*, thank you for your support and feedback with the miRNA project, it turned out being so interesting! *Armela*, thank you for solving all the autoclave issues. *Susan and Manu*, I would like to thank both of you for always having an open door listening to questions and giving me feedback. It was worth it! *Marcel*, you did a great job organizing material for me - no matter if it was 10 µl pipette tips or media that was officially out of sock - it was always just in time for my experiments, thank you!

Besides the many helpful hands at university, I would like to thank everyone outside the lab who made my time unforgettable: Everybody from the btS München, especially *Alex* and *Eli* as well as *Laura* and *Hendrik* with our weekly lunches, *Judith* and *Veit* for the Sunday brunches, *Carina* and *Leo* for the cooking sessions, *Birgit*, *Raphael* and *Boris* for the relaxing evening swimming rounds in the lake, and *Debby* and *Andi* for the effective distraction from lab work on epic board game battle fields. And thanks to both my parents-in law *Karin* and *Ralph* with *Hanne* for the relaxing holidays.

One of the biggest thanks goes to my sister *Denise* and my parents *Regine* and *Volker* - thank you for everything. Without your constant help, support, stability and encouragement, all of this would not have been possible without you!

Last but not least - *Henning*, thank you so much for everything. For your support and understanding, although having had so many kilometres between us and the necessary thing always in another flat during out remote marriage. As Oscar Wilde said: *"Everything is going to be fine in the end. If it's not fine it's not the end."*

XII. BIBLIOGRAPHY

Abeliovich A, Schmitz Y, Fariñas I, Choi-Lundberg D, Ho WH, Castillo PE, Shinsky N, Verdugo J, Armanini M, Ryan A, Hynes M, Phillips H, Sulzer D & Rosenthal A (2000) Mice lacking a-synuclein display functional deficits in the nigrostriatal dopamine system. *Neuron* 25, 239–252.

Agarwal V, Bell GW, Nam JW & Bartel DP (2015) Predicting effective microRNA target sites in mammalian mRNAs. *Elife* 4, 1–38.

Ahn BH, Rhim H, Shi Yeon Kim YMS, Lee MY, Choi JY, Wolozin B, Chang JS, Lee YH, Kwon TK, Chung KC, Yoon SH, Hahn SJ, Kim MS, Jo YH & Mina DS (2002) α-synuclein interacts with phospholipase D isozymes and inhibits pervanadate-induced phospholipase D activation in human embryonic kidney-293 cells. *J. Biol. Chem.* 277, 12334–12342.

Alim M, Hossain M, Arima K, Takeda K, Izumiyama Y, Nakamura M, Kaji H, Shinoda T, Hisanaga & Sueda K (2002) Tubulin seeds a-synuclein fibril formation. *J. Biol. Chem.* 277, 2112–2117.

Alliot F, Godin I & Pessac B (1999) Microglia derive from progenitors, originating from the yolk sac, and which proliferate in the brain. *Brain Res. Dev. Brain Res.* 117, 145–152.

Alston-Roberts C, Barallon R, Bauer SR, Butler J, Capes-Davis A, Dirks WG, Elmore E, Furtado M, Kerrigan L, Kline MC, Kohara A, Los G V., Macleod RAF, Masters JRW, Nardone M, Nardone RM, Nims RW, Price PJ, Reid YA, Shewale J, Steuer AF, Storts DR, Sykes G, Taraporewala Z & Thomson J (2010) Cell line misidentification: The beginning of the end. *Nat. Rev. Cancer* 10, 441–448.

Alvarez-Erviti L, Rodriguez-Oroz M, Cooper J, Caballero C, Ferrer I, Obeso J & Schapira A (2010) Chaperone-mediated autophagy markers in Parkinson disease brains. *Arch. Neurol.* 67, 1464–1472.

Anderson JP, Walker DE, Goldstein JM, De Laat R, Banducci K, Caccavello RJ, Barbour R, Huang J, Kling K, Lee M, Diep L, Keim PS, Shen X, Chataway T, Schlossmacher MG, Seubert P, Schenk D, Sinha S, Gai WP & Chilcote TJ (2006) Phosphorylation of Ser-129 is the dominant pathological modification of α-synuclein in familial and sporadic lewy body disease. *J. Biol. Chem.* 281, 29739–29752.

Andres-Mateos E, Mejias R, Sasaki M, Li X, Lin BM, Biskup S, Zhang L, Banerjee R, Thomas B, Yang L, Liu G, Beal MF, Huso DL, Dawson TM & Dawson VL (2009) Unexpected lack of hypersensitivity in LRRK2 knock-out mice to MPTP (1-methyl-4- phenyl-1,2,3,6-tetrahydropyridine). *J. Neurosci.* 29, J. Neurosci. 29:15846-15850.

Angenstein F, Greenough WT & Weiler IJ (1998) Metabotropic glutamate receptor-initiated translocation of protein kinase p90rsk to polyribosomes: a possible factor regulating synaptic protein synthesis. *Proc. Natl. Acad. Sci. U. S. A.* 95, 15078–15083.

Antar L, Dictenberg J, Plociniak M, Afroz R & Bassell G (2005) Localization of FMRP-associated mRNA granules and requirement of microtubules for activity-dependent trafficking in hippocampal neurons. *Genes, Brain Behav.* 4, 350–359.

Antar LN, Afroz R, Dictenberg JB, Carroll RC & Bassell GJ (2004) Metabotropic glutamate receptor activation regulates fragile X mental retardation protein and Fmr1 mRNA localization differentially in dendrites and at synapses. *J. Neurosci.* 24, 2648–2655.

Arlotta P & Pasca SP (2019) Cell diversity in the human cerebral cortex: from the embryo to brain organoids. *Curr. Opin. Neurobiol.* 56, 194–198.

Ashley CT, Wilkinson KD, Reines D & Warren ST (1993) FMR1 protein: Conserved RNP family domains and selective RNA binding. *Science* 262, 563–566.

Bagley JA, Reumann D, Bian S, Lévi-Strauss J & Knoblich JA (2017) Fused cerebral organoids model interactions between brain regions. *Nat. Methods* 14, 743–751.

Bagni C & Greenough WT (2005) From mRNP trafficking to spine dysmorphogenesis: The roots of fragile X syndrome. *Nat. Rev. Neurosci.* 6, 376–387.

Bandyopadhyay U & Cuervo A (2007) Chaperone-mediated autophagy in aging and neurodegeneration: Lessons from a-synuclein. *Exp. Gerontol.* 42, 120–128.

Bartel DP (2018) Metazoan MicroRNAs. *Cell* 173, 20–51.

Bartels T, Kim NC, Luth ES & Selkoe DJ (2014) N-alpha-acetylation of α-synuclein increases its helical folding propensity, GM1 binding specificity and resistance to aggregation. *PLoS One* 9, 1–10.

Bassell GJ & Warren ST (2008) Fragile X syndrome: loss of local mRNA regulation alters synaptic development and function. *Neuron* 60, 201–214.

Bayer TA, Jakala P, Hartmann T, Egensperger R, Buslei R, Falkei P & Beyreuther K (1999) Neural expression profile of a-synuclein in developing human cortex. *Neuroreport* 10, 2799–2803.

Bear MF & Connors BW (2015a) Chapter 5: Synaptic Transmission. In *Neuroscience: Exploring the Brain*. Jones and Bartlett Publishers, Inc, pp.109–142.

Bear MF & Connors BW (2015b) Chapter 6: Neurotransmitter Systems. In *Neuroscience: Exploring the Brain*. Jones and Bartlett Publishers, Inc, pp.143–178.

Bear MF, Huber KM & Warren ST (2004) The mGluR theory of fragile X mental retardation. *Trends Neurosci.* 27, 370–377.

Bekris LM, Mata IF & Zabetian CP (2010) The genetics of Parkinson disease. *J. Geriatr. Psychiatry Neurol.* 23, 228–242.

Bellucci A, Mercuri N, Venneri A, Faustini G, Longhena F, Pizzi M, Missale C & Spano P (2016) Review: Parkinson's disease: from synaptic loss to connectome dysfunction. Neuropathol. *Appl. Neurobiol.* 42, 77–94.

Bennett M, Bishop J, Leng Y, Chock P, Chase T & Mouradian M (1999) Degradation of a-synuclein by proteasome. *J. Biol. Chem.* 274, 33855–33858.

Benton G, Kleinman HK, George J & Arnaoutova I (2011) Multiple uses of basement membrane-like matrix (BME/Matrigel) in vitro and in vivo with cancer cells. *Int.*

J. Cancer 123, 1751–1757.

Berezikov E, Chung WJ, Willis J, Cuppen E & Lai EC (2007) Mammalian mirtron genes. *Mol. Cell* 28, 328–336.

Bernstein E, Kim SY, Carmell MA, Murchison EP, Alcorn H, Li MZ, Mills AA, Elledge SJ, Anderson K V. & Hannon GJ (2003) Dicer is essential for mouse development. *Nat. Genet.* 35, 215–217.

Bershteyn M, Nowakowski T, Pollen A, Lullo E, Nene A, Wynshaw-Boris A & Kriegstein A (2017) Human iPSC-derived cerebral organoids model cellular features of lissencephaly and reveal prolonged mitosis of outer radial glia. *Cell Stem Cell* 20, 432–449.

Beyer K, Domingo-Sàbat M, Humbert J, Carrato C, Ferrer I & Ariza A (2008) Differential expression of alpha-synuclein, parkin, and synphilin-1 isoforms in Lewy body disease. *Neurogenetics* 9, 163–172.

Beyer K, Lao JI, Carrato C, Mate JL, López D, Ferrer I & Ariza A (2004) Differential expression of α-synuclein isoforms in dementia with Lewy bodies. *Neuropathol. Appl. Neurobiol.* 30, 601–607.

Bianchi F, Malboubi M, Li Y, George JH, Jerusalem A, Szele F, Thomson M & Ye H (2018) Rapid and efficient differentiation of functional motor neurons from human iPSC for neural injury modelling. *Stem Cell Res.* 32, 126–134.

Biedler J, Roffler-Tarlov S, Schachner M & Freedman LS (1978) Multiple neurotransmitter synthesis by human neuroblastoma cell lines and clones. *Cancer Res.* 38, 3751–7.

Birey F, Andersen J, Makinson CD, Islam S, Wei W, Huber N, Fan HC, Metzler KRC, Panagiotakos G, Thom N, O'Rourke NA, Steinmetz LM, Bernstein JA, Hallmayer J, Huguenard JR & Pasca SP (2017) Assembly of functionally integrated human forebrain spheroids. *Nature* 545, 54–59.

Blumenstock S, Angelo MF, Peters F, Dorostkar MM, Ruf VC, Luckner M, Crux S, Slapakova L, Arzberger T, Claverol S, Herzog E & Herms J (2019) Early defects in translation elongation factor 1α levels at excitatory synapses in α-synucleinopathy. *Acta Neuropathol.* 138, 971–986.

Blumenstock S, Rodrigues EF, Peters F, Blazquez-Llorca L, Schmidt F, Giese A & Herms J (2017) Seeding and transgenic overexpression of alpha-synuclein triggers dendritic spine pathology in the neocortex. *EMBO Mol. Med.* 9, 716–731.

Bobela W, Zheng L & Schneider BL (2014) Overview of mouse models of Parkinson's disease. *Curr. Protoc. Mouse Biol.* 4, 121–139.

Bohush A, Niewiadomska G & Filipek A (2018) Role of mitogen activated protein kinase signaling in parkinson's disease. *Int. J. Mol. Sci.* 19, 2973.

Van De Bor V & Davis I (2004) mRNA localisation gets more complex. *Curr. Opin. Cell Biol.* 16, 300–307.

Borchert GM, Lanier W & Davidson BL (2006) RNA polymerase III transcribes human microRNAs. *Nat. Struct. Mol. Biol.* 13, 1097–1101.

Borghi R, Marchese R, Negro A, Marinelli L, Forloni G, Zaccheo D, Abbruzzese G & Tabaton M (2000) Full length a-synuclein is present in cerebrospinal fluid from Parkinson's disease and normal subjects. *Neurosci. Lett.* 287, 65– 67.

Boudreau RL, Jiang P, Gilmore BL, Spengler RM, Tirabassi R, Nelson JA, Ross CA, Xing Y & Davidson BL (2014) Transcriptome-wide discovery of microRNA binding sites in Human Brain. *Neuron* 81, 294–305.

Braak H & Braak E (1995) Staging of Alzheimer's disease-related neurofibrillary changes. *Neurobiol. Aging* 16, 271–284.

Braak H, Del Tredici K, Rüb U, De Vos RAI, Jansen Steur ENH & Braak E (2003) Staging of brain pathology related to sporadic Parkinson's disease. *Neurobiol. Aging* 24, 197–211.

Bramham CR & Wells DG (2007) Dendritic mRNA: Transport, translation and function. *Nat. Rev. Neurosci.* 8, 776–789.

Brand KG & Syverton JT (1962) Results of species-specific hemagglutination tests on "transformed", nontransformed, and primary cell cultures. *J. Natl. Cancer Inst.* 28, 147–57.

Brazdis RM, Alecu JE, Marsch D, Dahms A, Simmnacher K, Lörentz S, Brendler A, Schneider Y, Marxreiter F, Roybon L, Winner B, Xiang W & Prots I (2021) Demonstration of brain region-specific neuronal vulnerability in human iPSC-based model of familial Parkinson's disease. *Hum. Mol. Genet.* 29, 1180–1191.

Brenner S, Wersinger C & Gasser T (2015) Transcriptional regulation of the α-synuclein gene in human brain tissue. *Neurosci. Lett.* 599, 140–145.

Brown SJ, Boussaad I, Jarazo J, Fitzgerald JC, Antony P, Keatinge M, Blechman J, Schwamborn JC, Krüger R, Placzek M & Bandmann O (2021) PINK1 deficiency impairs adult neurogenesis of dopaminergic neurons. *Sci. Rep.* 11, 1–14.

Browne GJ & Proud CG (2002) Regulation of peptide-chain elongation in mammalian cells. *Eur. J. Biochem.* 269, 5360–5368.

Bunai F, Ando K, Ueno H & Numata O (2006) Tetrahymena eukaryotic translation elongation factor 1A (eEF1A) bundles filamentous actin through dimer formation. *J. Biochem.* 140, 393–399.

Burre J, Sharma M & Südhof T. (2014) a-Synuclein assembles into higher-order multimers upon membrane binding to promote SNARE complex formation. *Proc. Natl. Acad. Sci.* 111, E4274–E4283.

Burré J, Sharma M & Südhof TC (2018) Cell biology and pathophysiology of α-synuclein. *Cold Spring Harb. Perspect. Med.* 8, a024091.

Burré J, Sharma M, Tsetsenis T, Buchman V, Etherton MR & Südhof TC (2010) α-Synuclein promotes SNARE-complex assembly in vivo and in vitro. *Science* 329, 1663–1667.

Bussell RJ & Eliezer D (2003a) A structural and functional role for 11-mer repeats in a-synuclein and other exchangeable lipid binding proteins. *J. Mol. Biol.* 329, 763–778.

Bussell RJ & Eliezer D (2003b) A structural and functional role for 11-mer repeats in α-synuclein and other exchangeable lipid binding proteins. *J. Mol. Biol.* 329, 763–778.

Bussell RJ, Ramlall T & Eliezer D (2005) Helix periodicity, topology, and dynamics of membrane-associated a-synuclein. *Protein Sci.* 14, 862–872.

Bystron I, Blakemore C & Rakic P (2008) Development of the

human cerebral cortex: Boulder Committee revisited. *Nat. Rev. Neurosci.* 9, 110–122.

Cabin DE, Shimazu K, Murphy D, Cole NB, Gottschalk W, McIlwain KL, Orrison B, Chen A, Ellis CE, Paylor R, Lu B & Nussbaum RL (2002) Synaptic vesicle depletion correlates with attenuated synaptic responses to prolonged repetitive stimulation in mice lacking α-synuclein. *J. Neurosci.* 22, 8797–8807.

Cabrero FR & Morrison EH (2022) *Lewy bodies* Treasure I. FL, ed., StatPearls (Internet): Stat Pearls Publishing.

Cai Y, Hagedorn CH & Cullen BR (2004) Human microRNAs are processed from capped, polyadenylated transcripts that are also function as mRNAs. *RNA* 10, 1957–66.

Cajal SR (1888) Estructura de los centros nerviosos de las aves. *Rev. Trim. Histol. Norm. Patol.* 1, 1–10.

Camp JG, Badsha F, Florio M, Kanton S, Gerber T, Wilsch-Bräuninger M, Lewitus E, Sykes A, Hevers W, Lancaster M, Knoblich JA, Lachmann R, Pääbo S, Huttner WB & Treutlein B (2015) Human cerebral organoids recapitulate gene expression programs of fetal neocortex development. *Proc. Natl. Acad. Sci. U. S. A.* 112, 15672–15677.

Carmel I, Shomron N & Heifetz Y (2012) Does base-pairing strength play a role in microRNA repression? *RNA* 18, 1947–1956.

Catalanotto C, Cogoni C & Zardo G (2016) MicroRNA in control of gene expression: An overview of nuclear functions. *Int. J. Mol. Sci.* 17.

Ceman S, O'Donnell WT, Reed M, Patton S, Pohl J & Warren ST (2003) Phosphorylation influences the translation state of FMRP-associated polyribosomes. *Hum. Mol. Genet.* 12, 3295–3305.

Chambers S, Fasano C, Papapetrou E, Tomishima M, Sadelain M & Studer L (2009) Highly efficient neural conversion of human ES and iPS cells by dual inhibition of SMAD signaling. *Nat. Biotechnol.* 27, 275–280.

Chandra S, Chen X, Rizo J, Jahn R & Südhof TC (2003) A broken a-helix in folded a-Synuclein. *J. Biol. Chem.* 278, 15313–15318.

Chandra S, Gallardo G, Fernández-Chacón R, Schlütter OM & Südhof TC (2005) Alpha-synuclein cooperates with CSPalpha in preventing neurodegeneration. *Cell* 123, 383–896.

Chang D, Nalls MA, Hallgrímsdóttir IB, Hunkapiller J, Brug M van der, Cai F, Kerchner GA, Ayalon G, Bingol B, Sheng M, Hinds D, Behrens TW, Singleton AB, Bhangale TR & Graham RR (2017) A meta-analysis of genome-wide association studies identifies 17 new Parkinson's disease risk loci. *Nat. Genet.* 49, 1511–1516.

Chartier-Harlin M-C, Kachergus J, Roumier C, Mouroux V, Douay X, Lincoln S, Levecque C, Larvor L, Andrieux J, Hulihan M, Waucquier N, Defebvre L, Amouyel P, Farrer M & Destée A (2004) Alpha-synuclein locus duplication as a cause of familial Parkinson's disease. *Lancet* 364, 1167–1169.

Cheever A & Ceman S (2009) Phosphorylation of FMRP inhibits association with Dicer. *RNA* 15, 362–366.

Chen E, Sharman MR, Shi X, Agrawal RK & Joseph S (2015) Fragile X mental retardation protein regulates translation by binding directly to the ribosome. *Mol. Cell* 54, 407–417.

Chen M, Maimaitili M, Buchholdt SH, Jensen UB, Febbraro F & Denham M (2020) Generation of eight human induced pluripotent stem cell lines from Parkinson's disease patients carrying familial mutations. *Stem Cell Res.* 42, 0–4.

Chen RH, Wislet-Gendebien S, Samuel F, Visanji N., Zhang G, Marsilio D, Langman T, Fraser P. & Tandon A (2013) a-Synuclein membrane association is regulated by the Rab3a recycling machinery and presynaptic activity. *J. Biol. Chem.* 288, 7438–7449.

Chen Y, Dolt KS, Kriek M, Baker T, Downey P, Drummond NJ, Canham MA, Natalwala A, Rosser S & Kunath T (2019) Engineering synucleinopathy-resistant human dopaminergic neurons by CRISPR-mediated deletion of the SNCA gene. *Eur. J. Neurosci.* 49, 510–524.

Chendrimada TP, Gregory RI, Kumaraswamy E, Norman J, Cooch N, Nishikura K & Shiekhattar R (2005) TRBP recruits the Dicer complex to Ago2 for microRNA processing and gene silencing. *Nature* 436, 740–744.

Chesselet M, Richter F, Zhu C, Magen I, Watson M & Subramaniam S (2012) A progressive mouse model of Parkinson's disease: the Thy1-aSyn ("Line 61") mice. *Neurotherapeutics* 9, 297–314.

Chiba-Falek O, Kowalak JA, Smulson ME & Nussbaum RL (2005) Regulation of α-synuclein expression by poly (ADP Ribose) polymerase-1 (PARP-1) binding to the NACP-Rep1 polymorphic site upstream of the SNCA gene. *Am. J. Hum. Genet.* 76, 478–492.

Chipman LB & Pasquinelli AE (2019) miRNA Targeting: Growing beyond the Seed. *Trends Genet.* 35, 215–222.

Cho S-J, Jung, Jae-SKo BH, Jin I & Moon IS (2004) Presence of translation elongation factor-1A (eEF1A) in the excitatory postsynaptic density of rat cerebral cortex. *Neurosci. Lett.* 366, 29–33.

Cho S-J, Lee H, Dutta S, Seog D-H & Moon IS (2012) Translation elongation factor-1A1 (eEF1A1) localizes to the spine by domain III. *BMB Rep.* 45, 227–232.

Christoff K & Gabrieli JDE (2000) The frontopolar cortex and human cognition: Evidence for a rostrocaudal hierarchical organization within the human prefrontal cortex. *Psychobiology* 28, 168–186.

Claassen DA, Desler MM & Rizzino A (2009) ROCK inhibition enhances the recovery and growth of cryopreserved human embryonic stem cells and human induced pluripotent stem cells. *Mol. Reprod. Dev.* 76, 722–32.

Clayton DF & George JM (1998) The synucleins: A family of proteins involved in synaptic function, plasticity, neurodegeneration and disease. *Trends Neurosci.* 21, 249–254.

Clough RL, Dermentzaki G & Stefanis L (2009) Functional dissection of the α-synuclein promoter: Transcriptional regulation by ZSCAN21 and ZNF219. *J. Neurochem.* 110, 1479–1490.

Clough RL & Stefanis L (2007) A novel pathway for transcriptional regulation of α-synuclein. *FASEB J.* 21, 596–607.

Conway KA, Harper JD & Lansbury PT (1998) Accelerated in vitro fibril formation by a mutant α-synuclein linked to early-onset Parkinson disease. *Nat. Med.* 4, 1318–1320.

Conway KA, Lee SJ, Rochet J-C, Ding TT, Harper JD, Williamson

RE & Landsbury JR PT (2000) Accelerated oligomerization by Parkinson's disease linked alpha-synuclein mutants. *Ann. New York Acad. Sci.* 920, 42–45.

Crick FH (1958) On protein synthesis. *Symp. Soc. Exp. Biol.* 12, 138–63.

Cuervo A, Stefanis L, Fredenburg R, Lansbury P & Sulzer D (2004) Impaired degradation of mutant a-synuclein by chaperone-mediated autophagy. *Science* 305, 1292–1295.

Cuervo AM & Macian F (2014) Autophagy and the immune function in aging. *Curr. Opin. Immunol.* 29, 97–104.

Dahariya S, Paddibhatla I, Kumar S, Raghuwanshi S, Pallepati A & Gutti RK (2019) Long non-coding RNA: Classification, biogenesis and functions in blood cells. *Mol. Immunol.* 112, 82–92.

Dambal S, Shah M, Mihelich B & Nonn L (2015) The microRNA-183 cluster: The family that plays together stays together. *Nucleic Acids Res.* 43, 7173–7188.

Darnell JC, Van Driesche SJ, Zhang C, Hung KYS, Mele A, Fraser CE, Stone EF, Chen C, Fak JJ, Chi SW, Licatalosi DD, Richter JD & Darnell RB (2011) FMRP stalls ribosomal translocation on mRNAs linked to synaptic function and autism. *Cell* 146, 247–261.

Darnell JC & Klann E (2013) The translation of translational control by FMRP: therapeutic targets for FXS. *Nat. Neurosci.* 16, 150–1536.

Davidson W, Jonas A, Clayton D & George J (1998) Stabilization of a-synuclein secondary structure upon binding to synthetic membranes. *J. Biol. Chem.* 273, 9443– 944.

Day M, Wang Z, Ding J, An X, Ingham C, Shering A, Wokosin D, Ilijic E, Sun Z, Sampson A, Mugnaini E, Deutch A, Sesack S, Arbuthnott G & Surmeier D (2006) Selective elimination of glutamatergic synapses on striatopallidal neurons in Parkinson disease models. *Nat. Neurosci.* 9, 251 – 259.

Decressac M, Mattsson B, Weikop P, Lundblad M, Jakobsson J & Björklund A (2013) TFEB-mediated autophagy rescues midbrain dopamine neurons from α-synuclein toxicity. *Proc. Natl. Acad. Sci. U. S. A.* 110.

Delaidelli A, Jan A, Herms J & Sorensen PH (2019) Translational control in brain pathologies: biological significance and therapeutic opportunities. *Acta Neuropathol.* 137, 535–555.

Desplats P, Lee H, Bae E, Patrick C, Rockenstein E, Crews L, Spencer B, Masliah E & Lee S (2009) Inclusion formation and neuronal cell death through neuron-to-neuron transmission of a-synuclein. *Proc. Natl. Acad. Sci.* 106, 13010–13015.

Devine MJ, Ryten M, Vodicka P, Thomson AJ, Burdon T, Houlden H, Cavaleri F, Nagano M, Drummond NJ, Taanman JW, Schapira AH, Gwinn K, Hardy J, Lewis PA & Kunath T (2011) Parkinson's disease induced pluripotent stem cells with triplication of the α-synuclein locus. *Nat. Commun.* 2.

Didiano D & Hobert O (2008) Molecular architecture of a miRNA-regulated 3'UTR. *RNA* 14, 1297–1317.

Dikiy I & Eliezer D (2012) Folding and misfolding of alpha-synuclein on membranes. *Biochim. Biophys. Acta* 1818, 1013–8.

Dikiy I & Eliezer D (2014) N-terminal acetylation stabilizes N-terminal helicity in lipid- and micelle-bound α-synuclein and increases its affinity for physiological membranes. *J. Biol. Chem.* 289, 3652–3665.

Ding TT, Lee SJ, Rochet JC & Lansbury PT (2002) Annular α-synuclein protofibrils are produced when spherical protofibrils are incubated in solution or bound to brain-derived membranes. *Biochemistry* 41, 10209–10217.

Dölen G, Osterweil E, Rao BSS, Smith GB, Auerbach BD, Chattarji S & Bear MF (2007) Correction of Fragile X Syndrome in Mice. *Neuron* 56, 955–962.

Donadio V, Incensi A, Rizzo G, Capellari S, Pantieri R, Stanzani Maserati M, Devigili G, Eleopra R, Defazio G, Montini F, Baruzzi A & Liguori R (2017) A new potential biomarker for dementia with Lewy bodies: skin nerve alpha-synuclein deposits. *Neurology* 89, 318–326.

Doxakis E (2010) Post-transcriptional regulation of alpha-synuclein expression by mir-7 and mir-153. *J. Biol. Chem.* 285.

El-Agnaf OMA, Salem SA, Paleologiu KE, Cooper LJ, Fullwood NJ, Gibson MJ, Curran MD, Court JA, Mann DMA, Ikeada S ich., Cookson MR, Hardy J & Allsop D (2003) a-Synuclein implicated in Parkinson's disease is present in extracellular biological fluids, including human plasma. *FASEB J.* 17, 1945–1947.

Eliezer D, Kutluay E, Bussell Jr R & Browne G (2001) Conformational properties of alpha-synuclein in its free and lipid-associated states. *J. Mol. Biol.* 307, 1061–1073.

Ellis C, Murphy E, Mitchell D, Golovko M, Scaglia F, Barcelo-Coblijn G & Nussbaum R (2005) Mitochondrial lipid abnormality and electron transport chain impairment in mice lacking a-synuclein. *Mol. Cell Biol.* 25, 10190–10201.

Ellis CE, Schwartzberg PL, Grider TL, Fink DW & Nussbaum RL (2001) α-Synuclein is phosphorylated by members of the Src family of protein-tyrosine kinases. *J. Biol. Chem.* 276, 3879–3884.

Ellwanger DC, Büttner FA, Mewes HW & Stümpflen V (2011) The sufficient minimal set of miRNA seed types. *Bioinformatics* 27, 1346–1350.

Emmanouilidou E, Stefanis L & Vekrellis K (2010) Cell-produced a-synuclein oligomers are targeted to, and impair, the 26S proteasome. *Neurobiol. Aging* 31, 953–968.

Ensemble.org (2021) e!Ensembl (SNCA). Available at: https://www.ensembl.org/Homo_sapiens/Gene/Summary?db=core;g=ENSG00000145335;r=4:89700345-89838315 [Accessed December 14, 2021].

Eriksen JL, Przedborski S & Petrucelli L (2005) Gene dosage and pathogenesis of Parkinson's disease. *Trends Mol. Med.* 11, 19–96.

Falkenburger BH, Saridaki T & Dinter E (2016) Cellular models for Parkinson's Disease. *J. Neurochem.* 139, 121–130.

Fan X, Dong J, Zhong S, Wei Y, Wu Q, Yan L, Yong J, Sun L, Wang X, Zhao Y, Wang W, Yan J, Wang X, Qiao J & Tang F (2018) Spatial transcriptomic survey of human embryonic cerebral cortex by single-cell RNA-seq analysis. *Cell Res.* 28, 730–745. Available at: http://dx.doi.org/10.1038/s41422-018-0053-3.

Fang F, Yang W, Florio JB, Rockenstein E, Spencer B, Orain XM, Dong SX, Li H, Chen X, Sung K, Rissman RA, Masliah E,

Ding J & Wu C (2017) Synuclein impairs trafficking and signaling of BDNF in a mouse model of Parkinson's disease. *Sci. Rep.* 7, 1–13.

Fares MB, Ait-Bouziad N, Dikiy I, Mbefo MK, Jovičić A, Kiely A, Holton JL, Lee SJ, Gitler AD, Eliezer D & Lashuel HA (2014) The novel Parkinson's disease linked mutation G51D attenuates in vitro aggregation and membrane binding of α-synuclein, and enhances its secretion and nuclear localization in cells. *Hum. Mol. Genet.* 23, 4491–4509.

Farrer M, Kachergus J, Forno L, Lincoln S, Wang DS, Hulihan M, Maraganore D, Gwinn-Hardy K, Wszolek Z, Dickson D & Langston JW (2004) Comparison of kindreds with parkinsonism and α-synuclein genomic multiplications. *Ann. Neurol.* 55, 174–179.

Fernández E, Collins M, Uren R, Kopanitsa M, Komiyama N, Croning M, Zografos L, Armstrong J, Choudhary J & Grant S (2009) Targeted tandem affinity purification of PSD-95 recovers core postsynaptic complexes and schizophrenia susceptibility proteins. *Mol. Syst. Biol.* 5, 269.

Ferrer I (2009) Early involvement of the cerebral cortex in Parkinson's disease: Convergence of multiple metabolic defects. *Prog. Neurobiol.* 88, 89–103.

Ferrer I, Perez E, Dalfo E & Barrachina M (2007) Abnormal levels of prohibitin and ATP synthase in the substantia nigra and frontal cortex in Parkinson's disease. *Neurosci. Lett.* 415, 205–209.

Fiala J, Feinberg M, Popov V & Harris K (1998) Synaptogenesis via dendritic filopodia in developing hippocampal area CA1. *J. Neurosci.* 18, 8900–8911.

Fiala JC, Spacek J & Harris KM (2002) Dendritic spine pathology: cause or consequence of neurological disorders? *Brain Res.* 39.

Finkelstein DI, Hare DJ, Billings JL, Sedjahtera A, Nurjono M, Arthofer E, George S, Culvenor JG, Bush AI & Adlard PA (2016) Clioquinol improves Cognitive, motor function, and microanatomy of the alpha-synuclein hA53T transgenic mice. *ACS Chem. Neurosci.* 7, 119–129.

Flurkey K, Currer JM & Harrison DE (2007) The Mouse in Aging Research. In E. Fox J.G., et al., ed. *The Mouse in Biomedical Research*. Burlington: American College Laboratory Animal Medicine (Elsevier), pp.637–682.

Frahm S, Melis V, Horsley D, Rickard JE, Riedel G, Fadda P, Scherma M, Harrington CR, Wischik CM, Theuring F & Schwab K (2018) Alpha-Synuclein transgenic mice, h-α-SynL62, display α-syn aggregation and a dopaminergic phenotype reminiscent of Parkinson's disease. *Behav. Brain Res.* 339, 153–168.

Friedman RC, Farh KKH, Burge CB & Bartel DP (2009) Most mammalian mRNAs are conserved targets of microRNAs. *Genome Res.* 19, 92–105.

Fromm B, Keller A, Friedlander MR, Peterson KJ & Grif S (2020) Forum Quo vadis microRNAs ? *Trends Genet.* 36, 461–463.

Fu R, Shen Q, Xu P, Luo JJ & Tang Y (2014) Phagocytosis of microglia in the central nervous system diseases. *Mol. Neurobiol.* 49, 1422–1434.

Fujiwara H, Hasegawa M, Dohmae N, Kawashima A, Masliah E, Goldberg MS, Shen J, Takio K & Iwatsubo T (2002) A-Synuclein is phosphorylated in synucleinopathy lesions. *Nat. Cell Biol.* 4, 160–164.

Galvin J, Lee V & Trojanowski J (2001) Synucleinopathies - clinical and pathological implications. *Neurol. Rev.* 58, 186–1990.

Galvin JE, Schuck TM, Lee VM & Trojanowski JQ (2001) Differential expression and distribution of alpha-, beta-, and gamma-synuclein in the developing human substantia nigra. *Exp. Neurobiol.* 168, 347–355.

Garcia-Esparcia P, Hernández-Ortega K, Koneti A, Gil L, Delgado-Morales R, Castaño E, Carmona M & Ferrer I (2015) Altered machinery of protein synthesis is region- and stage-dependent and is associated with α-synuclein oligomers in Parkinson's disease. *Acta Neuropathol. Commun.* 3, 1–25.

Garcia-Reitböck R, Anichtchik O, Bellucci A, Iovino M, Ballini C, Fineberg E, Ghetti B, Della Corte L, Spano P, Togaris G, Goedert M & Spillantini M (2010) SNARE protein redistribution and synaptic failure in a transgenic mouse model of Parkinson's disease. *Brain* 133, 2032–2044.

Garner CC, Nash J & Huganir RL (2000) PDZ domains in synapse assembly and signalling. *Trends Cell Biol.* 10, 274–280.

Gehrke S, Imai Y, Sokol N & Lu B (2010) Pathogenic LRRK2 negatively regulates microRNA-mediated translational repression. *Nature* 466, 637–641.

Gelb DJ., Oliver E & Gilman S (1999) Diagnostic criteria for Parkinson disease. *Arch. Neurol.* 56, 33–39.

Geng J (2019) *Early changes in miRNAs expression in a mouse model of Parkinson's Disease*. LMU Munich.

Giandomenico SL, Mierau SB, Gibbons GM, Wenger LMD, Masullo L, Sit T, Sutcliffe M, Boulanger J, Tripodi M, Derivery E, Paulsen O, Lakatos A & Lancaster MA (2019) Cerebral organoids at the air–liquid interface generate diverse nerve tracts with functional output. *Nat. Neurosci.* 22, 669–679.

Giasson BI, Forman MS, Higuchi M, Golbe LI, Graves C, Kotzbauer PT, Trojanowski JQ & Lee VM-Y (2003) Initiation and synergistic fibrillization of tau and alpha-synuclein. *Science* 300, 636–640.

Gillet JP, Varma S & Gottesman MM (2013) The clinical relevance of cancer cell lines. *J. Natl. Cancer Inst.* 105, 452–458.

Goldberg MS, Fleming SM, Palacino JJ, Cepeda C, Lam HA, Bhatnagar A, Meloni EG, Wu N, Ackerson LC, Klapstein GJ, Gajendiran M, Roth BL, Chesselet MF, Maidment NT, Levine MS & Shen J (2003) Parkin-deficient mice exhibit nigrostriatal deficits but not loss of dopaminergic neurons. *J. Biol. Chem.* 278, 43628–43635.

Gómez-Tortosa E, Newell K, Irizarry MC, Sanders JL & Hyman BT (2000) α-synuclein immunoreactivity in dementia with Lewy bodies: Morphological staging and comparison with ubiquitin immunostaining. *Acta Neuropathol.* 99, 352–357.

Gonzalez C, Armijo E, Bravo-Alegria J, Becerra-Calixto A, Mays CE & Soto C (2018) Modeling amyloid beta and tau pathology in human cerebral organoids. *Mol. Psychiatry* 23, 2363–2374.

Gregory RI, Chendrimada TP, Cooch N & Shiekhattar R (2005) Human RISC couples microRNA biogenesis and posttranscriptional gene silencing. *Cell* 123, 631–640.

Gregory SG, Barlow K, ... & Bentley DR (2006) The DNA sequence and biological annotation of human chromosome 1. *Nature* 441, 315–321.

Greten-Harrison B, Polydoro M, Morimoto-Tomita M, Diao L, Williams AM, Nie EH, Makani S, Tian N, Castillo PE, Buchman VL & Chandra SS (2010) αβγ-Synuclein triple knockout mice reveal age-dependent neuronal dysfunction. *Proc. Natl. Acad. Sci.* 107, 19573–19578.

Griffiths-Jones S (2004) The microRNA registry. *Nucleic Acids Res.* 32, D109–D111.

Griffiths-Jones S, Saini HK, Van Dongen S & Enright AJ (2008) miRBase: Tools for microRNA genomics. *Nucleic Acids Res.* 36, 154–158.

Grimson A, Farh KK-H, Johnston WK, Garrett-Engele P, Lim LP & Bartel DP (2007) MicroRNA targeting specificity in mammals: determinants beyond seed pairing. *Mol. Cell* 27, 91–105.

Gross SR & Gross Kinzy T (2005) Translation elongation factor 1A is essential for regulation of the actin cytoskeleton and cell morphology. *Nat. Struct. Mol. Biol.* 12, 772–778.

Gründemann J, Schlaudraff F, Haeckel O & Liss B (2008) Elevated α-synuclein mRNA levels in individual UV-laser-microdissected dopaminergic substantia nigra neurons in idiopathic Parkinson's disease. *Nucleic Acids Res.* 36, 1–16.

Gureviciene I, Gurevicius K & Tanila H (2009) Aging and a-synuclein affect synaptic plasticity in the dentate gyrus. *J. Neural Transm.* 116, 13–22.

Gureviciene I, Gurevicius K & Tanila H (2007) Role of a-synuclein in synaptic glutamate release. *Neurobiol. Dis.* 28, 83–89.

Gwinn K, Devine MJ, Jin LW, Johnson J, Bird T, Muenter M, Waters C, Adler CH, Caselli R, Houlden H, Lopez G, Singleton A, Hardy J & Singleton A (2011) Clinical features, with video documentation, of the original familial lewy body parkinsonism caused by α-synuclein triplication (Iowa kindred). *Mov. Disord.* 26, 2134–2136.

Haase AD, Jaskiewicz L, Zhang H, Lainé S, Sack R, Gatignol A & Filipowicz W (2005) TRBP, a regulator of cellular PKR and HIV-1 virus expression, interacts with Dicer and functions in RNA silencing. *EMBO Rep.* 6, 961–967.

Haggerty T, Credle J, Rodriguez O, Wills J, Oaks A, Masliah E & Sidhu A (2011) Hyperphosphorylated tau in an a-synuclein-overexpressing transgenic model of Parkinson's disease. *Eur. J. Neurosci.* 33, 1598–1610.

Haghnejad L, Emamalizadeh B, Jamshidi J, Bidoki AZ, Ghaedi H, Ahmadi E, Abdollahi S, Shahmohammadibeni N, Taghavi S, Fazeli A, Motallebi M, Zarneh AES, Mohammadihosseinabad S, Abbaszadegan MR, Torkamandi S, Gavenaroudi MA, Pedram N, Shahidi GA, Tafakhori A, Darvish H & Movafagh A (2015) Variation in the miRNA-433 binding site of FGF20 is a risk factor for Parkinson's disease in Iranian population. *J. Neurol. Sci.* 355, 72–74.

Han J, Lee Y, Yeom K-H, Kim Y-K, Jin H & Kim N V. (2004) The Drosha-DGCR8 complex in primary microRNA processing. *Genes Dev.* 18, 3016–3027.

Han J, Lee Y, Yeom KH, Nam JW, Heo I, Rhee JK, Sohn SY, Cho Y, Zhang BT & Kim VN (2006) Molecular Basis for the Recognition of Primary microRNAs by the Drosha-DGCR8 Complex. *Cell* 125, 887–901.

Han J, Pedersen JS, Kwon SC, Belair CD, Kim Y-K, Yeom K-H, Yang W-Y, Haussler D, Blelloch R & Kim VN (2009) Posttranscriptional crossregulation between Drosha and DGCR8. *Cell* 136, 75–84.

Hansen TB, Venø MT, Jensen TI, Schaefer A, Damgaard CK & Kjems J (2016) Argonaute-associated short introns are a novel class of gene regulators. *Nat. Commun.* 7, 1–10.

Harris K & Stevens J (1989) Dendritic spines of CA 1 pyramidal cells in the rat hippocampus: serial electron microscopy with reference to their biophysical characteristics. *J. Neurosci.* 9, 2982–2997.

Harris K & Stevens J (1988) Dendritic spines of rat cerebellar Purkinje cells: serial electron microscopy with reference to their biophysical characteristics. *J. Neurosci.* 8, 4455–4469.

He L & Hannon GJ (2004) MicroRNAs: Small RNAs with a big role in gene regulation. *Nat. Rev. Genet.* 5, 522–531.

Heikkila R, Hess A & Duvoisin R (1984) Dopaminergic neurotoxicity of 1-methyl-4- phenyl-1,2,5,6-tetrahydropyridine in mice. *Science* 224, 1451–1453.

Hou L, Antion MD, Hu D, Spencer CM, Paylor R & Klann E (2006) Dynamic translational and proteasomal regulation of fragile X Mental retardation protein controls mGluR-dependent long-term depression. *Neuron* 51, 441–454.

Hsu LJ, Mallory M, Xia Y, Veinbergs I, Hasimoto M, Yoshimoto M, Thal LJ, Saitoh T & Masliah E (1998) Expression pattern of synucleins (non-Ab component of Alzheimer's disease amyloid precursor protein/a-synuclein) during murine brain development. *J. Neurochem.*, 338–344.

Hughes A, Daniel S, Kilford L & Lees A (1992) Accuracy of clinical diagnosis of idiopathic Parkinson's disease: a clinico-pathological study of 100 cases. *J. Neurol. Neurosurg. Psychiatry* 55, 181–184.

Hughes CS, Postovit LM & Lajoie GA (2010) Matrigel: a complex protein mixture required for optimal growth of cell culture. *Proteomics* 10, 1886–1890.

Hughes J (1958) Post-tetanic potentiation. *Physiol. Rev.* 38, 91–113.

Ibáñez P., Lohmann E., Pollak P., Durif F., Tranchant C., Agid Y., Dürr A. & Brice A (2004) Absence of NR4A2 exon 1 mutations in 108 families with autosomal dominant Parkinson disease. *Neurology* 62, 2133–2134.

Ibáñez P, Bonnet A, Debarges B, Lohmann E, Tison F, Pollak P, Agid Y & Brice A (2004) Causal relation between alpha-synuclein gene duplication and familial Parkinson's disease. *Lancet* 364, 1169–1171.

Ifrim MF, Williams KR & Bassell GJ (2015) Single-molecule imaging of PSD-95 mRNA translation in dendrites and its dysregulation in a mouse model of fragile X syndrome. *J. Neurosci.* 35, 7116–7130.

Iketani M, Iizuka A, Sengoku K, Kurihara Y, Nakamura F, Sasaki Y, Sato Y, Yamane M, Matsushita M, Nairn AC, Takamatsu K, Goshima Y & Takei K (2013) Regulation of neurite outgrowth mediated by localized phosphorylation of protein translational factor eEF2 in growth cones. *Dev. Neurobiol.* 73, 230–246.

Imprey S, Davare M, Lesiak A, Fortin D, Ando H, Varlamova O, Obrietan K, Sonderling R, Goodman R & Wayman G (2010) An activity-induced microRNA controls dendritic spine formation by regulating Rac1-PAK signaling. *Mol.*

Cell Neurosci. 43, 145–156.

Irwin DJ, Lee VMY & Trojanowski JQ (2013) Parkinson's disease dementia: Convergence of α-synuclein, tau and amyloid-β pathologies. *Nat. Rev. Neurosci.* 14, 626–636.

Iwai A, Masliah E, Yoshimoto M, Ge N, Flanagan L, de Silva HA, Kittel A & Saitho T (1995) The precursor protein of non-A beta component of Alzheimer's disease amyloid is a presynaptic protein of the central nervous system. *Neuron* 14, 467–475.

Jakes R, Spillantini MG & Goerdert M (1994) Identification of two distinct synucleins from human brain. *FEBS Lett.* 345, 27–32.

Jelling K & Lantos P (2010) Papp-Lantos inclusions and the pathogenesis of multiple system atrophy: an update. *Acta Neuropathol.* 119, 657–667.

Jellinger KA (2019) Is Braak staging valid for all types of Parkinson's disease? *J. Neural Transm.* 126, 423–431.

Jellinger KA & Korczyn AD (2018) Are dementia with Lewy bodies and Parkinson's disease dementia the same disease? *BMC Med.* 16, 1–16.

Jensen P, Hager H, Nielsen M, Hojrup P, Gliemann J & Jakes R (1999) a-Synuclein binds to Tau and stimulates the protein kinase A-catalyzed tau phosphorylation of serine residues 262 and 356. *J. Biol. Chem.* 274, 25481– 25489.

Jeon B, Jackson-Lewis V & Burke R (1995) 6-Hydroxydopamine lesion of the rat sub- stantia nigra: Time course and morphology of cell death. *Neurodegeneration* 4, 131–137.

Jo J, Xiao Y, Sun AX, Cukuroglu E, Tran HD, Göke J, Tan ZY, Saw TY, Tan CP, Lokman H, Lee Y, Kim D, Ko HS, Kim SO, Park JH, Cho NJ, Hyde TM, Kleinman JE, Shin JH, Weinberger DR, Tan EK, Je HS & Ng HH (2016) Midbrain-like organoids from human pluripotent stem cells contain functional dopaminergic and neuromelanin-producing neurons. *Cell Stem Cell* 19, 248–257.

Jones-Rhoades MW, Bartel DP & Bartel B (2006) MicroRNAs and their regulatory roles in plants. *Annu. Rev. Plant Biol.* 57, 19–53.

Jones E & Powell T (1969) Morphological variations in the dendritic spines of the neocortex. *J. Cell Sci.* 5, 509–529.

Kabaria S, Choi D, Chaudhuri A, Mouradian M & Junn E (2015) Inhibition of miR-34b and miR-34c enhances α-synuclein expression in Parkinson's disease. *FEBS Lett.* 689, 319–325.

Kadoshima T, Sakaguchi H, Nakano T, Soen M, Ando S, Eiraku M & Sasai Y (2013) Self-organization of axial polarity, inside-out layer in human ES cell–derived neocortex pattern, and species-specific progenitor dynamics. *Proc. Natl. Acad. Sci. U. S. A.* 110, 20284–20289.

Kang L, Moriarty GM, Woods LA, Ashcroft AE, Radford SE & Baum J (2012) N-terminal acetylation of α-synuclein induces increased transient helical propensity and decreased aggregation rates in the intrinsically disordered monomer. *Protein Sci.* 21, 911–917.

Kasai H, Fukuda M, Watanabe S, Hayashi-Takagi A & Noguchi J (2010) Structural dynamics of dendritic spines in memory and cognition. *Trends Neurosci.* 33, 121–129.

Kim H, Park HJ, Choi H, Chang Y, Park H, Shin J, Kim J, Lengner CJ, Lee YK & Kim J (2019) Modeling G2019S-LRRK2 sporadic Parkinson's disease in 3D midbrain organoids. *Stem Cell Reports* 12, 518–531.

Kim J (1997) Evidence that the precursor protein ofnon-A b component of Alzheimer's disease amyloid (NACP) has an extended structure primarily composed of random-coil. *Mol. Cell* 7, 78–83.

Kingsbury AE, Daniel SE, Sangha H, Eisen S, Lees AJ & Forster OJF (2004) Alteration in α-synuclein mRNA expression in Parkinson's disease. *Mov. Disord.* 19, 162–170.

Kirik D, Rosenbald C, Burger C, Lundberg C, Johansen TE, Muzyczka N, Mandel RJ & Björklund A (2002) Parkinson-like neurodegeneration induced by targeted overexpression of α-synuclein in the nigrostriatal system. *J. Neurosci.* 22, 2780–2791.

Kitada T, Pisani A, Porter D, Yamaguchi H, Tscherter A, Martella G, Bonsi P, Zhang C, Pothos E & Shen J (2007) Impaired dopamine release and synaptic plasticity in the striatum of PINK1-deficient mice. *PNAS* 140, 11441–11446.

Kitada T, Tong Y, Gautier C & Shen J (2009) Absence of nigral degeneration in aged parkin/DJ-1/PINK1 triple knockout mice. *J. Neurochem.* 111, 696–702.

Knight SW & Bass BL (2001) A role for the RNase III enzyme DCR-1 in RNA interference and germ line development in Caenorhabditis elegans. *Science* 293, 2269–2271.

Koga S, Sekiya H, Kondru N, Ross OA & Dickson DW (2021) Neuropathology and molecular diagnosis of Synucleinopathies. *Mol. Neurodegener.* 16, 1–24.

Kontopoulos E, PArvin J & Feany M (2005) a-Synuclein acts in the nucleus to inhibit histone acetylation and promote neurotoxicity. *Hum. Mol. Genet.* 15, 3012–3023.

Koppelkamm A, Vennemann B, Lutz-Bonengel S, Fracasso T & Vennemann M (2011) RNA integrity in post-mortem samples: influencing parameters and implications on RT-qPCR assays. *Int. J. Legal Med.* 125, 573–580.

Kordower J, Chu Y, Hauser R, Olanow C & Freeman T (2008) Transplanted dopaminergic neurons develop PD pathologic changes: A second case report. *Mov. Disord.* 23, 2303–2306.

Koressaar T, Lepamets M, Kaplinski L, Raime K, Andreson R & Remm M (2018) Primer3-masker: Integrating masking of template sequence with primer design software. *Bioinformatics* 34, 1937–1938.

Koressaar T & Remm M (2007) Enhancements and modifications of primer design program Primer3. *Bioinformatics* 23, 1289–1291.

Kozlowski MT, Crook CJ & Ku HT (2021) Towards organoid culture without Matrigel. *Commun. Biol.* 4, 1387.

Kozomara A & Griffiths-Jones S (2014) miR Base: annotating hih confidence microRNAs using deep sequencing data. *Nucleic Acids Res.* 42.

Kozomara A & Griffiths-Jones S (2011) miR Base: integrating microRNA annotation and deep-sequencing data. *Nucleic Acids Res.* 39.

Kramer M & Schulz-Schaeffer W (2007) Presynaptic alpha-synuclein aggregates, not lewy bodies, cause neurodegeneration in dementia with Lewy bodies. *J. Neurosci.*, 1405 – 1410.

Kremerskothen J, Teber I, Wendholt D, Liedtke T, Böckers TM &

Barnekow A (2002) Brain-specific splicing of α-actinin 1 mRNA. *Biochem. Biophys. Res. Commun.* 295, 678–681.

Krol J, Krol I, Alvarez CPP, Fiscella M, Hierlemann A, Roska B & Filipowicz W (2015) A network comprising short and long noncoding RNAs and RNA helicase controls mouse retina architecture. *Nat. Commun.* 6, 1–13. Available at: http://dx.doi.org/10.1038/ncomms8305.

Kurowska Z, Englund E, Widner H, Lindvall O, Li J & Brundin P (2011) Signs of degeneration in 12–22-year old grafts of mesencephalic dopamine neurons in patients with Parkinson's disease. *J. Parkinsons. Dis.* 1, 83–92.

Laggerbauer B, Ostareck D, Keidel EM, Ostareck-Lederer A & Fischer U (2001) Evidence that fragile X mental retardation protein is a negative regulator of translation. *Hum. Mol. Genet.* 10, 329–338.

Lai Y, Kim S, Varkey J, Lou X, Song J, Diao K, Langen R & Shin YK (2014) Nonaggregated a-synuclein influences SNARE-dependent vesicle docking via membrane binding. *Biochemistry* 53, 3889–3896.

Lancaster MA, Corsini NS, Wolfinger S, Gustafson EH, Phillips AW, Burkard TR, Otani T, Livesey FJ & Knoblich JA (2017) Guided self-organization and cortical plate formation in human brain organoids. *Nat. Biotechnol.* 35, 659–666.

Lancaster MA & Knoblich JA (2014) Generation of cerebral organoids from human pluripotent. *Nat. Protoc.* 9, 2329–2340.

Lancaster MA, Renner M, Martin CA, Wenzel D, Bicknell LS, Hurles ME, Homfray T, Penninger JM, Jackson AP & Knoblich JA (2013) Cerebral organoids model human brain development and microcephaly. *Nature* 501, 373–379.

Lander ES, Linton LM, ... & Chen YJ (2001) Initial sequencing and analysis of the human genome: International Human Genome Sequencing Consortium. *Nature* 412, 565–566.

Lannom MC & Ceman S (2021) *FMRP and MicroRNAs in Neuronal Protein Synthesis* W. Sossin, ed., New York, USA: Oxford University Press.

Lapasset L, Milhavet O, Prieur A, Besnard E, Babled A, Ät-Hamou N, Leschik J, Pellestor F, Ramirez JM, De Vos J, Lehmann S & Lemaitre JM (2011) Rejuvenating senescent and centenarian human cells by reprogramming through the pluripotent state. *Genes Dev.* 25, 2248–2253.

de Lau L & Breteler M (2006) Epidemiology of Parkinson's disease. *Lancet Neurol.* 5, 525535.

Lauwers E, Debyser Z, Van Dorpe J, De Stooper B, Nuttin B & Baekelandt V (2003) Neuropathology and neurodegeneration in rodent brain induced by lentiviral vectormediated overexpression of α-synuclein. *Brain Pathol.* 13, 364–372.

Lee H, Khoshaghideh F, Lee S & Lee S (2006) Impairment of microtubule-dependent trafficking by overexpression of a-synuclein. *Eur. J. Neurosci.* 24, 3153–3162.

Lee R, Feinbaum R & Ambros V (1993) The C. elegans heterochronic gene lin-4 encodes small RNAs with antisense complementarity to lin-14. *Cell* 75, 843–854.

Lee Y, Hur I, Park SY, Kim YK, Mi RS & Kim VN (2006) The role of PACT in the RNA silencing pathway. *EMBO J.* 25, 522–532.

Lee Y, Kim M, Han K, Yeom K-H, Lee S, Hee Baek S & Kim N V (2003) MicroRNA genes are transcribed by RNA polymerase II. *EMBO J.* 23, 4051–4060.

Lees A & Smith E (1983) Cognitive deficits in the early stages o fParkinson's disease. *Brain* 106, 257–270.

Lewitus E, Kelava I & Huttner WB (2013) Conical expansion of the outer subventricular zone and the role of neocortical folding in evolution and development. *Front. Hum. Neurosci.* 7, 1–12.

Lewy FH. (1912) *Paralysis agitans: pathologische Anatomie* Handbuch d. M. Lewandowski, ed., Berlin: Springer.

Li R, Fang A, Li P, Qu Q & Wang Yx (2017) Recapitulating cortical development with organoid culture in vitro and modeling abnormal spindle-like (ASPM related primary) microcephaly disease. *Protein Cell* 8, 823–833.

Li X, Patel JC, Wang J, Avshalumov MV, Nicholson C, Buxbaum JD, Elder GA, Rice ME & Yue Z (2010) Enhanced striatal dopamine transmission and motor performance with LRRK2 overexpression in mice is eliminated by familial Parkinson's disease mutation G2019S. *J. Neurosci.*, 1788–1797.

Li Z, Zhang Y, Ku L, Wilkinson KD, Warren ST & Feng Y (2001) The fragile X mental retardation protein inhibits translation via interacting with mRNA. *Nucleic Acids Res.* 29, 2276–2283.

Liddle RA (2018) Parkinson's disease from the gut. *Brain Res.* 1693, 201–206.

Lill CM (2016) Genetics of Parkinson's disease. *Mol. Cell. Probes* 30, 386–396.

Lim L, Glasner M, Yetka S, Burger C & Bartel D (2003) Vertebrate microRNA genes. *Science* 299, 1540.

Lim W & Song G (2014) Identification of novel regulatory genes in development of the avian reproductive tracts. *PLoS One* 9, e96175.

Lindersson E, Beedholm R, Hojrup P, Moos T, Gai W, Hendil K & Jensen P (2004) Proteasomal inhibition by a-synuclein filaments and oligomers. *J. Biol. Chem.* 279, 12924–12934.

Lindvall O, Sawle G, Widner H, Rothwell J, Björklund A, Brooks D, Brundin P, Frackowiak R, Marsden C, Odin P & Al. E (1994) Evidence for long-term survival and function of dopaminergic grafts in progressive Parkinson's disease. *Ann. Neurol.* 35, 172–180.

Ling S-C, Fahrner P, Greenough W & Gelfand V (2004) Transport of Drosophila fragile X mental retardation protein-containing ribonucleoprotein granules by kinesin-1 and cytoplasmic dynein. *Biol. Sci.* 101, 17428–17433.

Liu G, Tang J, Edmonds BT, Murray J, Levin S & Condeelis J (1996) F-actin sequesters elongation factor 1α from interaction with aminoacyl-tRNA in a pH-dependent reaction. *J. Cell Biol.* 135, 953–963.

Lotharius J & Brundin P (2002) Impaired dopamine storage resulting from alpha-synuclein mutations may contribute to the pathogenesis of Parkinson's disease. *Hum. Mol. Genet.* 11, 2395–2407.

Lotharius J, Falsig J, van Beek J, Payne S, Dringen R, Brundin P & Leist M (2005) Progressive degeneration of human mesencephalic neuron-derived cells triggered by dopamine-dependent oxidative stress is dependent on the mixed-lineage kinase pathway. *J. Neurosci.* 25,

6329–6342.

Lui JH, Hansen D V & Kriegstein AR (2011) Development and evolution of the human neocortex. *Cell* 146, 18–36.

Luk K, Kehm V, Carroll J, Zhang B, O'Brien P, Trojanowski J & Lee VM (2012) Pathological a-synuclein transmission initiates Parkinson-like neurodegeneration in nontransgenic mice. *Science* 338, 949–953.

Luk KC. & Lee VM-Y (2014) Modeling Lewy pathology propagation in Parkinson's disease. *Park. Relat. Disord.* 20, S85–S87.

Lumayag S, Haldin CE, Corbett NJ, Wahlin KJ, Cowan C, Turturro S, Larsen PE, Kovacs B, Witmer PD, Valle D, Zack DJ, Nicholson DA & Xu S (2013) Inactivation of the microRNA-183/96/182 cluster results in syndromic retinal degeneration. *Proc. Natl. Acad. Sci. U. S. A.* 110.

Luo C, Lancaster M, Castano R, Nery J, Lnoblich J & Ecker J (2017) Cerebral organoids recapitulate epigenomic signatures of the human fetal brain. *Cell Rep.* 17, 3349–3384.

MacRae IJ, Ma E, Zhou M, Robinson C V. & Doudna JA (2008) In vitro reconstitution of the human RISC-loading complex. *Proc. Natl. Acad. Sci. U. S. A.* 105, 512–517.

Mahmoudi S & Brunet A (2012) Aging and reprogramming: a two-way street. *Curr. Opin. Cell Biol.* 24, 744–756.

Maltsev AS, Ying J & Bax A (2012) Impact of N-terminal acetylation of α-synuclein on its random coil and lipid binding properties. *Biochemistry* 51, 5004–5013.

Maniataki E & Mourelatos Z (2005) A human, ATP-independent, RISC assembly machine fueled by pre-miRNA. *Genes Dev.* 19, 2979–2990.

Maroteaux L, Campanelli JT & Scheller RH (1988) Synuclein: A neuron-specific protein localized to the nucleus and presynaptic nerve terminal. *J. Neurosci.* 8, 2804–2815.

Marti MJ, Tolosa E & Campdelacreu J (2003) Clinical Overview of the synucleinopathies. *Mov. Disord.* 18, 21–27.

Martin K. & Ephrussi A (2009) mRNA localization: gene expression in the spatial dimension. *Cell* 136, 719–730.

Masliah E, Rockenstein E, Veinbergs I, Mallory M, Hashimoto M, Takeda A, Sagara Y, Sisk A & Mucke L (2000) Dopaminergic loss and inclusion body formation in α-synuclein mice: Implications for neurodegenerative disorders. *Science* 287, 1265–1269.

Mateyak MK & Kinzy TG (2010) eEF1A: Thinking outside the ribosome. *J. Biol. Chem.* 285, 21209–21213.

Matsuoka Y, Vila M, Lincoln S, McCormack A, Picciano M, LaFrancois J, Yu X, Dickson D, Langston W, McGowan E, Farrer M, Hardy J, Duft K, Przedborski S & Di Monte D (2001) Lack of nigral pathology in transgenic mice expressing human α-synuclein driven by the tyrosine hydroxylase promoter. *Neurobiol. Dis.* 8, 535–539.

McCann H, Stevens CH, Cartwright H & Halliday GM (2013) α-synucleinopathy subtypes. *Park. Relat. Disord.* 10, 1–17.

McGeary SE, Lin KS, Shi CY, Pham TM, Bisaria N, Kelley GM & Bartel DP (2019) The biochemical basis of microRNA targeting efficacy. *Science* 366.

McLean P, Kawamata H & Hyman B (2001) a-Synuclein-enhanced green fluorescent protein fusion proteins form proteasome sensitive inclusions in primary neurons. *Neuroscience* 104, 901–912.

McNaught K, Perl D, Brownell A & Olanow C (2004) Systemic exposure to proteasome inhibitors causes a progressive model of Parkinson's disease. *Ann. Neurol.* 56, 149–162.

McNeill TH, Brown SA, Rafols JA & Shoulson I (1988) Atrophy of medium spiny I striatal dendrites in advanced Parkinson's disease. *Brain Res.* 455, 148–152.

Medvedev SP, Shevchenko IA & Zakian MS (2010) Induced pluripotent stem cells: problems and advantages when applying them in regenerative medicine. *Acta Naturae* 2, 18–28.

Mendoza MB, Gutierrez S, Ortiz R, Moreno DF, Dermit M, Dodel M, Rebollo E, Bosch M, Mardakheh FK & Gallego C (2021) The elongation factor eEF1A2 controls translation and actin dynamics in dendritic spines. *Sci. Signal.* 5594.

Meng L, Ben M, Cook SJ, Neubauer M, Wan A, Jin Y & Yan D (2015) The cell death pathway regulates synapse elimination through cleavage of gelsolin in Caenorhabditis elegans neurons Lingfeng. *Cell Rep.* 11, 1737–1748.

Metzler-Baddeley C (2007) A review of cognitive impairments in dementia with Lewy bodies relative to Alzheimer's disease and Parkinson's disease with dementia. *Cortex* 43, 583–600.

Mezey E, Dehejia A, Harta G, Papp MI, Polymeropoulos MH & Brownstein MJ (1998) Alpha synuclein in neurodegenerative disorders: Murderer or accomplice? *Nat. Med.* 4, 755–757.

Miller JD, Ganat YM, Kishinevsky S, Bowman RL, Liu B, Tu EY, Mandal PK, Vera E, Shim JW, Kriks S, Taldone T, Fusaki N, Tomishima MJ, Krainc D, Milner TA, Rossi DJ & Studer L (2013) Human iPSC-based modeling of late-onset disease via progerin-induced aging. *Cell Stem Cell* 13, 691–705.

Miller M & Peters A (1981) Maturation of rat visual cortex. IIA combined Golgi-electron microscope study of pyramidal neurons. *J. Comput. Neurosci.* 203, 555–573.

Mohamed N-V, Sirois J, Ramamurthy J, Mathur M, Lépine P, Deneault E, Maussion G, Nicouleau M, Chen CX-Q, Abdian N, Soubannier V, Cai E, Nami H, Thomas RA, Wen D, Tabatabaei M, Beitel LK, Singh Dolt K, Karamchandani J, Stratton JA, Kunath T, Fon EA & Durcan TM (2021) Midbrain organoids with an SNCA gene triplication model key features of synucleinopathy. *Brain Commun.*, 1–21.

Moore DJ, West AB, Dawson VL & Dawson TM (2005) Molecular pathophysiology of Parkinson's disease. *Annu. Rev. Neurosci.* 28, 57–87.

Moreno JA, Radford H, Peretti D, Steinert JR, Verity N, Martin MG, Halliday M, Morgan J, Dinsdale D, Ortori CA, Barrett DA, Tsaytler P, Bertolotti A, Willis AE, Bushell M & Mallucci GR (2012) Sustained translational repression by eIF2α-P mediates prion neurodegeneration. *Nature* 485, 507–511.

Muddashetty RS, Vijayalaxmi CN, Gross C, Yao X, Xing L, Laur O, Warren S & Bassell GJ (2011) Reversible inhibition of PSD-95 mRNA translation by miR-125a, FMRP phosphorylation and mGluR signaling. *Mol. Cell* 61, 515–525.

Muenter MD, Forno LS, Hornykiewicz O, Kish SJ, Maraganore

DM, Caselli RJ, Okazaki H, Howard FM, Snow BJ & Calne DB (1998) Hereditary form of parkinsonism-dementia. *Ann. Neurol.* 43, 768–781.

Muguruma K, Nishiyama A, Kawakami H, Hashimoto K & Sasi Y (2015) Self-organization of polarized cerebellar tissue in 3D culture of human pluripotent stem cells. *Cell Rep.* 10, 537–550.

Mukherjee S, Klaus C, Pricop-Jeckstadt M, Miller JA & Struebing FL (2019) A microglial signature directing human aging and neurodegeneration-related gene networks. *Front. Neurosci.* 13, 1–12.

Murmu R, Li W, Holtmaat A & Li J-Y (2013) Dendritic spine instability leads to progressive neocortical spine loss in a mouse model of Huntington's disease. *J. Neurosci.* 33, 12997 – 13009.

Murphy DD, Rueter SM, Trojanowski JQ & Lee VM (2000) Synucleins are developmentally expressed, and alpha-synuclein regulates the size of the presynaptic vesicular pool in primary hippocampal neurons le. *J. Neurosci.* 20, 3214–20.

Nakajo S, Shioda S, Nakai Y & Nakaya K (1994) Localization of phosphoneuroprotein 14 (PNP 14) and its mRNA expression in rat brain determined by immunocytochemistry and in situ hybridization. *Brain Res. Mol. Brain Res.* 27, 81–86.

Nakamura T, Yamashita H, Takahashi T & Nakamura S (2001) Activated Fyn phosphorylates α-synuclein at tyrosine residue 125. *Biochem. Biophys. Res. Commun.* 280, 1085–1092.

Nalavadi VC, Muddashetty RS, Gross C & Bassell GJ (2012) Dephosphorylation-induced ubiquitination and degradation of FMRP in dendrites: A role in immediate early mGluR-stimulated translation. *J. Neurosci.* 32, 2582–2587.

Narayanan U, Nalavadi V, Nakamoto M, Pallas DC, Ceman S, Bassell GJ & Warren ST (2007) FMRP phosphorylation reveals an immediate-early signaling pathway triggered by group I mGluR and mediated by PP2A. *J. Neurosci.* 27, 14349–14357.

Narhi L, Wood SJ, Steavenson S, Jiang Y, Wu GM, Anafi D, Kaufman SA, Martin F, Sitney K, Denis P, Louis JC, Wypych J, Biere AL & Citron M (1999) Both familial Parkinson's disease mutations accelerate α-synuclein aggregation. *J. Biol. Chem.* 274, 9843–9846.

Negro A, Brunati AM, Donella-Deana A, Massimino ML & Pinna LA (2001) Multiple phosphorylation of α-synuclein by protein tyrosine kinase Syk prevents eosin-induced aggregation. *2The FASEB J.* 16, 210–212.

Neuner J, Ovsepian S V., Dorostkar M, Filser S, Gupta A, Michalakis S, Biel M & Herms J (2014) Pathological α-synuclein impairs adult-born granule cell development and functional integration in the olfactory bulb. *Nat. Commun.* 5, 1–12.

Neystat M, Lynch T, Przedborski S, Kholodilov N, Rzhetskaya M & Burke R (1999) α-Synuclein expression in substantia nigra and cortex in Parkinson's disease. *Mov. Disord.* 14, 417–422.

Nikolaus S, Antke C & Müller H-W (2009) In vivo imaging of synaptic function in the central nervous system. *Behav. Brain Res.* 204, 1 – 31.

Niu M, Xu R, Wang J, Hou B & Xie A (2016) MiR-133b ameliorates axon degeneration induced by MPP+ via targeting RhoA. *J. Neurosci.* 325, 39–49.

Nonaka T, Iwatsubo T & Hasegawa M (2005) Ubiquitination of alpha-synuclein. *Biochemistry* 44, 361–368.

Norris EH, Giasson BI. & Lee VM-Y (2004) Alpha-synuclein: normal function and role in neurodegenerative diseases. *Curr. Top. Dev. Biol.* 60, 17–54.

Obeso JA, Rodriguez-Oroz MC, Chana P, Lera G, Rodriguez M & Olanow CW (2000) The evolution and origin of motor complications in Parkinson's disease. *Neurology* 55, S13-20.

Ohmine S, Squillace KA, Hartjes KA, Deeds MC, Armstrong AS, Thatava T, Sakuma T, Terzic A, Kudva Y & Ikeda Y (2012) Reprogrammed keratinocytes from elderly type 2 diabetes patients suppress senescence genes to acquire induced pluripotency. *Aging (Albany. NY).* 4, 60–73.

Okamura K, Chung WJ & Lai EC (2008) The long and short of inverted repeat genes in animals: microRNAs, mirtrons and hairpin RNAs. *Cell Cycle* 7, 2840–2845.

Okamura K, Hagen JW, Duan H, Tyler DM & Lai EC (2007) The mirtron pathway generates microRNA-class regulatory RNAs in Drosophila. *Cell*, 89–100.

Okochi M, Walter J, Koyama A, Nakajo S, Baba M, Iwatsubo T, Meijer L, Kahle PJ & Haass C (2000) Constitutive phosphorylation of the Parkinson's disease associated α-synuclein. *J. Biol. Chem.* 275, 390–397.

Olanow C, Schapira A & Agid Y (2003) Neuroprotection for Parkinson's disease: Prospects and promises. *Ann. Neurol. Neurol.* 53, S1–S2.

Ormel PR, Vieira de Sá R, van Bodegraven EJ, Karst H, Harschnitz O, Sneeboer MAM, Johansen LE, van Dijk RE, Scheefhals N, Berdenis van Berlekom A, Ribes Martínez E, Kling S, MacGillavry HD, van den Berg LH, Kahn RS, Hol EM, de Witte LD & Pasterkamp RJ (2018) Microglia innately develop within cerebral organoids. *Nat. Commun.* 9, 4167.

Paleologou KE, Oueslati A, Shakked G, Rospigliosi CC, Kim HY, Lamberto GR, Fernandez CO, Schmid A, Chegini F, Gai WP, Chiappe D, Moniatte M, Schneider BL, Aebischer P, Eliezer D, Zweckstetter M, Masliah E & Lashuel HA (2010) Phosphorylation at S87 is enhanced in synucleinopathies, inhibits α-synuclein oligomerization, and influences synuclein-membrane interactions. *J. Neurosci.* 30, 3184–3198.

Park J, Wetzel I, Marriott I, Dréau D, D'Avanzo C, Kim DY, Tanzi RE & Cho H (2018) A 3D human triculture system modeling neurodegeneration and neuroinflammation in Alzheimer's disease. *Nat. Neurosci.* 21, 941–951.

Parkinson J (2002) An eassay on shaking palsy. London: Sherwood, Neely and Jones; 1817. Re-printed in: Neuropsychiatric classics. *J. Neuropsychiatry Clin. Neurosci.* 14, 223–236.

Parkkinen L, Kauppinen T, Pirttilä T, Autere JM & Alafuzoff I (2005) A-synuclein pathology does not predict extrapyramidal symptoms or dementia. *Ann. Neurol.* 57, 82–91.

Parnetti L, Gaetani L, Eusebi P, Paciotti S, Hansson O, El-Agnaf O, Mollenhauer B, Blennow K & Calabresi P (2019) CSF and blood biomarkers for Parkinson's disease. *Lancet*

Neurol. 18, 573–586.

Pasca AM, Sloan SA, Clarke LE, Tian Y, Makinson CD, Huber N, Kim CH, Park JY, O'Rourke NA, Nguyen KD, Smith SJ, Huguenard JR, Geschwind DH, Barres BA & Pasca SP (2015) Functional cortical neurons and astrocytes from human pluripotent stem cells in 3D culture. *Nat. Methods* 12, 671–678.

Patt S, Gertz HJ., Gerhard L. & Cervós-Navarro J (1991) Pathological changes in dendrites of substantia nigra neurons in Parkinson's disease: a Golgi study. *Histol. Histopathol.* 6, 373–80.

Peng X, Theranian R, Dietrich P, Stefanis L & RG P (2005) a-Synuclein activation of protein phosphatase 2A reduces tyrosine hydroxylase phosphorylation in dopaminergic cells. *J. Cell Sci.* 118, 3523–3530.

Penzes P, Cahill M, Jones K, VanLeeuwen J-E & Woolfrey K (2011) Dendritic spine pathology in neuropsychiatric disorders. *Nat. Neurosci.* 14, 285 – 293.

Perez RG, Waymire J, Lin E, Liu J, Guo F & Zigmond M (2002) A role for a-synuclein in the regulation of dopamine biosynthesis. *J. Neurosci.* 22, 3090–3099.

Perrin RJ, Woods WS, Clayton DF & George JM (2000) Interaction of human a-synuclein and Parkinson's disease variants with phospholipids. Structural analysis using site-directed mutagenesis. *J. Biol. Chem.* 275, 34393–34398.

Peskova L, Jurcikova D, Vanova T, Krivanek J, Capandova M, Sramkova Z, Sebestikova J, Kolouskova M, Kotasova H, Streit L & Barta T (2020) miR-183/96/182 cluster is an important morphogenetic factor targeting PAX6 expression in differentiating human retinal organoids. *Stem Cells* 38, 1557–1567.

Peters A & Kaiserman-Abramof I (1970) The small pyramidal neuron of the rat cerebral cortex. The perikaryon, dendrites and spines. *Am. J. Anat.* 127, 321–355.

Petersen K, Olesen OF & Mikkelsen JD (1999) Developmental expression of a-synuclein in rat hippocampus and cerebral cortex. *Neuroscience* 91, 651–659.

Pfeiffer BE & Huber KM (2006) Current advances in local protein synthesis and synaptic plasticity. *J. Neurosci.* 26, 7147–7150.

Phatak P & Donahue J (2017) Biotinylated Micro-RNA Pull Down Assay for Identifying miRNA Targets. *Bio-Protocol* 7, 5–9.

Picconi B, Piccoli G & Calabresi P (2012) Synaptic dysfunction in Parkinson's disease. *Adv. Exp. Med. Biol.* 970, 553–572.

Pierce ML, Weston MD, Fritzsch B, Gabel HW, Ruvkun G & Soukup GA (2008) MicroRNA-183 family conservation and ciliated neurosensory organ expression. *Evol. Dev.* 10, 106–113.

Plante I, Davidovic L, Ouellet DL, Gobeil LA, Tremblay S, Khandjian EW & Provost P (2006) Dicer-derived microRNAs are utilized by the fragile X mental retardation protein for assembly on target RNAs. *J. Biomed. Biotechnol.*, 1–12.

Polymeropoulos MH, Lavedan C, Leroy E, Ide SE, Dehejia A, Dutra A, Pike B, Root H, Rubenstein J, Boyer R, Stenroos ES, Chandrasekharappa S, Athanassiadou A, Papapetropoulos T, Johnson WG, Lazzarini AM, Duvoisin RC, Di Iorio G, Golbe LI & Nussbaum RL (1997) Mutation in the α-synuclein gene identified in families with Parkinson's disease. *Science* 276, 2045–2047.

Portera-Cailliau C (2012) Which comes first in fragile X syndrome, dendritic spine dysgenesis or defects in circuit plasticity? *Neuroscientist* 18, 28–44.

Price DL, Rockenstein E, Ubhi K, Phung V, Maclean-Lewis N, Askay D, Cartier A, Spencer B, Patrick C, Desplats P, Ellisman MH & Masliah E (2010) Alterations in mGluR5 expression and signaling in lewy body disease and in transgenic models of alpha- synucleinopathy - implications for excitotoxicity. *PLoS One* 5.

Prieto M, Folci A & Martin S (2020) Post-translational modifications of the Fragile X Mental Retardation Protein in neuronal function and dysfunction. *Mol. Psychiatry* 25, 1688–1703.

van der Putten H, Wiederhold K, Probst A, Barbieri S, Mistl C, Danner S, Kauffmann S, Hofele K, Spooren W, Ruegg M, Lin S, Caroni P, Sommer B, Tolnay M & Bilbe G (2000) Neuropathology in mice expressing human alpha-synuclein. *J. Neurosci.* 20, 6021–6029.

Qian X, Nguyen HN, Song MM, Hadiono C, Ogden SC, Hammack C, Yao B, Hamersky GR, Jacob F, Zhong C, Yoon KJ, Jeang W, Lin L, Li Y, Thakor J, Berg DA, Zhang C, Kang E, Chickering M, Nauen D, Ho CY, Wen Z, Christian KM, Shi PY, Maher BJ, Wu H, Jin P, Tang H, Song H & Ming GL (2016) Brain-Region-Specific Organoids Using Mini-bioreactors for Modeling ZIKV Exposure. *Cell* 165, 1238–1254.

Qian X, Song H & Ming GL (2019) Brain organoids: Advances, applications and challenges. *Development* 146.

Qian X, Su Y, Adam CD, Wolf JA, Qian X, Su Y, Adam CD, Deutschmann AU, Pather SR & Goldberg EM (2020) Sliced Human Cortical Organoids for Modeling Resource Sliced Human Cortical Organoids for Modeling Distinct Cortical Layer Formation. *Cell Stem Cell* 26, 1–16.

Qin M, Kang J, Burlin T V., Jiang C & Smith CB (2005) Postadolescent changes in regional cerebral protein synthesis: An in vivo study in the Fmr1 null mouse. *J. Neurosci.* 25, 5087–5095.

Qin M, Schmidt KC, Zametkin AJ, Bishu S, Horowitz LM, Burlin T V., Xia Z, Huang T, Quezado ZM & Smith CB (2013) Altered cerebral protein synthesis in fragile X syndrome: Studies in human subjects and knockout mice. *J. Cereb. Blood Flow Metab.* 33, 499–507.

Quadrato G, Nguyen T, Macosko EZ, Sherwood JL, Yang SM, Berger DR, Maria N, Scholvin J, Goldman M, Kinney JP, Boyden ES, Lichtman JW, Williams ZM, McCarroll SA & Arlotta P (2017) Cell diversity and network dynamics in photosensitive human brain organoids. *Nature* 545, 48–53.

Qureshi H & Oaudel H (2011) Parkinsonian neurotoxin 1-methyl-4-phenyl-1,2,3,6-tetrahydropyridine (MPTP) and a-synuclein mutations promote Tau protein phos-phorylation at Ser262 and destabilize microtubule cytoskeleton in vitro. *J. Biol. Chem.* 286, 5055–5068.

Raja WK, Mungenast AE, Lin YT, Ko T, Abdurrob F, Seo J & Tsai LH (2016) Self-organizing 3D human neural tissue derived from induced pluripotent stem cells recapitulate Alzheimer's disease phenotypes. *PLoS One* 11, 1–18.

Rajasethupathy P, Fiumara F, Sheridan R, Betel D, Puthanveettil, Russo, Sander C, Tuschl T & Kandel E (2009) Characterization of small RNAs in aplysia reveals a role

for miR-124 in constraining synaptic plasticity through CREB. *Neuron* 63, 803–817.

Rakic P (2009) Evolution of the neocortex: a perspektive from developmental biology. *Nat. Rev. Neurosci.* 10, 724–735.

Ramón y Cajal S, Segura MF & Hümmer S (2019) Interplay between ncRNAs and cellular communication: A proposal for understanding cell-specific signaling pathways. *Front. Genet.* 10, 1–11.

Rao A & Steward O (1991) Evidence that protein constituents of postsynaptic membrane specializations are locally synthesized: analysis of proteins synthesized within synaptosomes. *J. Neurosci.* 11, 2881–2895.

Ratti M, Lampis A, Ghidini M, Salati M, Mirchev MB, Valeri N & Hahne JC (2020) MicroRNAs (miRNAs) and long non-coding RNAs (lncRNAs) as new tools for cancer therapy: first steps from bench to bedside. *Target. Oncol.* 15, 261–278.

Ray Dorsey E, Elbaz A, ... & Murray CJL (2018) Global, regional, and national burden of Parkinson's disease, 1990–2016: a systematic analysis for the Global Burden of Disease Study 2016. *Lancet Neurol.* 17, 939–953.

Recasens A, Perier C & Sue CM (2016) Role of microRNAs in the regulation of α-synuclein expression: A systematic review. *Front. Mol. Neurosci.* 9, 1–12.

Reynolds B, Tetzlaff W & Weiss S (1992) A multipotent EGF-responsive striatal embryonic progenitor cell produces neurons and astrocytes. *J. Neurosci.* 12, 4565–4574.

Riley BE, Gardai SJ, Emig-Agius D, Bessarabova M, Ivliev AE, Schüle B, Alexander J, Wallace W, Halliday GM, Langston JW, Braxton S, Yednock T, Shaler T & Johnston JA (2014) Systems-Based Analyses of Brain Regions Functionally Impacted in Parkinson's Disease Reveals Underlying Causal Mechanisms. *PLoS One* 9, e102909.

Rochefort NL & Konnerth A (2012) Dendritic spines: from structure to in vivo function. *EMBO Rep.* 13, 299–708.

Rochet JC, Conway KA & Lansbury PT (2000) Inhibition of fibrillization and accumulation of prefibrillar oligomers in mixtures of human and mouse α-synuclein. *Biochemistry* 39, 10619–10626.

Romaniello R, Arrigoni F, Fry A, Bassi M, Rees M, Borgatti R, Pilz DT & Cushion TD (2018) Tubulin genes and malformations of cortical development. *Eur. J. Med. Genet.* 61, 744–754.

Rus D (2019) Preparation and co-culture of iPSC-derived dopaminergic neurons and astrocytes. *Curr. Protoc. Cell Biol.* 85, e98.

de Rus Jacquet A (2019) Preparation and Co-Culture of iPSC-Derived Dopaminergic Neurons and Astrocytes. *Curr. Protoc. Cell Biol.* 85, e98.

Santulli G, Giza DE & Calin GA (2015) microRNA and Chronic Lymphotic Leukemia. In *microRNA: Cancer. Advances in Experimental Medicine and Biology*. Springer, Cham.

Schell H, Hasegawa T, Neumann M & Kahle P (2009) Nuclear and neuritic distribution of serine-129 phosphorylated a-synuclein in transgenic mice. *Neuroscience* 160, 796–804.

Scherzer CR, Grass JA, Liao Z, Pepivani I, Zheng B, Eklund AC, Ney PA, Ng J, McGoldrick M, Mollenhauer B, Bresnick EH & Schlossmacher MG (2008) GATA transcription factors directly regulate the Parkinson's disease-linked gene α-synuclein. *Proc. Natl. Acad. Sci. U. S. A.* 105, 10907–10912.

Schikorski T & Stevens C (1999) Quantitative fine-structural analysis of olfactory cortical synapses. *Proc. Natl. Acad. Sci. U. S. A.* 96, 4107–4112.

Schratt G (2009a) Fine-tuning neural gene expression with microRNAs. *Curr. Opin. Neurobiol.* 19, 213–219.

Schratt G (2009b) MicroRNAs at the synapse. *Nat. Rev. Neurosci.* 10, 842–849.

Schüle B, Sterling L, Walter M & Ting D (2014) Discovery of functional non-coding conserved regions in the α-synuclein gene locus. *F1000 Res.* 3.

Schwarting R, Sedelis M, Hofele K, Auburger G & HUston J (1999) Strain- dependent recovery of open-field behavior and striatal dopamine deficiency in the mouseMPTP model of Parkinson's disease. *Neurotoxicology Res.* 1, 41–56.

Scott D & Roy S (2012) a-Synuclein inhibits intersynaptic vesicle mobility and maintains recycling-pool homeosta sis. *J. Neurosci.* 32, 10129–10135.

Shang S, Li D, Tian Y, Li R, Zhao H, Zheng L, Zhang Y, Chen YC & Yin X (2021) Hybrid PET-MRI for early detection of dopaminergic dysfunction and microstructural degradation involved in Parkinson's disease. *Commun. Biol.* 4, 1–9.

Shi Y, Sun L, Liu J, Zhong S, Wang M, Li R, Li P, Guo L, Fang A, Chen R, Ge W-P, Wu Q & Wang X (2019) Vascularized human cortical organoids model cortical development in vivo. *bioRxiv*, 682104.

Siegel G, Obernosterer G, Fiore R, Oehmen M, Bicker S, Christensen, M, Khudayberdiev S, Leuschner P, Busch CJ, Kane C, Hübel K, Dekker F, Hedberg C, Rengarajan B, Drepper C, Waldmann H, Kauppinen S, Greenberg ME, Draguhn A, Rehmsmeier, Martinez & Schratt G (2009) A functional screen implicates microRNA- 138-dependent regulation of the depalmitoylation enzyme APT1 in dendritic spine morphogenesis. *Nat. Cell Biol.* 11, 705–716.

Singleton AB, Farrer M, Johnson J, Singleton A, Hague S, Kachergus J, Hulihan M, Peuralinna T, Dutra A, Nussbaum R, Lincoln S, Crawley A, Hanson M, Maraganore D, Adler C, Cookson MR, Muenter M, Baptista M, Miller D, Blancato J, Hardy J & Gwinn-Hardy K (2003) α-Synuclein locus triplication causes Parkinson's disease. *Science* 302, 841.

Sloan SA, Darmanis S, Huber N, Khan TA, Birey F, Caneda C, Reimer R, Quake SR, Barres BA & Paşca SP (2017) Human Astrocyte Maturation Captured in 3D Cerebral Cortical Spheroids Derived from Pluripotent Stem Cells. *Neuron* 95, 779-790.e6.

Smith W, Jiang H, Pei Z, Tanaka Y, Morita H, Sawa A, Dawson V, Dawson T & Ross C (2005) Endoplasmic reticulum stress and mitochondrial cell death pathways mediate A53T mutant a-synuclein-induced toxicity. *Hum. Mol. Genet.* 14, 3801–3811.

Smits LM, Reinhardt L, Reinhardt P, Glatza M, Monzel AS, Stanslowsky N, Rosato-Siri MD, Zanon A, Antony PM, Bellmann J, Nicklas SM, Hemmer K, Qing X, Berger E, Kalmbach N, Ehrlich M, Bolognin S, Hicks AA, Wegner F, Sterneckert JL & Schwamborn JC (2019) Modeling

Parkinson's disease in midbrain-like organoids. *NPJ Park. Dis.* 5, 5.

Smrt RD & Zhao X (2010) Epigenetic regulation of neuronal dendrite and dendritic spine development. *Front. Biol. China* 5, 304–323.

Snead D & Eliezer D (2014) Alpha-Synuclein Function and Dysfunction on Cellular Membranes. *Exp. Neurobiol.* 23, 292–313.

Soares DC, Barlow PN, Newbery HJ, Porteous DJ & Abbott CM (2009) Structural models of human eEF1A1 and eEF1A2 reveal two distinct surface clusters of sequence variation and potential differences in phosphorylation. *PLoS One* 4, e6315.

Sofroniew M V. (2014) Astrogliosis. *Cold Spring Harb. Perspect. Biol.* 7, a020420.

Spillantini MG, Crowther RA, Jakes R, Hasegawa M & Goedert M (1998) α-Synuclein in filamentous inclusions of Lewy bodies from Parkinson's disease and dementia with Lewy bodies. *Proc. Natl. Acad. Sci. U. S. A.* 95, 6469–6473.

Spillantini MG, Schmidt ML, Lee VM-Y, Trojanow JQ, Ross J & Goedert M (1997) a -Synuclein in Lewy bodies. *Nature* 388, 839–840.

St Martin JL, Klucken J, Outeiro TF, Nguyen P, Keller-McGandy C, Cantuti-Castelvetri I, Grammatopoulos TN, Standaert DG, Hyman BT & McLean PJ (2007) Dopaminergic neuron loss and up-regulation of chaperone protein mRNA induced by targeted over-expression of alpha-synuclein in mouse substantia nigra. *J. Neurochem.* 100, 1449–1457.

Steidl J, Gomez-Isla T, Mariash A, Ashe KH & Boland LM (2003) Altered short-term hippocampal synaptic plasticity in mutant a-synuclein transgenic mice. *Neuroreport* 14, 219–223.

Sutton MA & Schuman EM (2005) Local translational control in dendrites and its role in long-term synaptic plasticity. *J. Neurobiol.* 64, 116–131.

Tagliafierro L & Chiba-Falek O (2016) Upregulation of SNCA Gene Expression: Implications to Synucleinopathies. *Physiol. Behav.* 176, 139–148.

Takahashi K & Yamanaka S (2006) Induction of pluripotent stem cells from mouse embryonic and adult fibroblast cultures by defined factors. *Cell* 126, 663–676.

Tan Y, Sgobio C, Arzberger T, Machleid F, Tang Q, Findeis E, Tost J, Chakroun T, Gao P, Höllerhage M, Bötzel K, Herms J, Höglinger G & Koeglsperger T (2020) Loss of fragile X mental retardation protein precedes Lewy pathology in Parkinson's disease. *Acta Neuropathol.* 139, 319–345.

Tashiro A & Yuste R (2003) Structure and molecular organization of dendritic spines. *Histol. Histopathol.* 18, 617–634.

Terry R, Masliah E, Salmon D, Butters N, DeTeresa R, Hill R, Hansen LA & Katzmann R (1991) Physical basis of cognitive alterations in alzheimer's disease: Synapse loss is the major correlate of cognitive impairment. *Ann. Neurol.* 30, 572–580.

Thomson JA (1998) Embryonic stem cell lines derived from human blastocysts. *Science* 282, 1145–1147.

Tofaris GK, Reitböck PG, Humby T, Lambourne SL, O'Connell M, Ghetti B, Gossage H, Emson PC, Wilkinson LS, Goedert M & Spillantini MG (2006) Pathological changes in dopaminergic nerve cells of the substantia nigra and olfactory bulb in mice transgenic for truncated human α-synuclein(1- 120): Implications for lewy body disorders. *J. Neurosci.* 26, 3942–3950.

Tong Y, Yamaguchi H, Giaime E, Boyle S, Kopan R, Kelleher R & Shen J (2010) Loss of leucine-rich repeat kinase 2 causes im- pairment of protein degradation pathways, ac-cumulation of α-synuclein, and apoptotic cell death in aged mice. *Proc. Natl. Acad. Sci. U. S. A.* 107, 9879–9884.

Torre RE & Steward O (1992) Demonstration of local protein synthesis within dendrites using a new cell culture system that permits the isolation of living axons and dendrites from their cell bodies. *J. Neurosci.* 12, 762–772.

Ubhi K, Rockenstein E, Kragh C, Inglis C, Spencer B, Michael S, Mante M, Adame A, Galasko D & Masliah E (2014) Widespread microRNA dysregulation in multiple system atrophy - disease-related alteration in miR-96. *Eur. J. Neurosci.* 39, 1026–1041.

Uchihara T & Giasson BI (2016) Propagation of alpha-synuclein pathology: hypotheses, discoveries, and yet unresolved questions from experimental and human brain studies. *Acta Neuropathol.* 131, 49–73.

Ueda K, Fukushima H, Masliah E, Xia Y, Iwai A, Yoshimoto M, Otero DAC, Kondo J, Ihara Y & Saitoh T (1993) Molecular cloning of cDNA encoding an unrecognized component of amyloid in Alzheimer disease. *Proc. Natl. Acad. Sci. U. S. A.* 90, 11282–11286.

Ungerstedt U (1968) 6-Hydroxy-dopamine induced degeneration of central monoamine neurons. *Eur. J. Pharmacol.* 5, 107–110.

Uniprot (2022) Uniprot - P12814 ACTN1_HUMAN. Available at: https://www.uniprot.org/uniprotkb/P12814/entry [Accessed May 31, 2021].

Untergasser A, Cutcutache I, Koressaar T, Ye J, Faircloth BC, Remm M & Rozen SG (2012) Primer3-new capabilities and interfaces. *Nucleic Acids Res.* 40, 1–12.

Vallelunga A, Iannitti T, Capece S, Somma G, Russillo MC, Foubert-Samier A, Laurens B, Sibon I, Meissner WG, Barone P & Pellecchia MT (2021) Serum miR-96-5P and miR-339-5P are potential diomarkers for multiple system atrophy and Parkinson's disease. *Front. Aging Neurosci.* 13, 1–7.

Velasco S, Kedaigle A, Simmons S, Nash A, Rocha M, Quadrato G, Paulsen B, Nguyen L, Adiconis X, Regev A, Levin J & Arlotta P (2019) Individual brain organoids reproducibly form cell diversity of the human cerebral cortex. *Physiol. Behav.* 176, 139–148.

Villalba RM & Smith Y (2010) Striatal spine plasticity in Parkinson's disease. *Front. Neuroanat.* 4, 133.

Van Der Walt JM, Noureddine MA, Kittappa R, Hauser MA, Scott WK, McKay R, Zhang F, Stajich JM, Fujiwara K, Scott BL, Pericak-Vance MA, Vance JM & Martin ER (2004) Fibroblast growth factor 20 polymorphisms and haplotypes strongly influence risk of Parkinson disease. *Am. J. Hum. Genet.* 74, 1121–1127.

Wang L, Das U, Scott DA, Tang Y, McLean PJ & Roy S (2014) a-Synuclein multimers cluster synaptic vesicles and attenuate recycling. *Curr. Biol.* 24, 2319–2326.

Wang Z-H, Zhang J-L, Duan Y-L, Zhang Q-S, Li G-F & Zheng D-L (2015) MicroRNA-214 participates in the neuroprotective effect of Resveratrol via inhibiting α-synuclein expression in MPTP-induced Parkinson's disease mouse. *Biomed. Pharmacotherarpy* 74, 252–256.

Watanabe K, Taskesen E, Van Bochoven A & Posthuma D (2017) Functional mapping and annotation of genetic associations with FUMA. *Nat. Commun.* 8, 1–10.

Watson JB., Hatami A., David H., MAsliah E., Roberts K., Evans CE. & LEvine MS. (2009) Alterations in corticostriatal synaptic plasticity in mice overexpressing human alpha-synuclein. *Neuroscience* 159, 501–513.

Waxman EA & Giasson BI (2008) Specificity and Regulation of Casein Kinase-Mediated Phosphorylation of a-Synuclein. *J. Neuropathol. Exp. Neurol.* PAP, 402–416.

Wayman GA, Davare M, Ando H, Fortin D, Varlamova O, Cheng HY, Marks D, Obrietan K, Soderling TR, Goodman RH & Impey S (2008) An activity-regulated microRNA controls dendritic plasticity by down-regulating p250GAP. *Proc. Natl. Acad. Sci. U. S. A.* 105, 9093–9098.

Webb J, Ravikumar B, Atkins J, Skepper J & Rubinsztein D (2003) a-Synuclein is degraded by both autophagy and the proteasome. *J. Biol. Chem.* 278, 25009–25013.

Wefers Z, Alecki C, Huang R, Jacob-tomas S & Vera M (2022) Analysis of the Expression and Subcellular Distribution of eEF1A1 and eEF1A2 mRNAs during Neurodevelopment. *Cells* 11.

Weinreb P, Zhen W, Poon AW, Conway KA & Lansbury PJ (1996) NACP, a protein implicated in Alzheimer's dis- ease and learning, is natively unfolded. *Biochemistry* 35, 13709–13715.

Winner B, Regensburger M, Schreglmann S, Boyer L, Prots I, Rockenstein E, Mante M, Zhao C, Winkler J, Masliah E & Gage F (2012) Winner B, Regensburger M, Schreglmann S, Boyer L, Prots I, Rockenstein E, Mante M, Zhao C, Winkler J, Masliah E et al. *J. Neurosci.* 32, 16906 – 16916.

Winter J, Jung S, Keller S, Gregory RI & Diederichs S (2009) Many roads to maturity: MicroRNA biogenesis pathways and their regulation. *Nat. Cell Biol.* 11, 228–234.

Withers GS, MGeorge JM, Bankera GA & Clayton DF (1997) Delayed localization of synelfin (synuclein, NACP) to presynaptic terminals in cultured rat hippocampal neurons. *Dev. Brain Res.* 99, 887–94.

Wu B, Liu Q, Duan C, Li Y, Yu S, Chan P, Ueda K & Yang H (2011) Phosphorylation of a-synuclein upregulates tyrosine hydroxylase activity in MN9D cells. *Acta Histochem.* 113, 23–35.

Xicoy H, Wieringa B & Martens GJM (2017) The SH-SY5Y cell line in Parkinson's disease research: a systematic review. *Mol. Neurodegener.* 12, 1–11.

Xie Y & Chen Y (2016) MicroRNAs: emerging targets regulating oxidative stress in the models of Parkinson's disease. *Front. Neurosci.* 10, 298.

Xionga R, Wanga Z, Zhaoa Z, Li H, Chen W, Zhanga B, Wanga L, Wu L, Wen L, Ding J & Chen S (2014) MicroRNA-494 reduces DJ-1 expression and exacerbates neurodegeneration. *Neurobiol. Aging* 35, 705–714.

Xu S, Witmer P, Lumayag S, Kovacs B & Valle D (2007) MicroRNA (miRNA) transcriptome of mouse retina and identification of a sensory organ-specific miRNA cluster. *J. Biol. Chem.* 282, 25053–25066.

Yang D, Demma M, Warren V, Dharmawardhane S & Condeelis J (1990) Identification of an actin-binding protein from Dictyostelium as elongation factor 1a. *Nature* 347, 494–496.

Yang D, Li T, Wang Y, Tang Y, Cui H, Tang Y, Zhang X, Chen D, Shen N & Le W (2012) miR-132 regulates the differentiation of dopamine neurons by directly targeting Nurr1 expression. *J. Cell Sci.* 125, 1673–1682.

Yavich L, Jakala P & Tanila H (2006) Abnormal compartmen-talization of norepinephrine in mouse dentate gyrus in a-synuclein knockout and A30P transgenic mice. *J. Neurochem.* 99, : 724–732.

Yavich L, Tanila H, Vepsalainen S & Jakala P (2004) Role ofa-synuclein in presynaptic dopamine recruitment. *J. Neurosci.* 24, 11165–11170.

Yoon SJ, Elahi LS, Pașca AM, Marton RM, Gordon A, Revah O, Miura Y, Walczak EM, Holdgate GM, Fan HC, Huguenard JR, Geschwind DH & Pașca SP (2019) Reliability of human cortical organoid generation. *Nat. Methods* 16, 75–78.

Zaja-Milatovic S, Milatovic D, Schantz AM, Zhang KS, Montine A, Samii A, Deutch Y & Montine TJ (2005) Dendritic degeneration in neostriatal medium spiny neurons in Parkinson disease. *Neurobiology* 64, 545–547.

Zhang S-C, Wernig M, Duncan ID, Brüstle O & Thomson JA (2001) In vitro differentiation of transplantable neural precursors from human embryonic stem cells. *Nat. Biotechnol.* 19, 169–177.

Zhang W & Benson DL (2001) Stages of synapse development defined by dependence on F-actin. *J. Neurosci.* 21, 5169–5181.

Zhang Z & Cheng Y (2014) miR-16-1 promotes the aberrant α-synuclein accumulation in Parkinson disease via targeting heat shock protein 70. *Sci. World J.* 2014, 938348.

Zhou L, Miller C, Miraglia LJ, Romero A, Mure LS, Panda S & Kay SA (2021) A Genome-wide microRNA screen identifies the microRNA-183/96/182 cluster as a modulator of circadian rhythms. *Proc. Natl. Acad. Sci. U. S. A.* 118, e2020454118.

Zhou R, Huang Y, Li X, Chen C, Shi Q, Wang G, Tian C, Wang Z, Jing Y, Gao C & Dong X (2010) Molecular inter- action ofa-synuclein with tubulin influences on the po-lymerization of microtubule in vitro and structure of microtubule in cells. *Mol. Biol. Rep.* 37, 3183–3192.

„… doch mit mehr Vergnügen trink‘ ich Bier!“

Auszug aus einem Brief Friedrich von Schillers
an Henriette v. Wolzogen, 13. November 1783